2008

Geochemical investigation of Meso- to Neoarchean (3075–2800 Ma) supracrustal rocks in the Nuuk region, southern west Greenland

Juan Carlos Ordóñez Calderón
University of Windsor

GEOCHEMICAL INVESTIGATION OF MESO- TO NEOARCHEAN (3075-2800 Ma) SUPRACRUSTAL ROCKS IN THE NUUK REGION, SOUTHERN WEST GREENLAND

by

Juan Carlos Ordóñez Calderón

A Dissertation

Submitted to the Faculty of Graduate Studies

through Earth and Environmental Sciences

in Partial Fulfillment of the Requirements for

the Degree of Doctor of Philosophy at the

University of Windsor

Windsor, Ontario, Canada

2008

Your file Votre référence
ISBN: 978-0-494-47117-3
Our file Notre référence
ISBN: 978-0-494-47117-3

Declaration of Co-Authorship / Previous Publication

I. Authorship Declaration

This thesis incorporates material that is the result of joint research. Field work was carried out through the collaborations with A. Polat, P.W.U. Appel, J.A.M. van Gool, and J.G. Raith. Field observations, laboratory analysis, data interpretation, key ideas, and manuscripts preparation were performed by the first author. The contribution of co-authors was primarily through criticism and review on original versions of the manuscripts. Therefore, I certify that this thesis is the product of my own work.

II. Declaration of Previous Publication

This thesis includes 3 original papers that have been previously published and submitted for publication in international peer reviewed journals. The percentages given by the authors' name represent the relative scientific contribution of each co-author.

Manuscript 1 (Chapter 2)

Ordóñez-Calderón, J.C. (55%), Polat, A. (20%), Fryer, B.J. (10%), Gagnon, J.E. (5%), Raith, J.G. (5%), Appel, P.W.U. (5%), 2008. Evidence for HFSE and REE mobility during calc-silicate metasomatism, Mesoarchean (~3075) Ivisaartoq greenstone belt, southern West Greenland. Precambrian Research. 161, 317-340. doi:10.1016/j.precamres.2007.09.004.

All co-authors provided insightful criticism on early versions of this manuscript. This project was possible through contributions of PREA and NSERC grant 250926 to A. Polat, and NSERC grant 83117 to B.J. Fryer. A. Polat collaborated with field work and through continuous discussions and guidance during the preparation of this manuscript.

B.J. Fryer and J.E. Gagnon cooperated with laboratory analysis. Their contribution was important in providing high-precision trace element analysis through continuous reviews of the ICP-MS operation protocol at GLIER. J.G. Raith showed me some important outcrops with calc-silicate alterations. P.W.U. Appel was the leader of the GEUS Nuuk Project and through his funding it was possible to conduct field work in Greenland. He also showed me the key outcrops and shared his field observations with me.

Manuscript 2 (Chapter 3)

Ordóñez-Calderón, J.C. (60%), Polat, A. (20%), Fryer, B.J. (10%), Appel, P.W.U. (4%), van Gool, J.A.M. (2%), Dilek, Y. (2%), Gagnon, J.E. (2%), 2008. Geochemistry and tectonic origin of Mesoarchean oceanic crust in the Ujarassuit and Ivisaartoq greenstone belts, SW Greenland. Lithos (Submitted in May, 2008).

All co-authors provided insightful criticism on early versions of this manuscript. This project was possible through contributions of PREA and NSERC grant 250926 to A. Polat, and NSERC grant 83117 to B.J. Fryer. A. Polat collaborated with field work and through continuous discussions and guidance during the preparation of this manuscript. B.J. Fryer and J.E. Gagnon cooperated with laboratory analysis. Their contribution was important in providing high-precision trace element analysis through continuous reviews of the ICP-MS operation protocol at GLIER. P.W.U. Appel was the leader of the GEUS Nuuk Project and he also provided logistics of the field work in Greenland. During the field season in the Ujarassuit belt, J.A.M. van Gool shared with me his work experience on the complex structural geology of the Nuuk Region. Y. Dilek provided significant comments on Phanerozoic ophiolites.

Manuscript 3 (Chapter 4)

Ordóñez-Calderón, J.C. (65%), Polat, A. (20%), Fryer, B.J. (10%), Gagnon, J.E. (5%), 2008. The Neoarchean 2800-2840 Ma Storø greenstone belt, SW Greenland: Field and geochemical evidence for an intra-oceanic supra-subduction zone geodynamic setting. Precambrian Research (Submitted in July, 2008).

All co-authors provided insightful criticism on early versions of this manuscript. This project was possible through contributions of PREA and NSERC grant 250926 to A. Polat, and NSERC grant 83117 to B.J. Fryer. A. Polat collaborated with field work and through continuous discussions and guidance during the preparation of this manuscript. B.J. Fryer and J.E. Gagnon cooperated with laboratory analysis. Their contribution was important in providing high-precision trace element analysis through continuous reviews of the ICP-MS operation protocol at GLIER. P.W.U. Appel was the leader of the Nuuk Region Project and through his funding it was possible to conduct field work in Greenland.

Abstract

This study presents new structural observations and high precision major and trace element data for metamorphosed volcanic and sedimentary rocks in the Ivisaartoq (ca. 3075 Ma), Ujarassuit (ca. 3070 Ma), and Storø (2800-2840 Ma) greenstone belts, Nuuk region, southwestern Greenland. The new data are used to investigate postdepositional alteration, petrogenesis of volcanic rocks, provenance of sedimentary rocks, and geodynamic setting.

The Mesoarchean Ivisaartoq belt underwent two stages of calc-silicate alteration. Stage-I alteration appears to have resulted from sea-floor hydrothermal alteration. Stage-II alteration was developed during the regional metamorphism. Both stages of alteration caused mobilization of major elements, large ion lithophile elements (LILE: Rb, Cs, Sr, Ba, Pb), and light rare earth elements (LREE). Heavy rare earth elements (HREE) and high field strength elements (HFSE: Th, Nb, Ta, Zr, Ti) remained relatively immobile during stage-I alteration but were variably disturbed during the stage-II metasomatism. Transition metals (e.g., Ni, V, Co, Cr, and Sc) were immobile during both metasomatic events.

The geochemical characteristics of metavolcanic rocks in the Mesoarchean Ujarassuit and Ivisaartoq greenstone belts suggest that these belts include island arc tholeiites (IAT), andesites, boninites, subduction-related picrites, and normal-mid-ocean ridge basalts (N-MORB). Metasedimentary rocks have low chemical indexes of alteration values (CIA = 46 to 62), enriched LREE patterns, and high contents of transition metals, indicating that they have been derived from poorly weathered felsic to mafic source rocks. Accordingly, the Ujarassuit and Ivisaartoq greenstone belts are interpreted to represent dismembered

fragments of Mesoarchean supra-subduction zone oceanic crust formed either in a forearc or back-arc tectonic setting.

The Neoarchean Storø greenstone exhibit a tectonic contact with the surrounding tonalite-throndjemite-granodite (TTG) gneisses. Metavolcanic rocks in this belt possess near-flat to slightly enriched LREE patterns and pronounced negative Nb-Ta anomalies indicating a subduction zone geochemical signature. Metasedimentary rocks are characterized by low chemical indexes of alteration values (CIA = 50 to 71), high contents of transition metal, and enriched LREE patterns. These characteristics suggest a mixed-provenance consisting of poorly weathered felsic to mafic igneous source rocks. Collectively, the lithogeochemical characteristics of the Storø greenstone belt are consistent with a supra-subduction zone geodynamic setting.

Acknowledgments

I want to thank to my thesis advisors Dr. Ali Polat and Dr. Brian J. Fryer for their funding, excellent guidance, and continuous scientific discussions during this study. This project was funded through contributions of PREA and NSERC grant 250926 to A. Polat, and NSERC grant 83117 to B.J. Fryer. Field worked in SW Greenland was funded by the Bureau of Minerals and Petroleum in Nuuk and the Geological Survey of Denmark and Greenland (GEUS) through a contribution to Dr. P.W.U. Appel. I am especially thankful to Dr. A. Polat for being an excellent mentor and giving me the freedom to be an independent thinker during this study. I was fortunate to team up during field work with Dr. Jeroen A.M. van Gool and Dr. Ole Stecher. I am grateful to them for sharing with me their extensive experience in field geology and for the incisive discussions in which we engaged during the 2005 field season in SW Greenland. Special thanks to Drs. P.W.U. Appel, Johan G. Raith, and Joel E. Gagnon for providing excellent critiques and constructive comments on early versions of my manuscripts. I am indebted with Dr. Ian Samson for instilling the important idea of formulating fundamental questions. His teachings were inspiring. Thanks to Dr. Zhaoping Yang and Mr. J.C. Barrette for their help during the ICP-MS analyses. I also thank all the faculty and staff members in the Department of Earth and Environmental Sciences for their academic and administrative support. During the last 4 years, long discussions with my colleagues Mr. Nelson O. Campos-Alvarez and Dr. Shanmugam J. Pannalal have been fundamental in recognizing potential new directions in Earth Science research. Our coffee breaks have been an excellent opportunity for intellectual growth. My deepest gratitude to my brother Cesar Miguel Ordóñez-Calderón for taking care of my parents in the last 4 years. Without Cesar, my Ph.D. experience would not have been joyful and memorable.

Table of Contents

List of Tables

List of Figures

CHAPTER 1

Introduction

1.1. Background on Archean geodynamics

The Archean eon (ca. 3.8-2.5 Ga) corresponds to approximately 30% of earth history (cf. Van Kranendonk, 2007). Therefore, Archean cratons contain invaluable information on the geological processes in the early Earth. These cratons consist of associations of greenstone belts and tonalite-trondhjemite-granodiorite (TTG) orthogneisses. Metamorphic grade may range from prehnite-pumpellyite facies, through greenschist, to amphibolite facies (Wilkins, 1997). The oldest volcanic and sedimentary rocks on earth are preserved in the Archean greenstone belts. These belts are composed of ultramafic, mafic, intermediate, and felsic volcanic and volcaniclastic rocks. They also include chemical and siliciclastic sedimentary rocks. Volcanic rocks (~80 %) normally occur in greater proportion than the sedimentary counterparts (~20 %) (Condie, 1994). Therefore, any attempt to determine the depositional tectonic setting, or settings, of Archean greenstone belts requires an understanding of the magmatic processes in these belts. The surrounding TTG-gneisses may form the depositional basement of greenstone belts; or alternatively, they may exhibit intrusive or tectonic contacts (Ridley et al., 1997; Bleeker, 2002; Thurston, 2002; Thurston and Ayres, 2004). Accordingly, greenstone belts may be either allochtonous or autochthonous, relative to the adjacent felsic crustal rocks. However, the original structural, stratigraphic, magmatic, and mineralogical characteristics of granite-greenstone terranes are rarely preserved, given strong overprinting by multiple episodes of ductile deformation, metamorphism, plutonism, and hydrothermal alteration.

The diverse lithological and geochemical characteristics of Archean greenstone belt volcanic rocks suggest various magma sources, petrological processes, and geodynamic environments (Eriksson et al., 2004). However, petrological studies of Archean greenstone belts are complicated, because advanced hydrothermal alteration and polyphase metamorphism modify the original geochemical characteristics of volcanic and sedimentary rocks (Gélinas, 1982; Ludden et al., 1982; Gruau et al., 1992; 1996; Polat and Hofmann, 2003; Terabayashi et al., 2003; Weiershäuser and Spooner, 2005). The recognition and characterization of volcanic rocks with near-primary magmatic geochemical signatures and those with altered geochemical patterns is one of the most fundamental problems to be resolved in geochemical studies of Archean greenstone belts.

Structural, geochronological, geochemical, and geophysical investigations have provided evidence, although disputed in some cases, indicating that Archean plate tectonic processes were comparable with those in the Phanerozoic earth (see Cawood et al., 2006). Some of the most significant evidence include: 1) the discovery of Paleoarchean sheeted dykes in the Isua greenstone belt (Furnes et al., 2007); 2) the recognition of Archean eclogites in the Baltic Shield (Volodichev et al., 2004); 3) fragments of Neoarchean (2505 Ma) suprasubduction zone oceanic crust in the North China craton (Kusky et al., 2004; Polat et al., 2006); 4) well recorded, subduction accretion processes and strike-slip fault tectonics in the 2.7 Ga Abitibi and Wawa subprovinces of the Superior Province (Mueller et al., 1996; Polat et al., 1998; Polat and Kerrich, 2001; Daigneault et al., 2002); 5) occurrence of Archean hot subduction zone volcanic rocks including boninites, picrites, adakites, high-Mg andesites, and Nb-enriched basalts (Polat and Kerrich, 2006); and 6) recognition of seismic reflectors extending for approximately 30 km down into the lithospheric mantle, indicating a 2.7 Ga old fossil

subduction zone in the Superior Province (Calvert et al., 1995). In addition, Archean greenstone belts also include well-documented continental rift volcano-sedimentary sequences. Some of those belts occur in the Slave province, Rae province, Dharwar craton, and Baltic shield (see Chardon et al., 1998; Thurston and Kozhevnikov, 2000; Bleeker, 2002; Srivastava et al., 2002; Hartlaub et al., 2004).

Accordingly, greenstone belts may have formed in various tectonic settings including intra-oceanic subduction zones and active continental margins, mid-ocean ridges, oceanic plateaus, and continental rifts (cf. Abbott, 1996; Ohta et al., 1996; Percival, et al., 1997; Polat et al., 1998; Kloppenburg et al., 2001; Polat and Kerrich, 2001; Bleeker, 2002; Nutman et al., 2002; Dostal and Mueller, 2004; Smithies et al., 2004; Thurston and Ayres, 2004). A single greenstone belt may comprise a collage of rock units formed in different tectonic environments, resembling modern subduction-accretion complexes (Percival et al., 1997, Polat and Kerrich 2001; Hickman, 2004). Therefore, there is not a unique tectonic environment applicable to all greenstone belts (Polat and Kerrich, 2006).

Despite the acceptance of Archean plate tectonics by many researchers, Archean geodynamic processes remain controversial (see Hamilton, 1993; 1998; 2003; Eriksson and Catuneanu, 2004; Kerrich and Polat, 2006). Vertical tectonics, as opposed to Phanerozoic-like horizontal tectonics, has been suggested to explain the origin of dome and keel structures that characterize some Archean granite-greenstone terranes (e.g., Chardon et al., 1998; Hamilton, 1998). Vertical tectonics appears to be the result of granitic diapirism, which is driven by convective overturn of a density inverted crustal profile with a lower to middle granitic crust overlain by a hot upper basaltic crust (Rey et al., 2003). In this model, greenstone belts are the products of intra-continental magmatism, similar to continental flood basalts or continental rifts. The regional structure of the East

Pilbara granite-greenstone terrane has been interpreted as a result of vertical tectonics owing to prolonged plume-related magmatism (Hickman, 2004; Van Kranendonk, et al., 2004; Smithies et al., 2007). Some researchers have suggested that both vertical and horizontal tectonic processes operated in the Archean (Van Kranendonk et al., 2004; Lin, 2005; Smithies et al., 2007).

The operation of Phanerozoic-style plate tectonic processes in the Archean implies that Archean greenstone belts with volcanic rocks having intra-oceanic geochemical signatures may be the equivalents of Phanerozoic ophiolite complexes (Dilek and Polat, 2008; Sylvester et al., 1997). However, the existence of Archean ophiolites has been questioned, given the apparent absence of Archean greenstone belts with a complete Penrose-type ophiolite pseudostratigraphy (cf. McCall, 2003). A complete and undeformed Penrose-type ophiolite will display a layer cake pseudostratigraphy consisting of, from bottom to top, tectonized upper mantle, ultramafic to mafic cumulates, mafic sheeted dykes, pillowed and massive basaltic lava flows, and an uppermost layer of sediments (Anonymous, 1972). However, over the last 50 years, comparative studies of Phanerozoic ophiolites and modern ocean floor have revealed more complex and diverse stratigraphic, geochemical, and petrological characteristics (see Dilek, 2003; Kusky, 2004a,b; De Wit, 2004; Dilek and Polat, 2008). These studies have shown that ophiolites may form in diverse geodynamic settings, different from mid-ocean ridges. Therefore, neither Phanerozoic nor Archean ophiolites need to display a typical Penrose-type internal structure (Sylvester et al., 1997; Kusky, 2004b).

Despite the significance of Archean greenstone belts to understanding the evolution of early earth systems, 80% of those belts, worldwide, have not been investigated in detail (see De Wit, 2004). To resolve the above outstanding issues in Archean greenstone belts,

I have investigated the structural and geochemical characteristics of several unstudied Meso- to Neoarchean greenstone belts in the Nuuk Region of southern West Greenland (Fig. 1.1). These include the Ivisaartoq, Ujarassuit, and Storø greenstone belts. Detailed field observations and new high precision major and trace element data are reported for ultramafic to intermediate volcanic rocks, and associated siliciclastic sedimentary rocks, to understand their postmagmatic hydrothermal alteration, petrogenesis, tectonic settings of origin, and sedimentary provenance. This study provides new evidence supporting Phanerozoic-style plate tectonic processes in the Archean, and the existence of dismembered Archean ophiolites formed at suprasubduction zone settings.

1.2. Meso- to Neoarchean greenstone belts of the Nuuk Region, SW Greenland

The Nuuk region of southern West Greenland is part of the Archean North Atlantic craton (Nutman, 1997). The region is formed by associations of Eo- to Neoarchean (3850 to 2800 Ma) TTG-gneisses, greenstone belts, anorthosite-gabbro complexes, and layered and massive ultramafic rocks (Garde, 2003) (Fig. 1.1). Numerous studies have been conducted in the region since the recognition of orthogneisses older than 3600 Ma, and volcanic and sedimentary rocks, in Isua greenstone belt, of approximately 3800 to 3700 Ma in age (McGregor, 1973; Moorbath et al., 1973; Bridgwater et al., 1974; Nutman et al., 1996, 2001, 2004). Detailed structural, geochronological, and geochemical studies have indicated that the Nuuk region comprises a collage of several allochtonous terranes (Fig. 1.1) with different geological history prior to their final juxtaposition (Friend et al. 1987, 1988, 1996; Nutman et al., 1989, 1993, 1996, 2001, 2004, 2007; McGregor et al. 1991; Crowley et al., 2002; Friend and Nutman, 2005). These studies have proposed that the amalgamation of tectono-stratigraphic terranes occurred within a period of approximately

400 Ma, as a result of multiple continent-continent collisions taking place between 2960 to 2600 Ma. Therefore, the Nuuk region appear to be one of the best documented examples of Archean collisional orogenesis (see Nutman and Friend, 2007), and its tectonic evolution is believed to be an analogue of Phanerozoic Alpine-Himalayan and Altaid orogens (cf. Coney et al., 1980; Şengör, 1990; Şengör and Natal'in, 2004).

The tectono-stratigraphic terrane model proposed for the Nuuk region predicts the development of intra-oceanic and intra-continental subduction zones, and obduction of oceanic terranes such as oceanic plateaus, mid-ocean ridges, and island arcs. Consequently, the Ivisaartoq, Ujarassuit, and Storø greenstone belts may represent remnants of Archean oceanic crust, juxtaposed with felsic crust during collisional orogenesis (Fig. 1.1). Therefore, these greenstone belts could be the Archean equivalents of fragments of Phanerozoic ophiolites (cf. Şengör, 1990; De Wit, 2004; Şengör and Natal'in, 2004; Dilek and Polat, 2008). Or alternatively, they may represent continental rift and continental flood basalts, deformed and metamorphosed during collisional orogenesis.

The Eoarchean Isua greenstone belt comprises ultramafic to mafic volcanic rocks with geochemical characteristics that are consistent with an intra-oceanic subduction zone setting (Polat et al., 2003; 2004). In the Akia terrane (Fig. 1.1), the Mesoarchean Qussuk greenstone belt has been interpreted to represent a relict island arc build on basaltic oceanic crust (Garde, 2007). Thus, the structural and geochemical characteristics of Isua and Qussuk greenstone belts are consistent with the collisional model proposed for the Nuuk region. However, this interpretation cannot be extended to other unstudied Meso- to Neoarchean greenstone belts in the area (Fig. 1.1).

Despite the recent advances in understanding the geological evolution of the Nuuk region, several problems remain to be resolved: 1) the first-order structural and geochemical characteristics of the majority of greenstone belts have not been studied in detail; 2) the geodynamic setting of these belts is not known; and 3) their magmatic and postmagmatic evolution is not well understood. To resolve these problems, in this thesis I have studied the results of a detailed field and geochemical investigation of the Mesoarchean Ujarassuit and Ivisaartoq greenstone belts, and the Neoarchean Storø greenstone belt (Fig. 1.1). These belts were chosen given that they belong to the central Nuuk region where the tectonic terrane model has been best investigated (Fig. 1.1), and because they are part of different tectono-stratigraphic terranes. Therefore, these greenstone belts are key elements in testing the current geological models for the region, and also provide an excellent opportunity to understand Archean geodynamic processes.

1.3. Objectives

There are several fundamental questions regarding on the origin of the Meso- to Neoarchean greenstone belts in the Nuuk region:

1) Are greenstone belts in the Nuuk Region the product of intra-oceanic or intra-continental magmatism?
2) Are volcanic rocks in these belts comparable with those erupted in Phanerozoic volcanic arcs, oceanic plateaus, mid-ocean ridges, continental rifts, or continental flood basalts?
3) What are the effects of high-grade metamorphism and postmagmatic alteration on the original magmatic geochemical signatures?

4) What are the characteristics of the Archean mantle source for ultramafic to mafic rocks in the belts?
5) Do these belts represent relict Archean oceanic crust?
6) How different is the Archean volcanism recorded in these greenstone belts from modern volcanism?
7) Are siliciclastic sedimentary rocks contained in these belts derived from older continental rocks or juvenile volcanic-plutonic rocks?
8) What are the implications of these greenstone belts for the geological evolution of the Nuuk region and Archean geodynamics?

To resolve these questions and to test terrane accretion and crustal evolution models in the Nuuk region, the following objectives were proposed in this study:

1) To study the structural characteristics of greenstone belts in the Nuuk region.
2) To analyze volcanic and sedimentary rocks for their rare earth elements (REE), high field strength elements (HFSE), large ion lithophile elements (LILE), and transition metal concentrations.
3) To investigate the effects of postmagmatic alteration on the near-primary geochemical characteristics of these rocks.
4) To understand the petrologic evolution of individual volcanic associations.
5) To asses the role of crustal contamination.
6) To characterize the tectonic setting or settings.
7) To investigate the provenance for siliciclastic sedimentary rocks in these belts.
8) To compare the geochemical and structural characteristics of greenstone belts in the study area with other greenstones in the area and worldwide.

1.4. Outline of thesis structure

This thesis consists of 5 chapters. Chapter 1 is the introduction for the thesis and Chapter 5 presents a summary of this study. Chapters 2 to 4 are a collection of three manuscripts published and submitted to peer reviewed scientific journals.

A version of Chapter 2 was published as a research article in Precambrian Research. This chapter investigates in detail the postmagmatic geochemical changes experienced by mafic and ultramafic volcanic rocks, in the Ivisaartoq greenstone belt, during multistage hydrothermal alteration. Through detailed field work and petrographic observations, at least two stages of calc-silicate metasomatism were identified. Stage-I metasomatic alteration occurred during sea floor hydrothermal alteration, whereas stage-II alteration occurred during regional prograde metamorphism at upper amphibolite facies conditions. High precision major and trace element geochemistry of 40 samples including altered and unaltered mafic to ultramafic rocks were analyzed to understand the cumulative effects of prolonged alteration on the primary magmatic geochemical signatures.

A version of Chapter 3 has been submitted to be considered for publication in a Lithos special issue on "Mantle dynamics and crust-mantle interactions in collisional orogens". This chapter discusses the structural and geochemical evolution of the Ujarassuit and Ivisaartoq greenstone belts. Structural observations indicate at least three phases of ductile deformation at upper amphibolite facies metamorphic conditions. High precision major and trace element data are reported for 34 samples of volcanic rocks to understand their postmagmatic geochemical changes, petrogenesis, mantle source characteristics, and geodynamic setting of origin. In addition, 13 samples of sedimentary rocks were also analyzed for their geochemistry in order to understand the weathering

history of source rocks, their provenance, and to provide additional constraints on the geodynamic setting of Ujarassuit and Ivisaartoq greenstone belts.

A version of Chapter 4 has been submitted to Precambrian Research. This chapter discusses the field and geochemical characteristics of volcanic and sedimentary rocks in the Storø greenstone belt. A comprehensive analysis of postmagmatic alteration, petrogenesis, mantle source characteristics, and sediment provenance is integrated into a model to explain the geodynamic setting of origin of this belt. In addition, the field observations and geochemical data of supracrustal rocks in the Storø greenstone belt are compared with those of the Qussuk, Ujarassuit, and Ivisaartoq greenstone belts (Fig. 1.1).

1.5. References

Anonymous, 1972. Penrose field conference on ophiolites. Geotimes 17, 24-25.

Abbott, D.H., 1996. Plumes and hotspots as sources of greenstone belts. Lithos 37,113-127.

Bickle, M.J., Nisbet, E.G., Martin, A., 1994. Archean greenstone belts are not oceanic crust. Journal of Geology 102, 121-138.

Bleeker, W., 2002. Archean tectonics, a review, with illustrations from the Slave craton. In: Fowler, C.M.R., Ebinger, C.J., Hawkesworth, C.J. (Eds.). The Early Earth: Physical, Chemical and Biological Development. Geological Society of London Special Publications 199, 151-181.

Bridgwater, D., McGregor, V.R., Myers, J.S., 1974. A horizontal tectonic regime in the Archean of Greenland and its implications for early crustal thickening. Precambrian Research 1, 179-197.

Calvert, A.J., Sawyer, E.W., Davis, W.J., Luden, J.N., 1995. Archean subduction inferred from seismic images of a mantle suture in the Superior Province. Nature 375, 670-674.

Cawood, P.A., Kröner, A., Pisarevsky, S., 2006. Precambrian plate tectonics: Criteria and evidence. GSA Today 16, 4-11.

Chardon, D., Choukroune, P., Jayananda, M., 1998. Sinking of the Dharwar basin (South India): implications for Archaean tectonics. Precambrian Research 91, 15-39.

Condie, K.C., 1994. Greenstones through time. In: Condie, K.C., (Ed.). Archean Crustal Evolution. Developments in Precambrian Geology 11, 85-120.

Coney, P.J., Jones, D.L., Monger, J.W.H., 1980. Cordilleran suspect terranes. Nature 288, 329-333.

Crowley, J.L., Myers, J.S., Dunning, G.R., 2002. Timing and nature of multiple 3700-3600 Ma tectonic events in intrusive rocks north of the Isua greenstone belt, southern West Greenland. Geological Society of America Bulletin 114 (10), 1311-1325.

Daigneault, R., Mueller, W.U., Chown, E.H., 2002. Oblique Archean subduction: accretion and exhumation of an oceanic arc during dextral transpression, southern volcanic zone, Abitibi Subprovince Canada. Precambrian Research 115, 261-290.

De Wit, M.J., 2004. Archean greenstone belts do contain fragments of ophiolites. In: Kusky, T.M., (Ed.). Precambrian ophiolites and related rocks. Developments in Precambrian Geology 13, 599-614.

Dostal, J., Mueller, W.U., 2004. Komatiite geochemistry. In: Eriksson, P.G., Altermann, W., Nelson, D.R., Müeller, W.U., Catuneanu, O., (Eds.). The Precambrian Earth: Tempos and Events. Developments in Precambrian Geology 12, 290-298.

Dilek, Y., 2003. Ophiolite concept and its evolution. In: Dilek, Y., Newcomb, S., (Eds.). Ophiolite concept and the evolution of geological thought. Geological Society of America Special Paper 373, 1-16.

Dilek, Y., Polat, A., 2008. Suprasubduction zone ophiolites and Archean tectonics. Geology 36, 431-432.

Eriksson, P.G., Catuneanu, O., 2004. A commentary on Precambrian plate tectonics. In: Eriksson, P.G., Altermann, W., Nelson, D.R., Müeller, W.U., Catuneanu, O., (Eds.). The Precambrian Earth: Tempos and Events. Developments in Precambrian Geology 12, 201-213.

Eriksson, P.G., Catuneanu, O., Nelson, D.R., Mueller, W.U., Alterman, W., 2004. Towards a synthesis. In: Eriksson, P.G., Altermann, W., Nelson, D.R., Müeller, W.U., Catuneanu, O., (Eds.). The Precambrian Earth: Tempos and Events. Developments in Precambrian Geology 12, 739-769.

Friend, C.R.L., Nutman, A.P., 2005. New pieces of the Archaean terrane jigsaw puzzle in the Nuuk Region, southern West Greenland: Steps in transforming a simple insight into a complex regional tectonothermal model. Journal of the Geological Society of London 162, 147-162.

Friend, C.R.L., Nutman, A.P., Baadsgaard, H., Kinny, P.D., McGregor, V.R., 1996. Timing of late Archean terrane assembly, crustal thickening and granite emplacement in the Nuuk region, southern West Greenland. Earth and Planetary Science Letters 142, 353-365.

Friend, C.R.L., Nutman, A.P., McGregor, V.R., 1987. Late-Archaean tectonics in the Færingehavn-Tre Brødre area, south of Buksefjorden, southern West Greenland. Journal of the Geological Society of London 144, 369-376.

Friend, C.R.L., Nutman, A.P., McGregor, V.R., 1988. Late Archean terrane accretion in the Godthåb region, southern West Greenland. Nature 335, 535-538.

Furnes, H., De Wit, M., Staudigel, H., Rosing, M., Muehlenbachs, K., 2007. A Vestige of Earth's Oldest Ophiolite. Science 315, 1704-1707.

Garde, A.A., 2003. An overview of the Archaean evolution of the Nuuk region: From long-lived evolution of a sea of gneisses to episodic accretion of small continental terranes along boundary structures. In: Appel, P.W.U., Garde, A.A., Jørgensen, M.S., Moberg, E., Rasmussen, T.M., Schjøth, F., Steenfelt, A., (Eds.). Preliminary evaluation of the economic potential of the greenstone belts in the Nuuk Region: General geology and evaluation of compiled geophysical, geochemical and ore geological data. Denmark Og Grønlands Geologiske Undersøgelse Rapport 2003/94, 19-44.

Garde, A.A., 2007. A mid-Archean island arc complex in the eastern Akia terrane, Godthåbsfjord, southern West Greenland. Journal of the Geological Society of London 164, 565-579.

Gélinas, L., Mellinger, M., Trudel, P., 1982. Archean mafic metavolcanics from the Rouyn-Noranda district, Abitibi Greenstone Belt, Quebec. 1. Mobility of the major elements. Canadian Journal of Earth Sciences 19, 2258-2275.

Gruau, G., Rosing, M., Bridgwater, D., Gill, R.C.O., 1996. Resetting of Sm-Nd systematics during metamorphism of >3.7-Ga rocks: implications for isotopic models of early Earth differentiation. Chemical Geology 133, 225-240.

Gruau, G., Tourpin, S., Fourcade, S., Blais S., 1992. Loss of isotopic (Nd, O) and chemical (REE) memory during metamorphism of komatiites: New evidence from eastern Finland. Contributions to Mineralogy and Petrology 112, 66-82.

Hamilton, W.B., 1993. Evolution of the Archean mantle and crust. In: The geology of North America. C-2, 597-614.

Hamilton, W.B., 1998. Archean magmatism and deformation were not products of plate tectonics. Precambrian Research 91, 143-179.

Hamilton, W.B., 2003. An alternative earth. GSA Today 13 (11), 4-12.

Hartlaub, R.P., Heaman, L.M., Ashton, K.E., Chacko, T., 2004. The Archean Murmac Bay Group: evidence for a giant Archean rift in the Rae Province, Canada. Precambrian Research 131, 345-372.

Hickman, A.H., 2004. Two contrasting granite-greenstone terranes in the Pilbara Craton, Australia: Evidence for vertical and horizontal tectonic regimes prior to 2900 Ma. Precambrian Research 131, 153-172.

Kerrich, R., Polat, A., 2006. Archean greenstone-tonalite duality: Thermochemical mantle convection models or plate tectonics in the early Earth global dynamics? Tectonophysics 415, 141-165.

Kloppenburg, A., White, S.H., Zegers, T.E., 2001. Structural evolution of the Warrawoona greenstone belt and adjoining granitoid complexes, Pilbara craton, Australia: Implications for Archean tectonic processes. Precambrian Research 112, 107-147.

Kusky, T.M., 2004a. Epilogue: What if anything have we learned about Precambrian ophiolites and early earth processes? In: Kusky, T.M., (Ed.). Precambrian ophiolites and related rocks. Developments in Precambrian Geology 13, 727-737.

Kusky, T.M., 2004b. Introduction. In: Kusky, T.M., (Ed.). Precambrian ophiolites and related rocks. Developments in Precambrian Geology 13, 1-34.

Kusky, T.M., Li, J., Glass, A., Huang, X.N., 2004. Origin and emplacement of Archean ophiolites of the central orogenic belt, North China craton. In: Kusky, T.M., (Ed.). Precambrian ophiolites and related rocks. Developments in Precambrian Geology 13, 223-274.

Lin, S., 2005. Synchronous vertical and horizontal tectonism in the Neoarchean: Kinematic evidence from a synclinal keel in the northwestern Superior craton, Canada. Precambrian Research 139, 181-194.

Ludden, J. N., Gelinas, L., Trudel, P., 1982. Archean metavolcanics from the Rouyn-Noranda district, Abitibi greenstone belt, Quebec. 2. Mobility of trace elements and petrogenetic constraints. Canadian Journal of Earth Sciences 19, 2276-2287.

McCall, G.J.H., 2003. A critique of the analogy between Archaean and Phanerozoic tectonics on regional mapping of the Mesozoic-Cenozoic plate convergent zone in the Makran, Iran. Precambrian Research 127, 5-17.

McGregor, V.R., 1973. The early Precambrian gneisses of the Godthåb district, West Greenland. Phil. Trans. R. Soc. London A. 273, 343-358.

McGregor, V.R., Friend, C.R.L., Nutman, A.P., 1991. The late Archaean mobile belt through Godthåbsfjord, southern West Greenland: a continental collision zone? Bulletin of the Geological Society of Denmark 39, 179-197.

Moorbath, S., O'Nions, R.K., Pankhurst, R.J., 1973. Early Archaean age for the Isua iron formation, West Greenland. Nature 245, 138-139.

Mueller, W.U., Daigneault, R., Mortensen, J.K., Chown, E.H., 1996. Archean terrane docking: upper crust collision tectonics, Abitibi greenstone belt, Quebec, Canada. Tectonophysics 265, 127-150.

Nutman, A.P., 1997. The Greenland sector of the North Atlantic Craton. In: De Wit, M., Ashwal, L.D., (Eds.). Greenstone belts. Oxford Monographs on Geology and Geophysics 35, 665-674.

Nutman, A.P., Friend, C.R.L., 2007. Adjacent terranes with ca. 2715 and 2650 Ma high-pressure metamorphic assemblages in the Nuuk region of the North Atlantic Craton, southern West Greenland: Complexities of Neoarchaean collisional orogeny. Precambrian Research 155, 159-203.

Nutman, A.P., Friend, C.R.L., Baadsgaard, H., McGregor, V.R., 1989. Evolution and assembly of Archean gneiss terranes in the Godthåbsfjord region, southern West Greenland: Structural, metamorphic, and isotopic evidence. Tectonics 8 (3), 573-589.

Nutman, A.P., Friend, C.R.L., Barker, S.L.L., McGregor, V.R., 2004. Inventory and assessment of Palaeoarchaean gneiss terrains and detrital zircons in southern West Greenland. Precambrian Research 135, 281-314.

Nutman, A.P., Friend, C.R.L., Benett, V.C., 2001. Review of the oldest (4400-3600 Ma) geological and mineralogical record: Glimpses of the beginning. Episodes 24 (2), 1-9.

Nutman, A.P., Friend, C.R.L., Benett, V.C., 2002. Evidence for 3650-3600 Ma assembly of the northern end of the Itsaq Gneiss Complex, Greenland: Implications for early Archean tectonics. Tectonics DOI: 10.1029/2000TC001203.

Nutman, A.P., Friend, C.R.L., Horie, K., Hidaka, H., 2007. The Itsaq gneiss complex of southern West Greenland and the construction of Eoarchaean crust at convergent plate boundaries. In: Van Kranendonk, M.J., Smithies, R.H., Bennett, V.C., (Eds.). Earth's oldest rocks. Developments in Precambrian Geology 15, 187-218.

Nutman, A.P., Friend, C.R.L., Kinny, P.D., McGregor, V.R., 1993. Anatomy of an early Archean gneiss complex: 3900 to 3600 Ma crustal evolution in southern West Greenland. Geology 21, 415-418.

Nutman, A.P., McGregor, V.R., Friend, C.R.L., Benett, V.C., Kinny, P.D., 1996. The Itsaq Gneiss Complex of southern West Greenland; the world's most extensive record of early crustal evolution (3900-3600 Ma). Precambrian Research 78, 1-39.

Ohta, H., Maruyama, S., Takahashi, E., Watanabe, Y., Kato, Y., 1996. Field occurrence, geochemistry and petrogenesis of the Archean Mid-Ocean Ridge Basalts (AMORBs) of the Cleaverville area, Pilbara Craton, Western Australia. Lithos 37, 199-221.

Percival, J.A., Roering, C., van Reenen, D.D., Smit, C.A., 1997. Tectonic evolution of Associated Greenstone Belts and High-Grade Terrains. In: De Wit, M., Ashwal, L.D., (Eds.). Greenstone Belts. Oxford Monographs on Geology and Geophysics 35, 398-420.

Polat, A., Herzberg, C., Münker, C., Rodgers, R., Kusky, T., Li, J., Fryer, B., and Delaney, J., 2006. Geochemical and petrological evidence for a supra-subduction zone origin of Neoarchean (ca. 2.5 Ga) peridotites, central orogenic belt, North China craton. Geological Society of America Bulletin 118, 771-784.

Polat, A., Hofmann, A.W., 2003. Alteration and geochemical patterns in the 3.7-3.8 Ga, Isua greenstone belt, West Greenland. Precambrian Research 126, 197-218.

Polat, A., Hofmann, A.W., Appel, P.W.U., 2004. Geochemical diversity in volcanic rocks of the > 3.7 Ga Isua Greenstone Belt, southern west Greenland: implications for mantle composition and geodynamic processes. In: Eriksson, P.G., Altermann, W., Nelson, D.R., Müeller, W.U., Catuneanu, O., (Eds.). The Precambrian Earth: Tempos and Events. Developments in Precambrian Geology 12, 74-88.

Polat, A., Hofmann, A.W., Rosing, M.T., 2002. Boninite like volcanic rocks in the 3.7-3.8 Ga Isua greenstone belt, West Greenland: geochemical evidence for intra-oceanic subduction zone processes in the early Earth. Chemical Geology 184, 231-254.

Polat, A., Kerrich, R., 2001. Geodynamic processes, continental growth, and mantle evolution recorded in late Archean greenstone belts of the southern Superior Province, Canada. Precambrian Research 112, 5-25.

Polat, A., Kerrich, R., 2006. Reading the geochemical fingerprints of Archean hot subduction volcanic rocks: Evidence for accretion and crustal recycling in a mobile tectonic regime. In: Benn, K., Mareschal, J-C., Condie, K.C., (Eds.). Archean geodynamics and environments. American Geophysical Union Geophysical Monograph 164, 189-213.

Polat, A., Kerrich, R., Wyman, D.A., 1998. The late Archean Schreiber-Hemlo and White River-Dayohessarah greenstone belts, Superior Province: collages of oceanic plateaus, oceanic arcs, and subduction-accretion complexes. Tectonophysics 289, 295-326.

Rey, P.F., Philippot, P., Thébaud, N., 2003. Contribution of mantle plumes, crustal thickening and greenstone blanketing to the 2.75-2.65 Ga global crisis. Precambrian Research 127, 43-60.

Ridley, J.R., Vearncombe, J.R., Jelsma, H.A., 1997. Relations between Greenstone Belts and Associated Granitoids. In: de Wit, M., Ashwal, L.D., (Eds.). Greenstone Belts. Oxford Monographs on Geology and Geophysics 35, 376-397.

Şengör, A.M.C., 1990. Plate tectonics and orogenic research after 25 years: A Tethyan perspective. Earth Science Reviews 27, 1-201.

Şengör, A.M.C., Natal'in, B.A., 2004. Phanerozoic analogues of Archean oceanic basement fragments: Altaid ophiolites and ophirags. In: Kusky, T.M., (Ed.).

Precambrian ophiolites and related rocks. Developments in Precambrian Geology, Elsevier 13, 675-726.

Smithies, R.H., Champion, D.C., Sun, S., 2004. The case for Archean boninites. Contributions to Mineralogy and Petrology 147, 705-721.

Smithies, R.H., Van Kranendonk, M.J., Champion, D.C., 2007. The Mesoarchean emergence of modern-style subduction. Gondwana Research 11, 50-68.

Srivastava, R.K., Singh, R.K., Verma, S.P., 2002. Neoarchaean mafic volcanic rocks from the southern Bastar greenstone belt, Central India: Petrological and tectonic significance. Precambrian Research 131, 305-322.

Sylvester, P.J., Harper, G.D., Byerly, R.G., Thurston, P.C., 1997. Volcanic aspects. In: De Wit, M., Ashwal, L.D., (Eds.). Greenstone Belts. Oxford Monographs on Geology and Geophysics 35, 55-90.

Terabayashi, M., Masada, Y., Ozawa, H., 2003. Archean ocean-floor metamorphism in the North Pole area, Pilbara Craton, Western Australia. Precambrian Research 127, 167-180.

Thurston, P.C., 2002. Autochthonous development of Superior Province greenstone belts? Precambrian Research 115, 11-36.

Thurston, P.C., Ayres, L.D., 2004. Archean and Proterozoic Greenstone Belts: Setting and evolution. In: Eriksson, P.G., Altermann, W., Nelson, D.R., Müeller, W.U., Catuneanu, O., (Eds.). The Precambrian Earth: Tempos and Events. Developments in Precambrian Geology 12, 311-333.

Thurston, P.C., Kozhevnikov, V.N., 2000. An Archean quartz arenite-andesite association in the eastern Baltic Shield, Russia: implications for assemblage types and shield history. Precambrian Research 101, 313-340.

Van Kranendonk, M.J., Collins, W.J., Hickman, A., Pawley, M.J., 2004. Critical tests of vertical vs. horizontal tectonic models for the Archean East Pilbara Granite-Greenstone Terrane, Pilbara Craton, Western Australia. Precambrian Research 131, 173-211.

Van Kranendonk, M.J., 2007. Tectonics of early earth. In: Van Kranendonk, M.J., Smithies, R.H., Bennett, V.C., (Eds.). Earth's oldest rocks. Developments in Precambrian Geology 15, 1105-1116.

Volodichev, O.I., Slabunov, A.I., Bibikova, E.V., Konilov, A.N., Kuzenko, T.I., 2004. Archean eclogites in the Belomorian mobile belt, Baltic Shield. Petrology 12, 540-560.

Weiershäuser, L., Spooner, E.T.C., 2005. Seafloor hydrothermal fluids, Ben Nevis area, Abitibi greenstone belt; implications for Archean (approximately 2.7 Ga) seawater properties. Precambrian Research 138, 89-123.

Wilkins, C., 1997. Regional and Contact Metamorphism. In: De Wit, M., Ashwal, L.D., (Eds.). Greenstone Belts. Oxford Monographs on Geology and Geophysics 35, 126-163.

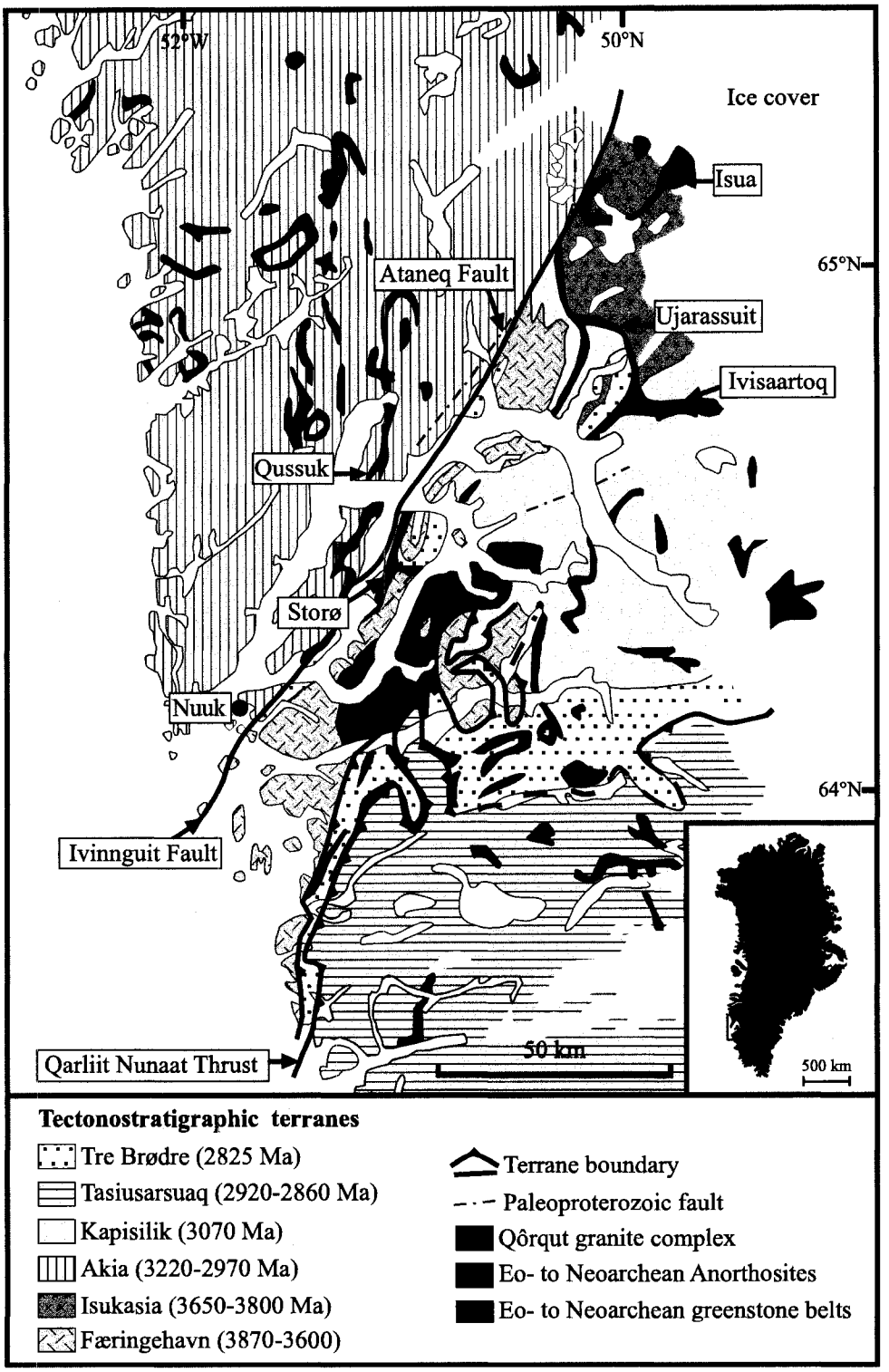

Figure 1.1. Geological map showing the Eo- to Neoarchean tectonostratigraphic terranes of the Nuuk Region. Also indicated are the locations of Isua, Ujarassuit, Ivisaartoq, Qussuk, and Storø greenstone belts. The map is adapted from Friend and Nutman (2005), and Nutman and Friend (2007).

CHAPTER 2

Evidence for HFSE and REE mobility during calc-silicate metasomatism, Mesoarchean (~3075 Ma) Ivisaartoq greenstone belt, southern West Greenland

2.1. Introduction

Many Archean greenstone belts display geochemical and petrographic evidence for post-magmatic alteration resulting from fluid-rock interaction during sea-floor, regional, and contact metamorphism (Fryer et al., 1979; Gruau et al., 1992; 1996; Lahaye et al., 1995; Polat et al., 2003; Terabayashi et al., 2003; Weiershäuser and Spooner, 2005). Alteration processes in the Archean appear to have significantly modified the primary igneous textures and geochemical signatures of greenstone belts. Post-depositional alteration generally results in the mobility of most major elements and LILE (e.g., K, Sr, Rb, Cs, Ba, Pb), whereas the abundances of the REE (La-Lu), HFSE (e.g., Zr, Hf, Nb, Ta, Ti, Y), and transition metals (e.g., Ni, Cr, Co, V, Sc) are not significantly changed (Gélinas et al., 1982; Ludden et al., 1982; Middelburg et al., 1988; Polat and Hofmann, 2003). Therefore, most Archean metavolcanic rocks appear to have preserved only near-primary REE, HFSE, and transition metal geochemical compositions.

Systematic investigation of chemical changes occurring at different stages of post-magmatic alteration is important to understand the origin and geodynamic evolution of Archean greenstone belts. However, resolving post-magmatic alteration events is sometimes hindered by multiple episodes of deformation, metamorphism, and plutonism that invariably affected greenstone belts.

Despite amphibolite facies metamorphism and polyphase deformation (Hall and Friend, 1979; Chadwick, 1985, 1990; Friend and Nutman, 2005), the Ivisaartoq belt

exhibits well preserved field relationships allowing the recognition of at least two successive stages of calc-silicate metasomatism. An early metasomatic event (stage-I) occurred during sea-floor hydrothermal alteration and was followed by intense metasomatism (stage-II) coeval with the regional dynamothermal metamorphism (Polat et al., 2007). The stage-I metasomatism is best recorded in pillow cores and rims, displaying a metasomatic zonation decreasing in intensity towards the pillow rims. The stage-II calc-silicate metasomatism is best recorded in concordant to discordant boudinaged calc-silicate layers preferentially located along shear zones.

The occurrence of non-metasomatized versus concentrically zoned pillow basalts, and their highly deformed counterparts (mafic amphibolites) variably affected by the stage-II calc-silicate alteration provides a unique opportunity to evaluate the geochemical effects associated with the different stages of post-magmatic alteration. The effects of the stage-I metasomatism on the primary geochemical characteristics of mafic and ultramafic rocks of the Ivisaartoq belt were investigated by Polat et al. (2007a). However, the geochemical changes resulting from the subsequent stage-II metasomatism and its effects on the near-primary magmatic composition of Ivisaartoq volcanic rocks are unknown. Accordingly, we present new field, petrographic, and geochemical data from the second stage metasomatic rocks and associated mafic and ultramafic amphibolites to understand the chemical and mineralogical changes that occurred during this alteration event. We report new, high precision major and trace element data for a total of 40 samples (25 amphibolites, and 15 calc-silicate rocks) to asses the effects of stage-II metasomatism on element mobility. The data presented in this study provide new insights into the geochemical effects of post-magmatic alteration on mafic to ultramafic rocks of the

Ivisaartoq greenstone belt and their implications on the petrogenetic and geodynamic evolution of the belt.

2.2. Regional geology and field characteristics

The Ivisaartoq greenstone belt is one of the largest and best preserved Archean greenstone belts in the Nuuk region, SW Greenland (Fig. 2.1). This belt forms an asymmetric syncline approximately 30 km long and 1 to 5 km wide. Structural and geochronological studies have shown that the Nuuk region is formed by several tectono-stratigraphic terranes ranging in age from 2860 to 3870 Ma (Friend et al., 1987, 1988, 1996; Nutman et al. 1989, 1993; Friend and Nutman, 2005; Garde, 2007). The Ivisaartoq belt is located within the *ca.* 3075-2960 Ma Kapisilik terrane and has an average U-Pb zircon age of ~3075 Ma (Friend and Nutman, 2005; Polat et al., 2007). The minimum age of the belt is indicated by 2963±12 Ma old granites intruding the belt (Friend and Nutman, 2005).

The Ivisaartoq belt is composed primarily of mafic and ultramafic amphibolites with minor intercalations of paragneisses, pelitic schists, quartzites, and ultramafic schists with relict olivine (Fig. 2.2). These rocks are the result of intense deformation and amphibolite-facies metamorphism of basalts, picrites, gabbros, diorites, siliciclastic sedimentary rocks, sulphide-bearing siliceous volcaniclastic (?) rocks, and ultramafic cumulates (Hall, 1980; Brewer et al., 1984; Chadwick, 1985, 1986; 1990; Polat et al., 2007). Despite deformation and metamorphism, primary magmatic features such as pillow flows, concentric cooling-cracks and drainage cavities in pillows (Fig. 2.3a-b), volcanic breccia, ocelli structures in basalts, magmatic layering, and cumulate textures are well preserved in low-strain zones.

Chadwick (1990) subdivided the belt into upper and lower amphibolite groups (Fig. 2.2). Primary magmatic features are well preserved in the upper group. In contrast, the lower group is more deformed, and most of the primary magmatic features have been obliterated. These lithotectonic groups are bounded by an ENE-trending alteration zone approximately 50 m thick and ~10 km long. A nearly continuous thin (~10 m thick) sheet of magnetite-rich ultramafic amphibolite, called the magnetic marker, occurs within this zone and has been used as a lithologic marker separating the upper and lower groups (Chadwick, 1985, 1990). Deformation in mafic and ultramafic rocks of the upper amphibolite group increases towards the magnetic marker. Therefore, mafic and ultramafic amphibolites around the contact zone are the highly strained counterparts of the less-deformed basaltic and picritic pillowed lavas occurring higher up in the sequence. These structural characteristics suggest that major deformation was accommodated at the contact between the lower and the upper groups. This zone has been interpreted as a tectonic contact (Polat et al., 2007).

The stage-I calc-silicate alteration overprints mineral assemblages in pillow cores, pillow interstitials, and contacts between pillows and gabbros (Fig. 2.3a-b). This alteration is well exposed in the upper amphibolite group. Metasomatized pillow basalts exhibit concentric structure with distinct mineralogical and chemical composition (Fig. 2.3a-b). From core to rim these include (1) empty or quartz-filled drainage cavities, (2) calc-silicate rich (diopside ± epidote ± scapolite) inner pillow cores, (3) calc-silicate free outer pillow cores, and (4) amphibole-rich pillow rims (metamorphosed chilled margins). Outer pillow cores preserve near-primary basaltic composition (Polat et al., 2007). This concentric mineralogical and chemical zonation (Fig. 2.3b) appears to have resulted from circulation of hydrothermal fluids through drainage cavities during the early stage of sea-

floor alteration predating the regional metamorphism and deformation (Appel, 1994, 1997; Raith et al., 2006; Polat et al., 2007).

The stage-II calc-silicate rocks exhibit mineral assemblages indicating prograde (assemblages IIa, IIb) to retrograde (assemblage IIc) metamorphic conditions (Table 2.1). Prograde calc-silicates occur as centimeter- to meter-scale boudinaged layers and are concordant to the regional foliation (Fig. 2.3c-d). They contain relict enclaves of amphibolites up to 1 m long and 0.5 m wide (Fig. 2.3d). Retrograde calc-silicates occur as brittle veins crosscutting the regional foliation and as patchy alterations overprinting the prograde assemblages (Fig. 2.3e-f). The stage-II calc-silicate rocks are associated with shear zones and are dominant along the contact between the upper and lower amphibolite groups in the vicinity of the magnetic marker (Fig. 2.2).

2.3. Petrography

Mafic amphibolites are composed of hornblende (60-80%) + plagioclase (5-20%) + quartz (5-20%) + titanite (0-2%) ± Fe-Ti oxides (0-5%) ± apatite (< 1%) (Fig. 2.4a). Biotite and fibrolitic actinolite and tremolite locally replace hornblende. In some locations amphibole is replaced by epidote and diopside. These calc-silicate minerals occur as disseminations and as thin layers (1-5 mm) concordant to the prevalent foliation. Amphibolites with mylonitic fabrics are locally present. They contain hornblende porphyroclasts with undulose extinction, subgrains, and kink folding (Fig. 2.4b-c).

Ultramafic amphibolites are composed primarily of actinolite, with minor tremolite and hornblende (<10%) (Fig. 2.4d). Actinolite and tremolite form aggregates with preferential orientation. Some ultramafic amphibolites are partially to completely replaced by chlorite. Calcite and biotite are occasionally associated with this alteration.

Mylonitic fabrics similar to those displayed by the mafic amphibolites are also present in ultramafic amphibolites.

Detailed petrographic description of stage-I calc-silicates are given in Polat et al. (2007). The stage-II calc-silicate rocks are of stratabound appearance, replacing the mafic and ultramafic amphibolites, and gabbroic dykes (Fig. 2.3c-f). They are composed of diopside (10-80%) + epidote (30-85%) + quartz (1-20%) + plagioclase (0-5%) ± garnet (0-5%) ± Fe-Ti oxides (< 1%) ± titanite (< 1%) ± calcite (< 1%) (Table 2.1, Fig. 2.5a-f). Scheelite and vesuvianite have been documented by Appel (1983, 1994, 1997).

The stage-II calc-silicates include two phases of prograde (assemblages IIa, IIb) and one phase of retrograde (assemblage IIc) metamorphism (Table 2.1). The prograde metasomatic assemblage IIa is characterized by fine-grained aggregates of epidote + clinozoisite + clinopyroxene + quartz + plagioclase + titanite ± apatite (Fig. 2.5a). Clinopyroxene is rich in diopside component (Polat et al., 2007). This assemblage is the most abundant and occurs as concordant (relative to the regional foliation) boudinaged layers replacing the mafic and ultramafic amphibolites.

The prograde metasomatic assemblage IIb consists of coarse-grained clinopyroxene (second generation) and garnet (Fig. 2.5b). Garnet is composed of grossular-andradite, and clinopyroxene is dominated by diopside (Polat et al., 2007). The assemblage IIb replaces the epidote-rich metasomatic assemblage IIa. Diopside and garnet have smooth contacts indicating growth at equilibrium conditions. Diopside also forms massive pods of coarse-grained (up to 4 cm) crystals overprinting the metasomatic assemblage IIa.

The retrograde metasomatic assemblage IIc consists predominantly of epidote (second generation) with minor quartz, amphibole, and calcite. This assemblage occurs as patchy alterations and brittle veins (Table 2.1). Coarse-grained patchy epidote overprints

earlier assemblages (IIa and IIb) and contains relict skeletal inclusions of garnet, diopside, and idioblastic titanite (Fig. 2.5c). This assemblage shows cataclastic texture with angular porphyroclasts of diopside, quartz, and plagioclase (assemblages IIa and IIb) cemented by a groundmass of late epidote, clinozoisite, and minor calcite (Fig. 2.5d). Tremolite is locally associated with this assemblage and mantles diopside. Epidote veins are highly discordant and crosscut amphibolites, stage-I calc-silicates, and calc-silicate assemblages IIa and IIb. Fine veinlets (< 0.5 mm) of epidote and rare calcite crosscut the prograde assemblages (Fig. 2.5e-f).

2.4. Analytical methods and data presentation

Samples were pulverized using an agate mill in the Department of Earth and Environmental Sciences of the University of Windsor, Canada. Major elements and some trace elements (Sc and Zr) were analyzed on a Thermo Jarrel-Ash ENVIRO II ICP-OES by Activation laboratories Ltd. (ATCLABS) in Ancaster, Canada. The samples were mixed with a flux of lithium metaborate and lithium tetraborate, and fused at 1000 °C in an induction furnace. The molten beads were rapidly digested in a solution of 5% HNO_3 containing an internal standard, and mixed continuously until complete dissolution. Loss on ignition (LOI) was determined by measuring weight loss upon heating to 1100 °C over a three hour period. Totals of major elements are 100 ± 1 wt.% and their analytical precisions are of 1-2%. The analytical precisions for Sc and Zr are better than 5%. Transition metals (Ni, Co, Cr, and V), REE, HFSE, and LILE were analyzed on a high-sensitivity Thermo Elemental X7 ICP-MS in the Great Lakes Institute for Environmental Research (GLIER), University of Windsor, Canada, following the protocols of Jenner et al. (1990). Samples dissolution was conducted under clean lab conditions with double

distilled acids. Approximately 100-130 mg of sample powder was used for acid digestion. Samples were dissolved in Teflon bombs in a concentrated mixture of HF-HNO_3 at a temperature of 120 °C for 3 days and then further attacked with 50% HNO_3 until no visible solid residue was left. Hawaiian basalt standards BHVO-1 and BHVO-2 were used as reference materials to estimate precision and accuracy. Analytical precisions are estimated as follows: 3-10% for REE, Y, Nb, Rb, Sr, Cs, Ba, Cu, and Co; 10-20% for Li, Ni, Zn, Ta, Th, and U; and 20-30% for Pb, V, and Cr.

Major element analyses were recalculated to 100 wt.% anhydrous basis for inter-comparisons. Chondrite and primitive mantle reservoir compositions are those of Sun and McDonough (1989) and Hofmann (1988), respectively. The Eu (Eu/Eu*), Ce (Ce/Ce*), Nb (Nb/Nb*), Ti (Ti/Ti*), and Zr (Zr/Zr*) anomalies were calculated with the following equation after Taylor and McLennan (1985):

$$A/A^* = A_N/([(B_N)(C_N)]^{1/2}$$

where

A/A^* = Element anomaly

A_N = Chondrite normalization for Eu and Ce anomalies, and primitive mantle normalization for Nb, Ti, and Zr anomalies.

B_N and C_N = Neighboring immobile elements as follow: Sm and Gd for Eu/Eu*; La and Pr for Ce/Ce*, Th and La for Nb/Nb*, Nd and Sm for Zr/Zr*, and Tb and Dy for Ti/Ti*.

These geochemical anomalies are used for petrogenesis only in samples with near primary magmatic composition. Mg-numbers (%) were calculated as the molecular ratio of $Mg^{2+}/(Mg^{2+} + Fe^{2+})$ where Fe^{2+} is assumed to be 90% of the total Fe.

2.5. Geochemical results

2.5.1. Mafic amphibolites

Mafic amphibolites are characterized by Mg-numbers ranging from 43 to 67. They have variable SiO_2 (42.9 to 56.9 wt.%), MgO (4.6-11.4 wt.%), Na_2O (0.80-4.0 wt.%), K_2O (< 0.01-0.87 wt.%), Fe_2O_3 (7.1-20.6 wt.%), and CaO (7.3-14.7 wt.%) contents. Zirconium ranges from 31 to 95 ppm (Figs. 2.6-2.7; Table 2.2). They do not display significant correlations on Zr versus Na_2O, K_2O, Fe_2O_3, and LILE (Rb, Sr, and Pb) diagrams (Figs. 2.6-2.7). Niobium, Th, and LREE show variably scattered patterns on Zr variation diagrams. In contrast, HREE, Al_2O_3, TiO_2, Ni, Sc, V, and Co show good correlation with Zr. The majority of samples possess Zr/Y ratios similar to those found in modern tholeiitic basalts (1.0-3.7 vs. < 2.0-4.5 in tholeiites) (cf. Barrett and MacLean, 1994).

Mafic amphibolites can be subdivided into four groups on the basis of the trace element systematics (Fig. 2.8). Group 1 amphibolites display near-flat REE patterns (La/Yb_{cn}=0.8-1.1). They possess negative Nb (Nb/Nb*=0.42-0.67), and negative to slightly positive Ti (Ti/Ti*=0.67-1.14) and Zr (Zr/Zr*=0.83-1.19) anomalies (Table 2.2; Fig. 2.8a-b). The europium anomalies (Eu/Eu*=0.88-1.05) are not pronounced.

Group 2 amphibolites are characterized by U-shape REE patterns (La/Sm_{cn}=2.6-3.0, Gd/Yb_{cn}=0.28-0.43). They display positive Nb (Nb/Nb*=1.3-1.5) and Eu (Eu/Eu*=1.95-2.32) anomalies, and strong negative to positive Ti (Ti/Ti*=0.23-6.27) and Zr (Zr/Zr*=0.41-8.2) anomalies (Table 2.2; Fig. 2.8c-d).

Group 3 amphibolites display variably depleted LREE patterns (La/Sm_{cn}=0.3-0.9). They possess negative Nb (Nb/Nb*=0.2-0.9), and negative to positive Ti (Ti/Ti*=0.35-1.17), Zr (Zr/Zr*=0.79-1.17), and Eu (Eu/Eu*= 0.55-1.10) anomalies (Fig. 2.8e-f).

Group 4 amphibolites have positively fractionated REE patterns (La/Yb_{cn}=1.0-3.5; Gd/Yb_{cn}=1.5-1.6). They exhibit negative to positive Zr (Zr/Zr*=0.58-1.18) anomalies, and negative Nb (Nb/Nb*=0.22-0.54), Ti (Ti/Ti*=0.72-0.88), and Eu (Eu/Eu*= 0.89-0.91) anomalies.

2.5.2. Ultramafic amphibolites

Ultramafic amphibolites are compositionally variable at 44.2-53.4 wt.% SiO_2, 15.5-25.6 wt.% MgO, 6.8-12.4 wt.% Fe_2O_3, 0.2-2.4 wt.% Na_2O, and 0.02-0.30 wt.% K_2O (Figs. 2.6-2.7). Mg-numbers range from 73 to 87. Low Zr contents (7-32 ppm) are consistent with an ultramafic composition. On Zr variation diagrams, TiO_2 and Al_2O_3 display positive correlations, whereas Ni shows a negative correlation (Figs. 2.6-2.7). They exhibit Zr/Y ratios mostly between 1.6 and 3.5 (Table 2.2).

Ultramafic amphibolites show variable characteristics on chondrite- and primitive mantle-normalized trace element diagrams (Fig. 2.9). Some ultramafic amphibolites have consistent negative Nb (Nb/Nb*=0.23-0.40) anomalies, slightly enriched LREE, and near-flat HREE (La/Yb_{cn}=1.7-3.3; Gd/Yb_{cn}=0.8-1.2) patterns (Fig. 2.9a-b). Other samples display negative to positive Nb (Nb/Nb*=0.06-2.64) anomalies, and depleted to highly enriched LREE (La/Yb_{cn}=0.44-22.1) patterns (Fig. 2.9c-d).

2.5.3. Calc-silicate rocks

As a group, the stage-II calc-silicate rocks have highly variable geochemical characteristics (Figs. 2.6-2.7). Relative to the mafic and ultramafic amphibolites, they have comparable compositional ranges of SiO_2 (43-57 wt.%), TiO_2 (0.17-1.84 wt.%), Al_2O_3 (1.0-16.4 wt.%), Zr (9-113 ppm), and Y (3.4-50.3 ppm) (Table 2.3). They have

higher CaO (15-30 wt.%), and lower MgO (2-11 wt.%), K_2O (<0.01-0.15 wt.%), and Fe_2O_3 (5.7-14.9 wt.%) than amphibolites at a given Zr content. They have large variations in Na_2O (0.09-2.7 wt.%), MnO (0.10-0.64 wt.%), Sr (40-2000 ppm), and Pb (2-36 ppm) contents.

The calc-silicate rocks display variable trace element characteristics on chondrite- and primitive mantle-normalized diagrams (Fig. 2.10). They exhibit two distinct Nb anomalies: (1) negative (Nb/Nb*=0.43-0.94) (Fig. 2.10b), and (2) positive Nb (Nb/Nb*=1.01-7.28) anomalies (Fig. 2.10d). They have near-flat REE patterns with minor depletion or enrichment of LREE and HREE (La/Yb_{cn}=0.64-2.0; Gd/Yb_{cn}=0.8-1.7). They possess negative to positive Eu (Eu/Eu*=0.7-3.6), Ti (Ti/Ti*=0.4-3.5), and Zr (Zr/Zr*=0.4-2.5) anomalies. Sample 485411 displays a LREE depleted trace element pattern similar to group 3 amphibolites (Fig. 2.10c-d).

2.6. Discussion

2.6.1. Regional metamorphism and metasomatism

The contrasting ages and complex metamorphic histories of the granite-greenstone associations of the Nuuk region have been explained in terms of allochthonous terranes docked by horizontal lithospheric motions comparable to those of Phanerozoic collisional and accretionary orogens (Bridgwater et al., 1974; Friend et al., 1987, 1988, 1996; Nutman et al., 1989, 1993; McGregor et al., 1991; Polat et al., 2002; Polat and Hofmann, 2003; Friend and Nutman, 2005; Nutman, 2006). On the basis of field relations and geochemical characteristics, Polat et al. (2007a) suggested that the Ivisaartoq belt formed in a juvenile intra-oceanic island arc setting. The amphibolite-facies regional metamorphism recorded by the Ivisaartoq greenstone belt might have taken place during

the terrane accretion, possibly during the docking of the Mesoarchean Kapisilik (*ca.* 3000 Ma) and Paleoarchean Isukasia (> 3600 Ma) terranes, shortly before the intrusion of the weakly deformed *ca.* 2.960 Ma marginal granites (see Friend and Nutman, 2005).

The stage-II calc-silicate rocks are the products of prolonged metasomatic reactions. They provide evidence for changing physical and chemical conditions during metamorphism. For example, the replacement of the epidote-rich metasomatic assemblage IIa by the anhydrous garnet-clinopyroxene assemblage IIb indicates an increase in temperature. Metasomatic garnet and clinopyroxene replacing mineral assemblages in metasedimentary rocks, metabasalts, komatiites, and iron formations have been documented to be formed at relatively high-T and intermediate-P (600-700 °C and 4.0-6.0 kbar ~ 12-18 km) during regional and/or contact metamorphism (e.g., Raith, 1991; Pan and Fleet, 1992; Mueller et al., 2004). The occurrence of garnet-diopside assemblage associated with ductile structures such as shear zones, tectonic boudins, and mylonitic foliations indicate that this assemblage was formed during the prograde stage of the regional amphibolite-facies metamorphism. In contrast, the metasomatic assemblage IIc exhibits cataclastic textures reflecting transitional ductile to brittle conditions. This brittle deformation and cataclasis might have accompanied the retrograde metamorphic evolution of the Ivisaartoq belt, possibly under upper greenschists-facies as indicated by the presence of accessory chlorite, tremolite, and calcite.

Transformation of mafic and ultramafic rocks into calc-silicates requires significant fluid-rock interaction, mass transfer, and reactions with Ca-rich fluids (see Rose et al., 1996). Fluids in metamorphic environments can be magmatic, derived from devolatilization reactions, meteoric, and mixtures of those fluid types (Rosing and Rose, 1993; Oliver, 1996; Ferry and Gerdes, 1998). There are no stable isotope or fluid

inclusion studies to unequivocally address the origin of the fluids responsible for the stage-II calc-silicate metasomatism of the Ivisaartoq belt. However, some constraints can be placed on the basis of field relationships. For instance, the contacts between the Ivisaartoq belt and the neighboring TTG-gneisses are marked by mylonites. Granites and granodiorites (*ca.* 2960 Ma) intruding the margins of the belt are only weakly deformed indicating that they postdate the regional metamorphism (Friend and Nutman, 2005). Granites and pegmatites occurring in the central parts of the belt transect the regional metamorphic fabrics and intrude the calc-silicate rocks. All these characteristics suggest that the intrusions exposed in the area are unlikely to be the source of metasomatic fluids. However, unexposed deep-seated syn-metamorphic intrusive rocks cannot be ruled out as the potential source of heat and fluids.

An alternative source of fluids could be metamorphic dehydration reactions. Fluids released during prograde metamorphism might have remobilized calcium from carbonates precipitated during sea-floor hydrothermal alteration in the sedimentary and volcanic rocks of the Ivisaartoq belt. Dehydration of clastic metasedimentary rocks in greenstone belts have been recognized as a significant source of fluids during regional metamorphism, causing intense metasomatism and ore deposition in the mafic and ultramafic metavolcanic counterparts (cf. Van Hees et al., 1999; Shelton et al., 2004). The lowermost part of the Ivisaartoq belt comprises a 500 m thick clastic metasedimentary unit (Figs. 2.1 and 2.2) composed of quartz-feldspathic gneisses and pelitic schists. We speculate that this unit could have played an important role in the generation of fluids that reacted with mafic and ultramafic rocks to produce the prograde metasomatic assemblages IIa and IIb.

2.6.2. Element mobility during the stage-I metasomatic alteration

Polat et al. (2008) investigated the geochemical and Sm-Nd isotope characteristics of well preserved picritic to basaltic pillow lavas and ultramafic cumulate rocks of the upper amphibolite unit. These rocks display flat to slightly enriched REE patterns, negative anomalies of HFSE (mainly Nb-Ta), and positive initial ε_{Nd} (+0.30 to +4.97) values. The preservation of primary magmatic textures including relict igneous clinopyroxene, and the coherent geochemical and isotopic characteristics suggests that these rocks retain a near-primary magmatic composition (see Polat et al., 2008).

In addition, some basaltic pillow lavas from the upper amphibolite unit exhibit mineralogical and chemical zonation providing evidence for sea-floor hydrothermal alteration (Fig. 2.3a-b). Epidote-rich inner pillow cores appear to have resulted from reactions with fluids circulating through drainage cavities; whereas the amphibole-rich pillow rims most likely represent chloritized chilled margins owing to interaction with sea water (see Polat et al., 2007). The outer pillow cores (Fig. 2.3b) appear to be an interface that remained relatively unaffected by sea-floor hydrothermal alteration. The average composition of these mineralogically and chemically zoned pillow basalts is presented in Table 2.2.

To assess the chemical changes that resulted from sea-floor alteration we present two isocon diagrams in Figure 2.11. In the isocon method, the elemental concentrations of the precursor versus the altered counterpart are plotted to quantify mass changes and element mobility owing to metasomatism. Accordingly, immobile elements will plot along a straight line (isocon) intercepting the origin. The slope of this line quantifies the total mass change in the altered rocks. Gains and losses of mobile elements are indicated by

their position either above or below the isocon line respectively (see Gresens, 1967; Grant, 1986; Baumgartner and Olsen, 1995).

Relative to the least altered outer pillow cores, the isocon slopes (Fig. 2.11, Table 2.2) indicate a total mass gain of 3.6% in the inner pillow cores and a total mass loss of 5.5% in the pillow rims. The isocon diagrams confirm large mobility of major elements (Ca, K, Na, Fe, Mg), LILE (Pb, Rb, Cs, Ba), and LREE (mostly La, Ce, and Eu) in the inner cores and pillow rims. In contrast, HREE, Th, Nb, Ta, Zr, and Ti consistently plot along and close to the isocon lines indicating their relatively low mobility.

The outer pillow cores display flat to slightly enriched LREE, near-flat HREE, and Nb-depleted trace element patterns similar to the least altered pillow basalts. These geochemical patterns have been interpreted as near-primary magmatic characteristics (Polat et al., 2007).

2.6.3. Origin of the geochemical patterns in the metavolcanic rocks

The deformation of the pillow lavas increases towards the magnetic marker giving rise to amphibolites with penetrative foliation. Group 1 amphibolites exhibit similar trace element patterns (Fig. 2.8a-b) to those of the least altered pillow basalts suggesting that their REE and HFSE have not been significantly modified by the strong metasomatic alteration that affected the areas along the magnetic marker (Fig. 2.3c-f). Therefore, Group 1 amphibolites preserve near-primary geochemical characteristics.

The trace element patterns of Group 2, 3, and 4 amphibolites are significantly different from those of the least altered pillow lavas (Fig. 2.8c-h). Several processes including source heterogeneity, crustal contamination, magma mixing, different degrees of partial melting, fractional crystallization, and hydrothermal alteration can produce the

contrasting trace element patterns of these amphibolites. Therefore, they could represent either volcanic flows with contrasting petrogenesis, or their trace element patterns may reflect complex hydrothermal alteration of the pillow lavas.

The U-shape REE patterns of Group 2 amphibolites resemble those of Phanerozoic boninites (Fig. 2.8c-d). These REE patterns in boninites result from partial melting of strongly depleted refractory mantle that has been refertilized by subduction fluids or melts prior to, or during melt production (Hickey and Frey, 1982; Crawford et al., 1989; Falloon and Danyushevsky, 2000). Although secular variations of the earth mantle prevents strict comparisons with modern magmatism (e.g., Glikson, 2001), the petrogenesis of Archean boninite-like melts, like their modern counterparts, requires a mantle source that has been depleted through several partial melting events prior to boninitic volcanism (Smithies et al., 2004). Melting of a refractory source would result in high-Mg (4.0-22 wt.%) magmas with low TiO_2 (< 0.5 wt.%) and Zr (< 55 ppm) contents, and high concentrations of transition metals (Ni ~ 47-520 ppm; Cr > 196-2343 ppm) (cf. Smithies, 2002; Smithies et al., 2004, and references therein). In comparison to modern boninitic lavas, the Mesoarchean Ivisaartoq Group 2 amphibolites display higher contents of TiO_2 (up to 1.4 wt.%) and Zr (up to 80 ppm), and lower abundances of MgO (10-11 wt.%), Ni (71-75 ppm), and Cr (116-196 ppm), implying that Group 2 amphibolites are not metamorphosed boninitic lavas. In addition, these amphibolites display strong positive Eu anomalies (Fig. 2.8c). Accordingly, we suggest that the geochemical characteristics of Group 2 amphibolites reflect the mobility of many major and trace elements, including LILE, REE, and HFSE during post-magmatic metasomatic alteration. The concentrations of Ti and Zr in samples 485402 and 485403 are comparable to those of Group 1 amphibolites and least altered pillow basalts, indicating that they were derived

from pillow basalt protoliths occurring in the upper volcanic sequence (upper amphibolites). Significant loss of the MREE, relative to Ti and Zr, would explain the U-shape REE patterns and the pronounced positive Ti and Zr anomalies of these samples (Fig. 2.8c-d). In contrast, sample 485406 displays strong negative Ti and Zr anomalies suggesting that these elements were locally remobilized along with the REE.

The flat HREE and depleted LREE patterns of Group 3 amphibolites resemble N-MORB (Fig. 2.8e-f). Unlike MORB, however, these amphibolites present negative Nb-Ta anomalies in primitive mantle-normalized diagrams. Crustal contamination and mixing with felsic magmas can result in negative HFSE anomalies and produce the enrichment of LREE from Group 3 to Groups 1 and 4 amphibolites. However, given the low concentration of transition metals (e.g, Ni, Co, and Cr) and MgO in felsic rocks, these processes would significantly decrease the content of these elements. In contrast, the concentration of transition metals and MgO of all amphibolite groups is comparable at a given Zr content (Figs. 2.6-2.7). Compelling evidence against significant crustal contamination and mixing in the petrogenesis of the Ivisaartoq volcanic rocks is provided by positive ε_{Nd} values of the associated mafic (+0.30 to +3.1) and ultramafic (+4.2 to +5.0) lavas (Polat et al., 2008).

Polat et al. (2007a) suggested that the Ivisaartoq belt formed in a suprasubduction zone. Basaltic rocks formed across those settings display complex trace element variations ranging from MORB-like REE patterns with negative Nb anomalies to typical arc lavas enriched in LREE and negative HFSE anomalies. These contrasting trace element patterns stem from different degrees of melting of heterogeneous depleted-mantle sources variably modified by subduction components (Klein and Karsten, 1995; Karsten et al., 1996; Sinton et al., 2003; Godard et al., 2006). Accordingly, these complex processes

may well produce the negative Nb-Ta anomalies and the enrichment of LREE from Groups 3 to Groups 1 and 4 amphibolites. However, these processes would also result in lavas with distinct contents of MgO, transition metals, Zr, TiO_2, Y, and HREE reflecting the degree of melting and depletion of the sources. In contrast, the concentration of those elements in Groups 1, 3 and 4 amphibolites is virtually the same at a given Zr content (Figs. 2.6-2.8).

In addition, crystal fractionation of a parental magma cannot explain the crossed LREE patterns between different amphibolite groups. Even within Group 3 amphibolites, some samples (e.g., 485407 and 485401) display extremely low La/Sm_{cn} ratios and strong depletion of Nb despite their high HREE content (Fig. 2.8e-f). These patterns cannot be explained by fractionation but suggest that the LREE and Nb were remobilized.

Although melting of a heterogeneous mantle source could have played a major role in the formation of diverse geochemical compositions in the Ivisaartoq volcanic rocks, the evidence for significant element mobility in the vicinity of calc-silicate formations indicates that the large geochemical variations in the belt have resulted from post-magmatic alteration processes (Fig. 2.3c-f). In addition, all groups of amphibolites locally occur within the same outcrops (*e.g.*, samples 485401, 485402, 405405, and 485410) without structural discontinuity. This suggests that their contrasting trace element patterns most likely resulted from alteration of the pillow basalts.

The ultramafic amphibolites provide additional evidence for significant post-magmatic alteration. For example, some ultramafic rocks, 485434 (ε_{Nd} = +8.3; La/Yb_{cn} = 20) and 485436 (ε_{Nd} = +9.5; La/Yb_{cn} = 24), display highly enriched LREE patterns (Fig. 2.9c-d) and strong positive ε_{Nd} values (see Polat et al., 2008). These samples are from the same outcrop as sample 485435 (ε_{Nd} = +2.9; La/Yb_{cn} = 1.8). Enrichment of LREE by crustal

contamination cannot explain the more positive ε_{Nd} values. These contrasting geochemical variations have been attributed to post-magmatic alteration (Polat et al., 2008). Altered ultramafic rocks display slightly depleted to extremely enriched LREE patterns and variable negative to positive anomalies of Eu, Nb, Ta, Ti, and Zr (Fig. 2.9c-d). In contrast, some samples still preserve geochemical characteristics comparable to the least altered ultramafic pillows and cumulates (Fig. 2.9a-b) (Polat et al., 2007). They possess slight LREE-enriched patterns and consistent negative anomalies of HFSE (especially Nb and Ta). We interpret these rocks as the least altered ultramafic amphibolites.

On variation diagrams, Zr is used as an alteration and differentiation index (Figs. 2.6-2.7) because of its immobile behaviour in different geological conditions, and consistent incompatibility during fractionation of ultramafic to mafic magmas (Winchester and Floyd, 1977; Barrett and MacLean, 1994; Pearce, 1996). Accordingly, immobile elements will display systematic correlations with Zr consistent with magmatic fractionation. Some major elements such as Si, Mg, Ca, Fe, Na, K, and trace elements including Rb, Sr, Ba, Pb show no correlation on variation diagrams indicating large mobility in all amphibolites (Figs. 2.6-2.7). Scatter of REE, Ti, Th, Nb, and Y on variation diagrams is consistent with various degrees of mobility of these elements. Transition metals Ni, V, Sc, Co, and Cr present excellent correlation with Zr (Fig. 2.7) in all amphibolites indicating that these elements were practically immobile during alteration.

Despite element mobility, systematic trends of increasing Al, REE, and HFSE with increasing Zr can be resolved. These trends are shared by all amphibolites. It is unlikely that the linear trends on variation diagrams of Zr represent a liquid line of descent given the differences in ε_{Nd} values between ultramafic and mafic pillows. However, the

collective geochemical correlations suggest crystal fractionation. For example, ultramafic rocks exhibit a steep negative correlation of Ni versus Zr consistent with olivine fractionation (Fig. 2.7). Aluminum content increases with increasing Zr in ultramafic amphibolites but decreases in the mafic amphibolites suggesting that plagioclase was only important during fractionation of the basaltic melts (Fig. 2.6). The trends of Sc and V reflect clinopyroxene fractionation. Fractionation of these mineral phases is consistent with the occurrence of olivine-bearing ultramafic sheets grading upwards into gabbroic rocks, clinopyroxene-rich cumulates, anorthosites intrusions, and plagioclase-rich ocelli structures in gabbros and basalts.

There is no unequivocal evidence indicating the relative timing of this alteration. However, the samples in this study were collected along a high strain zone at the contact between the upper and lower amphibolite groups. This zone was a fluid pathway during the regional metamorphism as indicated by ductile calc-silicate layers, quartz veins, and silicic mylonites (Chapter 2.6.1). We postulate that the alteration patterns displayed by Groups 2-4 amphibolites were formed during the regional metamorphic event coeval with the stage-II calc-silicate metasomatism.

2.6.4. Element mobility during the stage-II calc-silicate metasomatism

The stage-II calc-silicate rocks resulted from prolonged metasomatic reactions in ultramafic to mafic rocks. Local mobility of REE and HFSE in the magmatic precursors makes a quantitative estimation of elemental mass changes difficult because most methods use ratios of immobile elements as a datum (Gresens, 1967; Grant, 1986; MacLean and Kranidiotis, 1987; MacLean, 1988, 1990). Thus, we present a qualitative

evaluation of the chemical changes occurring during the stage-II calc-silicate metasomatism.

As a group, the stage-II calc-silicate rocks represent significant additions of Ca and losses of Na and K relative to the volcanic protoliths (Fig. 2.6). Manganese, Fe, and Mg, were consistently lost during formation of the prograde assemblage IIa, and gained to form the garnet-clinopyroxene metasomatic assemblage IIb. Some LILE such as Rb, Sr, Ba, and Pb were variably enriched in the calc-silicate assemblages IIb and IIc.

Primitive mantle- and chondrite-normalized trace element patterns of the stage IIa calc-silicates are slightly depleted in HREE, however, the concentration levels of trace elements are comparable to those of the least altered mafic amphibolites and pillow basalts (filled symbols, Fig. 2.10a-b). Moreover, the concentrations of Ni, Sc, V, Cr, and Co in this assemblage are consistent with a basaltic protolith (Fig. 2.7). These characteristics indicate that Th, Nb, Ta, Ti, Zr, REE (excepting Eu), and transition metals were not significantly changed during the development of the metasomatic assemblage IIa.

Large additions of Ca (CaO = 17-30 vs. 15-22 wt.% in the assemblage IIa) in calc-silicate assemblages IIb and IIc resulted in low REE and HFSE abundances (< 3 x primitive mantle values) due to residual dilution (Fig. 2.10). For instance, sample 499718 (CaO ~30 wt.%) exhibits low concentrations of transition metals (e.g., Ni = 29; Cr = 47, and Co = 11 ppm) coupled with low REE and HFSE contents (Fig. 2.10a-b). However, low trace element abundances in some calc-silicates may reflect the composition of their protoliths. Samples 499740 and 499741 were collected from calc-silicate boudins spatially associated with ultramafic amphibolites (see Fig. 2.3d). They display high Ni (>

1300 ppm), Co (> 100 ppm), and Cr (> 1500 ppm) contents, and low abundances of REE and HFSE consistent with an ultramafic precursor (Fig. 2.10c-d).

The stage IIb and IIc calc-silicate rocks exhibit evidence for REE and HFSE mobility. Sample 485411 (Fig. 2.10c-d) displays a strongly depleted LREE pattern similar to those of Group 3 amphibolites (Fig. 2.8e-f) suggesting loss of LREE. Gains and losses of HFSE are indicated by strong positive (samples 499715, 499716, and 499741) and complementary large negative (sample 485411) Nb-Ta anomalies in primitive mantle-normalized diagrams (Fig. 2.10d). Despite strong Ca enrichment, samples 499715 and 499716 posses high REE contents. This suggests that REE were enriched in these samples.

Retrograde overprinting makes it difficult to determine whether the REE, Nb, and Ta were mobilized during the development of the metasomatic assemblage IIb or the retrograde assemblage IIc. Calc-silicate metasomatism of volcanic rocks in other Archean greenstone belts has resulted in significant mobility of the REE and HFSE mainly during the formation of prograde garnet-pyroxene assemblages (e.g., Galley et al., 2000). In addition, experimental and empirical studies indicate that HFSE are more easily mobilized at high temperatures (cf. Rubin et al., 1993; Van Baalen, 1993; Tilley and Eggleton 2005; Wood, 2005). Therefore, we suggest that the observed remobilization of HFSE and REE may have occurred during the formation of garnet-clinopyroxene assemblage IIb, probably over 500 °C.

2.7. Conclusions and Implications

Geochemical investigations of Archean volcanic rocks, as a proxy to understand the magmatic and tectonic evolution of greenstone belts, rely on the systematics of elements that are not easily disturbed during hydrothermal alteration and metamorphism. Most

major elements (Si, Na, K, Ca, Mg, and Fe) and LILE (Rb, Cs, Ba, Sr, Pb, U) are highly mobile during fluid-rock interaction limiting their use in petrologic and tectonic investigations (Hart et al., 1974; Condie et al., 1977; Ludden and Thompson, 1979; Ludden et al., 1982; Ague, 1994; Staudigel et al., 1996; Alt, 1999; Masters and Ague, 2005). In contrast, transition metals (Ni, Sc, Co, Cr, and V), HFSE (Zr, Ti, Nb, Ta, and Th), and REE (mainly the HREE) have been reliably used to investigate the evolution of variably altered and metamorphosed greenstone belts due to their largely immobile behaviour (Arndt, 1994; Polat and Hofmann, 2003; Polat et al., 2003).

This study has provided evidence for remobilization of those (e.g., REE and HFSE) normally immobile trace elements during a second stage of calc-silicate metasomatism yielding the following results:

1. Although almost all normally 'immobile' elements were disturbed, the collective geochemical correlations with Zr suggest different degrees of mobility. Accordingly, trace element mobility in the stage-II calc-silicate rocks and associated amphibolites increases from Zr, Ti, Ni, V, and Co, through HREE, Th, Nb, Ta, Y, Al, Sc, and Cr, to LREE and MREE. Petrographic and geochemical characteristics of calc-silicate rocks appear to indicate that the mobility of HFSE and REE occurred during the prograde stage of the regional metamorphism at upper amphibolite facies conditions (stage-II metasomatism). This trace element mobility contrasts with the consistent immobile behaviour of HREE and HFSE during an early stage of sea-floor hydrothermal alteration (stage-I metasomatism).

2. Altered amphibolites and calc-silicate rocks exhibit complementary trace element patterns of enriched and depleted LREE, Th, Nb, and Ta (Fig. 2.12). It is noteworthy that the mobility of these elements occurred along shear zones and resulted in the formation of

amphibolites with trace element characteristics resembling those displayed by volcanic rocks formed at contrasting tectonic settings such as boninites and N-MORB-like lavas (cf. Dostal et al., 1980). Considering these trace element patterns as primary can lead to misleading geodynamic interpretations.

3. The close spatial association of strongly altered and least altered metavolcanic rocks indicates that the REE and HFSE (mainly Th, Nb and Ta) were mobile on a local scale (1-4 m). It appears that the REE were removed at some localities, giving rise to Group 2 and 3 amphibolites, and re-precipitated within several meters, generating the LREE-enriched patterns of Group 4 amphibolites and some ultramafic rocks (Figs. 2.8-2.9).

4. Despite large element mobility, mafic and ultramafic amphibolites display discernable linear trends on diagrams of Zr versus REE, HFSE, and transition metals (Figs. 2.6-2.7). Net gains or losses of major elements during hydrothermal alteration (e.g., silicification, chloritization, calc-silicate alteration, etc) may well produce positive linear trends of immobile elements due to residual dilution or enrichment effects (Finlow-Bates and Stumpfl, 1981; MacLean and Kranidiotis, 1987; MacLean, 1990; MacLean and Hoy, 1991; Barrett and MacLean, 1994; Ague, 1994). Although Ca, Mg, Fe, and Si were mobile during post-magmatic alteration, the abundance of these elements in the Ivisaartoq amphibolites is still consistent with basaltic to picritic compositions (see also Polat et al. 2007a). This suggests that alteration and metamorphism did not produce significant mass changes, except where intense calc-silicate replacement occurred. Therefore, the correlation of REE, HFSE, and transition metals with Zr resulted from magmatic processes.

5. Near-primary magmatic signatures in the amphibolites are indicated by inflections on variation diagrams (e.g., Zr versus Al, Ni, Sc, and V) which are more likely produced by magmatic fractionation (Figs. 2.6-2.7). Although differences in ε_{Nd} values between mafic and ultramafic pillows and cumulates rule out a parental magma (Polat et al., 2008), taken all together, the covariations of transition metals and Al with Zr indicate fractionation of olivine, clinopyroxene, and plagioclase.

6. The geochemical characteristics of the Ivisaartoq volcanic rocks indicate that they are part of the same mafic to ultramafic volcanic suite. The least altered Group 1 amphibolites and ultramafic rocks (Figs. 2.8a-b and 2.9a-b) exhibit trace element patterns with flat to slightly enriched LREE, consistent negative Nb-Ta anomalies, and flat-HREE. These geochemical characteristics are consistent with subduction zone geochemical signatures (see Hawkesworth et al., 1993; Pearce and Peate, 1995) and partial melting of a garnet-free shallow mantle source region.

2.8. Acknowledgments

We thank Z. Yang, and J.C. Barrette for their help during the ICP-MS analyses. This is a contribution of PREA and NSERC grant 250926 to A. Polat, and NSERC grant 83117 to B. Fryer. Field worked was funded by the Bureau of Minerals and Petroleum in Nuuk and the Geological Survey of Denmark and Greenland (GEUS). Two anonymous reviewers are thanked for providing excellent critiques and constructive comments on an early version of this paper which resulted in significant improvement of this study.

2.9. References

Ague, J.J., 1994. Mass transfer during Barrovian metamorphism of pelites, south-central Connecticut. I: Evidence for changes in composition and volume. American Journal of Science 294, 989-1057.

Alt J. C., 1999. Hydrothermal alteration and mineralization of oceanic crust: Mineralogy, geochemistry, and processes. In: Barrie, C.T., Hannington, M.D., (Eds). Volcanic-Associated Massive Sulphide Deposits: Processes and Examples in Modern and Ancient Settings. Reviews in Economic Geology 8, 133-155.

Appel, P.W.A., 1983. Tungsten in the Godthåb area, West Greenland. Rapport Grønlands Geologiske Undersøgelse 1115, 59-64.

Appel, P.W.A., 1994. Stratabound scheelite in altered Archean komatiites, West Greenland. Mineralium Deposita 29, 341-352.

Appel, P.W.A., 1997. High bromine contents and low Cl/Br ratios in hydrothermally altered Archean komatiitic rocks, West Greenland. Precambrian Research 82, 177-189.

Arndt, N.T., 1994. Archean komatiites. In: Condie, K.C. (Ed). Archean Crustal Evolution. Developments in Precambrian Geology 11, 11-44.

Barrett, T.J., MacLean, W.H., 1994. Chemostratigraphy and hydrothermal alteration in exploration for VHMS deposits in greenstones and younger volcanic rocks. In: Lentz, D.R., (Ed.). Alteration and alteration processes associated with ore-forming systems. Geological Association of Canada, Short course notes 11, 433-467.

Baumgartner, L.P., Olsen, S.N., 1995. A least-squares approach to mass transport calculations using the isocon method. Economic Geology 90, 1261-1270.

Brewer, M., Chadwick, B., Coe, K. & Park, J.F.W., 1984. Further field observations in the Ivisârtoq Region of southern West Greenland. Rapport Grønlands Geologiske Undersøgelse 120, 55-67.

Bridgwater, D., McGregor, V.R.,. Myers, J.S., 1974. A horizontal tectonic regime in the Archean of Greenland and its implications for early crustal thickening. Precambrian Research 1, 179-197.

Chadwick, B., 1985. Contrasting styles of tectonism and magmatism in the late Archaean crustal evolution of the northeastern part of the Ivisârtoq region, inner Godthåbsfjord, southern West Greenland. Precambrian Research 27, 215-238.

Chadwick, B., 1986. Malene stratigraphy and late Archean structure: new data from Ivisaartoq, inner Godthåbsfjord, southern West Greenland. Rapport Grønlands Geologiske Undersøgelse 130, 74-85.

Chadwick, B., 1990. The stratigraphy of supracrustal rocks within high-grade orthogneisses and its bearing on Late Archean structure in southern West Greenland. Journal of the Geological Society of London 147, 639-652.

Chadwick, B., Coe, K., 1988. Geological map of Greenland, 1:100 000, Ivisaartoq sheet 64 V. Nord. Copenhagen, Geological Survey of Greenland.

Condie, K.C., Viljoen, M.J., Kable, E.J.D., 1977. Effects of alteration on element distributions in Archean tholeiites from the Barberton greenstone belt, South Africa. Contributions to Mineralogy and Petrology 64, 75-89.

Crawford, A.J, Falloon, T.J, Green, D.H., 1989. Classification, petrogenesis and tectonic setting of boninites. In: Crawford, A.J. (Ed), Boninites and related rocks. Unwin-Hyman, London, 1-49.

Dostal, J., Strong D.F., Jamieson, R.A., 1980. Trace element mobility in the mylonite zone within the ophiolite aureole, St. Anthony Complex, Newfoundland. Earth and Planetary Science Letters 49, 188-192.

Falloon, T.J., Danyushevsky, L.V., 2000. Melting of refractory mantle at 1.5, 2 and 2.5 GPa under anhydrous and H_2O-undersaturated conditions: Implications for the petrogenesis of high-Ca boninites and the influence of subduction components on mantle melting. Journal of Petrology 41 (2), 257-283.

Ferry, J.M., Gerdes, M.L., 1998. Chemically reactive fluid flow during metamorphism. Annual Review of Earth and Planetary Sciences 26, 255-287.

Finlow-Bates, T., Stumpfl, E.F., 1981. The behavior of so called immobile elements in hydrothermally altered rocks associated with volcanogenic submarine-exhalative ore deposits. Mineralium Deposita 16, 319-328.

Friend, C.R.L., Nutman, A.P., 2005. New pieces to the Archaean terrane jigsaw puzzle in the Nuuk Region, southern West Greenland: Steps in transforming a simple insight into a complex regional tectonothermal model. Journal of the Geological Society of London 162, 147-162.

Friend, C.R.L., Nutman, A.P., Baadsgaard, H., Kinny, P.D., McGregor, V.R., 1996. Timing of late Archean terrane assembly, crustal thickening and granite emplacement in the Nuuk region, southern West Greenland. Earth and Planetary Science Letters 142, 353-365.

Friend, C.R.L., Nutman, A.P. & McGregor, V.R., 1987. Late-Archaean tectonics in the Færingehavn-Tre Brødre area, south of Buksefjorden, southern West Greenland. Journal of the Geological Society of London 144, 369-376.

Friend, C.R.L., Nutman, A.P., McGregor, V.R., 1988. Late Archean terrane accretion in the Godthåb region, southern West Greenland. Nature 335, 535-538.

Fryer, B.J., Fyfe, W.S., Kerrich, R., 1979. Archean volcanogenic oceans. Chemical Geology 24, 25-33.

Galley, A.G., Jonasson, I.R., Watkinson, D.H., 2000. Magnetite-rich calc-silicate alteration in relation to synvolcanic intrusions at the Ansil volcanogenic massive sulfide deposit, Rouyn-Noranda, Quebec, Canada. Mineralium Deposita 35, 619-637.

Garde, A.A., 2007. A mid-Archean Island arc complex in the Eastern Akia terrane, Godthåbsfjord, southern West Greenland. Journal of the Geological Society of London 164, 565-579.

Gélinas, L., Mellinger, M., Trudel, P., 1982. Archean mafic metavolcanics from the Rouyn-Noranda district, Abitibi Greenstone Belt, Quebec. 1. Mobility of the major elements. Canadian Journal of Earth Sciences 19, 2258-2275.

Glikson, A.Y., 2001. The astronomical connection of terrestrial evolution: crustal effects of post-3.8 Ga mega-impact clusters and evidence for major 3.2±0.1 Ga bombardment of the Earth–Moon system. Journal of Geodynamics 32, 205–229.

Godard, M., Bosch, D., Einaudi, F., 2006. A MORB source for low-Ti magmatism in the Semail ophiolite. Chemical Geology 234 (1-2), 58-78.

Grant, J.A., 1986. The isocon diagram-A simple solution to Gresens' equation for metasomatic alteration. Economic Geology 81, 1976-1982.

Gresens, R.L., 1967. Composition-volume relationships of metasomatism. Chemical Geology 2, 47-65.

Gruau, G., Rosing, M., Bridgwater, D., Gill, R.C.O., 1996. Resetting of Sm-Nd systematics during metamorphism of >3.7-Ga rocks: implications for isotopic models of early Earth differentiation. Chemical Geology 133, 225-240.

Gruau, G., Tourpin, S., Fourcade, S., Blais S., 1992. Loss of isotopic (Nd, O) and chemical (REE) memory during metamorphism of komatiites: new evidence from eastern Finland. Contributions to Mineralogy and Petrology 112, 66-82.

Hart S. R., Erlank A. J., Kable E. J. D., 1974. Sea-floor basalt alteration: Some chemical and isotopic effects. Contributions to Mineralogy and Petrology 44, 219–230.

Hawkesworth, C.J., Gallanger, K., Hergt, J.M., McDetmott, F., 1993. Mantle and slab contributions in arc magmas. Annual Reviews of Earth and Planetary Sciences 21, 175-204.

Hall, R.P., 1980. The tholeiitic and komatiitic affinity of Malene metavolcanic amphibolites from Ivisaartoq, southern West Greenland. Rapport Grønlands Geologiske Undersøgelse 97, 20 pp.

Hall, R.P., Friend, C.R.L., 1979. Structural evolution of the Archean rocks in Ivisârtoq and the neighboring inner Godthåbsfjord region, southern West Greenland. Geology 7, 311-315.

Hickey, R.L., Frey, F.A., 1982. Geochemical characteristics of boninitic series volcanics: implications for their source. Geochimica et Cosmochimica Acta 46, 2099–2115.

Hofmann, A.W., 1988. Chemical differentiation of the Earth: the relationship between mantle, continental crust, and oceanic crust. Earth and Planetary Science Letters 90, 297-314.

Jenner, G. A., Longerich, H. P., Jackson, S. E., Fryer, B. J., 1990. ICP-MS; a powerful tool for high-precision trace-element analysis in earth sciences; evidence from analysis of selected U.S.G.S. Reference samples. Chemical Geology 83, 133-148.

Karsten, J.L., Klein, E.M., Sherman, S.B., 1996. Subduction zone geochemical characteristics in ocean ridge basalts from the southern Chile Ridge: Implications of modern ridge subduction systems for the Archean. Lithos 37 (2-3), 143-161.

Klein, E.M., Karsten, J.L., 1995. Ocean-ridge basalts with convergent-margin geochemical affinities from the Chile Ridge. Nature 374, 52-57.

Lahaye, Y., Arndt, N.T., Byerly, G., Chauvel, C., Fourcade, S., Gruau, G., 1995. The influence of alteration on the trace-element and Nd isotopic compositions of komatiites. Chemical Geology 126, 43-64.

Ludden, J. N., Gelinas, L., Trudel, P., 1982. Archean metavolcanics from the Rouyn-Noranda district, Abitibi greenstone belt, Quebec. 2. Mobility of trace elements and petrogenetic constraints. Canadian Journal of Earth Sciences 19, 2276-2287.

Ludden, J. N., Thompson, G., 1979. An evaluation of the behavior of the rare earth elements during the weathering of sea-floor basalts. Earth and Planetary Science Letters 43, 85–92.

MacLean, W.H., 1988. Rare earth element mobility at constant inter-REE ratios in the alteration zone at the Phelps Dodge massive sulphide deposit, Matagami, Quebec. Mineralium Deposita 23, 231-238.

MacLean, W.H., 1990. Mass change calculations in altered rocks series. Mineralium Deposita 25, 1-6.

MacLean, W.H., Hoy, L.D., 1991. Geochemistry of hydrothermally altered rocks at the Horn mine, Noranda, Quebec. Economic Geology 86, 506-528.

MacLean, W.H., Kranidiotis, P., 1987. Immobile elements as monitors of mass transfer in hydrothermal alteration: Phelps Dodge massive sulfide deposit, Matagami, Quebec. Economic Geology 82, 951-962.

McGregor, V.R., Friend, C.R.L., Nutman, A.P., 1991. The late Archean mobile belt through the Godthåbsfjord, southern West Greenland; a continent-continent collision zone? Bull. Geol. Soc. Denmark 39, 179-197.

Masters, R.L., Ague, J.J., 2005. Regional-scale fluid flow and element mobility in Barrow's metamorphic zones, Stonehaven, Scotland. Contributions to Mineralogy and Petrology 150, 1-18.

Middelburg, J.J., Van der Weijden, C.H., Woittiez, J.R.W., 1988. Chemical processes affecting the mobility of major, minor and trace elements during weathering of granitic rocks. Chemical Geology 68 (3-4), 253-273.

Mueller, A.G., Nemchin, A.A., Frei, R., 2004. The Nevoria Gold Skarn Deposit, Southern Cross Greenstone Belt, Western Australia: II. Pressure-Temperature-Time Path and Relationship to Postorogenic Granites. Economic Geology, 99, 453-478.

Nutman, A.P., 2006. Antiquity of the oceans and continents. Elements 2 (4), 223-227.

Nutman, A.P., Friend, C.R.L., Baadsgaard, H., McGregor, V.R., 1989. Evolution and assembly of Archean Gneiss Terranes in the Godthåbsfjord Region, Southern West Greenland: structural, metamorphic, and isotopic evidence. Tectonics 8 (3), 573-589.

Nutman, A.P., Friend, C.R.L., Kinny, P.D., McGregor, V.R., 1993. Anatomy of an early Archean gneiss complex: 3900 to 3600 Ma crustal evolution in southern West Greenland. Geology 21, 415-418.

Oliver, N.H.S., 1996. Review and classification of structural controls on fluid flow during regional metamorphism. Journal of metamorphic Geology 14, 477-492.

Pan, Y., Fleet, M.E., 1992. Mineralogy and genesis of calc-silicates associated with Archean volcanogenic massive sulphide deposits at the Manitouwadge mining camp, Ontario. Canadian Journal of Earth Sciences 29, 1375-1388.

Pearce, J.A., 1996. A user's guide to basalt discrimination diagrams. In: Wyman, D.A. (Ed.). Trace element geochemistry of volcanic rocks: applications for massive sulphide exploration. Geological Association of Canada, GAC Short Course Notes 12, 79-113.

Pearce, J.A., Peate, D.W., 1995. Tectonic implications of the composition of volcanic arc magmas. Annual Reviews of Earth and Planetary Sciences 23, 251-285.

Polat, A., Appel, P.W.U., Frei, R., Pan, Y., Dilek, Y., Ordóñez-Calderón, J.C., Fryer, B., Hollis, J.A., Raith, J.G., 2007. Field and Geochemical Characteristics of the Mesoarchean (~3075 Ma) Ivisaartoq greenstone belt, southern West Greenland: Evidence for sea floor hydrothermal alteration in supra-subduction oceanic crust. Gondwana Research 11, 69-91.

Polat, A., Frei, R., Appel, P.W.U., Dilek, Y., Fryer, B., Ordóñez-Calderón, J.C., Yang, Z., 2008. The origin and compositions of Mesoarchean oceanic crust: Evidence from the 3075 Ma Ivisaartoq greenstone belt, SW Greenland. Lithos doi: 10.1016/j.lithos.2007.06.021.

Polat, A., Hofmann, A.W., 2003. Alteration and geochemical patterns in the 3.7-3.8 Ga Isua greenstone belt, West Greenland. Precambrian Research 126, 197-218.

Polat, A., Hofmann, A.W., Münker, C., Regelous, M., Appel, PW.U., 2003. Contrasting geochemical patterns in the 3.7-3.8 Ga pillow basalt cores and rims, Isua greenstone belt, Southwest Greenland: implications for post-magmatic alteration processes. Geochimica et Cosmochimica Acta 67 (3), 441-457.

Polat, A., Hofmann, A.W., Rosing, M.T., 2002. Boninite-like volcanic rocks in the 3.7-3.8 Ga Isua greenstone belt, West Greenland: geochemical evidence for intra-oceanic subduction zone processes in the early Earth. Chemical Geology 184, 231-254

Raith, J.G., 1991. Stratabound tungsten mineralization in regional metamorphic calc-silicate rocks from the Australpine crystalline complex, Australia. Mineralium Deposita 26, 72-80.

Raith, J.G., Polat, A., Appel, P.W.U., 2006. Hydrothermal alteration of Archean oceanic crust in the Ivisaartoq greenstone belt, southern West Greenland. Pangeo Conference Series, Austria, 264-265.

Rose, N.M., Rosing, M.T., Bridgwater, D., 1996. The origin of metacarbonate rocks in the Archaen Isua supracrustal belt, west Greenland. American Journal of Science 296, 1004-1044.

Rosing, M.T., Rose, N.M., 1993. The role of ultramafic rocks in regulating the concentrations of volatile and non-volatile components during deep crustal metamorphism. Chemical Geology 108, 187-200.

Rubin, J.N., Henry, C.D., Price, J.G., 1993. The mobility of zirconium and other "immobile" elements during hydrothermal alteration. Chemical Geology 110, 29-47.

Shelton, K.L., McMenamy, T.A., Van Hees, E.H.P., Falck, H., 2004. Deciphering the Complex Fluid History of a Greenstone-Hosted Gold Deposit: Fluid Inclusion and Stable Isotope Studies of the Giant Mine, Yellowknife, Northwest Territories, Canada. Economic Geology 99, 1643-1663.

Sinton, J.M., Ford, L.L., Chappell, B., McCulloch, M.T., 2003. Magma genesis and mantle heterogeneity in the Manus back-arc basin, Papua New Guinea. Journal of Petrology 44 (1), 159-195.

Smithies, R.H., 2002. Archean boninites-like rocks in an intracratonic setting. Earth and Planetary Science Letters 197, 19-34.

Smithies, R.H., Champion, D.C., Sun, S., 2004. The case for Archean boninites. Contributions to Mineralogy and Petrology 147, 705-721.

Staudigel, H., Plank, T., White, B., Schmincke, H-U., 1996. Geochemical fluxes during sea floor alteration of the basaltic upper oceanic crust: DSDP sites 417 and 418. In: Bebout, G.E., Scholl, S.W., Kirby, S.H., Platt, J.P. (Ed.). Subduction: Top to bottom. American Geophysical Union, Washington, 19-38.

Sun, S.S., McDonough, W.F., 1989. Chemical and isotopic systematics of oceanic basalts: implications for mantle composition and processes. Geological Society of London, Special Publications 42, 313-345.

Taylor, S. R., McLennan, S. M., 1985. The continental crust: Its composition and evolution. Blackwell, Oxford, 312 pp.

Terabayashi, M., Masada, Y., Ozawa, H., 2003. Archean ocean-floor metamorphism in the North Pole area, Pilbara Craton, Western Australia. Precambrian Research 127, 167-180.

Tilley, D.B., Eggleton, R.A., 2005. Titanite low-temperature alteration and Ti mobility. Clays and Clay Minerals 53 (1), 100-107.

Van Baalen, M.R., 1993. Titanium mobility in metamorphic systems: a review. Chemical Geology 110, 233-249.

Van Hees, E.H.P., Shelton, K.L., McMenamy, T.A., Ross, L.M., Jr., Cousens, B.L., Falck, M., Robb, M.E., and Canam, T.W., 1999. Metasedimentary influence on metavolcanic-rock-hosted greenstone gold deposits: Geochemistry of the Giant mine, Yellowknife, Northwest Territories, Canada. Geology 27, 71–74.

Weiershäuser, L., Spooner, E.T.C., 2005. Seafloor hydrothermal fluids, Ben Nevis area, Abitibi greenstone belt; implications for Archean (approximately 2.7 Ga) seawater properties. Precambrian Research 138, 89-123.

Winchester, J.A., Floyd, P.A., 1977. Geochemical discrimination of different magma series and their differentiation products using immobile elements. Chemical Geology 20, 325-343.

Wood, S.A., 2005. The aqueous geochemistry of zirconium, hafnium, niobium and tantalum. In: Linnen, R.L., Samson, I.M. (Eds). Rare-element geochemistry and mineral deposits. Geological Association of Canada, GAC Short Course Notes 17, 217-268.

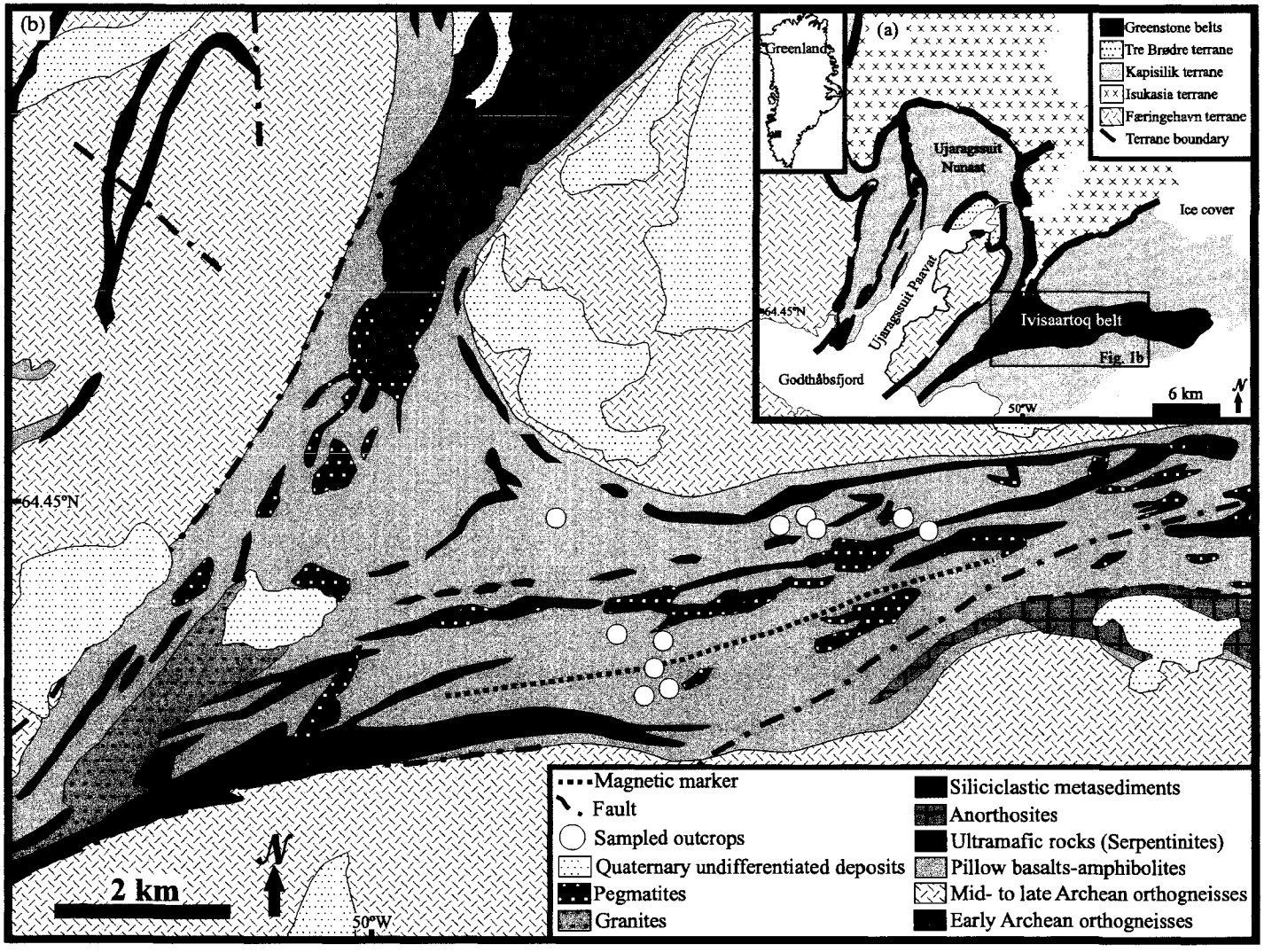

Figure 2.1. (a) Early to late Archean tectonic terranes map of the northeastern Nuuk region (modified after Friend and Nutman, 2005). (b) Geological map of central Ivisaartoq belt and surrounding areas (modified from Chadwick and Coe, 1988).

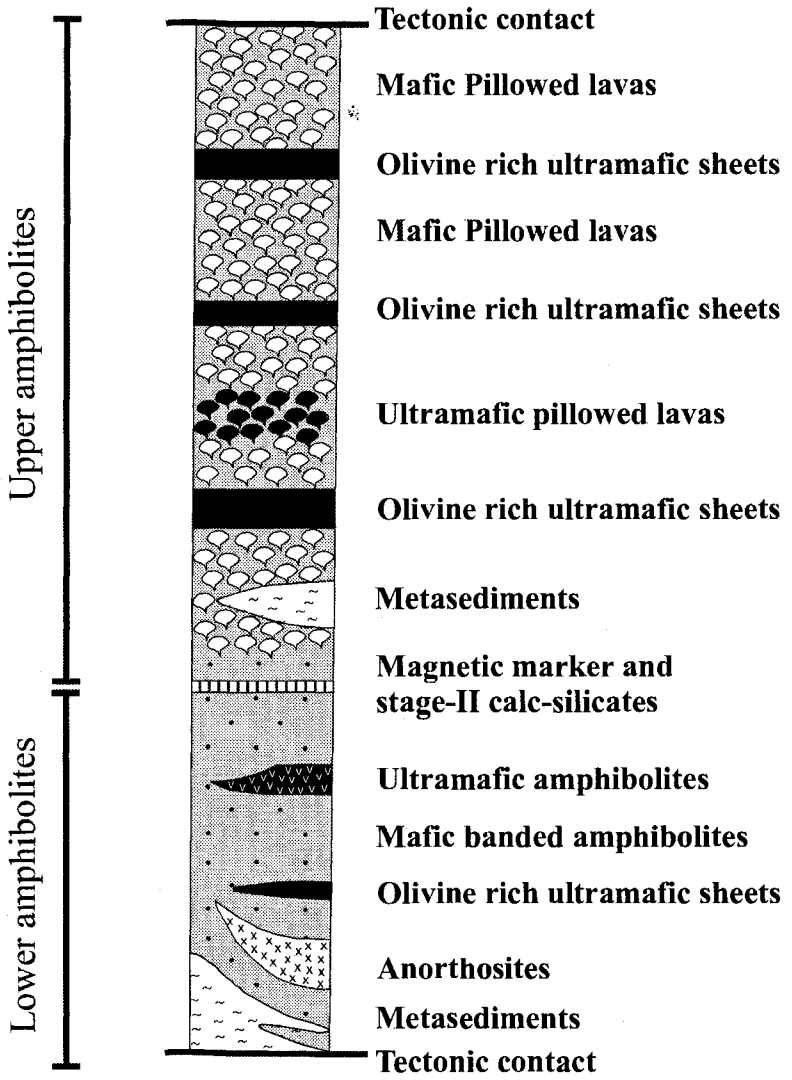

Figure 2.2. Simplified stratigraphic column of the Ivisaartoq greenstone belt (modified after Chadwick, 1990).

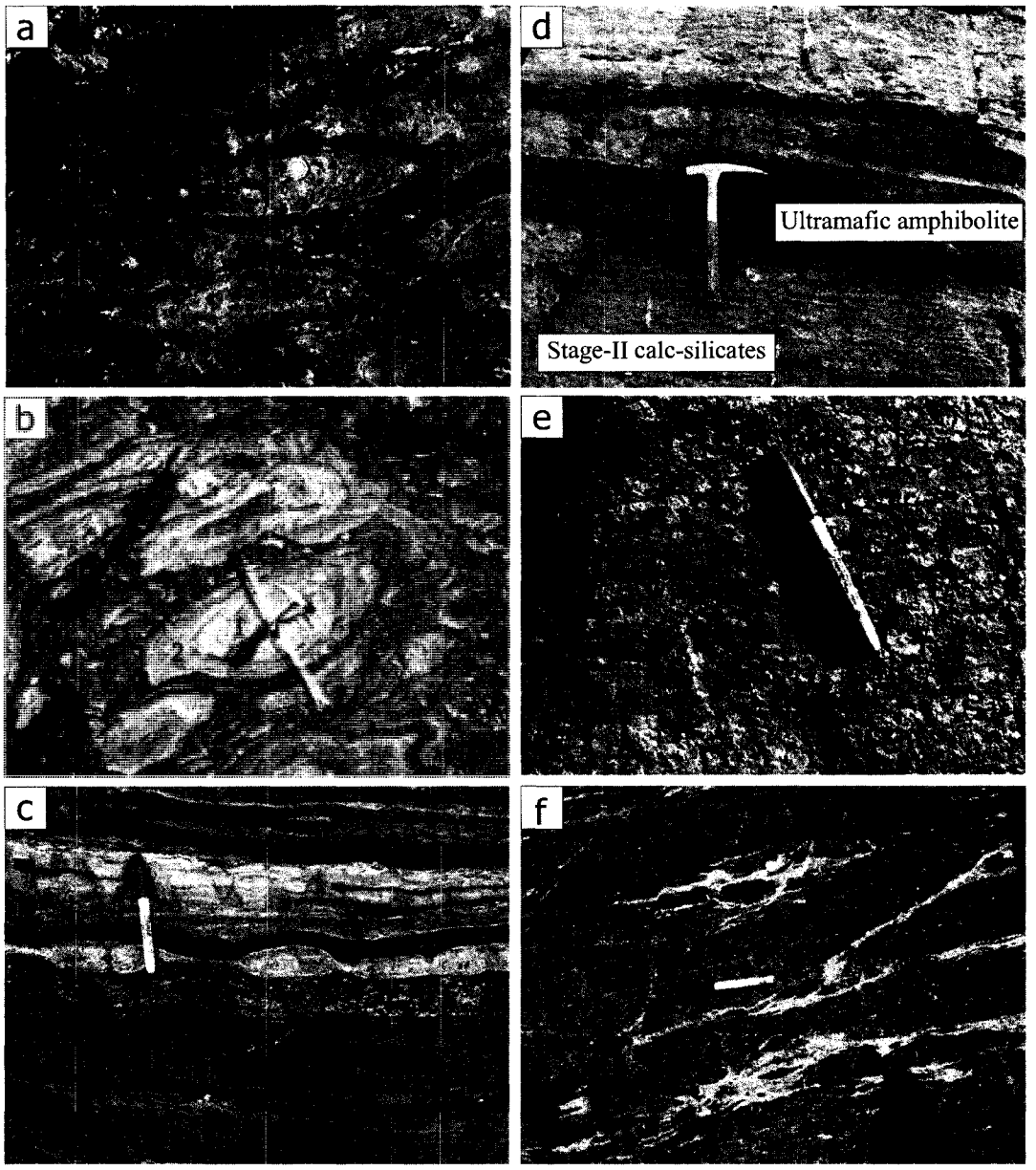

Figure 2.3. Field photographs of outcrops from the Ivisaartoq greenstone belt. (a) Pillowed lavas with well preserved drainage cavities (arrow), epidosite cores (stage-I metasomatism), and pillow rims. (b) Concentrically zoned pillow lava displaying epidote-rich inner pillow core (1), calc-silicate free outer pillow core (2), and amphibole-rich pillow rim (3). (c) Boudins of stage-II calc-silicate rocks. (d) Relict ultramafic enclave in a thick layer of epidote + diopside (assemblage IIa). (e) Coarse-grained epidote-rich assemblage IIc (arrows) partially replacing the assemblage IIa. (f) Brittle discordant veins of epidote (assemblage IIc) crosscutting mafic amphibolites.

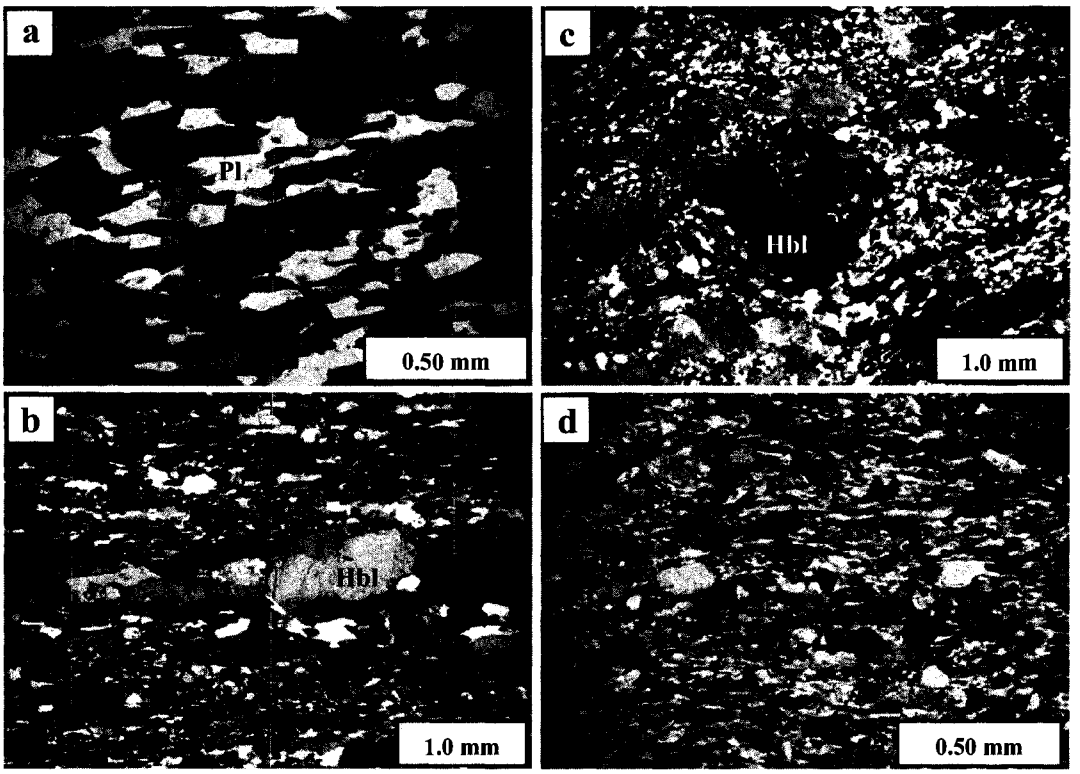

Figure 2.4. Photomicrographs of metavolcanic rocks. (a) Mafic amphibolites with characteristic foliation defined by oriented hornblende. (b) Mylonitic amphibolite with recrystallized ribbons of hornblende. (c) Mylonitic amphibolite with deformed porphyroclasts of hornblende embedded in a dynamically recrystallized groundmass. (d) Actinolite-rich ultramafic amphibolite. Plane polarized light for (a). Crossed polarized light for (b-d). Abbreviations: Hbl = hornblende; Pl = plagioclase.

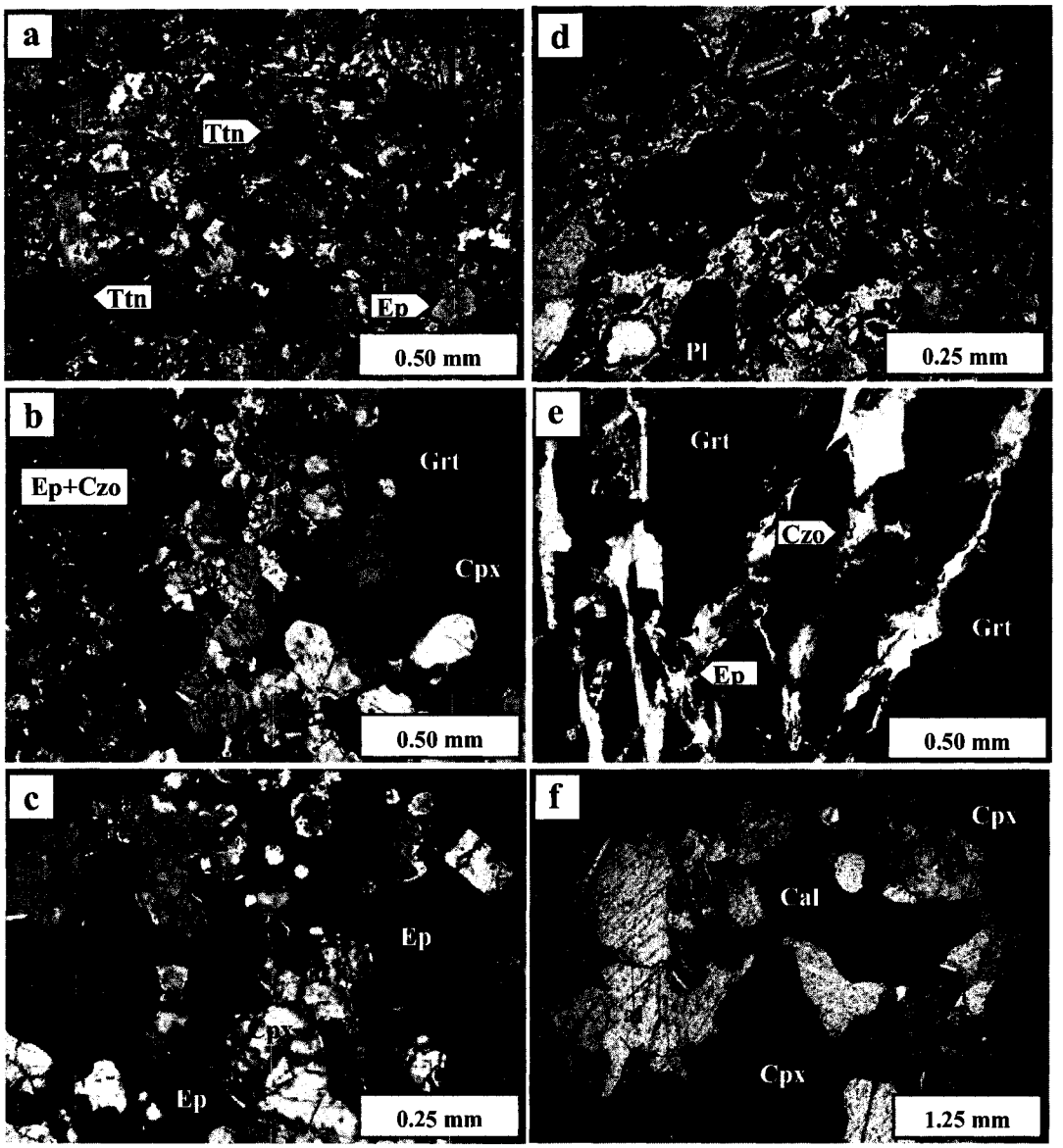

Figure 2.5. Photomicrographs of stage-II calc-silicate assemblages (crossed polarized light). (a) Fine grained epidote-rich metasomatic assemblage IIa. (b) Coarse grained garnet-clinopyroxene assemblage IIb overprinting the fine grained assemblage IIa. (c) Patchy epidote (metasomatic assemblage IIc) replacing clinopyroxene of the assemblage IIb. (d) Relict clinopyroxene and plagioclase partially replaced by epidote (arrows) of the assemblage IIc. (e) Fine veinlets of epidote and clinozoisite replacing fractured garnet porphyroblast. (f) Calcite overprinting the assemblage IIb. Abbreviations: Ttn = titanite; Ep = epidote; Grt = garnet; Cpx = clinopyroxene; Czo = clinozoisite; Cal = calcite.

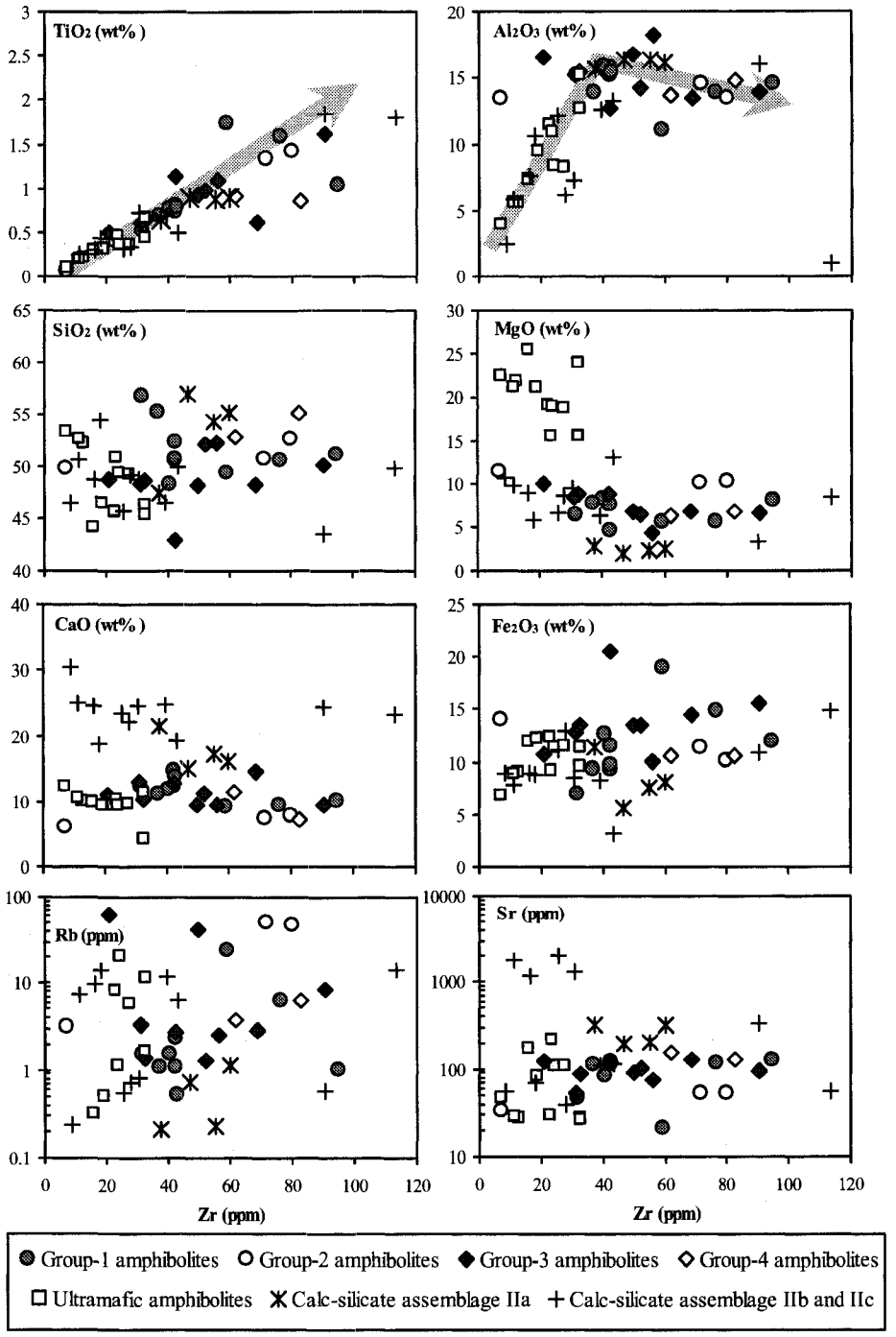

Figure 2.6. Variation diagrams of Zr versus selected major elements and LILE. Ultramafic amphibolites from Polat et al. (2008) and this study (Table 2.2). Amphibolites and their associated calc-silicates have been plotted to show the chemical changes associated with the stage II calc-silicate alteration. The amphibolites exhibit concentration levels of TiO_2, Al_2O_3, and MgO consistent with an ultramafic to mafic protolith. Arrows indicate differentiation trends (see text).

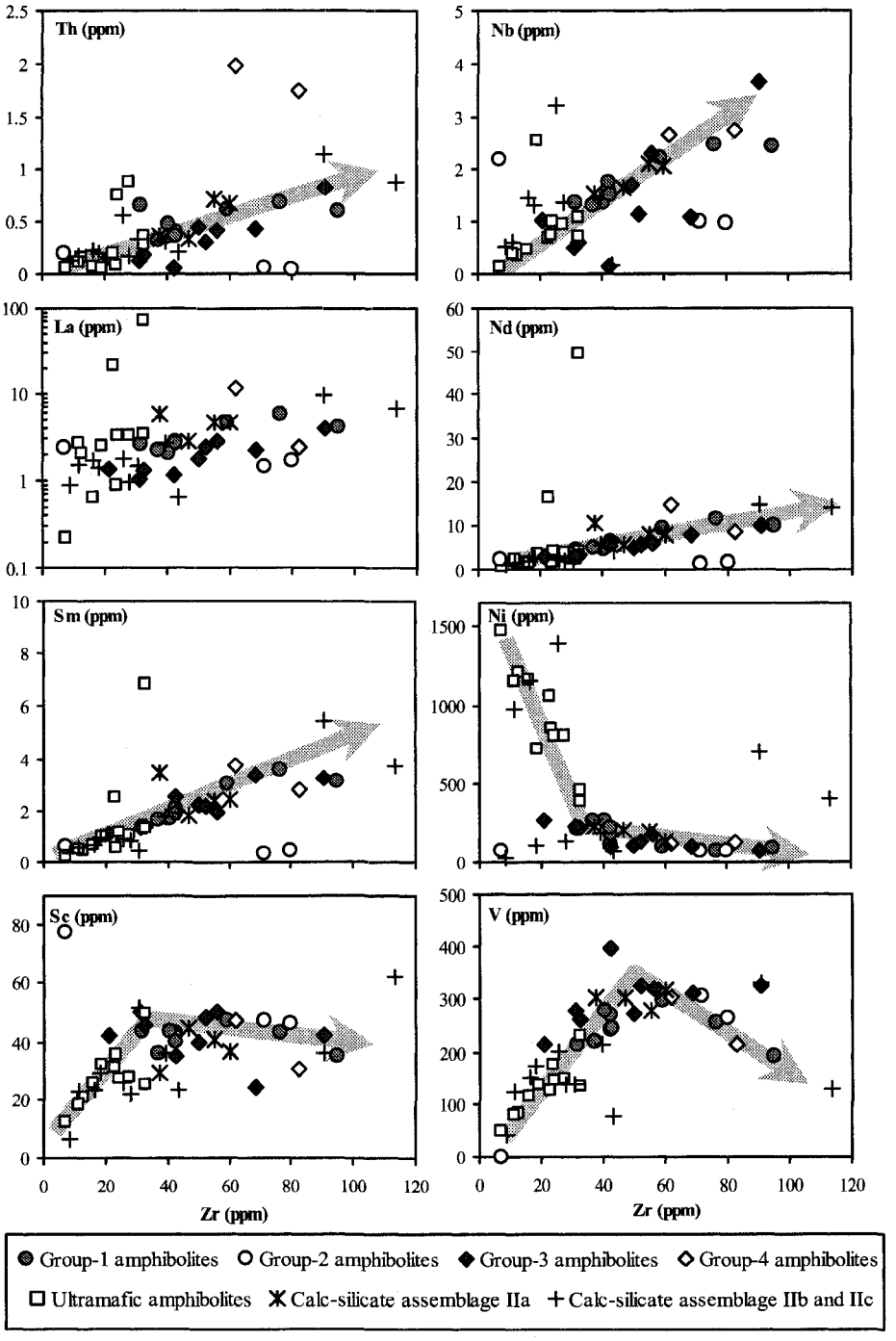

Figure 2.7. Variation diagrams of Zr versus selected REE, HFSE, and transition metals. Ultramafic amphibolites from Polat et al. (2008) and this study (Table 2.2). Differentiation trends are indicated by arrows. The trace element variations of amphibolites are consistent with an ultramafic to mafic protolith. The stage II calc-silicate rocks overlap the compositional trend of the amphibolites.

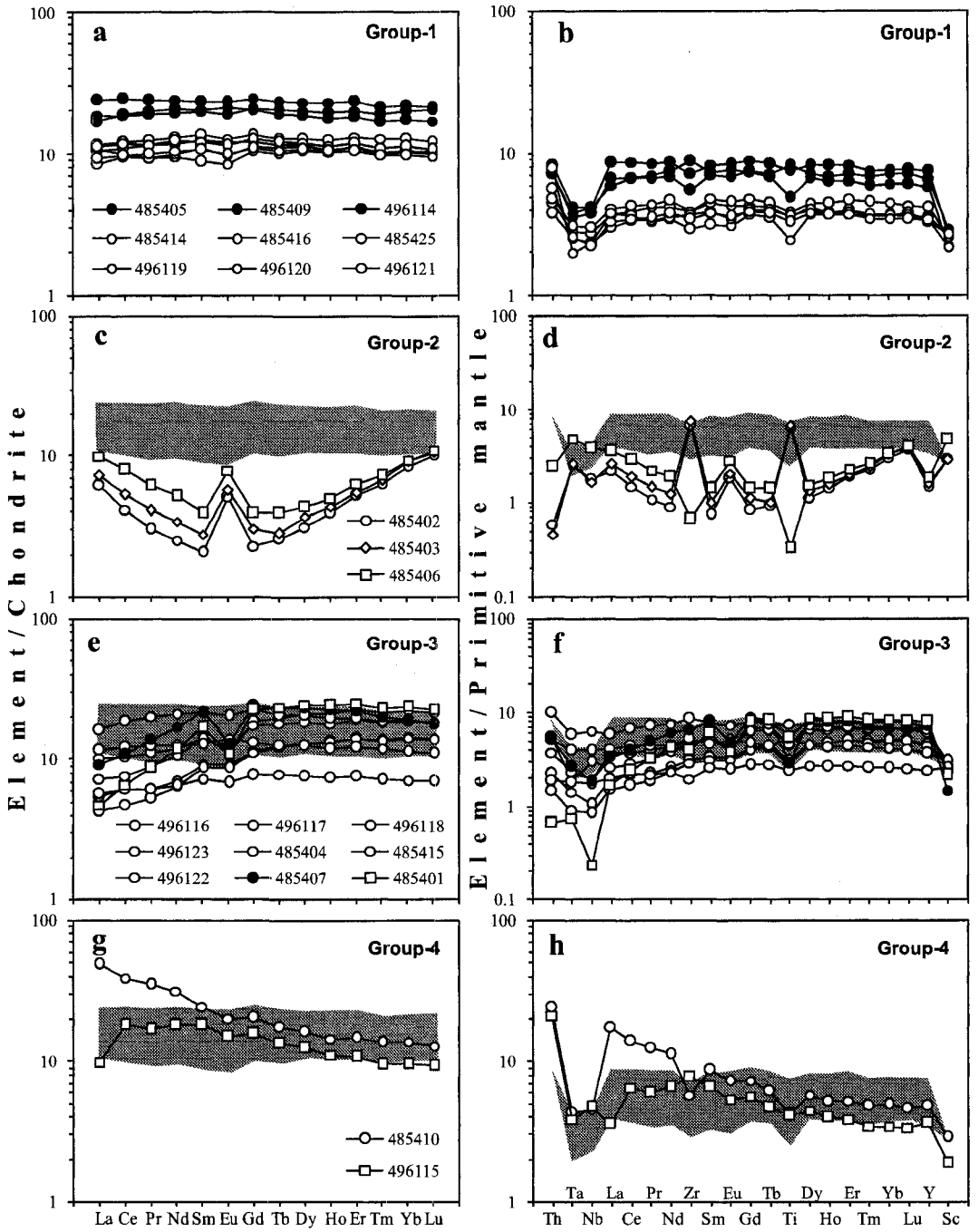

Figure 2.8. Chondrite- and primitive mantle-normalized diagrams showing different groups of mafic amphibolites. The compositional field of Group 1 amphibolites (shaded area) is overlap to Groups 2-4 amphibolites for intercomparisons. Chondrite normalization values from Sun and McDonough (1989), and primitive mantle normalization values from Hofmann (1988).

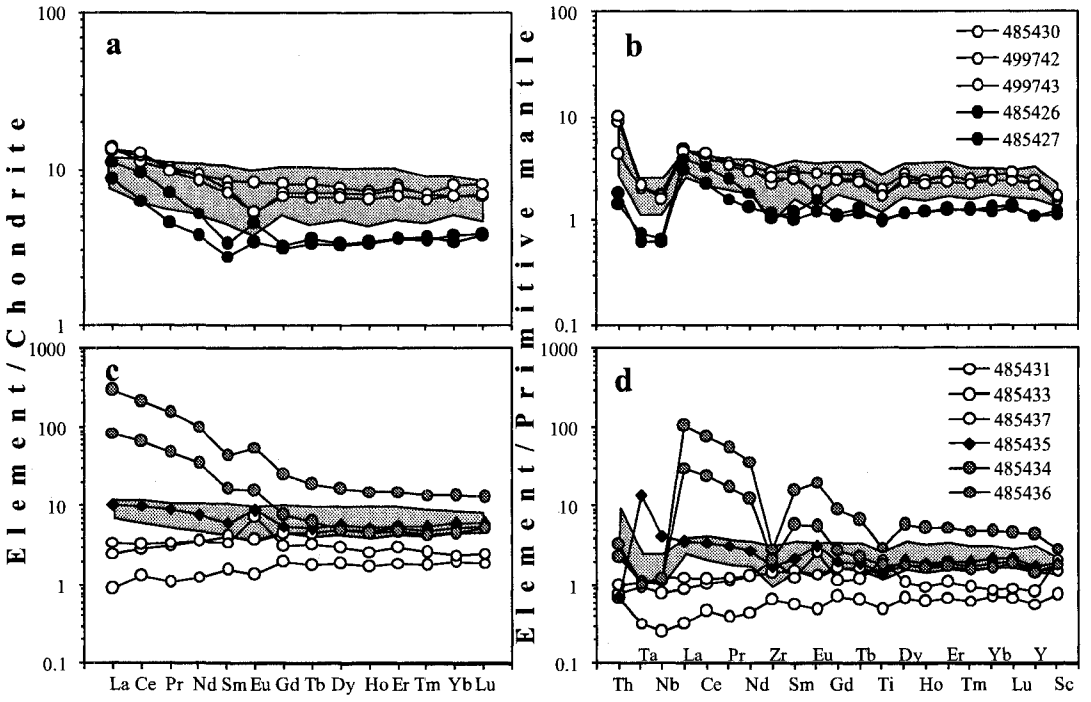

Figure 2.9. Chondrite- and primitive mantle-normalized diagrams of ultramafic amphibolites. Samples 499742 and 499743 from this study (Table 2.2), other ultramafic amphibolites from Polat et al. (2008). The shaded area represents the composition of the least altered ultramafic pillows and cumulates of Polat et al. (2007).

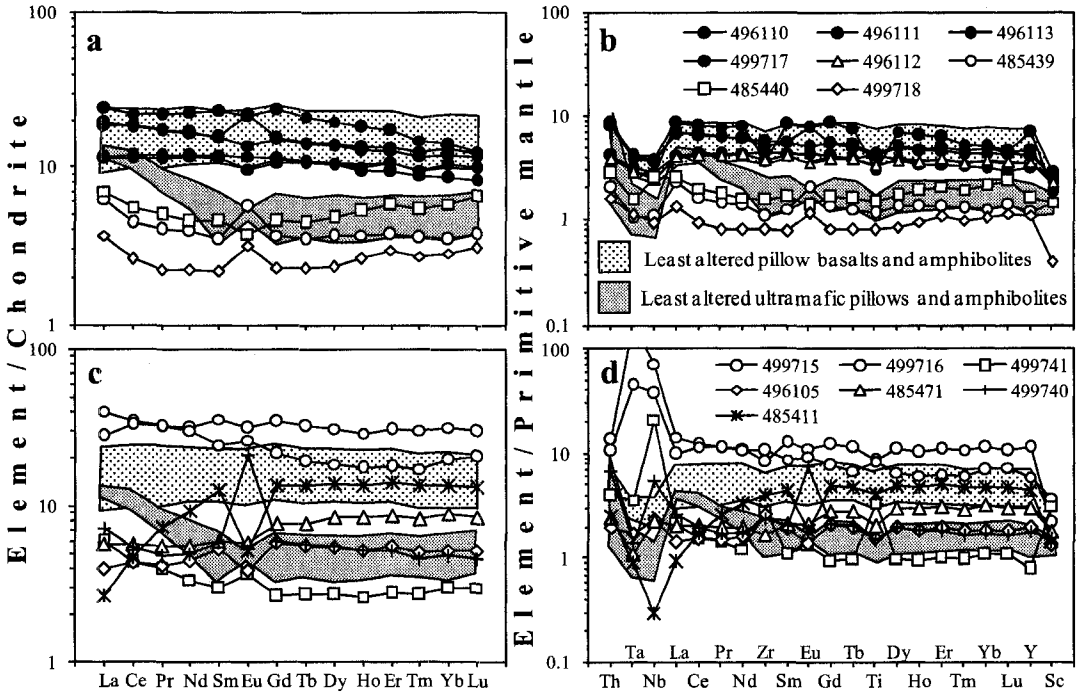

Figure 2.10. Chondrite- and primitive-mantle normalized diagrams of stage-II calc-silicate rocks. Filled circles = samples with the metasomatic assemblage IIa; other symbols = samples variably overprinted by the metasomatic assemblages IIb and IIc. Fields of the least altered mafic and ultramafic rocks from Polat et al. (2007, 2008) and this study.

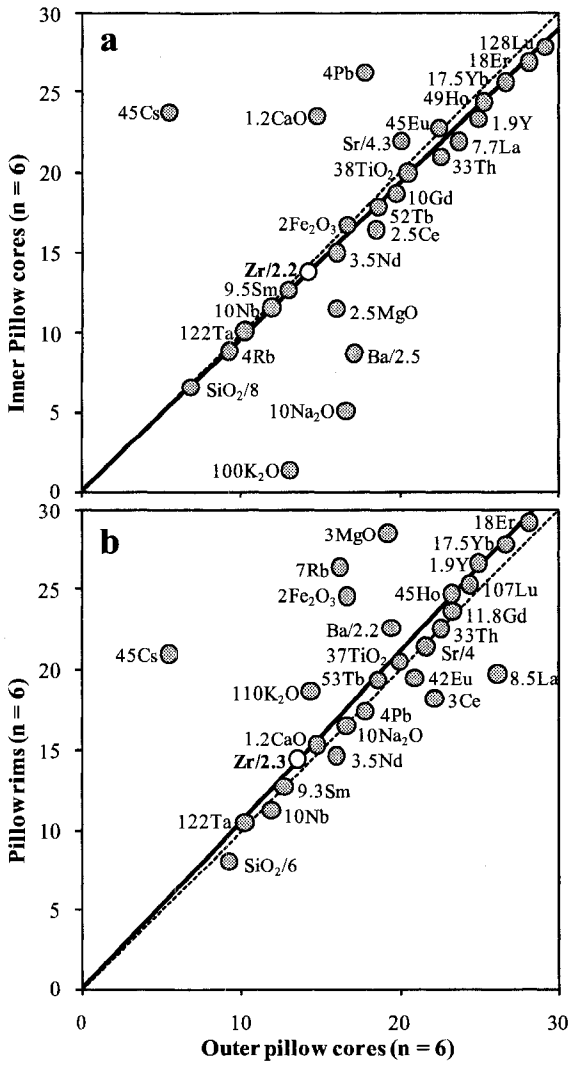

Figure 2.11. Isocon diagrams of pillow basalts with core and rim structures resulting from stage-I calc-silicate alteration (see also Figure 2.3b). Non-metasomatized outer pillow cores are compared with (a) strongly metasomatized inner pillow cores, and (b) amphibole-rich pillow rims. Sample compositions are average estimates from Polat et al. (2007) (See Table 2.2). The isocon plots (solid lines) are defined using Zr as immobile element. Dashed line represents the line of constant mass (see Grant, 1986). Major elements are plotted in weigh percent and trace elements in ppm. Data are scaled as indicated.

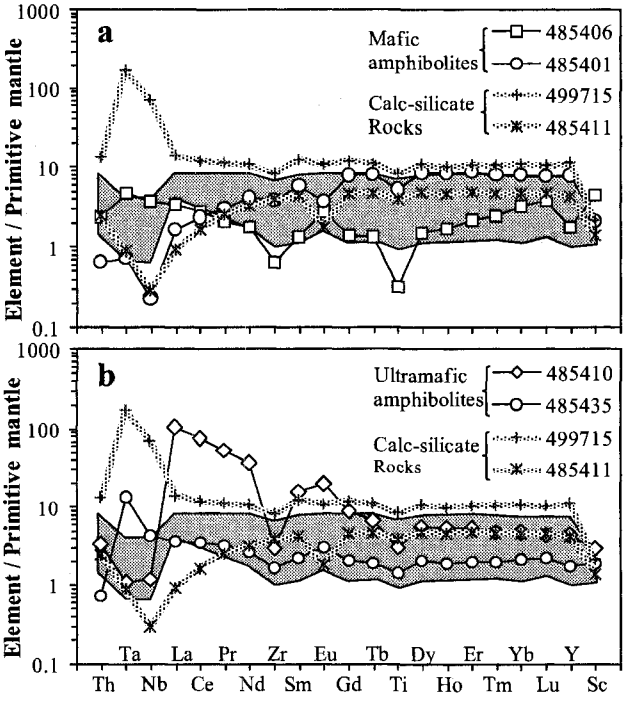

Figure 2.12. Summary of the geochemical patterns displayed by mafic (a) and ultramafic (b) amphibolites and associated stage-II calc-silicates. Shaded area represents the composition of least altered mafic and ultramafic metavolcanic rocks of the Ivisaartoq belt (from Polat et al., 2007, 2008; this study).

Table 2.1. Sequence of metasomatic assemblages of the stage-II calc-silicate rocks.

Assemblage	Mineralogy	Characteristics
Prograde assemblage IIa	Epidote + clinozoisite + clinopyroxene + quartz + plagioclase + titanite ± apatite	Pervasive alteration replacing mafic and ultramafic metavolcanic rocks. Occur as concordant boudinaged layers (Figs. 2.3c-d and 2.5a).
Prograde assemblage IIb	Garnet + clinopyroxene + titanite ± vesuvianite ± Scheelite	Coarse grained assemblages overprinting the metasomatic assemblage IIa and stage-I calc-silicate rocks (Fig. 2.5 b).
Retrograde assemblage IIc	Epidote + quartz ± tremolite ± calcite	Occur as patchy alterations replacing the prograde assemblages IIa and IIb, and as brittle irregular veins transecting the amphibolites and stage-I calc-silicate rocks (Figs. 2.3e-f and 2.5c-f).

Table 2.2. Major (wt.%) and trace element (ppm) concentrations and significant element ratios for mafic and ultramafic amphibolites and calc-silicate rocks

	Group-1 amphibolites								
	485405	485409	496114	485414	485416	485425	496119	496120	496121
SiO_2 (wt.%)	51.2	50.6	49.4	50.6	52.5	56.9	48.2	50.8	55.3
TiO_2	1.04	1.59	1.74	0.75	0.81	0.52	0.78	0.79	0.70
Al_2O_3	14.60	13.98	11.06	15.23	15.85	15.22	15.87	15.47	13.90
Fe_2O_3	12.03	14.85	19.00	11.58	9.41	7.08	12.73	9.75	9.46
MnO	0.19	0.22	0.30	0.18	0.22	0.17	0.20	0.20	0.18
MgO	8.14	5.67	5.67	7.62	4.59	6.46	8.27	7.57	7.73
CaO	10.12	9.53	9.23	12.46	14.71	12.45	11.91	13.90	11.19
Na_2O	2.36	2.95	2.80	1.39	1.71	1.08	1.74	1.25	1.36
K_2O	0.08	0.33	0.57	0.08	0.18	0.11	0.21	0.17	0.13
P_2O_5	0.19	0.26	0.26	0.05	0.07	0.04	0.06	0.06	0.06
LOI (%)	0.79	0.36	0.50	0.85	0.69	0.52	0.67	0.69	0.68
Mg-number (%)	57	43	37	57	49	64	56	61	62
Sc (ppm)	35	43	47	43	42	44	44	41	36
V	195	256	299	243	272	217	278	245	221
Cr	245	104	190	122	981	2030	275	269	235
Co	42	39	34	49	53	51	53	53	48
Ni	92	70	105	117	187	218	236	274	232
Rb	1.0	6.4	24.0	1.1	2.4	1.6	1.5	0.5	1.1
Sr	129.7	119.6	21.6	126.1	115.1	46.9	84.4	118.0	116.7
Y	25.5	32.7	28.5	15.3	18.0	14.5	15.6	16.5	14.8
Zr	94.8	76.4	59.1	42.4	42.4	31.5	40.5	42.6	37.1
Nb	2.45	2.48	2.21	1.61	1.76	1.36	1.37	1.49	1.29
Cs	0.05	0.38	3.33	0.14	0.27	0.29	0.06	LDL	0.21
Ba	17.4	47.4	53.4	17.5	24.3	31.4	14.2	25.0	23.1
Ta	0.15	0.17	0.14	0.11	0.12	0.08	0.10	0.11	0.10
Pb	2.01	6.59	4.50	1.88	1.57	2.79	3.63	2.18	1.35
Th	0.60	0.68	0.61	0.37	0.40	0.66	0.47	0.36	0.32
U	0.13	0.17	0.11	0.06	0.16	0.16	0.06	0.07	0.06
La	4.09	5.86	4.57	2.57	2.82	2.63	2.06	2.75	2.28
Ce	12.03	15.56	11.83	6.98	7.64	6.43	6.05	7.61	6.21
Pr	1.90	2.30	1.82	1.11	1.18	0.89	0.90	1.12	0.95
Nd	9.82	11.47	9.14	5.54	6.17	4.54	4.71	5.81	5.01
Sm	3.14	3.57	3.03	1.90	2.08	1.36	1.69	1.88	1.64
Eu	1.24	1.35	1.10	0.70	0.74	0.50	0.57	0.66	0.58
Gd	4.18	5.06	4.25	2.45	2.76	2.12	2.28	2.57	2.23
Tb	0.71	0.88	0.75	0.43	0.47	0.37	0.41	0.45	0.40
Dy	4.70	5.85	5.06	2.93	3.20	2.66	2.83	3.03	2.72
Ho	1.01	1.30	1.09	0.60	0.70	0.58	0.61	0.64	0.59
Er	2.99	3.85	3.32	1.85	2.16	1.73	1.82	1.94	1.73
Tm	0.43	0.54	0.48	0.26	0.33	0.26	0.26	0.28	0.25
Yb	2.83	3.56	3.28	1.70	2.08	1.68	1.72	1.86	1.61
Lu	0.43	0.54	0.51	0.25	0.31	0.27	0.26	0.27	0.24
(La/Yb)cn	0.97	1.11	0.94	1.02	0.91	1.05	0.81	1.00	0.95
(La/Sm)cn	0.82	1.03	0.95	0.85	0.85	1.22	0.77	0.92	0.87
(Gd/Yb)cn	1.20	1.15	1.05	1.17	1.07	1.02	1.07	1.12	1.12
(Eu/Eu*)cn	1.05	0.97	0.94	0.99	0.94	0.90	0.88	0.92	0.93
(Ce/Ce*)cn	1.04	1.02	0.99	0.99	1.01	1.01	1.07	1.04	1.02
Al_2O_3/TiO_2	14.05	8.78	6.36	20.31	19.60	29.11	20.47	19.59	19.93
Nb/Ta	15.97	14.84	15.65	14.47	14.43	17.09	13.78	13.61	12.75
Zr/Y	3.71	2.34	2.08	2.77	2.35	2.17	2.60	2.58	2.51
Ti/Zr	65.69	124.95	176.29	106.05	114.33	99.40	114.80	111.13	112.74
(Nb/Nb*)pm	0.64	0.51	0.54	0.67	0.67	0.42	0.57	0.61	0.62
(Zr/Zr*)pm	1.19	0.83	0.79	0.91	0.83	0.89	1.00	0.90	0.91
(Ti/Ti*)pm	0.73	0.90	1.14	0.85	0.84	0.67	0.92	0.87	0.86
ΣREE	49.50	61.70	50.23	29.29	32.64	26.02	26.17	30.87	26.44
North	64°43.838'	64°43.631'	64°43.657'	64°44.055'	64°44.069'	64°44.920'	64°43.927'	64°44.058'	64°44.005'
West	49°55.618'	49°55.799'	49°56.762'	49°56.286'	49°56.307'	49°57.202'	49°56.222'	49°56.756'	49°57.191'

LDL = Lower than detection limit

*Calc-silicates with metasomatic assemblage IIa, other calc-silicate samples are variably replaced by the assemblages IIb and IIc

[a] Avaraged pillow basalt composition from Polat et al. (2007)

Table 2.2. (*Continued*)

	Group-2 amphibolites			Group-3 amphibolites						
	485402	485403	485406	485401	485407	496116	496117	496118	496123	485404
SiO_2 (wt.%)	50.7	52.7	49.7	42.9	48.1	48.1	48.6	48.3	52.2	50.0
TiO_2	1.34	1.42	0.07	1.14	0.61	0.93	0.65	0.61	0.98	1.61
Al_2O_3	14.61	13.49	13.43	12.74	13.45	16.82	15.42	15.25	14.23	13.87
Fe_2O_3	11.46	10.21	14.11	20.55	14.53	13.50	13.59	12.84	13.58	15.62
MnO	0.13	0.13	0.17	0.15	0.13	0.14	0.19	0.21	0.21	0.23
MgO	10.15	10.26	11.40	8.76	6.77	6.79	8.84	8.47	6.46	6.62
CaO	7.41	7.96	6.11	12.89	14.50	9.44	10.40	13.13	11.21	9.41
Na_2O	3.70	3.45	3.18	0.90	1.77	3.34	2.13	1.08	0.80	2.15
K_2O	0.46	0.35	LDL	LDL	0.13	0.87	0.15	0.05	0.26	0.26
P_2O_5	LDL	LDL	1.78	LDL	0.02	0.08	0.05	0.04	0.08	0.19
LOI (%)	1.98	1.61	0.09	0.73	0.80	0.77	0.99	0.95	0.48	0.62
Mg-number (%)	64	67	62	46	48	50	56	57	48	46
Sc (ppm)	47	46	77	35	24	40	46	50	48	42
V	308	266	LDL	399	312	273	262	278	327	327
Cr	129	116	197	73	151	119	252	395	138	133
Co	37	35	46	58	49	48	56	58	48	43
Ni	73	72	75	97	101	106	227	239	139	74
Rb	52.5	48.6	3.2	2.8	2.9	42.3	1.4	3.4	1.3	8.4
Sr	52.9	53.6	34.2	119.4	127.7	92.1	88.5	53.8	104.5	93.4
Y	6.3	6.9	7.8	34.9	31.2	30.2	19.5	19.3	26.4	28.0
Zr	71.5	80.1	7.1	42.3	68.7	49.9	32.6	31.2	52.3	90.8
Nb	1.00	0.96	2.21	0.14	1.08	1.70	0.61	0.50	1.15	3.68
Cs	7.26	6.71	3.22	0.93	0.67	10.16	0.36	1.25	0.05	2.35
Ba	60.2	56.1	13.7	3.2	19.7	264.4	17.6	8.9	33.5	112.5
Ta	0.10	0.10	0.19	0.03	0.10	0.08	0.06	0.03	0.09	0.23
Pb	1.76	1.71	1.51	1.46	4.33	3.86	3.69	2.87	5.62	3.70
Th	0.05	0.04	0.20	0.06	0.44	0.45	0.18	0.12	0.31	0.81
U	0.02	0.02	0.03	0.04	0.21	0.11	0.10	0.04	0.09	0.19
La	1.49	1.74	2.41	1.16	2.25	1.78	1.33	1.04	2.46	3.93
Ce	2.62	3.34	5.03	4.21	6.87	4.83	3.87	3.00	6.53	11.79
Pr	0.29	0.39	0.58	0.84	1.30	0.85	0.59	0.51	1.05	1.92
Nd	1.19	1.62	2.45	5.54	8.03	5.01	3.36	3.04	5.61	9.94
Sm	0.31	0.42	0.59	2.56	3.39	2.22	1.41	1.34	2.14	3.27
Eu	0.29	0.33	0.45	0.62	0.76	0.64	0.53	0.50	0.72	1.18
Gd	0.46	0.61	0.80	4.55	4.85	3.78	2.31	2.25	3.54	4.55
Tb	0.10	0.10	0.14	0.86	0.86	0.73	0.46	0.45	0.66	0.76
Dy	0.78	0.93	1.08	6.14	5.82	5.24	3.24	3.23	4.59	5.14
Ho	0.22	0.24	0.28	1.36	1.26	1.18	0.75	0.74	1.01	1.09
Er	0.85	0.90	1.04	4.10	3.66	3.67	2.32	2.34	3.15	3.22
Tm	0.16	0.17	0.18	0.58	0.50	0.55	0.35	0.34	0.46	0.47
Yb	1.36	1.50	1.51	3.83	3.14	3.62	2.36	2.32	3.06	3.10
Lu	0.26	0.27	0.27	0.56	0.45	0.54	0.36	0.34	0.46	0.46
(La/Yb)cn	0.74	0.78	1.07	0.20	0.48	0.33	0.38	0.30	0.54	0.85
(La/Sm)cn	2.99	2.58	2.55	0.28	0.42	0.50	0.59	0.49	0.72	0.76
(Gd/Yb)cn	0.28	0.33	0.43	0.96	1.25	0.84	0.79	0.78	0.93	1.18
(Eu/Eu*)cn	2.32	1.95	2.01	0.55	0.57	0.68	0.90	0.88	0.79	0.93
(Ce/Ce*)cn	0.96	0.97	1.02	1.03	0.97	0.94	1.05	0.99	0.98	1.03
Al_2O_3/TiO_2	10.92	9.47	191.01	11.22	22.22	18.06	23.58	25.06	14.56	8.64
Nb/Ta	10.03	9.58	11.61	4.60	10.37	22.50	10.80	14.28	12.34	15.92
Zr/Y	11.43	11.67	0.92	1.21	2.20	1.65	1.67	1.62	1.98	3.25
Ti/Zr	112.11	106.60	59.09	161.01	52.81	111.87	120.46	117.00	112.06	106.04
(Nb/Nb*)pm	1.51	1.52	1.29	0.22	0.45	0.78	0.50	0.57	0.54	0.84
(Zr/Zr*)pm	8.20	6.76	0.41	0.79	0.92	1.05	1.05	1.08	1.06	1.11
(Ti/Ti*)pm	6.27	5.87	0.23	0.63	0.35	0.61	0.69	0.65	0.72	1.04
ΣREE	10.39	12.57	16.82	36.93	43.15	34.64	23.24	21.44	35.45	50.83
North	64°43.803'	64°43.803'	64°43.877'	64°43.771'	64°43.877'	64°43.839'	64°43.849'	64°43.904'	64°43.953'	64°43.813'
West	49°55.723'	49°55.723'	49°55.729'	49°55.605'	49°55.729'	49°56.668'	49°56.814'	49°56.527'	49°56.600'	49°55.612'

Table 2.2. (*Continued*)

	Goup-3 amphibolites		Goup-4 amphibolites		Ultramafic amphibolites					
	485415	496122	485410	496115	485426	485427	485430	485431	485433	485434
SiO_2 (wt.%)	52.3	48.7	52.9	55.1	52.4	52.7	46.4	53.4	44.2	45.7
TiO_2	1.09	0.50	0.91	0.86	0.21	0.21	0.44	0.10	0.30	0.39
Al_2O_3	18.27	16.56	13.73	14.83	5.67	5.59	12.68	3.98	7.40	11.48
Fe_2O_3	10.06	10.71	10.61	10.63	9.11	8.96	11.52	6.84	11.99	12.41
MnO	0.20	0.21	0.23	0.13	0.13	0.14	0.22	0.12	0.18	0.15
MgO	4.37	9.93	6.23	6.79	21.83	21.29	15.52	22.59	25.58	19.22
CaO	9.60	10.96	11.40	7.25	10.12	10.54	11.44	12.42	10.02	9.57
Na_2O	3.89	2.07	3.33	4.00	0.54	0.59	1.46	0.56	0.33	0.93
K_2O	0.17	0.32	0.50	0.24	0.02	LDL	0.30	0.04	LDL	0.15
P_2O_5	0.05	0.04	0.17	0.12	0.01	0.01	0.03	LDL	0.02	0.03
LOI (%)	0.45	1.23	0.65	1.06	3.02	2.69	1.75	2.69	6.35	3.81
Mg-number (%)	46	65	54	56	83	82	73	87	81	75
Sc (ppm)	50	42	47	31	21	19	26	12	26	31
V	321	216	304	214	82	80	136	48	116	127
Cr	233	301	405	255	12347	12146	1953	6534	10711	7020
Co	67	54	43	41	83	82	67	81	93	98
Ni	180	279	123	128	1211	1160	469	1479	1162	1064
Rb	2.6	62.6	3.7	6.4	LDL	LDL	11.6	LDL	0.3	8.4
Sr	74.4	123.6	154.4	129.0	28.4	29.5	28.0	47.0	178.2	30.7
Y	16.0	10.5	21.1	15.9	4.7	4.7	10.1	2.6	7.0	6.5
Zr	56.1	21.2	62.0	82.7	12.4	11.4	32.7	7.2	16.0	22.9
Nb	2.31	1.01	2.66	2.74	0.37	0.39	1.09	0.15	0.47	0.70
Cs	0.12	13.65	0.08	1.42	0.08	0.06	3.05	0.10	0.23	2.49
Ba	42.7	51.0	190.8	92.3	4.6	4.9	55.4	33.7	12.4	33.8
Ta	0.16	0.07	0.17	0.15	0.02	0.03	0.08	0.01	0.04	0.04
Pb	2.14	10.45	12.62	3.60	0.99	0.90	1.83	5.02	5.98	5.38
Th	0.42	0.15	1.98	1.75	0.15	0.12	0.36	0.06	0.07	0.19
U	0.11	0.04	0.50	0.30	0.26	0.43	0.13	0.02	0.03	0.24
La	2.81	1.38	11.79	2.42	2.11	2.76	3.38	0.22	0.64	21.39
Ce	7.65	3.92	24.67	11.47	4.01	6.05	7.12	0.84	1.91	42.49
Pr	1.19	0.58	3.34	1.61	0.43	0.67	0.95	0.11	0.31	4.73
Nd	5.81	3.09	14.85	8.59	1.75	2.47	4.39	0.62	1.74	16.70
Sm	1.95	1.12	3.73	2.79	0.43	0.51	1.31	0.25	0.66	2.53
Eu	0.82	0.40	1.16	0.87	0.20	0.26	0.47	0.08	0.23	0.91
Gd	2.65	1.56	4.13	3.19	0.62	0.67	1.64	0.41	0.97	1.62
Tb	0.46	0.29	0.64	0.50	0.12	0.13	0.30	0.07	0.18	0.24
Dy	3.11	1.91	4.08	3.14	0.82	0.84	1.96	0.49	1.30	1.33
Ho	0.67	0.42	0.82	0.63	0.19	0.19	0.40	0.10	0.28	0.27
Er	2.01	1.24	2.42	1.79	0.59	0.59	1.29	0.33	0.89	0.81
Tm	0.30	0.18	0.34	0.24	0.09	0.09	0.17	0.05	0.13	0.12
Yb	1.86	1.17	2.26	1.58	0.61	0.56	1.11	0.34	0.90	0.79
Lu	0.28	0.18	0.32	0.24	0.10	0.09	0.17	0.05	0.14	0.14
(La/Yb)cn	1.02	0.79	3.51	1.03	2.33	3.32	2.05	0.44	0.48	18.35
(La/Sm)cn	0.91	0.78	1.99	0.55	3.11	3.42	1.62	0.56	0.62	5.31
(Gd/Yb)cn	1.15	1.08	1.48	1.63	0.82	0.96	1.19	0.99	0.87	1.67
(Eu/Eu*)cn	1.10	0.92	0.91	0.89	1.16	1.37	0.99	0.77	0.88	1.37
(Ce/Ce*)cn	1.01	1.05	0.95	1.40	1.01	1.07	0.95	1.32	1.03	1.02
Al_2O_3/TiO_2	16.77	32.99	15.17	17.22	26.60	27.27	28.77	37.94	24.75	29.23
Nb/Ta	14.88	14.14	15.56	17.81	15.16	13.57	13.61	11.38	12.37	15.86
Zr/Y	3.51	2.01	2.94	5.21	2.67	2.41	3.22	2.81	2.30	3.51
Ti/Zr	116.41	142.17	87.51	62.47	102.91	107.91	80.93	87.36	111.91	102.73
(Nb/Nb*)pm	0.86	0.90	0.22	0.54	0.26	0.28	0.40	0.54	0.92	0.14
(Zr/Zr*)pm	1.17	0.80	0.58	1.18	1.01	0.71	0.95	1.29	1.05	0.25
(Ti/Ti*)pm	1.17	0.86	0.72	0.88	0.86	0.79	0.74	0.73	0.79	0.89
ΣREE	31.56	17.43	74.57	39.04	12.07	15.89	24.67	3.95	10.29	94.05
North	64°44.062'	64°43.891'	64°43.623'	64°43.764'	64°44.903'	64°44.903'	64°44.900'	64°44.900'	64°44.940'	64°44.940'
West	49°56.298'	49°57.609'	49°55.941'	49°56.692'	49°53.261'	49°53.261'	49°53.466'	49°53.466'	49°53.402'	49°53.402'

Table 2.2. (*Continued*)

	Ultramafic amphibolites					Calc-silicate rocks				
	485435	485436	485437	499742	499743	496110*	496111*	496113*	499717*	496112
SiO_2 (wt.%)	46.5	45.4	50.8	49.3	49.2	55.1	54.4	57.0	47.4	46.5
TiO_2	0.31	0.67	0.47	0.36	0.36	0.90	0.87	0.89	0.64	0.69
Al_2O_3	9.46	15.22	10.92	8.38	8.30	16.16	16.36	16.35	15.67	12.55
Fe_2O_3	12.28	9.63	9.28	11.51	11.59	8.21	7.65	5.71	11.43	8.30
MnO	0.20	0.23	0.16	0.20	0.20	0.15	0.13	0.11	0.23	0.35
MgO	21.18	24.10	15.53	19.07	18.91	2.40	2.37	2.03	2.87	6.32
CaO	9.52	4.51	10.36	9.43	9.78	16.20	17.23	14.99	21.51	24.76
Na_2O	0.50	0.24	2.39	1.39	1.44	0.73	0.91	2.73	0.11	0.29
K_2O	0.05	LDL	0.04	0.28	0.19	0.02	0.03	0.14	LDL	0.12
P_2O_5	0.02	0.02	0.02	0.03	0.03	0.08	0.08	0.07	0.11	0.06
LOI (%)	4.34	7.74	2.00	2.04	1.91	1.42	2.52	2.32	1.38	1.15
Mg-number (%)	77	83	77	77	76	37	38	41	33	60
Sc (ppm)	33	50	36	27	28	37	41	45	29	36
V	139	232	176	147	149	317	279	305	305	215
Cr	11378	1222	4698	1862	1896	250	375	208	245	168
Co	90	98	85	77	77	29	43	46	40	45
Ni	734	397	860	819	820	141	198	209	239	189
Rb	0.5	1.7	1.1	20.9	6.0	1.1	0.2	0.7	0.2	12.0
Sr	85.5	27.4	221.1	112.0	112.6	320.1	204.4	197.0	321.3	112.2
Y	7.8	19.9	3.6	10.7	9.7	19.4	17.9	13.4	30.2	15.1
Zr	18.9	32.6	23.5	24.3	27.7	60.1	55.1	46.9	37.6	39.4
Nb	2.56	0.71	0.76	0.99	0.94	2.05	2.11	1.64	1.54	1.41
Cs	0.07	0.88	0.32	10.41	3.10	0.10	0.08	0.06	0.06	5.50
Ba	16.1	9.2	37.0	61.2	19.4	11.5	8.1	27.0	12.5	16.4
Ta	0.55	0.04	0.04	0.09	0.09	0.15	0.16	0.12	0.11	0.11
Pb	2.53	2.14	5.85	3.61	3.21	10.12	4.96	3.30	15.62	2.30
Th	0.06	0.28	0.08	0.75	0.87	0.67	0.70	0.34	0.36	0.31
U	0.08	0.34	0.08	0.22	0.23	0.16	0.16	0.19	0.18	0.16
La	2.54	73.82	0.89	3.24	3.30	4.72	4.58	2.80	5.82	2.73
Ce	6.45	139.74	2.18	7.78	8.26	11.44	11.77	7.45	14.06	7.17
Pr	0.89	14.90	0.35	1.01	0.94	1.65	1.66	1.13	2.09	1.10
Nd	3.79	49.77	1.77	4.39	3.98	7.82	7.97	5.61	10.64	5.53
Sm	0.98	6.84	0.56	1.15	1.08	2.42	2.35	1.83	3.49	1.75
Eu	0.52	3.32	0.43	0.30	0.31	1.25	0.80	0.67	1.24	0.56
Gd	1.19	5.21	0.66	1.43	1.37	3.09	3.03	2.28	4.79	2.16
Tb	0.20	0.72	0.13	0.27	0.24	0.54	0.52	0.40	0.78	0.39
Dy	1.49	4.17	0.78	1.78	1.66	3.56	3.48	2.60	4.94	2.59
Ho	0.31	0.87	0.16	0.38	0.36	0.75	0.71	0.53	1.01	0.56
Er	0.95	2.58	0.51	1.24	1.10	2.23	2.12	1.54	2.84	1.74
Tm	0.15	0.36	0.07	0.18	0.16	0.32	0.30	0.22	0.38	0.24
Yb	1.01	2.25	0.41	1.28	1.10	2.12	1.95	1.39	2.29	1.67
Lu	0.16	0.33	0.07	0.21	0.17	0.31	0.29	0.20	0.32	0.25
(La/Yb)cn	1.69	22.06	1.47	1.70	2.02	1.50	1.58	1.36	1.71	1.10
(La/Sm)cn	1.62	6.78	1.00	1.76	1.93	1.23	1.22	0.96	1.05	0.98
(Gd/Yb)cn	0.95	1.87	1.29	0.90	1.00	1.18	1.26	1.33	1.69	1.05
(Eu/Eu*)cn	1.47	1.70	2.17	0.71	0.77	1.40	0.91	1.01	0.93	0.88
(Ce/Ce*)cn	1.03	1.01	0.94	1.04	1.13	0.99	1.03	1.01	0.97	1.00
Al_2O_3/TiO_2	30.34	22.65	23.44	23.19	22.82	17.92	18.75	18.30	24.55	18.15
Nb/Ta	4.66	16.42	17.42	11.49	10.72	13.46	13.16	13.54	13.88	12.34
Zr/Y	2.44	1.64	6.48	2.28	2.86	3.09	3.08	3.49	1.25	2.62
Ti/Zr	98.92	123.70	118.86	89.18	78.82	89.92	94.92	114.30	101.91	105.30
(Nb/Nb*)pm	2.64	0.06	1.13	0.26	0.23	0.47	0.48	0.69	0.43	0.62
(Zr/Zr*)pm	0.68	0.12	1.65	0.75	0.94	0.97	0.89	1.02	0.43	0.89
(Ti/Ti*)pm	0.73	0.50	1.90	0.67	0.73	0.83	0.83	1.12	0.42	0.88
ΣREE	20.64	304.87	8.94	24.64	24.02	42.21	41.52	28.68	54.70	28.43
North	64°44.943'	64°44.959'	64°44.962'	64°44.878'	64°44.878'	64°44.453'	64°44.460'	64°44.338'	64°44.458'	64°44.402'
West	49°53.379'	49°53.375'	49°53.313'	49°53.758'	49°53.758'	49°52.106'	49°52.433'	49°54.278'	49°52.393'	49°53.298'

Table 2.2. (*Continued*)

	Calc-silicate rocks									
	485411	499718	485439	485440	499715	499716	499740	499741	496105	485471
SiO_2 (wt.%)	54.4	46.5	50.6	48.7	43.4	49.8	45.6	48.7	49.1	54.5
TiO_2	0.87	0.17	0.24	0.31	1.84	1.80	0.31	0.72	0.33	0.43
Al_2O_3	16.36	2.46	5.86	7.68	15.98	1.03	12.17	7.25	6.15	10.64
Fe_2O_3	7.65	9.02	7.90	8.94	10.88	14.94	11.18	8.59	13.02	8.87
MnO	0.13	0.64	0.30	0.34	0.16	0.33	0.27	0.34	0.38	0.26
MgO	2.37	10.57	9.77	8.89	3.30	8.48	6.70	9.49	8.66	5.79
CaO	17.23	30.42	25.00	24.59	24.23	23.25	23.51	24.51	22.07	18.83
Na_2O	0.91	0.16	0.18	0.52	0.09	0.33	0.16	0.25	0.15	0.46
K_2O	0.03	0.02	0.07	0.06	LDL	0.06	0.06	0.11	0.09	0.15
P_2O_5	0.08	0.03	0.05	0.03	0.11	0.01	0.03	0.01	0.04	0.04
LOI (%)	2.52	6.21	1.96	1.67	1.09	0.01	1.42	0.80	0.36	0.66
Mg-number (%)	38	70	71	66	38	53	54	69	57	56
Sc (ppm)	23	6	23	23	36	62	26	52	22	29
V	77	41	123	151	332	129	203	139	138	174
Cr	73	47	6415	8290	1035	168	1780	1863	88	229
Co	16	11	90	106	66	81	100	152	55	46
Ni	71	29	976	1152	714	416	1391	2292	138	110
Rb	6.3	0.2	7.5	9.7	0.6	14.3	0.6	0.8	0.7	14.5
Sr	113.6	55.6	1773.8	1182.9	336.5	55.6	1991.8	1302.9	39.9	68.9
Y	19.3	4.7	4.9	6.8	50.3	26.1	7.6	3.4	8.5	13.1
Zr	43.4	8.6	11.4	16.3	90.6	113.4	25.8	30.6	27.9	18.1
Nb	0.17	0.54	0.62	1.43	42.54	22.39	3.21	12.36	1.37	1.31
Cs	11.63	0.37	0.46	8.84	0.34	0.38	0.28	0.30	0.33	1.05
Ba	18.0	3.5	67.4	60.2	11.7	285.5	12.9	62.9	5.5	53.9
Ta	0.04	0.04	0.04	0.06	7.01	1.79	0.05	0.14	0.07	0.04
Pb	3.71	2.55	22.27	19.12	12.47	5.52	35.85	31.35	3.77	4.13
Th	0.21	0.13	0.17	0.23	1.14	0.88	0.56	0.33	0.16	0.20
U	0.02	0.13	0.05	0.06	1.91	1.81	0.16	0.61	0.05	0.06
La	0.65	0.89	1.51	1.69	9.77	6.85	1.77	1.45	0.98	1.40
Ce	3.00	1.64	2.77	3.49	21.92	20.76	3.45	2.78	2.76	3.59
Pr	0.71	0.21	0.38	0.47	3.12	3.08	0.47	0.38	0.40	0.53
Nd	4.44	1.04	1.82	2.10	14.76	14.33	2.34	1.62	2.11	2.59
Sm	1.91	0.33	0.53	0.68	5.48	3.76	0.89	0.46	0.82	0.92
Eu	0.30	0.18	0.32	0.22	1.81	1.52	1.21	0.22	0.23	0.34
Gd	2.76	0.46	0.74	0.91	6.99	4.38	1.20	0.54	1.19	1.57
Tb	0.51	0.08	0.13	0.16	1.20	0.72	0.21	0.10	0.21	0.29
Dy	3.49	0.59	0.92	1.19	7.86	4.68	1.41	0.70	1.37	2.15
Ho	0.76	0.15	0.21	0.29	1.64	0.98	0.29	0.15	0.30	0.48
Er	2.33	0.49	0.61	0.94	5.05	2.96	0.85	0.47	0.91	1.43
Tm	0.34	0.07	0.09	0.14	0.77	0.44	0.12	0.07	0.13	0.21
Yb	2.22	0.46	0.57	0.94	5.21	3.21	0.79	0.50	0.86	1.47
Lu	0.34	0.08	0.09	0.16	0.75	0.52	0.12	0.08	0.13	0.22
(La/Yb)cn	0.20	1.30	1.78	1.21	1.26	1.44	1.51	1.97	0.77	0.64
(La/Sm)cn	0.21	1.70	1.78	1.55	1.12	1.15	1.25	1.97	0.75	0.95
(Gd/Yb)cn	1.01	0.80	1.05	0.78	1.09	1.10	1.23	0.89	1.12	0.87
(Eu/Eu*)cn	0.40	1.43	1.56	0.84	0.89	1.14	3.58	1.32	0.70	0.86
(Ce/Ce*)cn	1.07	0.91	0.88	0.94	0.96	1.09	0.92	0.90	1.06	1.00
Al_2O_3/TiO_2	18.75	14.71	24.13	25.17	8.70	0.57	38.98	10.03	18.78	24.47
Nb/Ta	4.89	12.30	15.09	24.17	6.07	12.53	58.84	85.61	19.96	30.38
Zr/Y	2.25	1.84	2.33	2.38	1.80	4.35	3.39	9.00	3.27	1.38
Ti/Zr	120.53	116.15	128.07	112.41	121.63	95.40	72.66	141.61	70.44	143.88
(Nb/Nb*)pm	0.19	0.65	0.51	0.94	5.19	3.72	1.31	7.28	1.40	1.01
(Zr/Zr*)pm	1.04	1.03	0.81	0.95	0.70	1.08	1.25	2.47	1.48	0.82
(Ti/Ti*)pm	0.84	0.96	0.90	0.89	0.77	1.26	0.73	3.45	0.79	0.70
ΣREE	23.76	6.68	10.70	13.38	86.33	68.19	15.10	9.52	12.40	17.19
North	64°43.691'	64°44.564'	64°44.859'	64°44.859'	64°44.279'	64°44.339'	64°44.878'	64°44.878'	64°44.253'	64°44.814'
West	49°55.570'	49°51.967'	49°53.752'	49°53.752'	49°53.227'	49°52.738'	49°53.758'	49°53.758'	49°52.855'	49°51.504'

Table 2.2. (*Continued*)

	Avarage Pillow basalts [a]		
	Pillow rims	Outer pillows	Inner Pillows
SiO_2 (wt.%)	48.5	55.7	52.1
TiO_2	0.55	0.54	0.53
Al_2O_3	14.19	14.47	14.08
Fe_2O_3	12.31	8.41	8.34
MnO	0.23	0.18	0.21
MgO	9.51	6.45	4.59
CaO	12.79	12.40	19.59
Na_2O	1.66	1.68	0.51
K_2O	0.17	0.13	0.01
P_2O_5	0.04	0.04	0.04
LOI (%)	0.92	1.17	0.91
Mg-number (%)	60	60	52
Sc (ppm)	44.5	43.8	43.5
V	224	227	213
Cr	328.97	307.09	721.71
Co	74.14	60.88	66.27
Ni	249.12	233.49	325.18
Rb	3.77	2.33	2.22
Sr	85.80	86.93	94.14
Y	14.01	13.19	12.25
Zr	33.2	31.4	30.3
Nb	1.12	1.20	1.16
Cs	0.47	0.12	0.53
Ba	49.72	43.07	21.89
Ta	0.09	0.08	0.08
Pb	4.36	4.49	6.57
Th	0.68	0.69	0.63
U	0.15	0.24	0.23
La	2.32	3.09	2.84
Ce	6.07	7.43	6.57
Pr	0.86	1.01	0.90
Nd	4.19	4.61	4.28
Sm	1.36	1.37	1.33
Eu	0.46	0.50	0.50
Gd	2.01	1.99	1.86
Tb	0.37	0.35	0.34
Dy	2.49	2.42	2.35
Ho	0.55	0.52	0.50
Er	1.62	1.57	1.49
Tm	0.24	0.23	0.22
Yb	1.59	1.53	1.46
Lu	0.24	0.23	0.22
(La/Yb)cn	0.98	1.36	1.31
(La/Sm)cn	1.07	1.41	1.34
(Gd/Yb)cn	1.02	1.05	1.03
(Eu/Eu*)cn	0.85	0.93	0.98
(Ce/Ce*)cn	1.04	1.02	0.99
Al_2O_3/TiO_2	25.65	26.71	26.83
Nb/Ta	13.07	14.23	14.00
Zr/Y	2.37	2.38	2.47
Ti/Zr	99.82	103.36	103.82
(Nb/Nb*)pm	0.36	0.33	0.35
(Zr/Zr*)pm	0.97	0.87	0.89
(Ti/Ti*)pm	0.74	0.75	0.76
ΣREE	24.37	26.84	24.86
North	64°44.906'	64°44.906'	64°44.906'
West	49°51.827'	49°51.827'	49°51.827'

Table 2.3. Selected compositional values and inter-element ratios for the least altered amphibolites and stage-II calc-silicate rocks.

	Mafic amphibolites	Ultramafic amphibolites	Stage-II calc-silicates
Mg-number	37 - 64	73 - 83	33 - 71
SiO_2 (wt.%)	48 - 57	46 - 53	43 - 57
Fe_2O_3	7.1 - 19	9.0 - 11.6	5.7 - 14.9
MgO	4.6 - 8.3	15.5 - 21.8	2.0 - 10.6
CaO	9.2 - 14.7	9.4 - 11.4	15.0 - 30.4
Zr (ppm)	32 - 95	11 - 33	9 - 113
Ni	70 - 274	469 - 1211	29 - 2292
Sc	35 - 47	19 - 28	6 - 62
Cr	104 - 2030	1862 - 12347	47 - 8290
ΣREE	26 - 62	12 - 25	7 - 86
(La/Yb)cn	0.81 - 1.11	1.7 - 3.3	0.2 - 2.0
(La/Sm)cn	0.77 - 1.22	1.6 - 3.4	0.2 - 2.0
(Gd/Yb)cn	1.0 - 1.2	0.8 - 1.2	0.8 - 1.7
Al_2O_3/TiO_2	6.4 - 29.1	22.8 - 28.8	0.6 - 39
Nb/Ta	12.8 - 17.1	10.7 - 15.2	4.9 - 86
Zr/Y	2.1 - 3.7	2.3 - 3.2	1.3 - 9.0
Ti/Zr	65.7 - 176.3	79 - 108	70 - 144
(Eu/Eu*)cn	0.9 -1.1	0.7 - 1.4	0.4 - 3.6
(Nb/Nb*)pm	0.4 - 0.7	0.2 - 0.4	0.2 - 7.3
(Zr/Zr*)pm	0.8 - 1.2	0.7 - 1.0	0.4 - 2.5
(Ti/Ti*)pm	0.7 - 1.1	0.7 - 0.9	0.4 - 3.45

CHAPTER 3

Geochemistry and tectonic origin of Mesoarchean oceanic crust in the Ujarassuit and Ivisaartoq greenstone belts, SW Greenland

3.1. Introduction

Archean greenstone belts are composed dominantly of volcanic rocks and include a significant fraction of siliciclastic, volcaniclastic, and chemical sedimentary rocks (Condie, 1994). Basaltic lava flows are prevalent and are commonly associated with felsic, intermediate, and ultramafic volcanic rocks. The lithogeochemical diversity of Archean greenstone belts is the product of complex igneous and sedimentological processes operating in a wide variety of tectonic settings either at intra-oceanic or intra-continental environments (Eriksson and Catuneanu, 2004). Accordingly, it has been suggested that greenstone belts may represent the volcanic remnants of Archean intra-oceanic island arcs, mid-ocean ridges, large igneous provinces, and intra-continental rifts (Bickle et al., 1994; Ohta et al., 1996; Polat et al., 1998; Polat and Kerrich, 2001; Hartlaub et al., 2004; Sandeman et al., 2004; Thurston and Ayres, 2004; Kusky, 2004). The recognition of intra-oceanic Archean greenstone belts is of fundamental importance because they provide invaluable information on the geodynamic origin of the Archean oceanic crust. In addition, given that oceanic volcanic rocks are less susceptible to crustal contamination than greenstone belts deposited on continental crust, they also provide information on thermal and geochemical characteristics of the Archean mantle (Bennett et al., 1993; Ohta et al., 1996; Pollack, 1997; Kerrich et al., 1999; Polat et al., 1999; Komiya et al., 2004; Condie, 2005a). However, the intra-oceanic origin of Archean greenstone belts is controversial because their original stratigraphic relationships and primary geochemical

signatures have been variably modified during hydrothermal alteration, regional metamorphism, polyphase deformation, and plutonism (Fryer et al., 1979; Gruau et al., 1992; Lahaye et al., 1995; Wilkins, 1997; Polat et al., 2003; Weiershäuser and Spooner, 2005).

The Nuuk region in southern West Greenland comprises several early to late Archean (3850-2800 Ma) tectono-stratigraphic terranes assembled into a single block in the late Archean (Friend et al., 1988; 1996; Nutman et al., 1989; McGregor et al., 1991; Friend and Nutman, 2005; Garde, 2007). The diachronous accretion of allochtonous terranes in the Nuuk region is one of the best documented examples of Archean collisional orogeny (Nutman and Friend, 2007). The collisional tectonic model proposed for the Nuuk region suggests that some greenstone belts may represent relict fragments of Archean ocean floor accreted onto continental crust during the closure of Archean ocean basins in the late stages of a Wilson cycle (cf. Casey and Dewey, 1984; Şengör, 1990). High-grade middle- to lower-crustal rocks are exposed in the Nuuk region at present. Therefore, the volcanic stratigraphy of most supracrustal belts is incomplete given that the uppermost crustal levels have been removed by erosion (Garde, 2007). Nevertheless, the region includes significant remnants of Mesoarchean intra-oceanic volcanic suites represented by rare island arc complexes (ca. 3071 Ma) in Qussuk and Bjørneøen (Garde, 2007) and incomplete fragments of supra-subduction zone oceanic crust (ca. 3075 Ma) in the Ivisaartoq greenstone belt (Polat et al., 2007, 2008).

The geochemical characteristics of metavolcanic rocks in the Ivisaartoq belt have been investigated by Polat et al. (2007, 2008) and Ordóñez-Calderón et al. (2008). However, no modern geochemical studies have been conducted in supracrustal rocks of the Ujarassuit Nunaat area to the NNW of the Ivisaartoq belt (Fig. 3.1). These rocks are

unofficially named as the Ujarassuit greenstone belt in this study. The Ujarassuit greenstone belt is dominated by hornblende-rich amphibolites with a basaltic composition (Fig. 3.1). The belt also includes volumetrically minor basaltic andesites, andesites, picrites, boninites, and volcanoclastic sedimentary rocks which are now, respectively, plagioclase-rich amphibolites, serpentinites, actinolite-tremolite-rich amphibolites, cummingtonite-rich amphibolites, biotite schists, and quartzitic gneisses (Table 3.1). This diverse lithological association provides an excellent opportunity to investigate Archean volcanogenic processes and geodynamic depositional environments.

In this contribution, we report new high-precision major and trace element data for 34 samples of metavolcanic rocks in the Ujarassuit greenstone belt with the following objectives: (1) to assess the effects of high-grade metamorphism and postmagmatic alteration on the primary geochemical signatures; (2) to investigate source characteristics and mantle processes; (3) to understand the geodynamic origin; and (4) for inter-comparison with well studied metavolcanic rocks of the Ivisaartoq and Qussuk belts (Garde, 2007; Polat et al., 2007, 2008; Ordóñez-Calderón et al., 2008). In addition, new geochemical data have been reported for 13 samples from metavolcanoclastic-sedimentary rocks in the Ivisaartoq and Ujarassuit greenstone belts to understand their provenance and to provide additional constraints on the depositional setting of these supracrustal belts.

3.2. Geological setting and field characteristics

Structural and U-Pb zircon geochronological studies have shown that the Nuuk region is composed of several Eo- to Neoarchean (3850-2800 Ma) tectono-stratigraphic terranes (Fig. 3.1) bounded by amphibolite facies mylonites (Friend et al., 1987, 1988,

1996; Nutman et al., 1989; McGregor et al., 1991; Crowley, 2002; Friend and Nutman, 2005). These allochtonous terranes comprise associations of tonalite-trondhjemite-granodiorite (TTG) orthogneisses and fragments of greenstone belts (Black et al., 1971; Moorbath et al., 1973; McGregor, 1973; Bridgwater et al., 1974; McGregor and Mason, 1977; Chadwick, 1990; Nutman et al., 1996; Garde, 2007; Polat et al., 2007). The region has undergone multiple phases of deformation and metamorphism at upper amphibolite facies conditions, which appears to be related to several episodes of terrane accretion operating between 2710 and 2960 Ma (Friend and Nutman, 1991; Friend et al., 1996; Friend and Nutman, 2005).

The Ivisaartoq greenstone belt is located within the ca. 3070-2970 Ma Kapisilik terrane (Fig. 3.1) (Chadwick, 1985, 1990). A minimum depositional age of ca. 3075 Ma has been constrained by U-Pb zircon geochronology in felsic volcaniclastic-sedimentary rocks (Friend and Nutman, 2005; Polat et al., 2007). The belt comprises a sequence of metamorphosed pillow basalts, with minor intercalations of picrites, gabbros, and volcaniclastic-sedimentary rocks (Chadwick, 1985, 1990; Polat et al., 2007, 2008). The Ivisaartoq belt has been subdivided into two lithotectonic groups (Chadwick, 1990). The upper group is less deformed than the lower group and contains primary magmatic features including pillow lavas (Fig. 3.2a), cumulate textures, and volcanic breccia (Chadwick, 1990; Polat et al., 2007, 2008). These primary features are rare in the lower lithotectonic group, which is more deformed. The base of the lower group includes a ca. 500 m thick unit of biotite schists and quartzitic gneisses interpreted as volcaniclastic-sedimentary rocks (Chadwick, 1990; this study) (Fig. 3.1). Biotite schists are the most abundant rock type (Table 3.1). Layers of quartzitic gneisses up to 1 m thick are locally intercalated. Despite strong deformation and penetrative foliation, the biotite schists

preserve rounded felsic cobbles 5 to 20 cm in length (Fig. 3.2b-c). In addition, a few layers of hornblende-rich amphibolites (up to 50 cm thick) parallel to the prevalent foliation are intercalated within this volcaniclastic-sedimentary unit.

The Ujarassuit greenstone belt appears to be the northern continuation of the Ivisaartoq belt (Fig. 3.1) (Hall and Friend, 1979; Chadwick, 1990; Friend and Nutman, 2005). The belt is less than 1 km wide owing to strong tectonic attenuation. Tonalite-trondhjemite-granodiorite plutons, now TTG-gneisses, intrude into the Ujarassuit greenstone belt. These TTG-gneisses have yielded Mesoarchean U-Pb zircon ages between 3070 and 2972 Ma (Friend and Nutman, 2005; Hollis et al., 2006a). These ages have been interpreted as the age of the magmatic event, and provide a minimum depositional age that is comparable with the ages reported for the Ivisaartoq greenstone belt (Friend and Nutman, 2005; Polat et al., 2007).

The Ujarassuit greenstone belt is dominated by hornblende-rich amphibolites (Table 3.1). They display homogenous or layered appearance at outcrop scale owing to variations in the abundance of plagioclase and hornblende. Primary volcanic features are not preserved. The contacts between amphibolites and orthogneisses are partially delimited by high grade mylonites (Fig. 3.2d-e) up to 0.5 m in thickness. The surrounding orthogneisses are strongly migmatitic (Fig. 3.2f) and include amphibolite xenoliths (Fig. 3.2g), which in some locations preserve evidence for an earlier tectonic foliation (Hollis et al., 2006b; this study). Amphibolites are also variably migmatitic. The proportion of quartzo-feldspathic leucosome increases towards the contacts with the orthogneisses (Fig. 3.2h). The amphibolites are complexly folded indicating that the belt has experienced polyphase deformation (Fig. 3.3a-d). Plagioclase-rich amphibolites, serpentinites, and actinolite-tremolite-rich amphibolites are locally intercalated with hornblende-rich

amphibolites (Table 3.1). The serpentinites and actinolite-tremolite-rich amphibolites (hereafter ultramafic rocks) occur as discontinuous boudinaged lenses 1 m to 1 km in length (Fig. 3.3e). They are strongly altered (Table 3.1), and rarely contain fresh olivine and clinopyroxene. Metagabbros with relict igneous textures are locally preserved. Biotite schists and quartzitic gneisses are minor components of the Ujarassuit greenstone belt (Fig. 3.3f). They occur as 0.5 to 1 m thick layers intercalated with hornblende-rich amphibolites. In some areas, this intercalation forms packages up to 30 m thick. Although no primary sedimentary structures are preserved in the Ujarassuit belt, biotite schists are petrographically similar to those exposed in the lower volcaniclastic-sedimentary unit of the Ivisaartoq greenstone belt (Chadwick, 1990). Cummingtonite-rich amphibolites are rare. They are intercalated with hornblende-rich amphibolites and ultramafic rocks.

The Ujarassuit greenstone belt displays evidence for postmagmatic hydrothermal alteration, which is indicated by localized concordant calc-silicate rocks and rusty layers of pyrite-bearing quartz-rich rocks (Fig. 3.3g-h). The calc-silicate rocks are parallel to the regional foliation, and have been affected by recumbent folding (Fig. 3.3c). These rocks are composed of diopside, epidote, and garnet. Similar calc-silicate layers in the Ivisaartoq belt have been ascribed to high temperature metasomatism coeval with the prograde stage of the regional metamorphism (Polat et al., 2007; Ordóñez-Calderón et al., 2008).

3.3. Structural characteristics of Ujarassuit greenstone belt

The internal structural characteristics of the Ujarassuit greenstone belt and its structural relationships with the surrounding TTG-gneisses were investigated (Fig. 3.4). The belt exhibits evidence for at least three major phases of ductile deformation at upper

amphibolite facies metamorphic conditions (cf. Hall and Friend, 1979; Friend and Nutman, 1991; Hollis et al., 2006b). The earliest deformation event (D_1) is indicated by relict rootless folds (F_1), which folded an earlier tectonic foliation (S_1) (Fig. 3.3a). The S_1 foliation is locally preserved in amphibolite xenoliths within the orthogneisses. A second phase of deformation (D_2) transposed S_1 into parallelism with the regional S_2 foliation. D_2 deformation resulted in tight F_2 isoclinal and recumbent folds (Fig. 3.3b-c). Felsic leucosome in migmatitic amphibolites and calc-silicate layers are folded around F_2 recumbent folds (Figs. 3.2h and 3.3c). The latest phase of ductile deformation (D_3) is characterized by upright F_3 folds that refolded and reoriented earlier tectonic structures (Fig. 3.3d).

The orientations of D_2 and D_3 structures in the supracrustal rocks and TTG-gneisses are conformable (Fig. 3.4). In the western flank of the belt, the π-fold axis (182°/23°) calculated from poles to S_2 foliations display a similar orientation to those of small-scale parasitic isoclinal F_2 fold axes with mean attitude of 171°/44° (Fig. 3.4a-b). In the eastern flank, isoclinal F_2 fold axes display comparable mean attitude (151°/36°) to those in the western flank (Fig. 3.4e). However, poles to S_2 foliations plot along a major circle with a π-fold axis (79°/55°) oblique to F_2 (Fig. 3.4d-e). In the east the belt is more attenuated and changes its direction from NS to NW which has been interpreted to reflect large-scale fold superposition during late Archean upright folding (see Hall and Friend, 1979). Accordingly, the oblique π-fold axis likely represents interference patterns owing to moderately plunging F_3 upright folds.

Mineral stretching lineations are defined by preferred orientation of hornblende, quartz ribbons, and stretched garnet. Lineations (L_2) in the western flank (155°/44°) parallel F_2 axes, and therefore they may have been developed during D_2 deformation and

reoriented during F_3 folding (Fig. 3.4b-c). In contrast, mineral lineations (L_3) in the eastern flank possess a mean attitude (34°/59°) that is closer to the inferred F_3 π-axis (Fig. 3.4f). This suggests that L_3 lineations were likely formed during D_3 deformation. The prevalence of L_3 lineations and dominant east dipping direction of S_2 foliations imply that strong tectonic attenuation and more intense strain in the eastern flank of the Ujarassuit greenstone belt resulted from D_3 deformation (Fig. 3.1).

3.4. Petrography

The mineralogical characteristics and interpreted protoliths of different rock types are presented in Table 3.1. The primary igneous mineralogy and sedimentary textures are not preserved. These rocks consist of amphibolite facies metamorphic assemblages with penetrative foliation.

Hornblende-rich amphibolites (Fig. 3.5a) are composed of hornblende (60-70 %), plagioclase (20-35 %), quartz (5-10 %), and accessory (< 2%) minerals such as zircon, apatite, magnetite, and titanite. Garnet, biotite, and cummingtonite are locally present. Biotite generally replaces hornblende and garnet.

Cummingtonite-rich amphibolites are rare (Fig. 3.5b; Table 3.1). They are rich in cummingtonite (40-50%) and poor in hornblende (< 5%). They contain minor amounts of anthophyllite (up to 10%), and abundant quartz (10-15%) and plagioclase (30-50%). Cummingtonite-rich amphibolites are spatially associated with ultramafic rocks.

Plagioclase-rich amphibolites are rare (Table 3.1). They contain less hornblende (10-20%), but more plagioclase (60-70%) and quartz (5-15 %) than hornblende-rich amphibolites.

Ultramafic rocks are composed of hydrated metamorphic assemblages giving rise to variable mineralogical compositions (Fig. 3.5c; Table 3.1). They include serpentine, talc, actinolite, tremolite, and rarely cummingtonite. Some ultramafic rocks (498257 and 498262) are composed mainly of weakly serpentinized olivine (Fig. 3.5d) and clinopyroxene with characteristic mesh texture.

Biotite schists are composed of quartz (15-40%), plagioclase (50-70%), and biotite (10-30%) (Fig. 3.5e; Table 3.1). Accessory minerals may include garnet (<3%), epidote, magnetite, and titanite. Some samples (498242 and 498243) contain muscovite (< 5%) and microcline (5%). Cummingtonite, anthophyllite, and hornblende occasionally occur in amounts up to 15% (sample 498292 and 498297). Tourmaline (2%) was found only in biotite schists from the Ivisaartoq greenstone belt (Fig. 3.1).

Quartzitic gneisses were found only in the Ivisaartoq belt (Table 3.1). They are fine-grained and consist of quartz (70%), plagioclase (10%), biotite (10-15%), and muscovite (5-20%) (Fig. 3.5f). Locally, they contain garnet (2%) and hornblende (3%). Accessory minerals include magnetite, rare tourmaline, and significant amounts of fine-grained zircon.

3.5. Analytical methods and sampling

Samples were pulverized using an agate mill in the Department of Earth and Environmental Sciences of the University of Windsor, Canada. Major elements and some trace elements (Sc and Zr) were analyzed on a Thermo Jarrel-Ash ENVIRO II ICP-OES in Activation laboratories Ltd. (ATCLABS) in Ancaster, Canada. The samples were mixed with a flux of lithium metaborate and lithium tetraborate, and fused at 1000 °C in an induction furnace. The molten beads were rapidly digested in a solution of 5% HNO_3

containing an internal standard, and mixed continuously until complete dissolution. Loss on ignition (LOI) was determined by measuring weight loss upon heating to 1100 °C over a three hour period. Totals of major elements are 100 ± 1 wt% and their analytical precisions are 1-2% for most major elements (Table 3.2). The analytical precisions for Sc and Zr are better than 10%.

Transition metals (Ni, Co, Cr, and V), REE, HFSE, and LILE were analyzed on a high-sensitivity Thermo Elemental X7 ICP-MS in the Great Lakes Institute for Environmental Research (GLIER), University of Windsor, Canada, following the protocols of Jenner et al. (1990). Sample dissolution was conducted under clean lab conditions with doubly distilled acids. Approximately 100-130 mg of sample powder was used for acid digestion. Samples were dissolved in Teflon bombs in a concentrated mixture of HF-HNO_3 at a temperature of 120 °C for 3 days and then further attacked with 50% HNO_3 until no solid residue was left. Hawaiian basalt standards BHVO-1 and BHVO-2 were used as reference materials to estimate analytical precisions (Table 3.2). Analytical precisions are estimated as follows: 3-10% for REE, Y, Nb, Ta, Rb, Sr, Cs, Ba, and Co; 10-20% for Ni, and Th; and 20-30% for U, Pb, V, and Cr.

Major element analyses were recalculated to 100 wt.% anhydrous basis for inter-comparisons. Chondrite and primitive mantle reservoir compositions are those of Sun and McDonough (1989) and Hofmann (1988), respectively. The Eu (Eu/Eu*), Ce (Ce/Ce*), Nb (Nb/Nb*), Ti (Ti/Ti*), and Zr (Zr/Zr*) anomalies were calculated with the following equation after Taylor and McLennan (1985):

$$A/A^* = A_N/([(B_N)(C_N)]^{1/2}$$

Where

A/A* = Element anomaly

A_N = Chondrite normalization for Eu and Ce anomalies, and primitive mantle normalization for Nb, Ti, and Zr anomalies.

B_N and C_N = Neighboring immobile elements as follow: Sm and Gd for Eu/Eu*; La and Pr for Ce/Ce*, Th and La for Nb/Nb*, Nd and Sm for Zr/Zr*, and Tb and Dy for Ti/Ti*.

Mg-numbers (%) were calculated as the molecular ratio of $Mg^{2+}/(Mg^{2+} + Fe^{2+})$ where Fe^{2+} is assumed to be 90% of the total Fe.

3.6. Geochemistry

3.6.1. Amphibolites

Hornblende- and cummingtonite-rich amphibolites show a basaltic composition on the Zr/Ti versus Nb/Y diagram (Figs. 3.6 and 3.7; Table 3.1). They have been subdivided into four major groups on the basis of their chondrite- and primitive mantle-normalized trace element patterns (Fig. 3.8a-h; Table 3.3). Groups 1, 2, and 3 are hornblende-rich amphibolites. They show similar mineralogical composition and can only be distinguished on the basis of their trace element characteristics. In contrast, Group 4 amphibolites are cummingtonite-rich amphibolites (Table 3.1).

Hornblende-rich amphibolites (Groups 1-3) possess Zr/Y ratios (Zr/Y = 1.5-4.6) similar to those of modern tholeiitic basalts (Zr/Y = 1.3-3.1) (see Barrett and MacLean, 1994). They have Mg-numbers ranging from 44 to 67 and variable concentrations of SiO_2 (47.2-54.8 wt%), TiO_2 (0.4-1.2 wt%), Fe_2O_3 (9.9-15.7 wt%), Al_2O_3 (13.1-16.3 wt%), MgO (5.6-11.3 wt%), Zr (18-67 ppm), and ΣREE (13.1-41.2 ppm) (Fig. 3.7, Table 3.3). Groups 1-3 amphibolites in the Ujarassuit belt, and Groups 1-3 amphibolites in the Ivisaartoq belt (Ordóñez-Calderón et al., 2008), display collinear trends for major

elements, HFSE, REE, and transition metals on variation diagrams of Zr indicating comparable compositions (Table 3.3). However, in the Ujarassuit belt they have slightly lower concentrations of Ni (59-190 ppm) than those in the Ivisaartoq belt (74-279 ppm) (see Ordóñez-Calderón et al., 2008). They show variable Eu (Eu/Eu* = 0.63-1.06), Zr (Zr/Zr* = 0.94-1.63), and Ti (Ti/Ti* = 0.59-0.94) anomalies on chondrite- and primitive mantle-normalized diagrams (Fig. 3.8).

Group 1 amphibolites occur in the eastern and western flanks of the Ujarassuit greenstone belt (Fig. 3.8a-b). This amphibolite group displays near-flat REE patterns (La/Sm_{cn} = 0.77-1.14; Gd/Yb_{cn} = 1.10-1.21) and negative Nb anomalies (Nb/Nb* = 0.60-0.79). These trace element characteristics are similar to those shown by well preserved pillow basalts in the Ivisaartoq greenstone belt (Polat et al., 2007). In addition, Group 1 amphibolites in this study are compositionally similar to the least altered Group 1 amphibolites in the Ivisaartoq greenstone belt (Ordóñez-Calderón et al., 2008).

Group 2 amphibolites occur in the western flank of the Ujarassuit greenstone belt (Fig. 3.8c-d). The trace element patterns of this group of amphibolites are characterized by depleted LREE (La/Sm_{cn} = 0.53-1.02) and slightly fractionated HREE (Gd/Yb_{cn} = 0.68-0.95) patterns. In addition, they show pronounced negative Nb (Nb/Nb* = 0.32-0.67) anomalies. The trace element patterns of Group 2 amphibolites are comparable with those of Group 3 amphibolites in the Ivisaartoq greenstone belt (Ordóñez-Calderón et al., 2008) and amphibolites in the Qussuk greenstone belt in the Akia terrane (Garde, 2007).

Group 3 amphibolites occur in the western flank of the Ujarassuit belt (Fig. 3.1). They exhibit depleted LREE patterns (La/Sm_{cn} = 0.69-0.84; Gd/Yb_{cn} = 0.96-1.22) and lack significant Nb (Nb/Nb* = 0.92-1.15) anomalies (Fig. 3.8e-f). The trace element

patterns of this group of amphibolites are comparable to those of average modern N-MORB (Hofmann, 1988).

Relative to Groups 1-3 amphibolites, cummingtonite-rich amphibolites (Group 4) have higher SiO_2 (50.9-53.7 wt%), MgO (10.8-13.1 wt%), and Mg-numbers (67-76) (Table 3.3), and lower CaO (7.2-9.5 wt%), Fe_2O_3 (6.9-10.8 wt%), TiO_2 (0.26-0.33 wt%), Zr (20-29 ppm), and ΣREE (15.9-19.8 ppm) (see Tables 3.3 and 3.5). They possess high Ni (124-178 ppm), Cr (99-765 ppm), and Sc (27-46 ppm) contents. Group 4 amphibolites possess higher Al_2O_3/TiO_2 (44-71), lower Ti/Zr (55-97), and comparable Nb/Ta (14-21) ratios than those of Group 1-3 amphibolites (Table 3.5). They display enriched LREE (La/Sm_{cn} = 1.64-2.42) patterns and flat to fractionated HREE (Gd/Yb_{cn} = 0.57-1.01) patterns (Fig. 3.8g-h). In addition, Group 4 amphibolites have pronounced negative Nb (Nb/Nb* = 0.28-0.42) and Ti (Ti/Ti* = 0.59-0.74) anomalies, and minor positive Eu (Eu/Eu* = 1.01-1.24) anomalies.

Plagioclase-rich amphibolites have higher contents of SiO_2 (55.3-67.4 wt%) than Group 1-4 amphibolites (Tables 3.3 and 3.5). On Zr/Ti versus Nb/Y diagram they straddle the field of basalts and andesites (Fig. 3.6). In addition, they exhibit Zr/Y (5.9-15.9) ratios comparable with those of transitional (Zr/Y = 4.5-7.0) and calc-alkaline (Zr/Y > 7.0) volcanic rocks (see Barrett and MacLean, 1994). They have variable Mg-numbers (48-62) and Zr (87-146 ppm) contents (Table 3.3). Relative to Groups 1-3 amphibolites, they possess comparable concentrations of TiO_2 (0.57-1.0 wt%), lower Fe_2O_3 (3.5-13.4 wt%), HREE (7.6-11.5 ppm), Sc (11-18 ppm), and V (86-152 ppm), and higher contents of Th (1.2-4.8 ppm) and LREE (74.9-94.2 ppm). On chondrite- and primitive mantle-normalized diagrams (Fig. 3.9a-b), they exhibit fractionated LREE and HREE patterns

(La/Sm_{cn} = 1.78-3.21; Gd/Yb_{cn} = 2.61-3.12), pronounced negative Nb anomalies (Nb/Nb* = 0.21-0.55), and slight negative Eu anomalies (Eu/Eu* = 0.87-0.93).

3.6.2. Ultramafic rocks

Ultramafic rocks have high MgO (19.7-39.1 wt%) contents and loss-on-ignition (LOI = 1.5-10.3 wt%) values that are consistent with hydrated ultramafic lithologies (Table 3.1 and 3.3). Relative to Groups 1-3 amphibolites, they have lower concentration levels of CaO (0.5-9.5 wt%), Al_2O_3, (3.8-9.4 wt%), TiO_2 (0.11-0.42 wt%), Zr (4.2-20.7 ppm), and ΣREE (2.4-17.2 ppm) and higher Ni (658-2212 ppm), Cr (2377-6312 ppm), and Co (74-130 ppm) contents. On chondrite- and primitive mantle-normalized diagrams (Fig. 3.9c-d) they display variably depleted to slightly enriched LREE (La/Sm_{cn} =0.65-1.83) and fractionated to flat HREE (Gd/Yb_{cn} = 0.47-1.32) patterns. Ultramafic rocks show negative Nb anomalies (Nb/Nb* = 0.31-0.94) and variable Eu (Eu/Eu* = 0.34-1.03), Zr (Zr/Zr* = 0.84-3.29), and Ti (Ti/Ti* = 0.8-1.59) anomalies.

3.6.3. Biotite schists and quartzitic gneisses

Biotite schists have large variations of SiO_2 (53.2-72.4 wt%), MgO (1.3-8.4 wt%), Fe_2O_3 (2.5-10.2 wt%), TiO_2 (0.32-0.92 wt%), and Al_2O_3 (12.6-24.0 wt%) contents (Fig. 3.7) (Table 3.4). Niobium and ΣREE (54-342 ppm) display positive correlations with Zr (108-253 ppm) (Fig. 3.7). They have relatively high concentrations of transition metals Ni (53-328 ppm), Sc (7-37 ppm), Cr (51-753 ppm), and V (49-187 ppm), which are comparable to those of Groups 1-3 amphibolites (Table 3.5). On the Zr/Ti versus Nb/Y diagram, they plot in the field of andesites and basaltic andesites (Fig. 3.6). On chondrite- and primitive mantle-normalized diagrams, they display fractionated REE patterns with

high La/Sm_{cn} (1.94-10.08) and Gd/Yb_{cn} (0.79-4.64) ratios (Fig. 3.10a-d). In addition, they display pronounced negative Nb (Nb/Nb* = 0.02-0.51), Eu (Eu/Eu* = 0.58-0.95), and Ti (Ti/Ti* = 0.42-0.82) anomalies, and negative to positive Zr (Zr/Zr* = 0.70-1.81) anomalies.

Quartzitic gneisses in the Ivisaartoq belt are silica rich (SiO_2 = 72.0-81.6 wt%). Relative to the biotite schists, they are enriched in Zr (237-702 ppm) and ΣREE (288-409 ppm), and depleted in Al_2O_3 (10.9-11.7 wt%), MgO (0.5-1.6 wt%), TiO_2 (0.15-0.61 wt%), and transition metals (Ni, Co, and Sc < 15 ppm) (Table 3.5). They have Zr/Ti and Nb/Y ratios similar to those of rhyolites and dacites (Fig. 3.6). On chondrite and primitive mantle normalized diagrams (Fig. 3.10e-f), they display slightly fractionated REE patterns (La/Sm_{cn} = 1.11-1.47; Gd/Yb_{cn} = 0.80-1.75). In addition, they possess pronounced negative Nb (Nb/Nb* = 0.38-0.48), Eu (Eu/Eu* = 0.40-0.53), and Ti (Ti/Ti* < 0.1) anomalies, and negative to positive Zr (Zr/Zr* = 0.78-1.43) anomalies.

3.7. Discussion

3.7.1. Relationship between deformation and metamorphism

The juxtaposition of Eo- to Neoarchean (3850-2800 Ma) allochtonous terranes of the Nuuk region occurred during several collisional events that is reminiscent of Phanerozoic-style continent-continent collisional orogens (Friend et al. 1987, 1988; Nutman et al. 1989; Crowley et al., 2002; Friend and Nutman, 2005; Nutman et al., 2004; Nutman and Friend, 2007). In the Ujarassuit greenstone belt, the effects of collisional tectonics are well indicated by high-grade mylonites (Fig. 3.2d-e), migmatitic TTG-gneisses and amphibolites (Fig. 3.2f-h), strong ductile tectonic attenuation and transposition (Fig. 3.3a-c), and complete obliteration of primary depositional features.

Relict D_1 structures likely formed during ca. 2960 Ma amphibolite facies metamorphism, which appears to be related to the collision of the Isukasia and Kapisilik terranes (Friend and Nutman, 2005; Nutman and Friend, 2007). The orientations of F_2 isoclinal folds and L_2 mineral stretching lineations (Fig. 3.4) in the Ujarassuit greenstone belt are remarkably similar to those reported in the tectono-stratigraphic terranes to the southwest of the studied area (Friend and Nutman, 1991). Therefore, it is likely that D_2, and the subsequent D_3 deformation, occurred in the late Archean during or after the final amalgamation of the different tectono-stratigraphic terranes of the Nuuk region between 2650 and 2600 Ma (see Nutman and Friend, 2007).

3.7.2. Assessing element mobility in amphibolites

It is widely accepted that the concentration of HFSE (Nb, Ta, Th, Zr, Ti), REE (mainly Gd-Lu), and transition metals (Ni, V, Cr, Sc, Co) is not significantly changed during sea floor hydrothermal alteration and regional metamorphism (Hart et al., 1974; Condie et al., 1977; Ludden and Thompson, 1979; Ludden et al., 1982; Middelburg et al., 1988; Ague, 1994; Arndt, 1994; Staudigel et al., 1996; Alt, 1999; Polat and Hofmann, 2003). However, some studies have shown that high-temperature alteration and high-grade metamorphism can modify the concentrations of those normally 'immobile' elements (Rubin et al., 1993; Van Baalen, 1993; Tilley and Eggleton, 2005; Galley et al., 2000; Jiang et al., 2005; Ordóñez-Calderón et al., 2008). In the Ujarassuit greenstone belt, the occurrence of high-temperature calc-silicate alteration, sulphide-bearing quartz-rich layers (Fig. 3.3g-h), and migmatites (Fig. 3.2f-h) suggest that the near-primary geochemical signatures of volcanic rocks could have been disturbed.

Several studies have shown that partial melting of amphibolites produces andesitic to tonalitic melts in equilibrium with restitic amphibolites rich in garnet (e.g. Hartel and Pattison, 1996; Storkey et al., 2005). For example, restitic amphibolites in the Harts Range Meta-Igneous Complex, central Australia, display near-flat LREE patterns and systematic enrichment of HREE (Lu up to 100 x chondrite) with increasing compatibility in chondrite-normalized diagrams (Storkey et al., 2005). These geochemical characteristics result from preferential retention of the heavier REE in garnet during partial melting. Accordingly, low modal abundance of garnet (0 to 2%), absence of quartzo-feldspathic segregations in the sampled outcrops, and lack of significant enrichment of HREE (Fig. 3.8) indicate that Groups 1-4 amphibolites are not the residues after partial melting.

Group 1 amphibolites (Fig. 3.8a-b) in the Ujarassuit greenstone belt are geochemically similar to least altered pillow basalts and Group 1 amphibolites in the Ivisaartoq greenstone belt (Polat et al., 2007; Ordóñez-Calderón et al., 2008). The presence of well preserved pillow lavas (Fig. 3.2a) and relict igneous clinopyroxene in the Ivisaartoq belt has allowed reliable identification of near-primary magmatic geochemical signatures (Polat et al., 2007, 2008). Therefore, the coherent near-flat REE patterns and negative Nb-Ta anomalies in Group 1 amphibolites (Fig. 3.8a-b) likely reflect the near-primary magmatic geochemical signature.

Group 2 amphibolites display depleted LREE patterns (Fig. 3.8c-d) similar to those reported in ca. 3071 Ma amphibolites (metabasalts) of the Qussuk peninsula in the Akia terrane (Garde, 2007), and Group 3 amphibolites of the Ivisaartoq belt (Ordóñez-Calderón et al., 2008). There are two alternative explanations for these trace element patterns. First, LREE may have been lost during amphibolite facies metamorphism (e.g.,

Ordóñez-Calderón et al., 2008). Second, Group 2 amphibolites retain their magmatic geochemical signatures (cf. Garde, 2007). It is noteworthy that amphibolites with stronger LREE depletion ($La/Yb_{cn} < 0.70$) possess the most pronounced negative Ti anomalies ($Ti/Ti^* < 0.75$) (Fig. 3.11). It is unlikely that this anomaly is related to fractionation of Fe-Ti oxides given the positive correlation of Ti with Zr (Fig. 3.7). Mineralogical studies have revealed that titanite and hornblende accounts for large amounts of the LREE, Ti, Th, Nb, and Ta in amphibolites (Mulrooney and Rivers, 2005; Storkey et al., 2005). It is possible that breakdown of hornblende and titanite during high-grade metamorphism could have caused losses of LREE, Nb, and Ta, resulting in LREE-depleted patterns and more pronounced negative Nb-Ta anomalies (Fig. 3.8c-d). In the Ivisaartoq belt, there is evidence for meter-scale mobility of LREE, Nb and Ta, and to a minor extent Ti, during the prograde stage of regional metamorphism (Ordóñez-Calderón et al., 2008). However, the pronounced negative Ti anomalies could also indicate residual amphibole in the mantle source. Geochemical studies of Mesozoic volcanic complexes indicate that fractional crystallization increases the ΣREE concentration and may result in progressive flattening of LREE patterns (e.g., Green et al., 2006). It is unlikely that Groups 1 and 2 amphibolites (Fig. 3.8) are related by fractionation given that they possess comparable concentrations of MgO, Zr, HREE, Ni, Cr, and Sc (Tables 3.3 and 3.5). Although we cannot rule out a primary origin for the trace element characteristics of Group 2 amphibolites, their geochemical similarity to well documented altered amphibolites in the Ivisaartoq belt and field evidence for high-temperature alteration (Fig. 3.3g-h) suggest that the trace element patterns of Group 2 amphibolites resulted from postmagmatic element mobility.

Group 3 amphibolites (Fig. 3.8e-f) have trace element patterns very similar to those of average modern N-MORB (Hofmann, 1988). The consistent parallelism of trace element patterns, lack of pronounced anomalies of Ce and Eu, and the absence of calc-silicate alterations indicate that they retain near-primary geochemical compositions.

Group 4 amphibolites do not display evidence for silicification, calc-silicate alteration, or anomalous enrichment of major elements such as SiO_2, CaO, Na_2O, or K_2O (Table 3.3, Fig. 3.7). Thus, their low abundance of HFSE and REE is not the result of trace element dilution owing to metasomatism. In addition, several samples (498228, 498239, and 498248) collected along a traverse of approximately 8 km (Fig. 3.1) display remarkably similar trace element patterns (Fig. 3.8g-h). Therefore, we suggest that Group 4 amphibolites have retained their primary geochemical signatures. Accordingly, their low Ti and Zr contents, enriched LREE patterns, sub-chondritic Gd/Yb_{cn} ratios, negative Nb-Ta anomalies, and high Al_2O_3/TiO_2 ratios (44 to 71) are consistent with a boninite-like geochemical signature (cf. Fallon and Crawford 1991; Polat et al., 2002; Smithies et al., 2004; Manikyamba et al., 2005). It is noteworthy that cummingtonite-rich amphibolites (Group 4) display lower concentrations of CaO and Fe_2O_3 and higher concentration of MgO than hornblende-rich amphibolites (Groups 1-3). The low content of CaO may have favored metamorphic reactions resulting in cummingtonite as opposed to hornblende, given that this mineral is a Ca-poor Mg-rich amphibole (cf. Evans and Ghiorso, 1995; Smith and Phillips, 2002).

Plagioclase-rich amphibolites exhibit crossed LREE patterns that are likely the result of LREE mobility (Fig. 3.9a-b). However, their transitional to calc-alkaline compositions ($Zr/Y > 5.0$) and overall enrichment of LREE and HFSE (mainly Th, Nb, Ta, and Ti) are consistent with basaltic andesite and andesite precursors (Fig. 3.6).

3.7.3. Origin of ultramafic rocks

Ultramafic rocks display mineralogical evidence for advanced serpentinization (Fig. 3.5c-d). Therefore, it is likely that the variations of LREE patterns are the result of postmagmatic alteration (Fig. 3.9c-d). Heavy REE, however, display coherent parallel patterns on chondrite normalized diagrams, and therefore may have remained immobile during alteration. It is noteworthy that two samples (498257 and 498262) with fresh olivine and low degrees of serpentinization display trace element patterns and transition metal concentration (Table 3.3) similar to those of least altered ultramafic rocks with picritic composition in the Ivisaartoq greenstone belt (Polat et al., 2007, Ordonez-Calderon et al., 2008).

Picrites are olivine-rich high-MgO rocks with > 12 wt% MgO (Le Bas, 2000). They are strongly porphyritic and may contain more than 50 vol% of olivine crystals (cf. Cameron, 1985, Kamenetsky et al., 1995; Rohrbach et al., 2005). Their high modal abundance of olivine appears to be the result of accumulation of olivine crystallized from primary picritic melts and xenocrysts disaggregated from the upper mantle owing to high degrees of partial melting (cf. Boudier, 1991; Rohrbach et al., 2005). In this study, most ultramafic rocks have extremely low contents of CaO (0.49-2.85 wt%) at very high concentrations of MgO (33 to 39 wt%) implying that olivine, rather than clinopyroxene, was the prevalent cumulate phase (Tables 3.3 and 3.5; Fig. 3.7). Strongly porphyritic picritic lavas in the Troodos ophiolite and Kamchatka, with 40 to 70 vol% olivine, show similar low CaO contents (< 3.6 wt%) at ca. 34 to 36 wt% MgO (cf. Cameron, 1985; Kamenetsky et al., 1995). Geochemical studies of olivine and associated melt inclusions in Mesozoic-Cenozoic picrites have shown that the primary melts are ultramafic in

composition, rather than basaltic, with 13 to 24 wt% MgO (Kamenetsky et al., 1995; Rohrbach et al., 2005). Sample 498210 possesses higher CaO (9.5 wt%) at lower MgO (19.7 wt%) content suggesting less entrained cumulate olivine, and therefore likely represents near-melt composition. In the Ivisaartoq belt, pillow basalts and picritic rocks display different initial ε_{Nd} values ruling out a consanguineous origin through fractional crystallization (Polat et al., 2007, 2008). Accordingly, ultramafic rocks (Fig. 3.3e; Table 3.1) in the Ujarassuit greenstone belt are interpreted to represent picritic cumulates.

3.7.4. Biotite schists and quartzitic gneisses: sedimentary versus metasomatic origin

Recognition of sedimentary protoliths in Archean high-grade terranes is not easy because metamorphism and multistage deformation have obliterated the primary sedimentary features (e.g., Fedo, 2000; Fedo and Whitehouse, 2002; Bolhar et al., 2005; Cates and Mojzsis, 2006; Manning et al., 2006). In the Ivisaartoq belt, evidence for siliciclastic or volcaniclastic-sedimentary origin is suggested by relict felsic cobbles set in a biotite-rich matrix (Fig. 3.2b-c). However, given the lack of well preserved sedimentary features, the biotite schists and quartzitic gneisses could also represent the metamorphosed equivalents of metasomatized basalts, or intermediate to felsic volcanic rocks.

Although mass changes owing to hydrothermal alteration can concentrate or dilute the composition of immobile elements (e.g., Al, Ti, Nb, Y, REE, Sc, and Ni), the inter-element ratios may remain relatively constant carrying information on the composition of the protolith (cf. Winchester and Floyd, 1977; Finlow-Bates and Stumpfl, 1981; MacLean and Kranidiotis, 1987; MacLean, 1990). For example, Zr/Ti and Nb/Y ratios in biotite schists and quartzitic gneisses (Fig. 3.6) are consistent with andesitic to rhyolitic

composition. Relative to Groups 1-4 amphibolites, biotite schists and quartzitic gneisses display different covariations of TiO_2, HREE, and Sc on variation diagrams of Zr (Fig. 3.7) ruling out amphibolite protoliths (c.f. MacLean and Barret, 1993; Ague, 1994; Roser and Nathan, 1997). Therefore, it is unlikely that these rocks represent metamorphosed alteration zones developed in basaltic rocks.

The chemical index of alteration (CIA) is a parameter widely used to quantify the degree of weathering of sediment sources (Nesbitt and Young, 1984; Fedo et al., 1995; Nesbitt et al., 1996). Biotite schists and quartzitic gneisses possess CIA values (47 to 67) comparable or slightly higher than those of unweathered igneous rocks (38 to 51) but lower than average Archean shales (ca. 76) (Condie, 1993) (Fig. 3.12a; Table 3.4). The characteristic low CIA values and moderate Al_2O_3 content (12 to 24 wt%) strongly suggest that quartzitic gneisses and biotite schists may represent volcanic flows or immature volcaniclastic-sedimentary rocks with scarce clay minerals in their modal composition. In addition, most samples plot across the predicted weathering trends for andesitic and granitic rocks in the A-CN-K diagram (Fig. 3.12a). This type of compositional trend in sedimentary rocks has been interpreted to indicate mixing of detrital sediments derived from various sources (McLennan et al., 1993, 2003).

Mixing of detrital sediments can also be monitored using inter-element ratios of transition metals (e.g., Cr, Co, and Sc) against HFSE (e.g., Th and Zr) and LREE (Condie and Wronkiewicz, 1990; Hofmann, 2005). These elements are excellent tracers of source composition because of their contrasting concentrations in mafic and felsic rocks and immobile behavior during alteration. Accordingly, biotite schists and quartzitic gneisses, in the Ujarassuit and Ivisaartoq belts, plot along a linear array defined by basaltic and granitic end members on the Co/Th versus La/Sc diagram (Fig. 3.12b). This diagram also

shows significant compositional overlap between biotite schists and amphibolites with andesitic composition of the Qussuk Peninsula (Garde, 2007). However, biotite schists and quartzitic gneisses possess higher La/Sc ratios than andesites suggesting a felsic component in their provenance (Fig. 3.12b). It is clear that the La/Sc ratios appear to indicate that the felsic component in quartzitic gneisses is more differentiated than the average early Archean (> 3.5 Ga) upper continental crust (Condie, 1993; Taylor and McLennan, 1995). This component may be represented by highly fractionated calc-alkaline granites and rhyolites. The presence of fractionated granitic sources is also implied by increasing negative Eu-anomaly (cf. Taylor et al., 1986) with decreasing Co/Th ratios (Fig. 3.12c).

On the Th/Sc versus Zr/Sc diagram (Fig. 3.12d), biotite schists also display a source-controlled compositional trend that reflects mafic through felsic source rocks. In contrast, the quartzitic gneisses possess higher Zr/Sc ratios (36 to 155) relative to the biotite schists (4.5 to 18) (Fig. 3.12d). High Zr/Sc ratios in modern sediments have been interpreted as evidence for zircon addition owing to sedimentary sorting (McLennan et al., 1993, 2003). Quartzitic gneisses have high contents of modal zircon and large concentrations of Zr (up to 702 ppm) which may indicate zircon accumulation (Table 3.4). However, their enrichment in REE and Th (Fig. 3.10e-f), and pronounced negative Ti anomalies resemble the geochemical characteristics of Archean high-silica rhyolites (SiO_2 > 74 wt%; Zr up to 680 ppm) reported in the Superior Province, Canada (Thurston and Fryer, 1983; Kerrich et al., 2008).

The evidence discussed above indicates that biotite schists represent immature volcaniclastic-sedimentary rocks, most likely graywackes, derived from poorly weathered intermediate to felsic sources and minor volcanic debris sourced from contiguous basaltic

rocks (Table 3.1). These immature sedimentary rocks generally occur at convergent margins and normally represent first-cycle sedimentary deposits (e.g., Cox et al., 1995). In contrast, major and trace elements (Figs. 3.6 and 3.12b-d) suggest that quartzitic gneisses represent compositionally more mature volcaniclastic-sedimentary rocks, quartz-rich arkoses, sourced from felsic rocks. In the absence of zircon age data, the high Zr/Sc ratios (Fig. 3.12d) have two possible explanations. First, quartzitic gneisses may represent reworked volcaniclastic-sedimentary rocks derived from Mesoarchean highly-fractionated rhyolites. Strong acidic hydrothermal alteration of felsic source rocks could have produced residual detritus enriched in SiO_2 and Zr (e.g., Sugitani et al., 2006). Second, high SiO_2 and Zr contents may reflect sedimentary reworking and recycling of older continental rocks as has been indicated for the enrichment of Zr in modern turbidites (McLennan et al., 1990). This would imply that the Ivisaartoq greenstone belt likely formed close to continental crust.

3.7.5. Petrogenesis, mantle processes, and geodynamic setting

Groups 1-4 amphibolites do not exhibit compositional variations indicating mixing trends with average Archean upper continental crust (e.g., Fig. 3.13a-b). They possess low Ce/Yb ratios (Fig. 3.13b) reminiscent of primitive lavas erupted in intra-oceanic arcs such as Tonga-Kermadec and South Sandwich Islands (Hawkesworth et al., 1993; Hawkins, 2003; Pearce, 2003). The fault-bounded contact between orthogneisses and amphibolites (Fig. 3.2d-e), and amphibolite xenoliths within some orthogneisses (Fig. 3.2g) suggest that volcanic rocks were not erupted over an underlying continental basement. These field and geochemical characteristics indicate that volcanic rocks likely formed in an intra-oceanic setting.

Phanerozoic volcanic rocks erupted at active continental margins and intra-oceanic island arcs show characteristic negative Nb-Ta anomalies in primitive mantle normalized diagrams (Kelemen et al., 2003). The distinctive trace element characteristics of primitive arc lavas reflect partial melting of the mantle wedge, which is variably metasomatized as the oceanic lithosphere is subducted and experiences dehydration and partial melting (Pearce and Peate, 1995; Becker et al., 2000; Schmidt and Poli, 2003). Accordingly, the negative Nb-Ta anomalies in arc magmas result from inefficient transfer of HFSE elements, relative to Th and LREE, from slab-derived fluids into the mantle wedge. Groups 1 and 2 amphibolites (Fig. 3.8a-d) display negative Nb-Ta anomalies and consistently plot in the field of volcanic arc lavas on the Th/Yb versus Nb/Yb diagram (Fig. 3.13a) (Pearce and Peate, 1995; Pearce, 2008). They are interpreted as island arc tholeiites (IAT).

Given the low solubility of Th in slab-derived aqueous fluids, and its low concentration in the depleted mantle, the enrichment of Th in intra-oceanic arc lavas (Fig. 3.13a) appears to require refertilization of the mantle wedge with hydrous melts derived from subducted siliciclastic sediments and oceanic crust (Plank and Langmuir, 1993; Hawkesworth et al., 1997; Becker et al., 2000; Kelemen et al., 2003; Dilek et al., 2007; Klimm et al., 2008). A sedimentary component fluxed into the mantle source of the Ivisaartoq belt pillow basalts appears to be indicated by variable initial ε_{Nd} values (+0.30 to +3.10), which have been interpreted as evidence for recycling of older continental crust via subduction (Polat et al., 2008). In the Archean, melting of the slab may have been more common than in the modern Earth owing to higher mantle temperatures and hotter lithospheric plates (Martin, 1999; Schmidt and Poli, 2003; Dilek and Polat, 2008).

Therefore, crustal input into the mantle wedge via subduction may have been significant in the Archean (cf. Pearce, 2008).

High-Mg Group 1-3 amphibolites (MgO > 8.0 wt%) show much higher Fe_2O_3 (11.1-13.4 wt%) than modern N-MORB (9.8 to 11.6 wt%) and primitive IAT (8.9-10.6 wt%) (Hofmann, 1988; Kelemen et al., 2003). They are also depleted in HREE and HFSE (mainly Ti, Zr, Nb, and Ta) compared to modern N-MORB (Fig. 3.8a-f). These geochemical characteristics suggest the following processes: 1) Archean tholeiites resulted from larger degrees of partial melting relative to modern tholeiites; 2) the Mesoarchean mantle beneath the Ivisaartoq-Ujarassuit greenstone belts was more depleted than the source of modern N-MORB (see Polat et al., 2007), and 3) conservative behavior of HFSE and HREE in slab fluxes.

A strongly depleted Mesoarchean sub-arc mantle implies an earlier history of partial melting before arc initiation, possibly associated with Archean sea floor spreading (cf. Ohta et al., 1996; Furnes et al., 2007). It is noteworthy that Group 3 amphibolites do not exhibit the negative HFSE anomalies that characterize subduction-related magmas (Fig. 3.8e-f). Instead, their trace element patterns resemble those of Archean (3.1 to 3.3 Ga) mid-ocean-ridge basalts (A-MORB) from the Pilbara Craton (Ohta et al., 1996) and modern N-MORB (Hofmann, 1988). Accordingly, Group 3 amphibolites may represent relict pre-arc A-MORB-like oceanic crust, trapped during the initiation of subduction, formed at a mid-ocean ridge or back-arc spreading system. Or alternatively, they may have formed during an episode of arc rifting (cf. Dilek and Flower, 2003).

In Group 4 amphibolites, high MgO (10.8-13.0 wt%) and Cr (99-765 ppm), and low TiO_2 (0.26-0.33 wt%), Zr (20.3-28.6 ppm), and HREE (HREE 1.9 to 3.2 x primitive mantle) contents are consistent with models for boninite generation by high degrees of

partial melting of a refractory mantle source (Sun and Nesbitt, 1978; Bloomer and Hawkins, 1987; Crawford et al., 1989; Pearce et al., 1992; Kim and Jacobi et al., 2002; Dilek et al., 2007). In addition, the LREE enriched patterns (La/Sm_{cn} = 1.8 to 2.4) and negative Nb-Ta anomalies (Fig. 3.8g-h) suggest that the depleted mantle wedge was metasomatized by fluids and possibly melts fluxed from the subducting slab, prior to or during partial melting (cf. Taylor and Nesbitt, 1988; Bédard, 1999). Boninites in modern arcs may form in the forearc, owing to forearc extension during the early stages of subduction (Stern and Bloomer, 1992; Kim and Jacobi, 2002; Reagan et al., 2008). They may also be erupted in the back-arc, as the back-arc spreading center propagates into the volcanic arc and interact with slab derived fluids (Deschamps and Lallemand, 2003).

If the depleted LREE patterns of Group 2 amphibolites (Fig. 3.8 c-d) are primary rather than reflecting alteration patterns (see Garde, 2007; Ordóñez-Calderon et al., 2008), they may represent depleted IAT. In the Caribbean island arc, Cretaceous LREE-depleted IAT and boninites were erupted in the forearc setting as a result of seafloor spreading during the earliest stages of arc development (cf. Viruete et al., 2006).

In the Ujarassuit and Ivisaartoq belt the absence of voluminous intermediate to felsic rocks is also consistent with an immature stage of arc development. Plagioclase-rich amphibolites (Table 3.1) with basaltic andesites and andesite compositions are rare. Nonetheless, they display negative Nb-Ta anomalies, enriched LREE, and fractionated HREE (Gd/Yb_{cn} = 2.6-3.1) patterns (Fig. 3.9a-b) consistent with a subduction zone geochemical signature and deep melting ($\geq$ 80 km) with residual garnet in the source (cf. Johnson, 1994; Hirschmann and Stolper, 1996; van Westrenen et al., 2001; Kelemen et al., 2003). Despite their LREE enrichment, plagioclase-rich amphibolites possess comparable TiO_2 and slightly lower HREE contents relative to Groups 1-2 amphibolites (Table 3.3;

Figs. 3.8-3.9). Therefore, they are not related by fractional crystallization. Instead, the high Mg-numbers (48-62) and high contents of Th, Nb, LREE, and transition metals suggest that intermediate rocks likely formed through interaction between melts derived from hydrated basaltic slab and the sub-arc mantle (e.g., Defant and Drummond, 1990; Martin, 1999; Smithies, 2000; Condie, 2005b; Martin et al., 2005).

High contents of MgO (> 19 wt%) and transition metals (Cr = 2377-6312 ppm, Ni = 658-2200 ppm), and low concentrations of REE (HREE 0.6 to 2.0 x primitive mantle) and HFSE (< 0.4 wt% TiO_2) in ultramafic rocks are consistent with picritic composition (Fig. 3.9c-d; Table 3.1). Mesozoic-Cenozoic picrites have formed in various geodynamic settings including, but not limited to, mid-ocean ridges, oceanic plateaus, and island arcs (Kerr et al., 1996; Perfit et al., 1996; Thompson et al., 2001). The least altered ultramafic rocks (498262 and 498257), however, possess the characteristic LREE-enriched patterns and negative Nb-Ta anomalies of island arc picrites in the lesser Antilles, Solomon, New Hebrides, and Kamchatka (e.g., Eggins, 1993; Kamenetsky et al., 1995; Woodland et al., 2002; Schuth et al., 2004). Therefore, the geochemical characteristic of picritic rocks in the Ujarassuit greenstone belt suggest that they formed by large degrees of partial melting of depleted sub-arc mantle. Least altered picritic cumulates in the Ivisaartoq belt display large positive initial ε_{Nd} values (+4.21 to +4.97) consistent with long-term depletion of the Ivisaartoq sub-arc mantle (Polat et al., 2007, 2008). It is worth noting that modern subduction-related picrites appear to be restricted to intra-oceanic settings (Rohrbach et al., 2005).

The lithogeochemical association of IAT (Groups 1-2 amphibolites), transitional to calc-alkaline basaltic andesites and andesites (plagioclase-rich amphibolites), arc-like picrites, and boninite-like rocks (Group 4 amphibolites) is consistent with a supra-

subduction zone tectonic setting for the Ujarassuit and Ivisaartoq greenstone belts (Figs. 3.8 and 3.9; Table 3.1). Given that picrites and boninites are the products of large degrees of partial melting, their occurrence in modern island arcs is related to strong thermal anomalies in the mantle wedge. Subduction of young, hot oceanic lithosphere, spreading-ridge subduction, subduction initiation across fracture zones, and suprasubduction zone extension appear to explain the unusual high-temperatures in the sub-arc mantle (e.g., Stern and Bloomer, 1992; Kim and Jacobi, 2002; Hall et al., 2003; Deschamps and Lallemand, 2003; Schuth et al., 2004; Ishizuka et al., 2006; Dilek et al., 2007). Accordingly, we postulate that the volcanic rocks in the Ujarassuit and Ivisaartoq greenstone belts likely represent Mesoarchean oceanic crust formed either in the forearc or back-arc region (Fig. 3.14) (see Polat et al., 2007, 2008).

3.7.6. Collisional orogenesis of the Nuuk region and implications for Archean ophiolites

The Phanerozoic-like continental collisional tectonics proposed for the Nuuk region (Friend and Nutman, 2005; Nutman and Friend, 2007) predicts the existence of convergent margins and marginal basins in the Archean record. Intra-oceanic terranes may have been trapped into colliding continents during the closure of Archean ocean basins in a similar fashion to Tethyan ophiolites in the Mediterranean region (Dewey, 2003; Şengör, 1990; Flower, 2003; Dilek and Flower, 2003; Şengör and Natal'in, 2004; Dilek et al., 2007).

Suprasubduction zone oceanic crust displays various petrological characteristics that record complex events during its formation including progression from mid-ocean ridge, subduction initiation, intra-arc volcanism, slab rollback, arc rifting, and back-arc basin opening (Stern and Bloomer, 1992; Shervais, 2001; Dilek and Flower, 2003; Flower,

2003; Dilek et al., 2007). The Ujarassuit greenstone belt is composed dominantly of metamorphosed IAT which are spatially and temporally associated with N-MORB-like basaltic rocks (Group 3 amphibolites), boninites, picrites, andesites, and volcaniclastic-sedimentary rocks, implying that the belt likely contains upper-most crustal components of Mesoarchean forearc or backarc oceanic crust. A similar tectonic setting was proposed for volcanic rocks in the Ivisaartoq belt (Polat et al., 2007, 2008), and the discovery of boninites in this study substantiates this interpretation. However, if the high contents of Zr in quartzitic gneisses from the Ivisaartoq belt resulted from recycling of older Archean felsic crust (Fig. 3.12d), the Ivisaartoq belt may have formed close to a continental block.

Immature volcaniclastic-sedimentary rocks (biotite schists) in the Ivisaartoq and Ujarassuit greenstone belts were derived mostly from nearby felsic to intermediate intra-arc volcanic complexes and deposited onto adjacent basaltic oceanic crust (Fig. 3.14). These Mesoarchean volcanic arc complexes, however, appear to be missing from the geological record in the study area. Nevertheless, uppermost crustal components from a contemporaneous 3071 Ma island arc complex is well preserved at Qussuk and Bjørneøen in the Akia terrane (Garde, 2007). This relict volcanic arc complex is composed of metamorphosed andesitic volcanic rocks erupted on top of more primitive basaltic crust with geochemical characteristics similar to those of Group 2 amphibolites in the Ujarassuit greenstone belt. The exposure of deep crustal structures in the Ujarassuit greenstone belt suggests that the uppermost crustal rocks have been removed by erosion. This may well explain the absence of intra-arc complexes which may have been located at shallower crustal levels (cf. Garde, 2007).

Comparable geochronological, lithological, and geochemical characteristics of metavolcanic and metavolcaniclastic-sedimentary rocks in Ujarassuit and Ivisaartoq belts

suggest that they likely represent volcanic suites formed along the same Mesoarchean convergent margin. Therefore, the Ivisaartoq and Ujarassuit greenstone belts are interpreted to represent dismembered fragments of Mesoarchean supra-subduction zone oceanic crust. Accordingly, the Nuuk region appears to include scattered fragments of incomplete Mesoarchean ophiolites formed at different paleogeographic settings (forearc, intra-arc, and back-arc) along and across a supra-subduction zone.

3.8. Conclusions

The following conclusions are drawn based on the field characteristics and geochemical signatures of metavolcanic and metavolcaniclastic-sedimentary rocks from the Mesoarchean Ivisaartoq and Ujarassuit greenstone belts:

1. These belts are dominated by metamorphosed IAT (Table 3.1). Basaltic andesites, andesites, picrites, boninites, and volcaniclastic-sedimentary rocks are a minor component. These lithological and geochemical characteristics suggest an immature island arc origin for the Ujarassuit and Ivisaartoq greenstone belts (Figs. 3.8-3.10; Table 3.1). In addition, the presence of boninite-like rocks spatially associated with picritic cumulates indicates that the Ujarassuit greenstone belt likely represents obducted fragments of Mesoarchean forearc or back-arc oceanic crust.
2. In the Ujarassuit greenstone belt, recognition of the stratigraphic relationships between subduction-related rocks including IAT, boninites, and picrites, and rare N-MORB-like tholeiites (Group 3 amphibolites) are obscured by late Archean polyphase deformation (Figs. 3.8-3.9; Table 3.1). Accordingly, the protolith of Group 3 amphibolites may well represent pre-arc oceanic crust formed at mid-ocean ridges or

back-arc spreading centers (e.g., Leat and Larter, 2003); or alternatively it may have formed during an episode of arc rifting.

3. The following geochemical evidence indicates that the Mesoarchean mantle beneath the Ivisaartoq-Ujarassuit greenstone belts was heterogeneous, more depleted in trace elements than modern depleted upper mantle, and variably metasomatized by slab-derived fluids: (1) Groups 1-4 amphibolites (Figs. 3.8-3.9) have lower abundance of REE and HFSE (mainly Ti, Zr, Nb, and Ta) than modern average N-MORB (Hofmann, 1988); (2) contrasting geochemical patterns of mafic and ultramafic rocks; (3) low-Ti high-Mg rocks (boninites and picrites) indicative of refractory mantle sources; and (4) primitive mantle-normalized diagrams with negative Nb and Ta anomalies, flat LREE patterns, and enrichment of Th relative to HFSE and HREE.
4. Biotite schists display major and trace element characteristics resembling immature volcaniclastic-sedimentary rocks (graywackes) derived from mixtures of poorly weathered (CIA = 47 to 67) andesitic to rhyolitic sources (Fig. 3.12a-d). In addition, high concentrations of transition metals (Ni up to 328 ppm) suggest that sedimentary rocks also contain volcanic debris derived from local ultramafic to mafic rocks. Felsic to intermediate detritus was likely sourced from distal volcanic arc edifices (Fig. 3.14), given that supracrustal belts are dominated by mafic rocks. Voluminous felsic to intermediate volcanic sequences are not represented in the area, and therefore appear to haven been eroded away. This could be related to the present level of erosion in the Nuuk region which exposes mainly middle to lower crustal rocks (see Garde, 2007).
5. Quartzitic gneisses in the Ivisaartoq greenstone belt have high contents of SiO_2, Zr, and ΣREE, high Zr/Sc ratios, and low concentrations of transition metals indicating a felsic provenance (Figs. 3.10e-f and 3.12). These geochemical characteristics may

have been inherited from highly-fractionated Mesoarchean rhyolites; or alternatively, recycling of older continental crust may have resulted in significant zircon addition (cf. McLennan et al., 1990; 2003). Given the oceanic origin of volcanic rocks, the later would imply that the Ivisaartoq volcanic rocks were erupted in the proximity of older Archean continental crust (cf. Polat et al., 2007, 2008).

6. The new field and geochemical data presented in this contribution and those of previous studies (Garde, 2007; Polat et al., 2007, 2008) have revealed that the Nuuk region comprises several dismembered fragments of Mesoarchean arc-backarc-forearc system. These include intra-arc volcanic complexes in Qussuk and Bjørneøen (Garde, 2007), and forearc or backarc complexes in the Ujarassuit and Ivisaartoq greenstone belts. This is consistent with the allochtonous terrane model whereby the closure of Archean ocean basins in the last stage of a Wilson cycle would have trapped Archean oceanic crust into the colliding continents (Friend and Nutman, 2005; Nutman and Friend, 2007). Future studies may reveal scattered volcanic complexes formed at different paleogeographic locations (e.g., back-arc basins) along and across a regional Mesoarchean supra-subduction zone.

3.9. Acknowledgements

We thank Z. Yang, and J.C. Barrette for their help during the ICP-MS analyses. This is a contribution of PREA and NSERC grant 250926 to A. Polat, and NSERC grant 83117 to B. Fryer. Field work was funded by the Bureau of Minerals and Petroleum in Nuuk and the Geological Survey of Denmark and Greenland (GEUS).

3.10. References

Ague, J.J., 1994. Mass transfer during Barrovian metamorphism of pelites, south-central Connecticut. I: Evidence for changes in composition and volume. American Journal of Science 294, 989-1057.

Alt, J.C., 1999. Hydrothermal alteration and mineralization of oceanic crust: Mineralogy, geochemistry, and processes. In: Barrie, C.T., Hannington, M.D., (Eds.). Volcanic-Associated Massive Sulphide Deposits: Processes and examples in modern and ancient settings. Reviews in Economic Geology 8, 133-155.

Arndt, N.T., 1994. Archean komatiites. In: Condie, K.C. (Ed.). Archean Crustal Evolution. Developments in Precambrian Geology 11, 11-44.

Barrett, T.J., MacLean, W.H., 1994. Chemostratigraphy and hydrothermal alteration in exploration for VHMS deposits in greenstones and younger volcanic rocks. In: Lentz, D.R., (Ed.). Alteration and alteration processes associated with ore-forming systems. Geological Association of Canada, Short course notes 11, 433-467.

Becker, H., Jochum, K.P., Carlson, R.W., 2000. Trace element fractionation during dehydration of eclogites from high-pressure terranes and the implications for element fluxes in subduction zones. Chemical Geology 163, 65-99.

Bédard, J.H., 1999. Petrogenesis of boninites from the Betts Cove ophiolite, Newfoundland, Canada: Identification of subducted source components. Journal of Petrology 40, 1853-1889.

Bennett, V.C., Nutman, A.P., McCulloch, M.T., 1993. Nd isotopic evidence for transient, highly depleted mantle reservoirs in the early history of the Earth. Earth and Planetary Science Letters 119, 299-317.

Bickle, M.J., Nisbet, E.G., Martin, A., 1994. Archean greenstone belts are not oceanic crust. Journal of Geology 102, 121-138.

Black, L.P., Gale, N.H., Moorbath, S., Pankhurst, R.J., McGregor, V.R., 1971. Isotopic dating of very early Precambrian amphibolite facies gneisses from the Godthaab district, West Greenland. Earth and Planetary Science Letters 12 (3), 245-259.

Bloomer, S.H., Hawkins, J.W., 1987. Petrology and geochemistry of boninite series volcanic rocks from the Mariana trench. Contribution to Mineralogy and Petrology 97, 361-377.

Bolhar, R., Kamber, B.S., Moorbath, S., Whitehouse, M.J., Collerson, K.D., 2005. Chemical characterization of earth's most ancient clastic metasediments from the Isua Greenstone Belt, southern West Greenland. Geochimica et Cosmochimica Acta 69 (6), 1555-1573.

Boudier, F., 1991. Olivine xenocrysts in picritic magmas: An experimental and microstructural study. Contributions to Mineralogy and Petrology 109,114-123.

Bridgwater, D., McGregor, V.R.,. Myers, J.S., 1974. A horizontal tectonic regime in the Archean of Greenland and its implications for early crustal thickening. Precambrian Research 1, 179-197.

Cameron, W.E., 1985. Petrology and origin of primitive lavas from the Troodos ophiolite, Cyprus. Contribution to Mineralogy and Petrology 89, 239-255

Casey, J.F., Dewey, J.F., 1984. Ophiolite emplacement and obduction initiation of subduction zones along transform and accreting plate boundaries, triple-junction evolution, and fore-arc spreading centres: Implications for ophiolitic geology and obduction. In: Gass, I.G., Lippard, S.J., Shelton, A.W., (Eds.). Ophiolites and oceanic lithosphere. Geological Society of London Special Publication 13, 269-290.

Cates, N.L., Mojzsis, S.J., 2006. Chemical and isotopic evidence for wide spread Eoarchean metasedimentary enclaves in southern West Greenland. Geochimica et Cosmochimica Acta 70, 4229-4257.

Chadwick, B., 1985. Contrasting styles of tectonism and magmatism in the late Archaean crustal evolution of the northeastern part of the Ivisârtoq region, inner Godthåbsfjord, southern West Greenland. Precambrian Research 27, 215-238.

Chadwick, B., 1986. Malene stratigraphy and late Archean structure: New data from Ivisaartoq, inner Godthåbsfjord, southern West Greenland. Rapport Grønlands Geologiske Undersøgelse 130, 74-85.

Chadwick, B., 1990. The stratigraphy of supracrustal rocks within high-grade orthogneisses and its bearing on Late Archean structure in southern West Greenland. Journal of the Geological Society of London 147, 639-652.

Chadwick, B., Coe, K., 1988. Geological map of Greenland, 1:100 000, Ivisaartoq sheet 64 V. Nord. Copenhagen, Geological Survey of Greenland.

Condie, K.C., 1993. Chemical composition and evolution of the upper continental crust: Contrasting results from surface samples and shales. Chemical Geology 104, 1-37.

Condie, K.C., 1994. Greenstones through time. In: Condie, K.C., (Ed.). Archean crustal evolution. Developments in Precambrian Geology 11, 85-120.

Condie, K.C., 2005a. High field strength element ratios in Archean basalts: A window to evolving sources of mantle plumes? Lithos 79, 491-504.

Condie, K.C., 2005b. TTGs and adakites: Are they both slab melts? Lithos 80, 33-44.

Condie, K.C., Viljoen, M.J., Kable, E.J.D., 1977. Effects of alteration on element distributions in Archean tholeiites from the Barberton greenstone belt, South Africa. Contributions to Mineralogy and Petrology 64, 75-89.

Condie, K.C., Wronkiewicz, D.J., 1990. The Cr/Th ratio in Precambrian pelites from the Kaapvaal Craton as an index of craton evolution. Earth and Planetary Science Letters 97 (3-4), 256-267.

Cox, R., Lowe, D.R., Cullers, R.L., 1995. The influence of sediment recycling and basement composition on evolution of mudrock chemistry in the southwestern United States. Geochimica et Cosmochimica Acta 59, 2919-2940.

Crawford, A.J., Falloon, T.J., Green, D.H., 1989. Classification, petrogenesis and tectonic setting of boninites. In: Crawford, A.J. (Ed.). Boninites and Related Rocks. Unwin Hyman, London, 1-49.

Crowley, J.L., 2002. Testing the model of late Archean terrane accretion in southern West Greenland: A comparison of the timing of geological events across the Qarliit Nunaat Fault, Buksefjorden region. Precambrian Research 116 (1-2), 57-79.

Defant, M.J., Drummond, M.S., 1990. Derivation of some modern arc magmas by melting of young subducted lithosphere. Nature 347, 662-665.

Deschamps, A., Lallemand, S., 2003. Geodynamic setting of Izu-Bonin-Mariana boninites. In: Larter, R.D., Leat, P.T., (Eds.). Intra-oceanic subduction systems: Tectonic and magmatic processes. Geological Society of London Special Publications 219, 163-185.

Dewey, J., 2003. Ophiolites and lost oceans: Rifts, ridges, arcs, and/or scrapings? In: Dilek, Y., Newcomb, S., (Eds.). Ophiolite concept and the evolution of geological thought. Geological Society of America Special Paper 373, 153-158.

Dilek, Y., Flower, M.F.J., 2003. Arc-trench rollback and forearc accretion: 2. A model template for ophiolites in Albania, Cyprus, and Oman. In: Dilek, Y., Robinson, P.T.,

(Eds.). Ophiolites in earth history. Geological Society of London, Special Publications 218, 43-68.

Dilek, Y., Furnes, H., and Shallo, M., Suprasubduction zone ophiolite formation along the periphery of Mesozoic Gondwana. Gondwana Research 11, 453-475.

Dilek, Y. and Polat, A., Suprasubduction zone ophiolites and Archean tectonics. Geology 36, 431-432.

Eggins, S.M., 1993. Origin and differentiation of picritic arc magmas, Ambae (Aoba), Vanuatu. Contributions to Mineralogy and Petrology 114, 79-100.

Eriksson, P.G., Catuneanu, O., 2004. A commentary on Precambrian plate tectonics. In: Eriksson, P.G., Altermann, W., Nelson, D.R., Mueller, W.U., Catuneanu, O., (Eds.). The Precambrian earth: Tempos and events. Developments in Precambrian Geology 12, 201-213.

Escher, J.C., Pulvertaf, T.C.R., 1995. Geological map of Greenland, 1:2.500.000. Copenhagen, Geological Survey of Greenland.

Evans, B.W., Ghiorso, M.S., 1995. Thermodynamics and petrology of cummingtonite. American Mineralogist 80, 649-663.

Fallon, T.J., Crawford, A.J., 1991. The petrogenesis of high-calcium boninite lavas dredged from the northern Tonga ridge. Earth and Planetary Science Letters 102, 375-394.

Fedo, C.M., 2000. Setting and origin for problematic rocks from the > 3.7 Ga Isua greenstone belt, southern west Greenland: Earth's oldest coarse clastic sediments. Precambrian Research 101, 69-78.

Fedo, C.M., Nesbitt, H.W., Young, G.M., 1995. Unraveling the effects of potassium metasomatism in sedimentary rocks and paleosols, with implications for paleoweathering conditions and provenance. Geology 23, 921-924.

Fedo, C.M., Whitehouse, M.J., 2002. Metasomatic origin of quartz-pyroxene rock, Akilia, Greenland, and implications for earth's earliest life. Science 296, 1448-1452.

Finlow-Bates, T., Stumpfl, E.F., 1981. The behavior of so called immobile elements in hydrothermally altered rocks associated with volcanogenic submarine-exhalative ore deposits. Mineralium Deposita 16, 319-328.

Flower, M.F.J., 2003. Ophiolites, historical contingency, and the Wilson cycle. In: Dilek, Y., Newcomb, S. (Eds.). Ophiolite concept and the evolution of the geological thought. Geological Society of America Special Paper 373, 111-135.

Friend, C.R.L., Nutman, A.P., 2005. New pieces of the Archaean terrane jigsaw puzzle in the Nuuk Region, southern West Greenland: Steps in transforming a simple insight into a complex regional tectonothermal model. Journal of the Geological Society of London 162, 147-162.

Friend, C.R.L., Nutman, A.P., 1991. Refolded nappes formed during late Archaean terrane assembly, Godthåbsfjord, southern West Greenland. Journal of the Geological Society of London 148, 507-519.

Friend, C.R.L., Nutman, A.P., Baadsgaard, H., Kinny, P.D., McGregor, V.R., 1996. Timing of late Archean terrane assembly, crustal thickening and granite emplacement in the Nuuk region, southern West Greenland. Earth and Planetary Science Letters 142, 353-365.

Friend, C.R.L., Nutman, A.P., McGregor, V.R., 1987. Late-Archaean tectonics in the Færingehavn-Tre Brødre area, south of Buksefjorden, southern West Greenland. Journal of the Geological Society of London 144, 369-376.

Friend, C.R.L., Nutman, A.P., McGregor, V.R., 1988. Late Archean terrane accretion in the Godthåb region, southern West Greenland. Nature 335, 535-538.

Fryer, B.J., Fyfe, W.S., Kerrich, R., 1979. Archean volcanogenic oceans. Chemical Geology 24, 25-33.

Furnes, H., de Wit, M., Staudigel, H., Rosing, M., Muehlenbachs, K., 2007. A Vestige of Earth's Oldest Ophiolite. Science 315, 1704-1707.

Galley, A.G., Jonasson, I.R., Watkinson, D.H., 2000. Magnetite-rich calc-silicate alteration in relation to synvolcanic intrusions at the Ansil volcanogenic massive sulfide deposit, Rouyn-Noranda, Quebec, Canada. Mineralium Deposita 35, 619-637.

Gao, S., Wedepohl, K.H., 1995. The negative Eu anomaly in Archean sedimentary rocks: Implications for decomposition, age and importance of their granitic sources. Earth and Planetary Science Letters 133 (1-2), 81-94.

Garde, A.A., 2007. A mid-Archean island arc complex in the eastern Akia terrane, Godthåbsfjord, southern West Greenland. Journal of the Geological Society of London 164, 565-579.

Greene, A.R., Debari, S.M., Kelemen, P.B., Blusztajn, J., Clift, P.D., 2006. A detailed geochemical study of island arc crust: The Talkeetna arc section, south-central Alaska. Journal of Petrology 47, 1051-1093.

Gruau, G., Tourpin, S., Fourcade, S., Blais S., 1992. Loss of isotopic (Nd, O) and chemical (REE) memory during metamorphism of komatiites: New evidence from eastern Finland. Contributions to Mineralogy and Petrology 112, 66-82.

Hall, R.P., 1980. The tholeiitic and komatiitic affinity of Malene metavolcanic amphibolites from Ivisaartoq, southern West Greenland. Rapport Grønlands Geologiske Undersøgelse 97, 20 pp.

Hall, R.P., Friend, C.R.L., 1979. Structural evolution of the Archean rocks in Ivisârtoq and the neighboring inner Godthåbsfjord region, southern West Greenland. Geology 7, 311-315.

Hall, C.E., Gurnis, M., Sdrolias, M., Lavier, L.L., Müller, R.D., 2003. Catastrophic initiation of subduction following forced convergence across fracture zones. Earth and Planetary Science Letters 212, 15-30.

Hart, S.R., Erlank, A.J., Kable, E.J.D., 1974. Sea-floor basalt alteration: Some chemical and isotopic effects. Contributions to Mineralogy and Petrology 44, 219-230.

Hartel, T.H.D., Pattison, D.R.M., 1996. Genesis of the Kapuskasing (Ontario) migmatitic mafic granulites by dehydration melting of amphibolite: The importance of quartz to reaction progress. Journal of Metamorphic Geology 14, 591-611.

Hartlaub, R.P., Heaman, L.M., Ashton, K.E., Chacko, T., 2004. The Archean Murmac Bay Group: Evidence for a giant Archean rift in the Rae Province, Canada. Precambrian Research 131, 345-372.

Hawkesworth, C.J., Gallagher, K., Hergt, J.M., McDetmott, F., 1993. Mantle and slab contributions in arc magmas. Annual Review of Earth and Planetary Sciences 21, 175-204.

Hawkesworth, C.J., Turner, S.P., McDermott, F., Peate, D.W., Van Calsteren, P., 1997. U-Th isotopes in arc magmas: Implications for element transfer from the subducted crust. Science 276, 551-555.

Hawkins, J.W., 2003. Geology of supra-subduction zones - Implications for the origin of ophiolites. In: Dilek, Y., Newcomb, S. (Eds.). Ophiolite concept and the evolution of the geological thought. Geological Society of America Special Paper 373, 227-268.

Hirschmann, M.M., Stolper, E.M., 1996. A possible role for garnet pyroxenite in the origin of "garnet signature" in MORB. Contribution to Mineralogy and Petrology 124, 185-208.

Hofmann, A., 2005. The geochemistry of sedimentary rocks from the Fig Tree Group, Barberton greenstone belt: Implications for tectonic, hydrothermal and surface processes during mid-Archaean times. Precambrian Research 143, 23-49.

Hofmann, A.W., 1988. Chemical differentiation of the Earth: The relationship between mantle, continental crust, and oceanic crust. Earth and Planetary Science Letters 90, 297-314.

Hollis, J.A., Kelly, N.M., Frei, D., Schmid, S., Van Gool, J.A.M., 2006a. U-Pb zircon geochronology results for Ujarassuit Nunaat supracrustal belts and surrounding gneisses. Interim report. Danmarks Og Grønlands Geologiske Undersøgelse Rapport 45, 56 pp.

Hollis, J.A., Schmid, S., Stendal, H., van Gool, J.A.M., Weng, W.L., 2006b. Supracrustal belts in Godthåbsfjord region, southern West Greenland. Progress report on 2005 field work: Geological mapping, regional hydrothermal alteration, and tectonic sections. Danmarks Og Grønlands Geologiske Undersøgelse Rapport 7, pp. 171.

Ishizuka, O., Kimura, J-I., Li, Y.B., Stern, R.J., Reagan, M.K., Taylor, R.N., Ohara, Y., Bloomer, S.H., Ishii, T., Hargrove, U.S., Haraguchi, S., 2006. Early stages in the evolution of Izu-Bonin arc volcanism: New age, chemical, and isotopic constraints. Earth and Planetary Science Letters 250, 385-401.

Jenner, G.A., Longerich, H.P., Jackson, S.E., Fryer, B.J., 1990. ICP-MS; a powerful tool for high-precision trace-element analysis in earth sciences; evidence from analysis of selected U.S.G.S. Reference samples. Chemical Geology 83, 133-148.

Jiang, S.Y., Wang, R.C., Xu, X.S., Zhao, K.D., 2005. Mobility of high field strength elements (HFSE) in magmatic-, metamorphic-, and submarine-hydrothermal systems. Physics and Chemistry of the Earth 30, 1020-1029.

Johnson, K., 1994. Experimental cpx/and garnet/melt partitioning of REE and other trace elements at high pressures: Petrogenetic implications. Mineralogical Magazine 58A, 454-455.

Kamenetsky, V.S., Sobolev, A.V., Joron J.L., Semet, M.P., 1995. Petrology and geochemistry of cretaceous ultramafic volcanics from eastern Kamchatka. Journal of Petrology 36, 637-662.

Kay, R.W., 1978. Aleutian magnesian andesites: Melts from subducted Pacific ocean crust. Journal of Volcanology and Geothermal Research 4, 117-132.

Kelemen, P.B., Hanghøj, K., Greene, A.R., 2003. One view of the geochemistry of subduction-related magmatic arcs, with emphasis on primitive andesite and lower crust. Treatise on Geochemistry, Elsevier, vol. 3, 593-659.

Kemp, A.I.S., Hawkesworth, C.J., 2003. Granitic perspectives on the generation and secular evolution of the continental crust. Treatise on Geochemistry, Elsevier, vol. 3, 349-410.

Kerr, A.C., Marriner, G.F., Arndt, N.T., Tarney, J., Nivia, A., Saunders, A.D., Duncan, R.A., 1996. The petrogenesis of Gorgona komatiites, picrites and basalts: New field, petrographic and geochemical constraints. Lithos 37, 245-260.

Kerrich, R., Polat, A., Wyman, D., Hollings, P., 1999. Trace element systematics of Mg-, to Fe-tholeiitic basalt suites of the Superior Province: Implications for Archean mantle reservoirs and greenstone belt genesis. Lithos 46, 163-187.

Kerrich, R., Polat, A., Xie, Q., 2008. Geochemical systematics of 2.7 Ga Kinojevis Group (Abitibi), and Manitouwadge and Winston Lake (Wawa) Fe-rich basalt-rhyolite associations: Backarc rift oceanic crust? Lithos 101, 1-23.

Kim, J., Jacobi, R.D., 2002. Boninites: Characteristics and tectonic constraints, northeastern Appalachians. Physics and Chemistry of the Earth 27, 109-147

Klimm, K., Blundy, J.D., Green, T.H., 2008. Trace element partitioning and accessory phase saturation during H_2O-saturated melting of basalt with implications for subduction zone chemical fluxes. Journal of Petrology 49, 523-553.

Komiya, T., Maruyama, S., Hirata, T., Yurimoto, H., Nohda, S., 2004. Geochemistry of the oldest MORB and OIB in the Isua supracrustal belt, southern west Greenland: Implications for the composition and temperature of early Archean upper mantle. The Island arc 13, 47-72.

Kusky, T.M., 2004. Introduction. In: Kusky, T.M., (Ed.). Precambrian ophiolites and related rocks. Elsevier, Amsterdam, 1-34.

Lahaye, Y., Arndt, N.T., Byerly, G., Chauvel, C., Fourcade, S., Gruau, G., 1995. The influence of alteration on the trace-element and Nd isotopic compositions of komatiites. Chemical Geology 126, 43-64.

Le Bas, M.J., 2000. IUGS Reclassification of the high-Mg and picritic volcanic rocks. Journal of Petrology 41, 1467-1470.

Leat, P.T., Larter, R.D., 2003. Intra-oceanic subduction systems: Introduction. In: Larter, R.D., Leat, P.T., (Eds.). Intra-oceanic subduction systems: Tectonic and magmatic processes. Geological Society of London Special Publications 219, 1-17.

Ludden, J. N., Gélinas, L., Trudel, P., 1982. Archean metavolcanics from the Rouyn-Noranda district, Abitibi greenstone belt, Québec. 2. Mobility of trace elements and petrogenetic constraints. Canadian Journal of Earth Sciences 19, 2276-2287.

Ludden, J. N., Thompson, G., 1979. An evaluation of the behavior of the rare earth elements during the weathering of sea-floor basalts. Earth and Planetary Science Letters 43, 85-92.

MacLean, W.H., 1990. Mass change calculations in altered rocks series. Mineralium Deposita 25, 1-6.

MacLean, W.H., Barrett, T.J., 1993. Lithogeochemical techniques using immobile elements. Journal of Geochemical Exploration 48, 109-133.

MacLean, W.H., Kranidiotis, P., 1987. Immobile elements as monitors of mass transfer in hydrothermal alteration: Phelps Dodge massive sulfide deposit, Matagami, Quebec. Economic Geology 82, 951-962.

Manikyamba, C., Naqvi, S.M., Subba Rao, D.V., Ram Mohan, M., Khanna, T.C., Rao, T.G., Reddy G.L.N., 2005. Boninites from the Neoarchaean Gadwal Greenstone belt, Eastern Dharwar Craton, India: Implications for Archaean subduction processes. Earth and Planetary Science Letters 230, 65- 83.

Martin, H., 1999. Adakitic magmas: Modern analogues of Archaean granitoids. Lithos 46, 411-429.

Martin, H., Smithies, R.H., Rapp, R., Moyen, J.-F., Champion, D., 2005. An overview of adakite, tonalite-trondhjemite-granodiorite (TTG), and sanukitoid: Relationships and some implications for crustal evolution. Lithos 79, 1-24.

Manning, C.E., Mojzsis, S.J., Harrison, T.M., 2006. Geology, age and origin of supracrustal rocks at Akilia, West Greenland. American Journal of Science 306 (5), 303-366.

McGregor, V.R., 1973. The early Precambrian gneisses of the Godthaab District, West Greenland. Philosophical Transactions of the Royal Society of London, Series A 273, 343-358.

McGregor, V.R., Friend, C.R.L., Nutman, A.P., 1991. The late Archaean mobile belt through Godthabsfjord, southern West Greenland: A continent-continent collision zone? Bulletin of the Geological Society of Denmark 39 (3-4), 179-197.

McGregor, V.R., Mason, B., 1977. Petrogenesis and geochemistry of metabasaltic and metasedimentary enclaves in the Amîtsoq gneisses, West Greenland. American Mineralogist 62, 887-904.

McLennan, S.M., Bock, B., Hemming, S.R., Hurowitz, J.A., Lev, S.M., McDaniel, DK., 2003. The role of provenance and sedimentary processes in the geochemistry of sedimentary rocks. In: Lentz, D.R. (Ed.). Geochemistry of sediments and sedimentary rocks: Evolutionary considerations to mineral-deposit forming environments. GeoText 4, Geological Association of Canada, 7-38.

McLennan, S.M., Hemming, S., McDaniel, DK., Hanson, G.N., 1993. Geochemical approaches to sedimentation, provenance, and tectonics. In: Johnsson, M.J., Basu, A., (Eds.). Processes controlling the composition of clastic sediments. Geological Society of America Special Paper 284, 21-40.

McLennan, S.M., Murray, R.W., 1999. Geochemistry of sediments. In: Marshall, C.P., Fairbridge, R.W. (Eds.). Encyclopedia of Geochemistry. Kluwer Academic Publishers, 282-292.

McLennan, S.M., Taylor, S.R., McCulloch, M.T., Maynard, J.B., 1990. Geochemical and Nd-Sr isotopic composition of deep-sea turbidites: Crustal evolution and plate tectonic associations. Geochimica et Cosmochimica Acta 54, 2015-2050.

Middelburg, J.J., van der Weijden, C.H., Woittiez, J.R.W., 1988. Chemical processes affecting the mobility of major, minor and trace elements during weathering of granitic rocks. Chemical Geology 68, 253-273.

Moorbath, S., O'Nions, R.K., Pankhurst, R.J., 1973. Early Archaean age for the Isua Iron Formation, West Greenland. Nature 245, 138-139.

Mulrooney, D., Rivers, T., 2005. Redistribution of the rare-earth elements among coexisting minerals in metamafic rocks across the epidote-out isograd: An example from the St. Anthony complex, northern Newfoundland, Canada. The Canadian Mineralogist 43, 263-294.

Myers, J.S., 1997. Tectonic evolution of deep crustal structures in the mid-Proterozoic Albany-Fraser Orogen, Western Australia. In: Sengupta, S., (Ed.). Evolution of geological structures in micro- to macro-scales. Chapman and Hall London, 473-485.

Nesbitt, H.W., Young, G.M., 1982. Early Proterozoic climates and plate motions inferred from major element chemistry of lutites. Nature 299, 715-717.

Nesbitt, H.W., Young, G.M., 1984. Prediction of some weathering trends of plutonic and volcanic rocks based on thermodynamic and kinetic considerations. Geochimica et Cosmochimica Acta 48, 1523-1534.

Nesbitt, H.W., Young, G.M., McLennan, S.M., Keays, R.R., 1996. Effects of chemical weathering and sorting on the petrogenesis of siliciclastic sediments, with implications for provenance studies. Journal of Geology 104, 525-542.

Nutman, A.P., 2006. Antiquity of the oceans and continents. Elements 2 (4), 223-227.

Nutman, A.P., Friend, C.R.L., 2007. Adjacent terranes with ca. 2715 and 2650 Ma high-pressure metamorphic assemblages in the Nuuk region of the North Atlantic Craton, southern West Greenland: Complexities of Neoarchaean collisional orogeny. Precambrian Research 155, 159-203.

Nutman, A.P., Friend, C.R.L., Baadsgaard, H., McGregor, V.R., 1989. Evolution and assembly of Archean Gneiss Terranes in the Godthåbsfjord Region, Southern West Greenland: Structural, metamorphic, and isotopic evidence. Tectonics 8 (3), 573-589.

Nutman, A.P., McGregor, V.R., Friend, C.R.L., Bennett, V.C., Kinny, P.D., 1996. The Itsaq gneiss complex of southern West Greenland; the world's most extensive record of early crustal evolution (3900-3600 Ma). Precambrian Research 78 (1-3), 1-39.

Ohta, H., Maruyama, S., Takahashi, E., Watanabe, Y., Kato, Y., 1996. Field occurrence, geochemistry and petrogenesis of the Archean Mid-Ocean Ridge Basalts (AMORBs) of the Cleaverville area, Pilbara Craton, Western Australia. Lithos 37, 199-221.

Ordóñez-Calderón, J.C., Polat, A., Fryer, B.J., Gagnon, J.E., Raith, J.G., Appel, P.W.U., 2008. Evidence for HFSE and REE mobility during calc-silicate metasomatism, Mesoarchean (~3075 Ma) Ivisaartoq greenstone belt, southern West Greenland. Precambrian Research 161 (3-4), 317-340.

Pan, Y., Fleet, M.E., 1992. Mineralogy and genesis of calc-silicates associated with Archean volcanogenic massive sulphide deposits at the Manitouwadge mining camp, Ontario. Canadian Journal of Earth Sciences 29, 1375-1388.

Pearce, J.A., 1996. A user's guide to basalt discrimination diagrams. In: Wyman, D.A. (Ed.). Trace element geochemistry of volcanic rocks: Applications for massive sulphide exploration. Geological Association of Canada, Short Course Notes 12, 79-113.

Pearce, J.A., 2003. Supra-subduction zone ophiolites: The search for modern analogues. In: Dilek, Y., Newcomb, S., (Eds.). Ophiolite concept and the evolution of the geological thought. Geological Society of America Special Paper 373, 269-293.

Pearce, J.A., 2008. Geochemical fingerprinting of oceanic basalts with applications to ophiolite classification and the search for Archean oceanic crust. Lithos 100, 14-48.

Pearce, J.A., Peate, D.W., 1995. Tectonic implications of the composition of volcanic arc magmas. Annual Reviews of Earth and Planetary Sciences 23, 251-285.

Pearce, J.A., van der Laan, S.R., Arculus, R.J., Murton, B.J., Ishii, T., Peate, D.W., Parkinson, I.J., 1992. Boninite and harzburgite from Leg 125 (Bonin-Mariana Fore-arc): A case study of magma genesis during the initial stages of subduction. In: Fryer, P., Pearce, J.A., Stocking, L.B., (Eds.). Proceedings of the Ocean Drilling Program, Scientific Results vol. 125, 623-659.

Perfit, M.R., Fornari, D.J., Ridley, W.I., Kirk, P.D., Casey, J., Kastens, K.A., Reynolds, J.R., Edwards, M., Desonie, D., Shuster, R., Paradis, S., 1996. Recent volcanism in the Siqueiros transform fault: Picritic basalts and implications for MORB magma genesis. Earth and Planetary Science Letters 141, 91-108.

Plank, T., Langmuir, C.H., 1993. Tracing trace elements from sediment input to volcanic output at subduction zones. Nature 362, 739-743.

Polat, A., Appel, P.W.U., Frei, R., Pan, Y., Dilek, Y., Ordóñez-Calderón, J.C., Fryer, B., Raith, J.G., 2007. Field and geochemical characteristics of the Mesoarchean (~3075

Ma) Ivisaartoq greenstone belt, southern West Greenland: Evidence for seafloor hydrothermal alteration in a supra-subduction oceanic crust. Gondwana Research 11, 69-91.

Polat, A., Frei, R., Appel, P.W.U., Dilek, Y., Fryer, B., Ordóñez-Calderón, J.C., Yang, Z., 2008. The origin and compositions of Mesoarchean oceanic crust: Evidence from the 3075 Ma Ivisaartoq greenstone belt, SW Greenland. Lithos 100, 293-321.

Polat, A., Hofmann, A.W., 2003. Alteration and geochemical patterns in the 3.7-3.8 Ga Isua greenstone belt, West Greenland. Precambrian Research 126, 197-218.

Polat, A., Hofmann, A.W., Münker, C., Regelous, M., Appel, PW.U., 2003. Contrasting geochemical patterns in the 3.7-3.8 Ga pillow basalt cores and rims, Isua greenstone belt, Southwest Greenland: Implications for postmagmatic alteration processes. Geochimica et Cosmochimica Acta 67 (3), 441-457.

Polat, A., Hofmann, A.W., Rosing, M.T., 2002. Boninite-like volcanic rocks in the 3.7-3.8 Ga Isua greenstone belt, West Greenland: Geochemical evidence for intra-oceanic subduction zone processes in the early Earth. Chemical Geology 184, 231-254

Polat, A., Kerrich, R., 2001. Geodynamic processes, continental growth, and mantle evolution recorded in late Archean greenstone belts of the southern Superior Province, Canada. Precambrian Research 112, 5-25.

Polat, A., Kerrich, R., Wyman, D.A., 1999. Geochemical diversity in oceanic komatiites and basalts from the late Archean Wawa greenstone belts, Superior Province, Canada: Trace element and Nd isotope evidence for a heterogeneous mantle. Precambrian Research, 94, 139-173.

Polat, A., Kerrich, R., Wyman, D.A., 1998. The late Archean Schreiber-Hemlo and White River-Dayohessarah greenstone belts, Superior Province: Collages of oceanic

plateaus, oceanic arcs, and subduction-accretion complexes. Tectonophysics 289, 295-326.

Pollack, H.N., 1997. Thermal characteristics of the Archean mantle. In: de Wit, M., Ashwal, L.D., (Eds.). Greenstone belts. Oxford Monographs on Geology and Geophysics 35, 223-232.

Raith, J.G., Polat, A., Appel, P.W.U., 2006. Hydrothermal alteration of Archean oceanic crust in the Ivisaartoq greenstone belt, southern West Greenland. Pangeo Conference Series, Austria, 264-265.

Reagan, M.K., Hanan, B.B., Heizler, M.T., Hartman, B.S., Hickey-Vargas, R., 2008. Petrogenesis of volcanic rocks from Saipan and Rota, Mariana Islands, and implications for the evolution of nascent island arcs. Journal of Petrology 49, 441-464.

Rohrbach, A., Schuth, S., Ballhaus, C., Münker, C., Matveev, S., Qopoto, C., 2005. Petrological constraints on the origin of arc picrites, New Georgia Group, Solomon Islands. Contributions to Mineralogy and Petrology 149, 685-698.

Roser, B.P., Nathan, S., 1997. An evaluation of element mobility during metamorphism of a turbidite sequence (Greenland Group, New Zealand). Geological Magazine 134 (2), 219-234.

Rubin, J.N., Henry, C.D., Price, J.G., 1993. The mobility of zirconium and other "immobile" elements during hydrothermal alteration. Chemical Geology 110, 29-47.

Sandeman, H.A., Hanmer, S., Davis, W.J., Ryan, J.J., Peterson, T.D., 2004. Neoarchaean volcanic rocks, Central Hearne supracrustal belt, Western Churchill Province, Canada: Geochemical and isotopic evidence supporting intra-oceanic, supra-subduction zone extension. Precambrian Research 134, 113-141.

Schiøtte, L., Compston, W., Bridgwater, D., 1988. Late Archaean ages for the deposition of clastic sediments belonging to the Malene supracrustals, southern West Greenland: Evidence from an ion probe U-Pb zircon study. Earth and Planetary Science Letters 87 (1-2), 45-58.

Schmidt, M.W., Poli, S., 2003. Generation of mobile components during subduction of the oceanic crust. Treatise on Geochemistry, Elsevier, vol. 3, 567-591.

Schuth, S., Rohrbach, A., Münker, C., Ballhaus, C., Garbe-Schönberg, D., Qopoto, C., 2004. Geochemical constraints on the petrogenesis of arc picrites and basalts, New Georgia Group, Solomon Islands. Contribution to Mineralogy and Petrology 148, 288-304.

Şengör, A.M.C., 1990. Plate tectonics and orogenic research after 25 years: A Tethyan perspective. Earth Science Reviews 27, 1-201.

Şengör, A.M.C., Natal'in, B.A., 2004. Phanerozoic analogues of Archean oceanic basement fragments: Altaid ophiolites and ophirags. In: Kusky, T.M., (Ed.). Precambrian ophiolites and related rocks. Developments in Precambrian Geology, Elsevier vol. 13, 675-726.

Shervais, J.W., 2001. Birth, death, and resurrection: The life cycle of suprasubduction zone ophiolites. Geochemistry, Geophysics, Geosystems 2, Paper number 2000GC000080.

Smith, C.G., Phillips, E.R., 2002. Cummingtonite in the Dalradian of NE Scotland. Mineralogical Magazine 66 (2), 337-352.

Smithies, R.H., 2000. The Archean tonalite-trondhjemite-granodiorite (TTG) series is not an analogue of Cenozoic adakite. Earth and Planetary Science Letters 182, 115-125.

Smithies, R.H., Champion, D.C., Sun, S., 2004. The case for Archean boninites. Contributions to Mineralogy and Petrology 147, 705-721.

Staudigel, H., Plank, T., White, B., Schmincke, H-U., 1996. Geochemical fluxes during sea floor alteration of the basaltic upper oceanic crust: DSDP sites 417 and 418. In: Bebout, G.E., Scholl, S.W., Kirby, S.H., Platt, J.P., (Ed.). Subduction: Top to bottom. American Geophysical Union, Washington, 19-38.

Stern, R.J., Bloomer, S.H., 1992. Subduction zone infancy: Examples from Eocene Izu-Bonin-Mariana and Jurassic California arcs. Geological Society of America Bulletin 104, 1621-1636.

Storkey, A.C., Hermann, J., Hand, M., Buick, I.S., 2005. Using in situ trace-element determinations to monitor partial-melting processes in metabasites. Journal of Petrology 46 (6), 1283-1308.

Sugitani, K., Yamashita, F., Nagaoka, T., Yamamoto, K., Minami, M., Mimura, K., Suzuki, K., 2006. Geochemistry and sedimentary petrology of Archean clastic sedimentary rocks at Mt. Goldsworthy, Pilbara Craton, Western Australia: Evidence for the early evolution of continental crust and hydrothermal alteration. Precambrian Research 147, 124-147.

Sun, S.S., McDonough, W.F., 1989. Chemical and isotopic systematics of oceanic basalts: Implications for mantle composition and processes. Geological Society of London Special Publications 42, 313-345.

Sun, S.S., Nesbitt, R.W., 1978. Geochemical regularities and genetic significance of ophiolitic basalts. Geology 6, 689-693.

Taylor, R.N., Nesbitt, R.W., 1988. Light rare-earth element enrichment of suprasubduction zone mantle: Evidence from the Troodos ophiolite, Cyprus. Geology 16, 448-451.

Taylor, S.R., McLennan, S. M., 1985. The continental crust: Its composition and evolution. Blackwell, Oxford, 312 pp.

Taylor, S.R., McLennan, S.M., 1995. The geochemical evolution of the continental crust. Reviews of Geophysics 33, 241-265.

Taylor, S.R., Rudnick, R.L., McLennan, S.M., Eriksson, K., 1986. Rare earth element patterns in Archean high-grade metasediments and their tectonic significance. Geochimica et Cosmochimica Acta 50, 2267-2279.

Terabayashi, M., Masada, Y., Ozawa, H., 2003. Archean ocean-floor metamorphism in the North Pole area, Pilbara Craton, Western Australia. Precambrian Research 127, 167-180.

Thompson, R.N., Gibson, S.A., Dickin, A.P., Smith, P.M., 2001. Early Cretaceous basalt and picrite dykes of the Southern Etendeka Region, NW Namibia: Windows into the role of the Tristan mantle plume in Paraná-Etendeka magmatism. Journal of Petrology 42, 2049-2081.

Thurston, P.C., Ayres, L.D., 2004. Archean and Proterozoic greenstone belts: Setting and evolution. In: Eriksson, P.G., Altermann, W., Nelson, D.R., Mueller, W.U., Catuneanu, O., (Eds.). The Precambrian earth: Tempos and events. Developments in Precambrian Geology 12, 311-333.

Thurston, P.C., Fryer, B.J., 1983. The geochemistry of repetitive cyclical volcanism from basalt through rhyolite in the Uchi-Confederation greenstone belt, Canada. Contributions to Mineralogy and Petrology 83, 204-226.

Van Baalen, M.R., 1993. Titanium mobility in metamorphic systems: A review. Chemical Geology 110, 233-249.

Van Westrenen, W., Blundy, J., Wood, B., 2001. High field strength element/rare earth fractionation during partial melting in the presence of garnet: Implications for identifications of mantle heterogeneities. Geochemistry, Geophysics, Geosystems 2, Paper number 2000GC000133.

Viruete, J.E., Díaz de Neira, A., Hernáiz Huerta, P.P., Monthel, J., García Senz, J., Joubert, M., Lopera, E., Ullrich, T., Friedman, R., Mortensen, J., Pérez-Estaún, A., 2006. Magmatic relationships and ages of Caribbean Island arc tholeiites, boninites and related felsic rocks, Dominican Republic. Lithos 90, 161-186.

Weiershäuser, L., Spooner, E.T.C., 2005. Seafloor hydrothermal fluids, Ben Nevis area, Abitibi greenstone belt: Implications for Archean (approximately 2.7 Ga) seawater properties. Precambrian Research 138, 89-123.

Wilkins, C., 1997. Regional and contact metamorphism. In: de Wit, M., Ashwal, L.D., (Eds.). Greenstone belts. Oxford Monographs on Geology and Geophysics 35, 126-163.

Winchester, J.A., Floyd, P.A., 1977. Geochemical discrimination of different magma series and their differentiation products using immobile elements. Chemical Geology 20, 325-343.

Wood, S.A., 2005. The aqueous geochemistry of zirconium, hafnium, niobium and tantalum. In: Linnen, R.L., Samson, I.M., (Eds.). Rare-element geochemistry and mineral deposits. Geological Association of Canada, GAC Short Course Notes 17, 217-268.

Woodland, S.J., Pearson, D.G., Thirlwall, M.F., 2002. A platinum group element and Re-Os isotope investigation of siderophile element recycling in subduction zones: Comparison of Grenada, Lesser Antilles arc, and the Izu-Bonin arc. Journal of Petrology 43, 171-198.

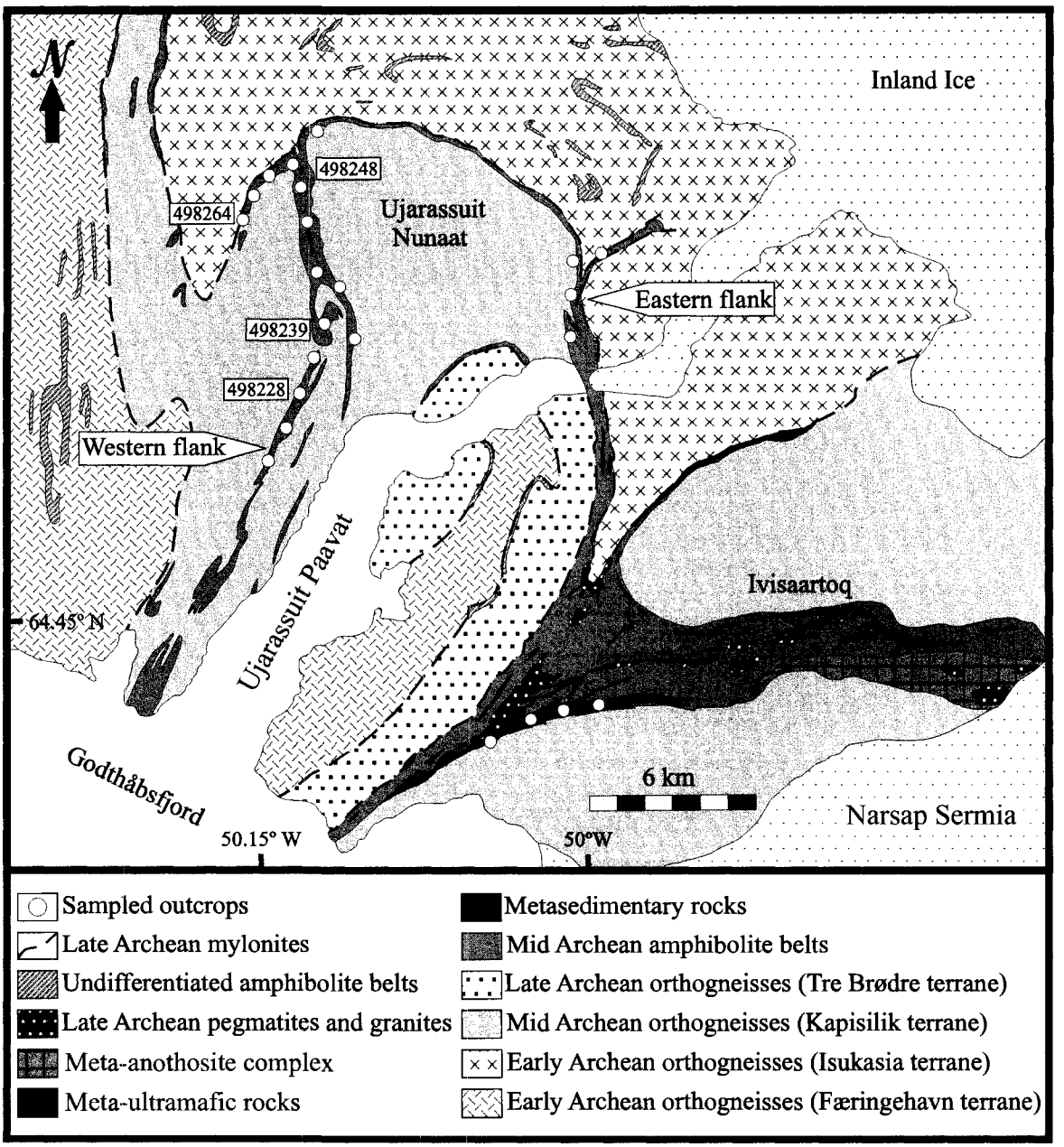

Figure 3.1. Geological map of the Ivisaartoq and Ujarassuit greenstone belts with approximate sample locations (Modified from Friend and Nutman, 2005 after Chadwick and Coe, 1988). Structural measurements and sampling of metavolcanic and metasedimentary rocks were conducted in the eastern and western flanks of the Ujarassuit greenstone belt. The lower metasedimentary unit of the Ivisaartoq greenstone belt was also sampled.

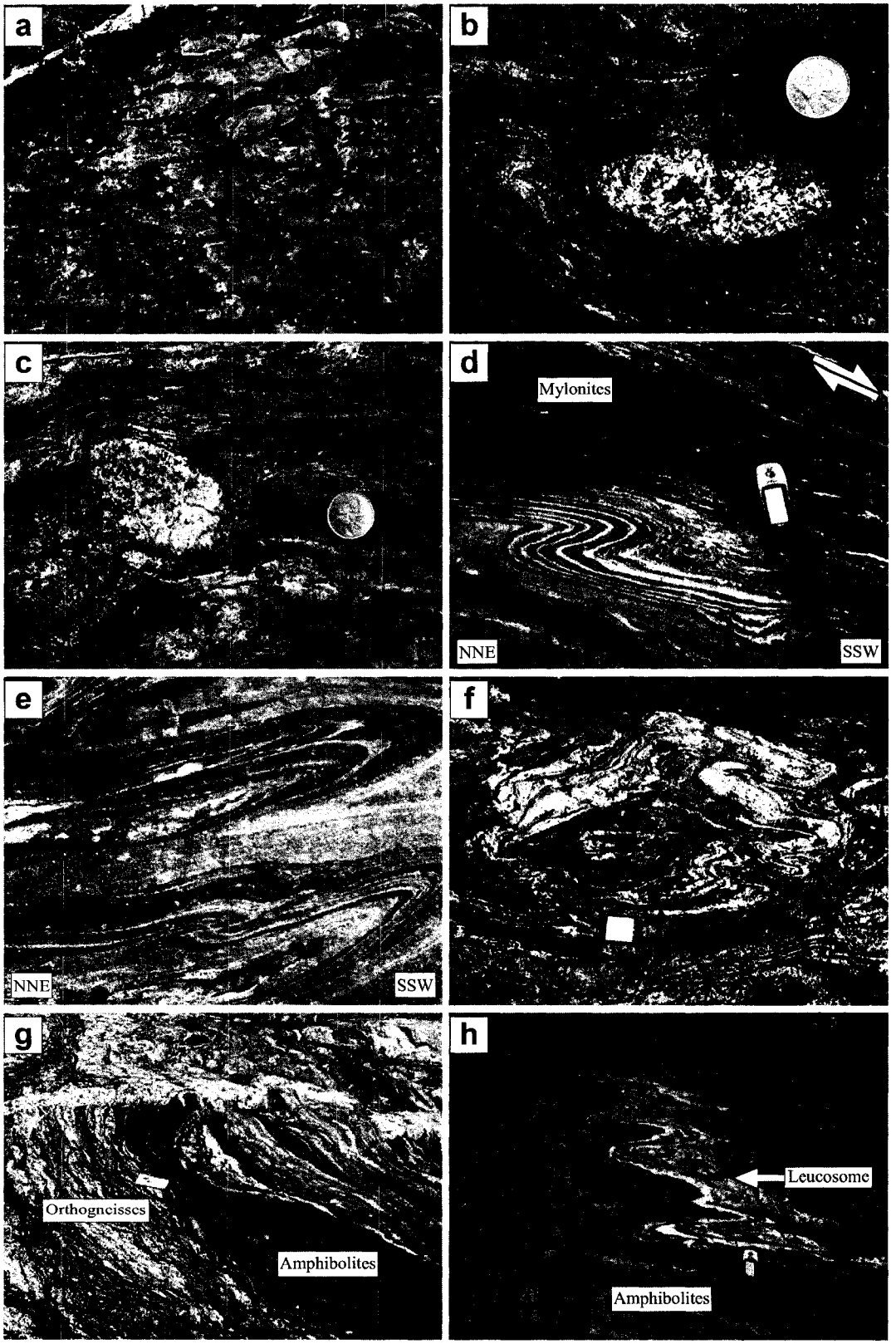

Figure 3.2. (*See next page for Figure caption*)

Figure 3.2. Field photographs of various rock types in the Ivisaartoq (a-c) and Ujarassuit (d-h) greenstone belts. (a) Pillow basalts from the Ivisaartoq belt. (b-c) Relict felsic cobbles in biotite schists of the Ivisaartoq greenstone belt. (d-e) Asymmetric and transposed folds in mylonites at the contact between TTG-gneisses and amphibolites. (f-g) Migmatitic TTG-gneisses, close to the contact with amphibolites, with large xenolithic inclusions of amphibolites. (h) Migmatitic amphibolites affected by recumbent F_2 folding.

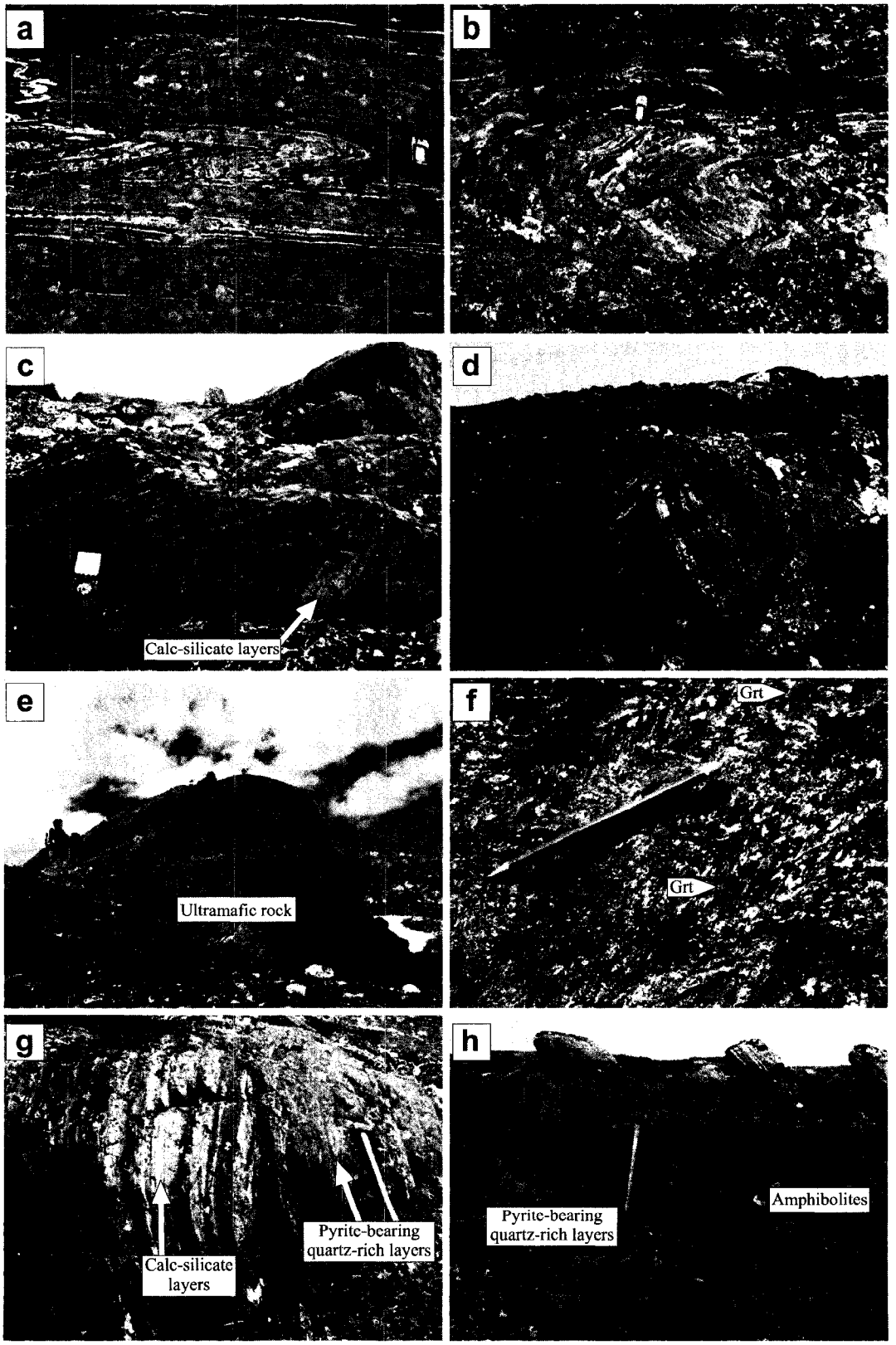

Figure 3.3. (*See next page for Figure caption*)

Figure 3.3. Field photographs of various rock types in the Ujarassuit greenstone belt. (a) Rootless F_1 isoclinal fold transposed into the prevalent regional S_2 foliation. (b-c) F_2 Recumbent folds in amphibolites. Calc-silicate alterations have been affected by F_2 recumbent folding. (d) Outcrop-scale F_3 upright folds in amphibolites. (e) Serpentinized olivine-rich ultramafic rocks with lens-shaped geometry. (f) Biotite schists with small-scale F_2 isoclinal folds. (g-h) Calc-silicate and pyrite-bearing quartz-rich layers hosted by hornblende-rich amphibolites.

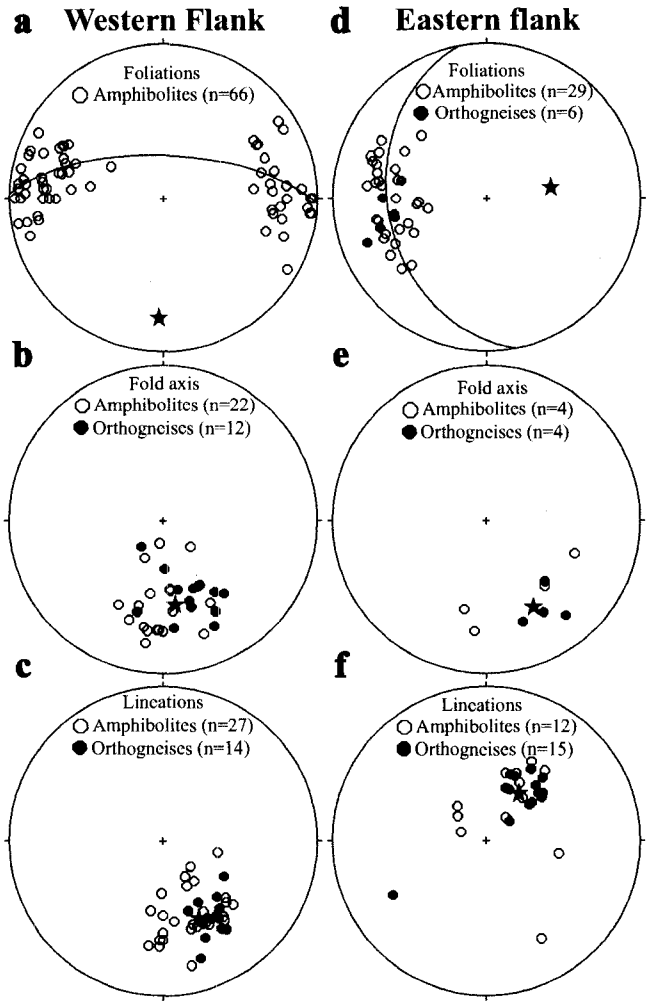

Figure 3.4. Equal-area lower hemisphere stereographic projections for the western (a-c) and eastern (d-f) flanks of the Ujarassuit greenstone belt. Stars represent: F_2 (a) and F_3 (d) π-fold axes defined by great circles through pole to foliations; average small-scale isoclinal F_2 fold axis (b and e); and average L_2 (c) and L_3 (f) mineral stretching lineations.

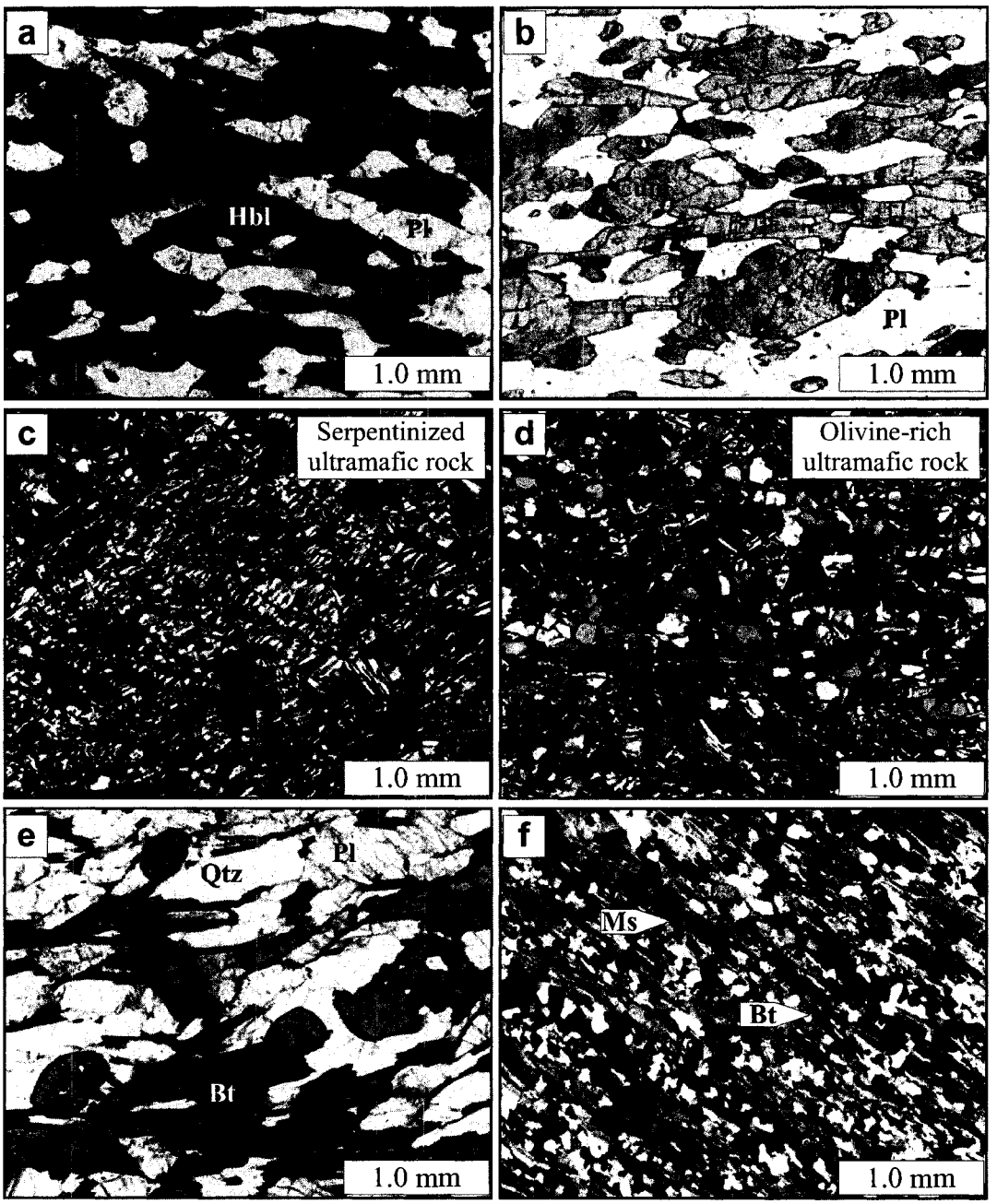

Figure 3.5. Photomicrographs of metavolcanic and metasedimentary rocks (see Table 3.1). (a) Hornblende-rich amphibolites (Groups 1-3 amphibolites). (b) Cummingtonite-rich amphibolites (Group 4 amphibolites). (c) Serpentinized olivine-rich ultramafic rock. (d) Unaltered olivine-rich ultramafic rock (see also Fig. 3.3e). (e) Biotite schist with accessory garnet. (f) Fine-grained quartzitic gneiss with abundant muscovite and minor biotite. Plane polarized light for (a-b) and (e), and crossed polarized light for (c-d) and (f). Abbreviations: Bt, biotite; Cum, cummingtonite; Grt, garnet; Hbl, hornblende; Ms, muscovite; Pl, plagioclase; Qtz, quartz.

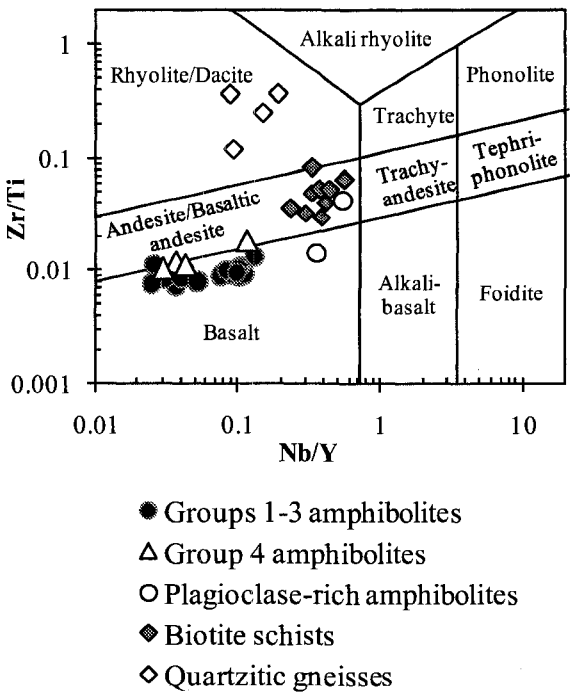

Figure 3.6. Zr/Ti versus Nb/Y classification diagram for metavolcanic rocks (amphibolites) in the Ujarassuit greenstone belt (Table 3.1). Metasedimentary rocks (biotite schists and quartzitic gneisses) are also plotted for intercomparisons. Compositional fields revised by Pearce (1996) after Winchester and Floyd (1977).

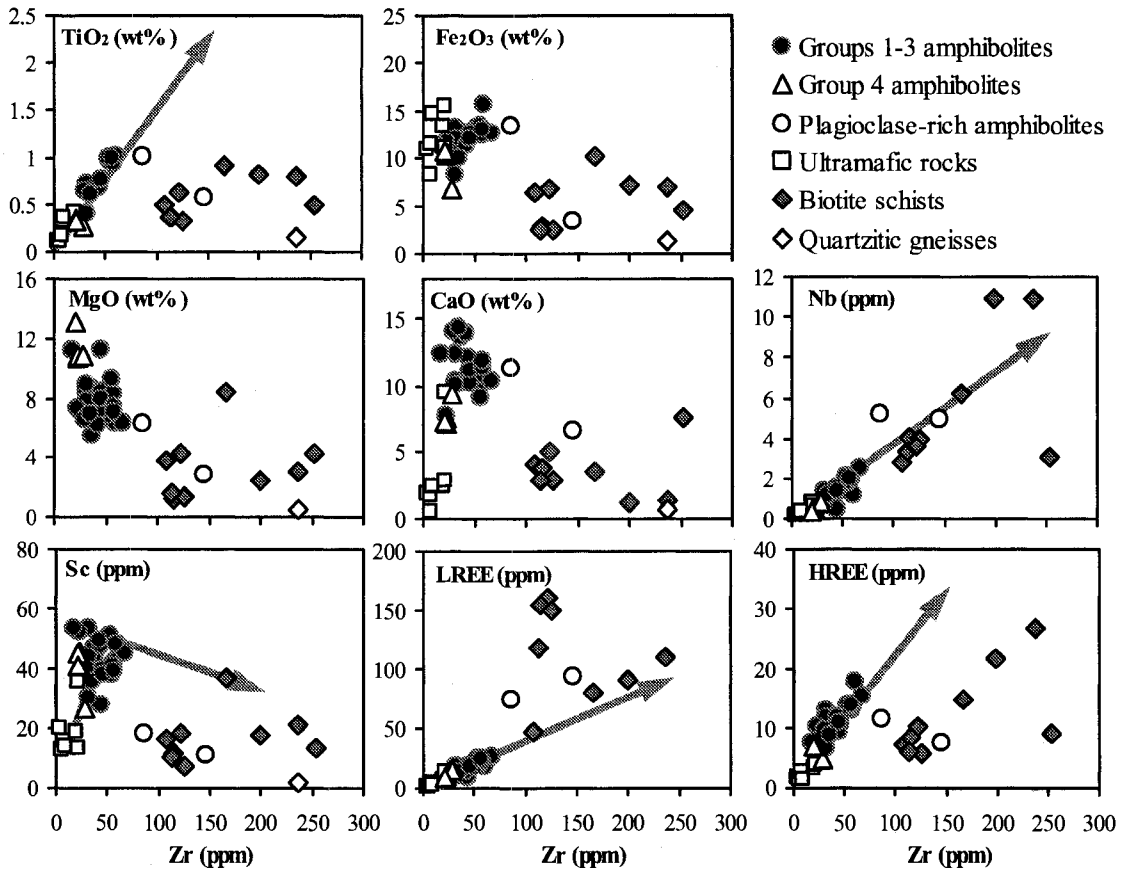

Figure 3.7. Variation diagrams of Zr versus selected major and trace elements for metavolcanic and metasedimentary rocks (Table 3.1). Arrows represent the deduced magmatic trends for metavolcanic rocks in the Ivisaartoq greenstone belt (see Ordóñez-Calderón et al., 2008).

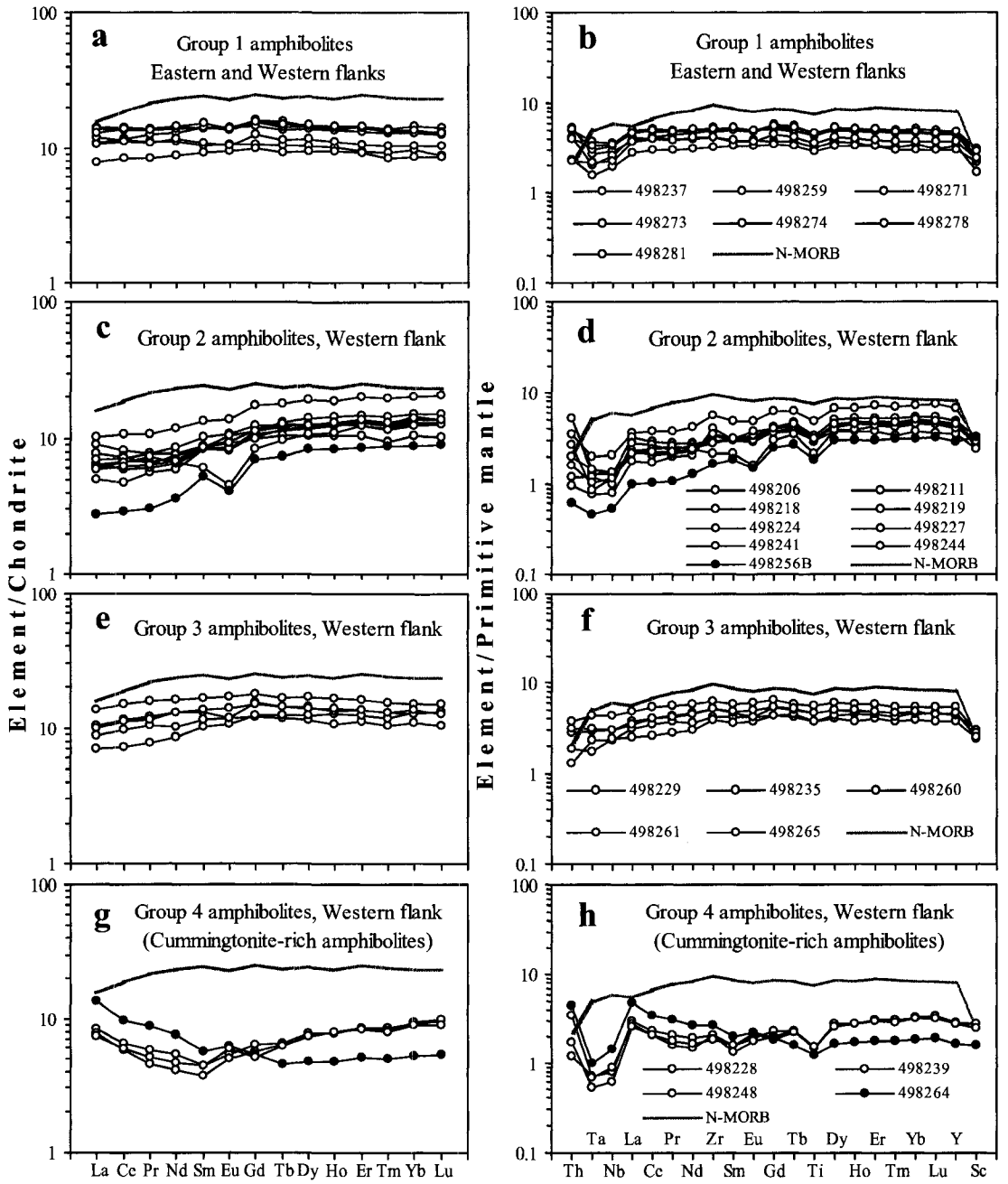

Figure 3.8. Chondrite- and primitive-mantle normalized diagrams for hornblende-rich (Groups 1-3) and cummingtonite-rich (Group 4) amphibolites in the Ujarassuit greenstone belt. Amphibolites were divided into groups according to the total trace element abundance, the presence or absence of Nb-Ta anomalies, and the degree of depletion of LREE. Chondrite normalization values from Sun and McDonough (1989). Primitive mantle normalization values and average geochemical composition of modern N-MORB from Hofmann (1988).

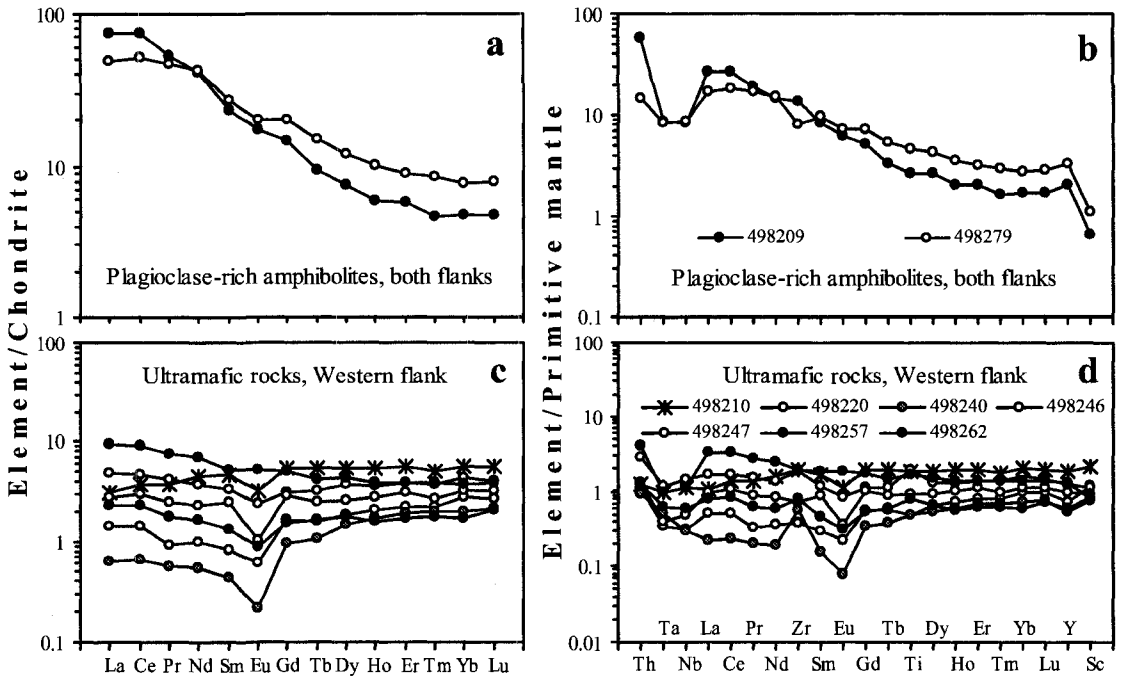

Figure 3.9. Chondrite- and primitive-mantle normalized diagrams for (a-b) Plagioclase-rich amphibolites with basaltic andesite and andesite geochemical composition. (c-d) ultramafic rocks (Table 3.1). Normalization values as in Figure 3.8.

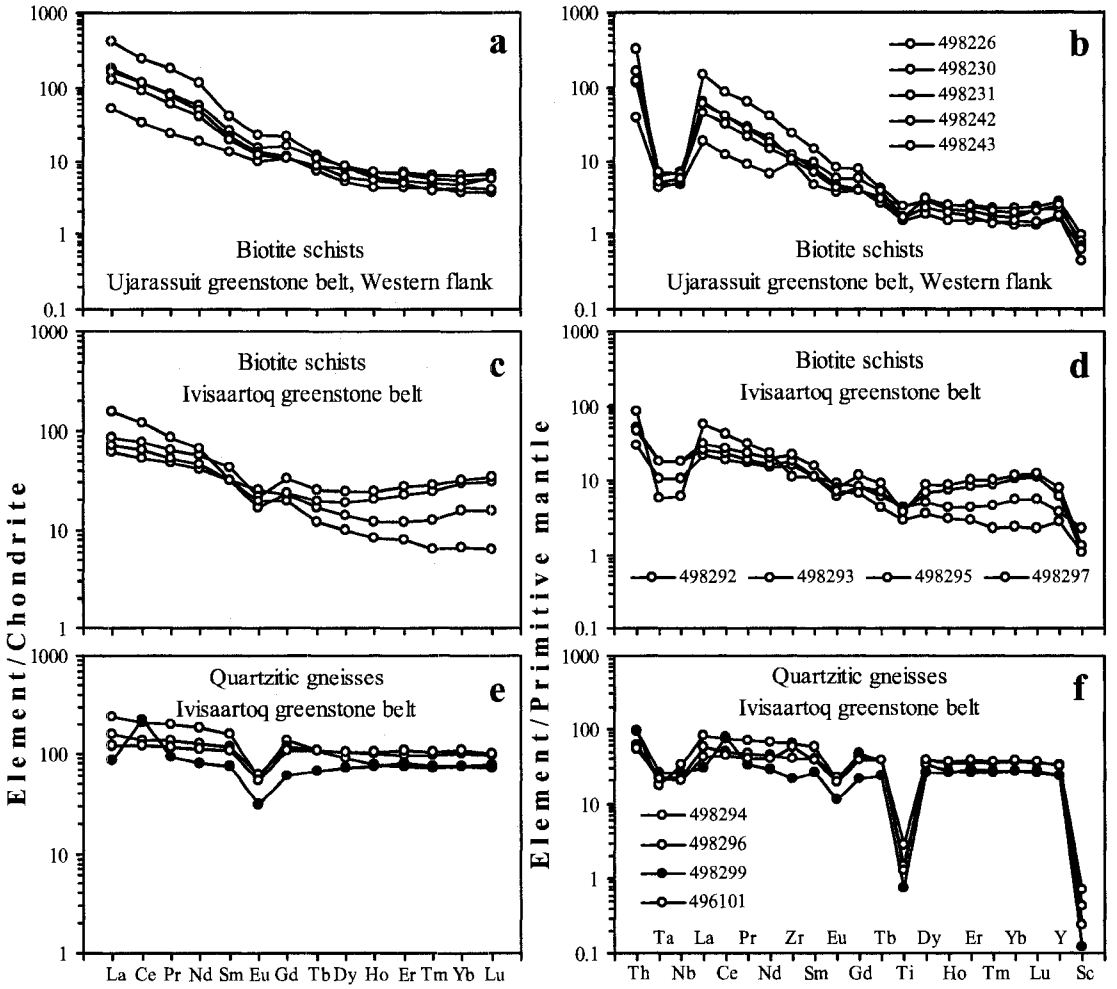

Figure 3.10. Chondrite- and primitive-mantle normalized diagrams for metasedimentary rocks. (a-b) Biotite schists in the western flank of the Ujarassuit greenstone belt. (c-f) Biotite schists and quartzitic gneisses in the lower metasedimentary unit of the Ivisaartoq belt. Normalization values as in Figure 3.8.

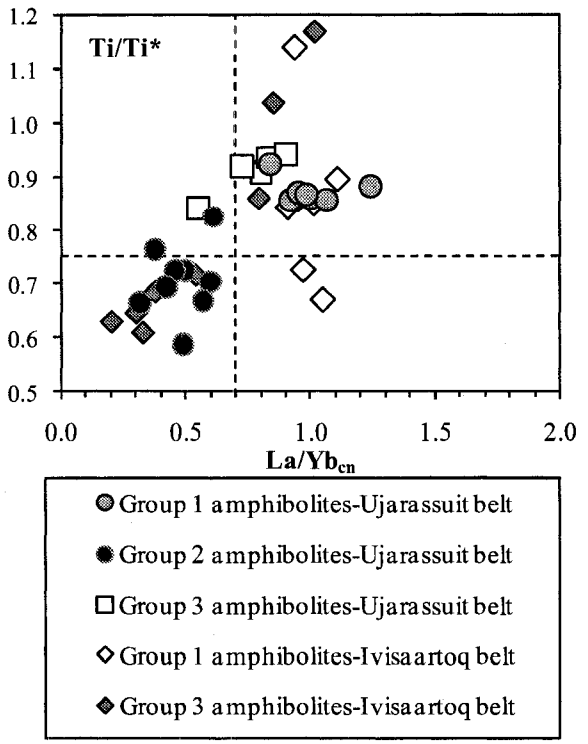

Figure 3.11. Ti/Ti* versus La/Yb_{cn} diagram for Groups 1-3 amphibolites in the Ujarassuit greenstone belt. Group 1 and 3 amphibolites from the Ivisaartoq belt are compositionally similar, respectively, to Groups 1 and 2 in this study (see Ordóñez-Calderón et al., 2008). This diagram illustrate that amphibolites with stronger negative anomalies of Ti are more depleted in LREE (see Chapter 3.7.2).

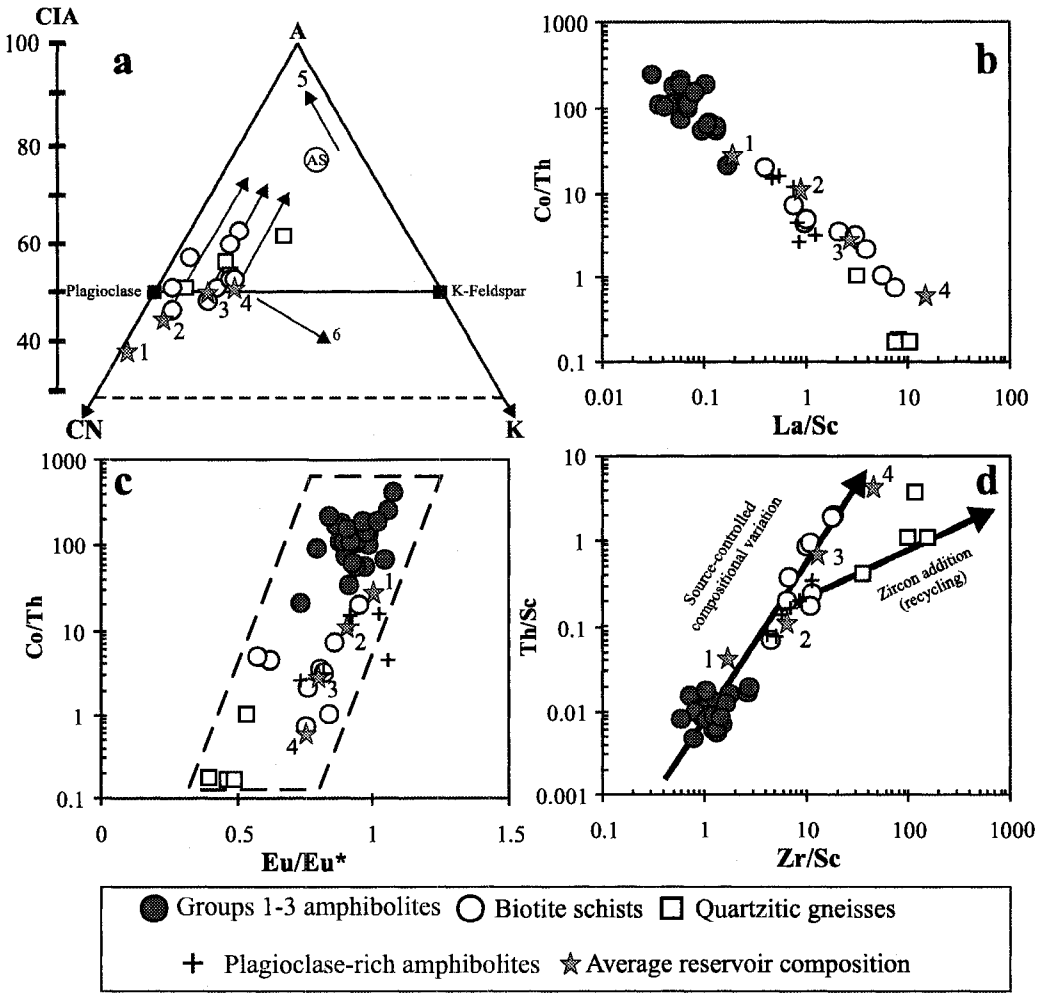

Figure 3.12. Ternary weathering diagram (a) and selected trace element ratios (b-d) for biotite schists and quartzitic gneisses from the Ivisaartoq and Ujarassuit greenstone belts. The ternary diagram is plotted in molecular proportions of Al_2O_3 (A)-CaO*+Na_2O (CN)-K_2O (K) where CaO* represents the amount of CaO in the silicate fraction (Nesbit and Young, 1982, 1984; Fedo et al., 1995). The scale for the chemical index of alteration (CIA) is illustrated to the left (McLennan and Murray, 1999). Numbered stars represent the following reservoir compositions: 1 = average oceanic island arc tholeiitic basalt (Kelemen et al., 2003); 2 = average andesite (Kelemen et al., 2003); 3 = average > 3.5 Ga upper continental crust (Condie, 1993); 4 = average Archean calc-alkaline granite (Kemp and Hawkesworth, 2003). In the ternary diagram: AS = Archean shale; arrows parallel to the A-CN side represent the predicted weathering trend for intermediate to felsic protoliths (stars 2-4); arrow 5 represent the trend of extremely weathered rocks, and arrow 6 the trend of sediments affected by potassium metasomatism. Groups 1-3 amphibolites are those in this study and Group 1 amphibolites in the Ivisaartoq belt (Ordóñez-Calderón et al., 2008). Plagioclase-rich amphibolites, with an andesitic geochemical composition, are from this study and those from the Qussuk greenstone belt (Garde, 2007).

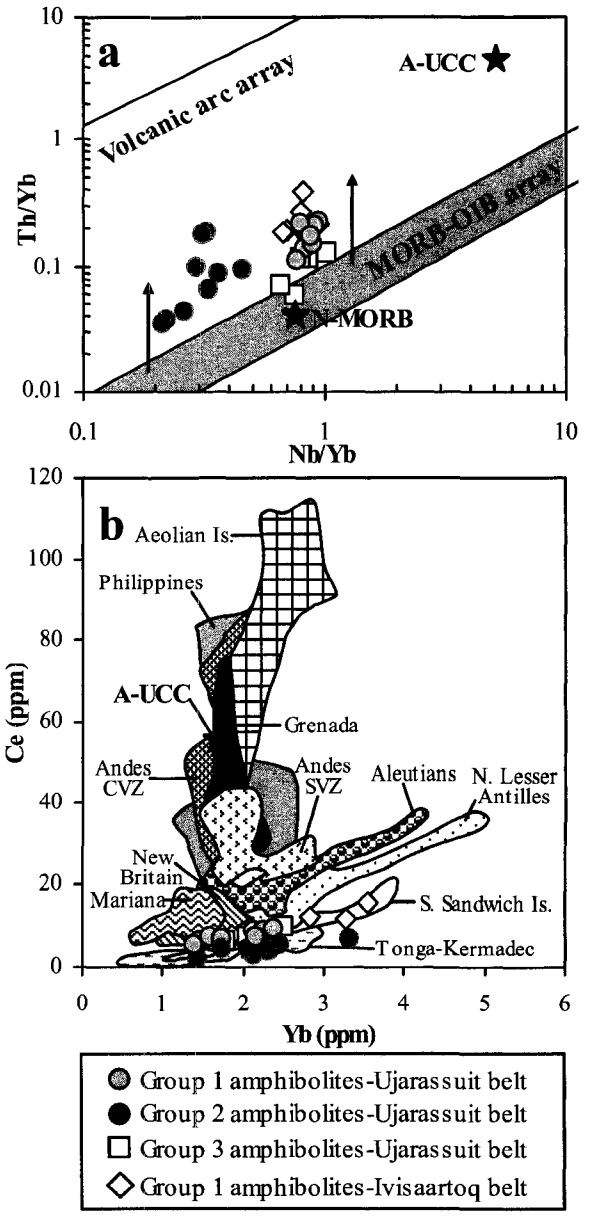

Figure 3.13. (a) Th/Yb versus Nb/Yb diagram showing the fields of modern MORB-OIB and volcanic arc arrays (see Pearce and Peate, 1995 and Pearce, 2008). (b) Ce versus Yb diagram with the compositional field for oceanic and continental arc basalts from Hawkesworth et al. (1993). The composition of least altered Group 1 amphibolites from the Ivisaartoq greenstone belt was plotted for intercomparisons (see Ordóñez-Calderón et al., 2008). Average composition of modern N-MORB and Archean (> 3.5 Ga) upper continental crust (A-UCC) after Hofmann (1988) and Condie (1993), respectively.

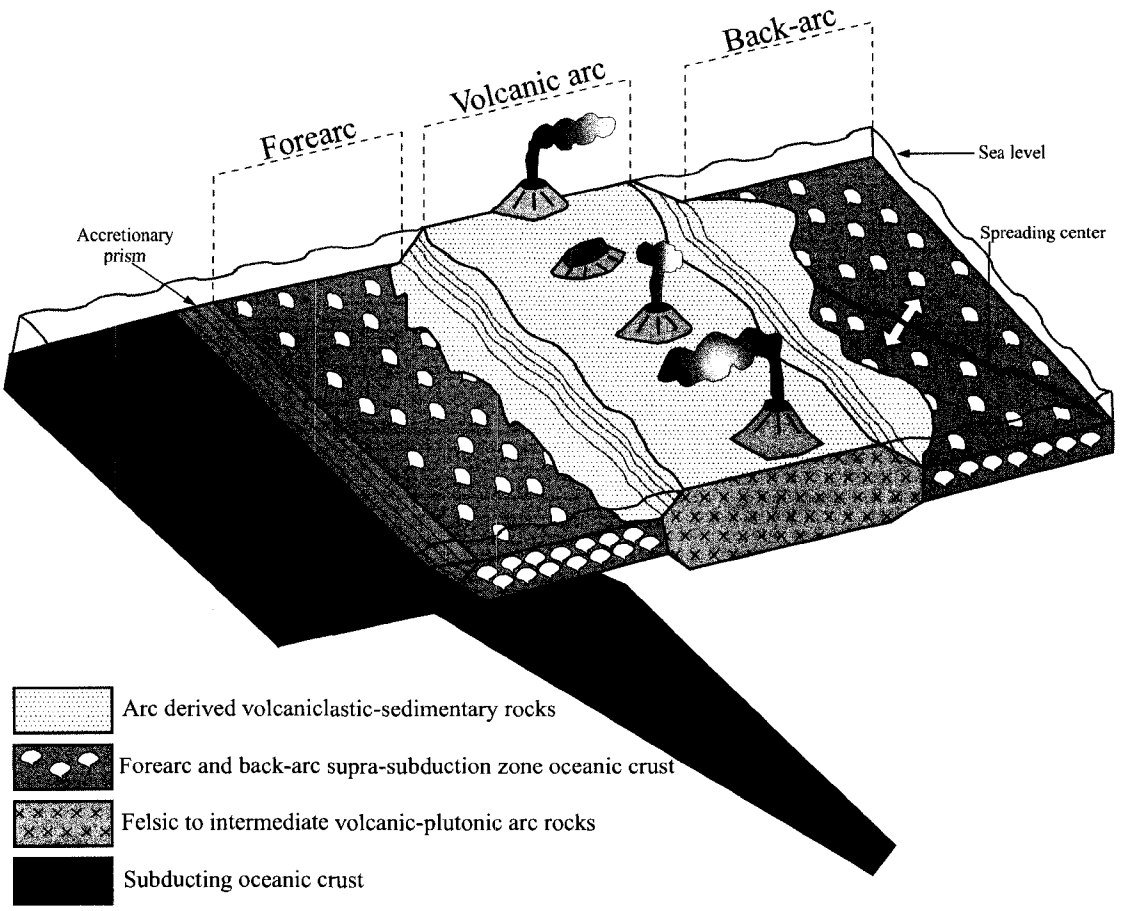

Figure 3.14. Schematic block diagram (not to scale), across a hypothetical intra-oceanic subduction zone setting, illustrating the proposed geodynamic origin of the Ujarassuit greenstone belt. The polarity of subduction is arbitrary. The protoliths of metavolcanic rocks in this study are interpreted to have been erupted either in the forearc or back-arc region. Biotite schists represent volcaniclastic-sedimentary rocks with a mixed provenance, which includes detritus derived from the erosion of felsic to intermediate arc volcanic and plutonic rocks, and local detritus derived from mafic to ultramafic volcanic rocks in the forearc or back-arc.

Table 3.1. Mineralogical characteristics and interpreted protoliths for the main rock types discussed in this study

Lithology	Mineralogical composition	Protolith
Hornblende-rich amphibolites (Groups 1-3 amphibolites)	Hornblende + plagioclase + quartz + zircon + titanite + apatite ± magnetite ± garnet ± biotite ± cummingtonite	Basaltic rocks. Groups 1-2 amphibolites represent island arc tholeiites (IAT). Group 3 amphibolites represent rare N-MORB-like tholeiites
Cummingtonite-rich amphibolites (Group 4 amphibolites)	Cummingtonite ± anthophyllite ± hornblende + plagioclase + quartz ± biotite ± magnetite	Boninite-like rocks
Plagioclase-rich amphibolites	Hornblende + plagioclase + quartz + zircon + titanite + apatite ± magnetite ± biotite	Transitional to calc-alkaline basaltic andesites and andesites
Serpentinized olivine-rich rocks and actinolite-tremolite-rich amphibolites (Ultramafic rocks)	Serpentine + talc + actinolite + tremolite + magnetite ± cummingtonite ± olivine ± clinopyroxene ± magnetite	Olivine-rich pricritic cumulus
Biotite schists	Biotite + plagioclase + quartz + magnetite ± garnet ± epidote ± titanite ± muscovite ± microcline ± hornblende ± cummingtonite ± anthophyllite ± tourmaline	Immature volcanoclastic graywackes derived from mafic to felsic source rocks
Quartzitic gneisses	Quartz + plagioclase + biotite + zircon + muscovite ± garnet ± hornblende ± magnetite ± tourmaline	quartz-rich arkoses derived from felsic source rocks

Table 3.2. Measured and recommended major and trace element concentrations for USGS standards W-2, BIR-1, BHVO-1, and BHVO-2

	W-2			BIR-1		
	Recommended	Measured (n = 5)	RSD (%)	Recommended	Measured (n = 5)	RSD (%)
SiO_2 (wt%)	52.68	52.11	1.4	47.92	47.92	0.9
TiO_2	1.06	1.07	0.8	0.96	0.97	1.1
Al_2O_3	15.45	15.23	0.9	15.50	15.56	1.2
Fe_2O_3	10.83	10.74	0.8	11.30	11.32	0.8
MnO	0.17	0.17	1.3	0.18	0.17	1.7
MgO	6.37	6.34	0.3	9.70	9.65	0.6
CaO	10.86	10.87	0.5	13.30	13.23	0.2
Na_2O	2.20	2.24	1.2	1.82	1.84	0.4
K_2O	0.63	0.62	1.9	0.03	0.03	21.7
P_2O_5	0.14	0.15	9.8	0.02	0.03	18.2
Total	99.89	99.54	0.9	100.26	100.70	0.6
Sc (ppm)	36.0	35.3	2.7	44.0	43.8	1.1
Zr	94.0	88.0	4.0	18.0	13.3	9.5

	BHVO-1			BHVO-2		
	Recommended	Measured (n = 12)	RSD (%)	Recommended	Measured (n = 18)	RSD (%)
V (ppm)		298.2	22.4	317	308.4	22.6
Cr		149.6	21.5	280	213.7	30.4
Co		45.1	9.7	45	44.3	7.9
Ni		148.7	17.4	119	152.0	9.8
Ga		65.3	3.6		65.2	4.0
Rb		9.1	3.4	9.8	8.8	5.5
Sr		395.2	2.2	389	379.2	9.8
Y	28	23.3	3.2	26	22.7	8.0
Zr	179	160.0	6.9	172	155.7	9.8
Hf	4.4	4.2	6.9	4.1	4.1	8.7
Nb	19	15.2	4.5	18	14.5	9.5
Cs	0.13	0.10	9.8		0.1	8.9
Ba	139	129.3	5.0	130	130.4	5.4
Ta	1.2	1.0	4.2	1.4	1.0	7.2
Pb	2.6	2.2	21.8		1.7	21.9
Th	1.1	1.4	7.1	1.2	1.8	18.4
U		0.4	23.6		0.4	15.9
La	16	15.0	4.4	15	14.8	5.0
Ce	39	37.7	4.8	38	37.3	4.5
Pr	5.4	5.3	5.1		5.3	5.1
Nd	25	23.9	4.9	25	24.1	4.9
Sm	6.4	6.0	5.1	6.2	6.0	5.2
Eu	2.06	2.01	4.0		2.0	2.6
Gd	6.4	6.3	4.8	6.3	6.3	3.5
Tb	0.96	0.90	3.2	0.90	0.90	5.4
Dy	5.2	5.2	4.8		5.1	4.4
Ho	0.99	0.95	5.1	1.04	0.94	4.2
Er		2.5	4.2		2.5	4.6
Tm	0.33	0.32	5.6		0.32	6.2
Yb	2.0	1.9	4.6	2	1.9	6.3
Lu	0.29	0.26	4.6	0.28	0.27	5.6

RSD = Relative standard deviation expressed as a percentage (%).

Table 3.3. Major (wt.%) and trace element (ppm) concentrations and significant element ratios for metavolcanic rocks

	Group 1 amphibolites							Group 2 amphibolites	
	498237	498259	498271	498273	498274	498278	498281	498206	498211
SiO_2 (wt.%)	49.3	52.5	47.9	52.5	50.5	51.6	49.2	50.1	47.2
TiO_2	0.96	1.00	0.70	0.61	0.76	0.94	1.00	0.66	1.01
Al_2O_3	15.58	13.57	14.60	13.55	15.30	13.83	14.70	14.90	16.15
Fe_2O_3	12.73	13.23	12.67	10.08	12.14	13.10	13.11	12.28	15.71
MnO	0.19	0.20	0.20	0.20	0.19	0.20	0.21	0.21	0.24
MgO	7.99	6.84	11.20	7.00	7.99	7.42	7.13	7.13	6.34
CaO	10.72	11.08	10.17	14.30	11.24	11.38	11.88	12.08	10.28
Na_2O	2.43	1.23	1.90	1.56	1.63	1.25	2.41	1.81	2.81
K_2O	0.06	0.30	0.61	0.19	0.18	0.21	0.26	0.79	0.13
P_2O_5	0.08	0.08	0.05	0.04	0.06	0.07	0.08	0.05	0.09
LOI (%)	0.66	0.58	1.78	0.58	1.50	0.46	0.53	1.24	0.35
Mg-number (%)	55	51	64	58	57	53	52	54	44
Sc (ppm)	38	51	28	35	38	48	39	47	48
V	266	307	206	227	237	305	282	279	297
Cr	238	211	196	603	244	257	187	307	143
Co	46	47	68	48	50	48	52	54	52
Ni	147	79	433	120	156	89	135	171	78
Ga	35	33	32	29	34	32	38	41	41
Rb	2	6	23	4	4	3	5	56	4
Sr	78	88	65	111	160	72	128	101	94
Y	19.8	20.9	14.4	13.3	16.3	20.0	21.0	18.7	29.5
Zr	54.2	53.2	44.9	35.3	45.2	58.1	57.1	44.1	60.1
Nb	1.70	2.08	1.49	1.15	1.33	1.96	2.00	0.47	1.21
Cs	0.20	0.17	2.77	0.12	0.22	0.33	0.29	1.30	0.16
Ba	25.38	28.83	57.91	35.85	46.44	21.09	43.51	91.84	31.73
Ta	0.11	0.15	0.08	0.06	0.09	0.12	0.14	0.03	0.08
Pb	1.90	2.64	4.92	5.45	6.84	3.76	5.87	6.09	3.27
Th	0.46	0.41	0.35	0.19	0.19	0.44	0.33	0.08	0.29
U	0.25	0.13	0.11	0.12	0.07	0.14	0.99	0.19	0.08
La	2.68	3.50	2.91	1.91	2.58	3.39	3.21	1.21	2.46
Ce	7.42	9.19	7.23	5.29	7.06	8.68	8.82	3.04	6.70
Pr	1.21	1.35	1.07	0.81	1.04	1.30	1.31	0.54	1.02
Nd	6.11	6.87	5.35	4.18	5.53	6.68	7.02	2.78	5.55
Sm	2.18	2.16	1.61	1.42	1.66	2.19	2.37	1.29	2.05
Eu	0.83	0.82	0.62	0.54	0.60	0.80	0.81	0.47	0.78
Gd	3.02	3.26	2.16	2.00	2.59	3.19	3.19	2.15	3.58
Tb	0.51	0.59	0.39	0.35	0.43	0.53	0.57	0.42	0.67
Dy	3.51	3.68	2.61	2.37	3.00	3.69	3.79	2.97	4.85
Ho	0.77	0.78	0.57	0.53	0.63	0.81	0.83	0.70	1.06
Er	2.23	2.42	1.56	1.53	1.78	2.35	2.40	2.12	3.39
Tm	0.33	0.36	0.23	0.21	0.27	0.34	0.35	0.32	0.51
Yb	2.15	2.39	1.58	1.40	1.73	2.14	2.26	2.14	3.31
Lu	0.32	0.36	0.22	0.22	0.27	0.33	0.33	0.32	0.53
La/Yb_{cn}	0.84	0.99	1.24	0.92	1.00	1.06	0.96	0.38	0.50
La/Sm_{cn}	0.77	1.02	1.14	0.85	0.98	0.97	0.85	0.59	0.75
Gd/Yb_{cn}	1.14	1.10	1.11	1.16	1.21	1.20	1.14	0.81	0.87
(Eu/Eu*)cn	0.98	0.94	1.02	0.98	0.88	0.92	0.91	0.87	0.88
(Ce/Ce*)cn	0.99	1.02	0.98	1.02	1.04	0.99	1.04	0.91	1.02
Al_2O_3/TiO_2	16.19	13.60	20.97	22.37	20.01	14.70	14.69	22.50	15.91
Nb/Ta	15.75	13.84	18.69	18.52	15.63	16.18	14.80	15.29	15.07
Zr/Y	2.74	2.55	3.12	2.66	2.77	2.90	2.72	2.36	2.03
Ti/Zr	106.36	112.55	92.92	102.77	101.37	97.18	105.07	89.92	101.20
(Nb/Nb*)pm	0.63	0.71	0.60	0.77	0.78	0.65	0.79	0.62	0.58
(Zr/Zr*)pm	1.04	0.97	1.07	1.01	1.04	1.06	0.98	1.63	1.25
(Ti/Ti*)pm	0.92	0.87	0.88	0.86	0.86	0.86	0.87	0.76	0.72
ΣREE	33.26	37.72	28.11	22.75	29.18	36.42	37.27	20.47	36.46
North	64°53.566'	64°55.080'	64°51.480'	64°53.002'	64°52.855'	64°53.398'	64°50.941'	64°50.962'	64°50.885'
West	50°12.867'	50°12.317'	49°59.689'	49°56.825'	49°57.233'	50°1.744'	49°59.203'	50°12.649'	50°12.389'

LDL = Lower than detection limit.

Metavolcanic rocks with sample number < 498270 belong to the Western flank of the Ujarassuit greenstone belt.

Metavolcanic rocks with sample number > 498270 belong to the Eastern flank of the Ujarassuit greenstone belt.

Table 3.3. (*Continued*)

	Group 2 amphibolites							Group 3 amphibolites	
	498218	498219	498224	498227	498241	498244	498256B	498229	498235
SiO_2 (wt.%)	48.1	49.3	48.6	54.0	54.8	50.1	49.2	48.1	51.2
TiO_2	0.65	0.72	0.62	0.65	0.45	0.66	0.40	0.80	0.79
Al_2O_3	16.03	14.93	15.80	13.09	16.27	15.87	13.81	16.24	14.60
Fe_2O_3	12.94	13.26	12.04	9.85	11.68	11.31	11.12	12.70	11.31
MnO	0.20	0.21	0.21	0.21	0.14	0.20	0.21	0.22	0.21
MgO	8.66	8.44	7.88	6.61	7.36	5.55	11.26	8.39	6.26
CaO	10.28	10.37	12.47	14.07	7.72	13.63	12.47	10.62	13.90
Na_2O	2.70	2.30	1.84	1.30	1.50	2.62	1.32	2.79	1.30
K_2O	0.35	0.44	0.50	0.19	0.02	0.06	0.14	0.13	0.34
P_2O_5	0.07	0.05	0.06	0.05	0.04	0.05	0.03	0.06	0.06
LOI (%)	1.08	0.97	1.01	1.84	LDL	2.87	1.21	1.28	1.20
Mg-number (%)	57	56	56	57	56	49	67	57	52
Sc (ppm)	43	54	44	40	52	47	54	40	50
V	240	285	251	244	292	234	224	247	285
Cr	244	301	263	351	37	238	618	263	319
Co	48	45	53	39	50	58	57	54	45
Ni	149	100	150	138	59	161	159	190	138
Ga	36	36	32	29	30	30	25	34	33
Rb	7	11	18	6	1	1	4	5	12
Sr	77	83	87	47	36	94	37	69	50
Y	19.2	21.4	19.5	15.2	17.4	19.5	12.5	16.4	18.9
Zr	36.3	31.5	31.5	30.6	23.0	36.9	18.2	45.7	42.5
Nb	0.75	0.77	0.59	0.78	0.68	0.69	0.31	1.35	1.39
Cs	0.26	0.48	0.46	0.22	0.07	0.10	0.42	0.21	0.75
Ba	51.91	55.65	36.29	33.84	11.62	13.90	18.10	32.57	17.95
Ta	0.05	0.06	0.05	0.06	0.04	0.03	0.02	0.09	0.07
Pb	5.15	6.22	5.29	1.54	2.05	2.73	2.37	7.40	6.57
Th	0.43	0.43	0.10	0.16	0.13	0.22	0.05	0.11	0.15
U	0.15	0.24	0.11	0.18	0.20	0.48	0.04	0.23	0.07
La	1.59	2.20	1.89	1.57	1.50	1.45	0.68	2.14	1.72
Ce	3.74	5.20	4.74	4.32	4.30	3.91	1.84	6.15	4.58
Pr	0.58	0.74	0.62	0.66	0.70	0.61	0.29	1.00	0.74
Nd	3.08	3.66	3.58	3.30	3.15	3.22	1.72	4.85	4.02
Sm	1.27	1.36	1.28	1.31	0.92	1.32	0.80	1.77	1.56
Eu	0.50	0.55	0.48	0.54	0.26	0.60	0.24	0.68	0.61
Gd	2.07	2.35	2.28	2.04	1.71	2.26	1.42	2.43	2.50
Tb	0.43	0.49	0.45	0.39	0.36	0.47	0.28	0.44	0.46
Dy	3.03	3.54	3.18	2.61	2.72	3.17	2.12	2.88	3.10
Ho	0.72	0.82	0.73	0.59	0.62	0.73	0.47	0.60	0.72
Er	2.18	2.45	2.23	1.71	2.03	2.24	1.41	1.85	2.07
Tm	0.32	0.37	0.32	0.24	0.30	0.33	0.22	0.27	0.30
Yb	2.33	2.45	2.22	1.73	2.05	2.30	1.43	1.80	2.11
Lu	0.35	0.38	0.35	0.26	0.32	0.35	0.22	0.26	0.33
La/Yb_{cn}	0.46	0.60	0.57	0.61	0.49	0.43	0.32	0.80	0.55
La/Sm_{cn}	0.79	1.02	0.92	0.75	1.02	0.69	0.53	0.76	0.69
Gd/Yb_{cn}	0.72	0.77	0.83	0.95	0.68	0.79	0.80	1.10	0.96
(Eu/Eu*)cn	0.94	0.94	0.85	1.00	0.63	1.06	0.68	1.01	0.95
(Ce/Ce*)cn	0.94	0.98	1.05	1.02	1.01	1.00	1.00	1.01	0.98
Al_2O_3/TiO_2	24.78	20.73	25.39	20.24	35.97	23.93	34.71	20.38	18.51
Nb/Ta	14.68	13.36	12.43	13.70	16.45	20.10	16.71	14.80	20.55
Zr/Y	1.89	1.47	1.62	2.01	1.33	1.89	1.46	2.79	2.25
Ti/Zr	106.91	137.11	118.35	126.89	117.81	107.74	130.89	104.45	111.19
(Nb/Nb*)pm	0.37	0.32	0.56	0.63	0.62	0.49	0.67	1.15	1.11
(Zr/Zr*)pm	1.28	0.99	1.03	1.03	0.94	1.25	1.09	1.09	1.19
(Ti/Ti*)pm	0.72	0.70	0.67	0.82	0.59	0.69	0.66	0.91	0.84
ΣREE	22.19	26.54	24.34	21.26	20.92	22.96	13.14	27.12	24.83
North	64°50.202'	64°51.000'	64°49.455'	64°51.388'	64°52.912'	64°52.715'	64°54.985'	64°51.485'	64°51.711'
West	50°12.887'	50°11.826'	50°13.696'	50°11.513'	50°13.083'	50°13.213'	50°12.391'	50°11.446'	50°11.921'

Table 3.3. (*Continued*)

	Group 3 amphibolites			Group 4 amphibolites				Plagioclase-rich amphibolites	
	498260	498261	498265	498228	498239	498248	498264	498209	498279
SiO_2 (wt.%)	49.0	50.5	49.0	53.3	53.7	52.0	50.9	67.4	55.3
TiO_2	1.01	1.20	1.00	0.32	0.33	0.33	0.26	0.57	1.00
Al_2O_3	15.62	15.54	15.55	15.19	15.83	14.63	18.61	14.75	10.59
Fe_2O_3	12.50	12.75	13.37	10.45	10.57	10.81	6.86	3.47	13.42
MnO	0.20	0.20	0.19	0.21	0.14	0.17	0.13	0.05	0.25
MgO	8.29	6.33	9.34	10.75	10.85	13.06	10.84	2.83	6.34
CaO	10.81	10.41	9.09	7.58	7.17	7.32	9.47	6.70	11.29
Na_2O	2.39	2.51	2.16	1.87	1.33	1.63	2.63	3.82	0.95
K_2O	0.14	0.41	0.18	0.32	0.02	0.04	0.23	0.16	0.74
P_2O_5	0.08	0.10	0.07	0.04	0.04	0.03	0.04	0.21	0.12
LOI (%)	0.28	0.07	1.37	2.68	0.44	1.48	1.50	0.34	0.98
Mg-number (%)	57	50	58	67	67	71	76	62	48
Sc (ppm)	42	45	41	46	45	41	27	11	18
V	264	323	277	223	232	233	124	86	152
Cr	251	219	238	456	379	765	99	132	229
Co	51	45	48	47	50	57	44	16	56
Ni	166	100	155	124	125	178	167	63	130
Ga	37	55	36	29	27	26	28	47	35
Rb	1	6	11	10	2	2	12	4	11
Sr	136	104	44	74	91	67	106	372	411
Y	20.0	23.6	20.3	12.6	11.9	12.1	7.3	9.2	14.7
Zr	57.3	67.2	55.4	22.5	22.0	20.3	28.6	145.7	86.6
Nb	1.77	2.54	1.79	0.46	0.51	0.36	0.83	4.92	5.20
Cs	0.11	0.18	1.39	1.27	0.40	0.53	1.75	0.98	0.31
Ba	41.61	173.98	38.00	50.48	18.07	28.51	27.69	127.10	63.15
Ta	0.12	0.17	0.13	0.03	0.03	0.02	0.04	0.35	0.33
Pb	2.68	6.20	1.84	12.71	11.22	6.91	4.77	4.89	11.29
Th	0.24	0.32	0.26	0.10	0.29	0.14	0.37	4.80	1.23
U	0.08	0.11	0.13	0.36	0.23	0.16	0.10	1.07	0.96
La	2.55	3.37	2.42	2.06	1.88	1.78	3.33	18.18	11.85
Ce	7.31	9.57	7.18	4.19	3.71	3.75	6.12	47.04	33.16
Pr	1.15	1.53	1.11	0.55	0.43	0.48	0.83	5.05	4.51
Nd	6.17	7.75	6.06	2.52	1.94	2.18	3.61	19.35	19.97
Sm	1.99	2.53	2.08	0.68	0.57	0.68	0.86	3.56	4.20
Eu	0.68	0.97	0.80	0.31	0.28	0.34	0.36	1.00	1.18
Gd	3.12	3.65	3.09	1.30	1.16	1.04	1.08	3.02	4.10
Tb	0.53	0.62	0.54	0.24	0.24	0.23	0.17	0.35	0.56
Dy	3.59	4.29	3.58	1.97	1.85	1.87	1.19	1.92	3.04
Ho	0.76	0.94	0.80	0.44	0.44	0.44	0.27	0.33	0.57
Er	2.26	2.69	2.25	1.43	1.41	1.40	0.84	0.95	1.49
Tm	0.33	0.39	0.33	0.22	0.21	0.20	0.13	0.12	0.22
Yb	2.07	2.50	2.23	1.52	1.55	1.48	0.87	0.78	1.27
Lu	0.33	0.38	0.32	0.25	0.25	0.23	0.14	0.12	0.20
La/Yb_{cn}	0.83	0.91	0.73	0.91	0.82	0.81	2.58	15.64	6.29
La/Sm_{cn}	0.80	0.84	0.73	1.91	2.08	1.64	2.42	3.21	1.78
Gd/Yb_{cn}	1.22	1.18	1.12	0.70	0.61	0.57	1.01	3.12	2.61
(Eu/Eu*)cn	0.84	0.98	0.96	1.01	1.07	1.24	1.15	0.93	0.87
(Ce/Ce*)cn	1.03	1.01	1.06	0.94	0.99	0.97	0.89	1.18	1.09
Al_2O_3/TiO_2	15.47	12.90	15.55	47.32	47.34	44.41	71.25	25.70	10.55
Nb/Ta	15.11	14.76	14.15	16.10	18.89	16.81	20.77	14.25	15.73
Zr/Y	2.87	2.85	2.74	1.79	1.84	1.69	3.93	15.87	5.90
Ti/Zr	105.70	107.46	108.13	85.56	91.01	97.12	54.81	23.61	69.50
(Nb/Nb*)pm	0.93	1.00	0.92	0.42	0.28	0.29	0.30	0.21	0.55
(Zr/Zr*)pm	1.14	1.06	1.09	1.20	1.47	1.17	1.13	1.23	0.66
(Ti/Ti*)pm	0.94	0.94	0.92	0.59	0.64	0.64	0.74	0.89	0.98
ΣREE	32.85	41.21	32.79	17.68	15.92	16.11	19.80	101.76	86.33
North	64°54.142'	64°53.816'	64°53.785'	64°51.483'	64°52.959'	64°54.043'	64°53.799'	64°50.855'	64°53.795'
West	50°13.996'	50°15.656'	50°15.157'	50°11.420'	50°13.087'	50°13.027'	50°15.778'	50°12.627'	50°03.025'

Table 3.3. (*Continued*)

	Ultramafic rocks						
	498210	498220	498240	498246	498247	498257	498262
SiO_2 (wt.%)	48.5	47.9	47.5	44.7	44.5	42.3	43.6
TiO_2	0.40	0.11	0.11	0.42	0.20	0.36	0.17
Al_2O_3	9.43	4.72	4.30	6.88	5.14	3.84	4.41
Fe_2O_3	11.14	11.00	8.32	13.37	11.47	15.51	14.72
MnO	0.16	0.15	0.11	0.18	0.11	0.18	0.22
MgO	19.73	33.87	39.14	31.76	36.67	34.51	34.06
CaO	9.53	1.91	0.49	2.46	1.80	2.85	2.45
Na_2O	0.91	0.23	0.05	0.17	0.07	0.27	0.28
K_2O	0.20	0.08	LDL	0.05	LDL	0.08	0.03
P_2O_5	0.03	0.03	0.02	0.04	0.02	0.07	0.01
LOI (%)	3.82	4.65	3.24	4.02	10.96	9.51	5.88
Mg-number (%)	78	86	90	82	86	82	82
Sc (ppm)	35	20	12	19	16	13	14
V	178	117	74	148	102	101	86
Cr	2377	4141	6312	5173	5216	2543	2634
Co	74	108	113	111	103	117	130
Ni	658	997	2212	1311	1403	1082	1400
Ga	16	9	7	14	9	9	8
Rb	1	3	0	1	0	1	0
Sr	38	16	1	11	2	6	6
Y	8.0	3.2	2.4	5.5	4.2	5.9	2.5
Zr	20.72	4.19	6.17	19.84	7.84	21.04	8.49
Nb	0.65	0.18	0.17	0.84	0.28	0.67	0.35
Cs	0.11	1.88	0.05	0.23	1.14	0.20	0.11
Ba	4.30	2.86	0.65	2.52	0.39	1.05	2.00
Ta	0.04	0.01	0.02	0.05	0.02	0.04	0.02
Pb	5.08	5.17	2.58	4.34	2.26	1.82	2.50
Th	0.11	0.09	0.08	0.24	0.11	0.33	0.10
U	0.12	0.05	0.04	0.08	0.05	0.18	0.03
La	0.75	0.35	0.16	1.18	0.68	2.30	0.56
Ce	2.41	0.91	0.42	2.99	1.91	5.85	1.48
Pr	0.36	0.09	0.05	0.41	0.24	0.74	0.17
Nd	2.10	0.48	0.26	1.79	1.11	3.27	0.80
Sm	0.73	0.13	0.07	0.52	0.38	0.79	0.20
Eu	0.19	0.04	0.01	0.14	0.06	0.30	0.05
Gd	1.08	0.33	0.19	0.63	0.59	1.02	0.31
Tb	0.20	0.06	0.04	0.12	0.09	0.16	0.06
Dy	1.35	0.47	0.38	0.94	0.67	1.10	0.46
Ho	0.31	0.12	0.10	0.20	0.16	0.22	0.09
Er	0.92	0.38	0.32	0.64	0.52	0.65	0.29
Tm	0.13	0.06	0.05	0.10	0.07	0.10	0.05
Yb	0.94	0.45	0.33	0.72	0.52	0.62	0.28
Lu	0.14	0.07	0.05	0.10	0.08	0.10	0.05
La/Yb_{cn}	0.54	0.53	0.31	1.10	0.88	2.48	1.35
La/Sm_{cn}	0.65	1.73	1.45	1.43	1.13	1.83	1.75
Gd/Yb_{cn}	0.94	0.59	0.47	0.71	0.91	1.32	0.91
(Eu/Eu*)cn	0.64	0.53	0.34	0.75	0.39	1.03	0.62
(Ce/Ce*)cn	1.11	1.23	1.11	1.04	1.12	1.08	1.16
Al_2O_3/TiO_2	23.45	44.55	40.58	16.52	26.08	10.78	26.00
Nb/Ta	16.54	12.85	8.40	17.97	17.66	17.51	14.25
Zr/Y	2.59	1.32	2.59	3.63	1.85	3.59	3.33
Ti/Zr	116.30	151.37	102.91	125.89	150.73	101.60	119.90
(Nb/Nb*)pm	0.94	0.41	0.64	0.65	0.42	0.31	0.60
(Zr/Zr*)pm	1.17	1.19	3.29	1.45	0.84	0.92	1.48
(Ti/Ti*)pm	0.99	0.80	1.09	1.59	1.01	1.10	1.27
ΣREE	11.60	3.93	2.44	10.48	7.08	17.21	4.86
North	64°50.624'	64°50.813'	64°52.959'	64°52.654'	64°52.668'	64°54.983'	64°53.816'
West	50°12.603'	50°12.733'	50°13.087'	50°12.887'	50°12.784'	50°12.314'	50°15.656'

Table 3.4. Major (wt.%) and trace element (ppm) concentrations and significant element ratios for metasedimentary rocks

	Ujarassuit belt, Western flank					Ivisaartoq belt, lower metasedimentary unit			
	Biotite schists					Biotite schists			
	498226	498230	498231	498242	498243	498292	498293	498295	498297
SiO_2 (wt.%)	62.8	53.1	69.2	72.4	71.5	58.1	71.2	70.7	59.9
TiO_2	0.50	0.50	0.36	0.32	0.35	0.92	0.82	0.80	0.63
Al_2O_3	16.15	24.04	15.42	14.51	14.81	15.29	12.83	12.59	16.38
Fe_2O_3	6.36	4.60	2.82	2.53	2.54	10.17	7.13	6.95	6.89
MnO	0.12	0.07	0.04	0.04	0.04	0.17	0.10	0.09	0.14
MgO	3.75	4.23	1.25	1.34	1.62	8.40	2.44	3.11	4.23
CaO	4.09	7.70	3.82	2.80	2.84	3.56	1.29	1.39	5.11
Na_2O	3.16	4.71	3.97	2.96	2.94	2.67	2.36	2.66	4.86
K_2O	2.95	0.99	2.97	2.99	3.20	0.61	1.68	1.57	1.66
P_2O_5	0.12	0.02	0.14	0.14	0.13	0.11	0.13	0.11	0.20
LOI (%)	1.67	2.49	1.99	1.33	1.27	0.83	1.49	1.23	1.21
Mg-number (%)	54	65	47	51	56	62	40	47	55
CIA (%)	51	51	49	53	46	58	62	60	47
Sc (ppm)	16	13	11	7	10	37	17	21	18
V	110	57	71	49	64	187	117	125	134
Cr	115	141	94	51	73	753	121	129	131
Co	24	20	21	14	31	52	19	19	25
Ni	75	114	272	57	108	328	67	53	93
Ga	68	47	120	150	138	54	81	75	155
Rb	381	76	115	74	83	16	49	48	49
Sr	205	378	136	281	214	334	106	95	175
Y	12.0	9.3	11.0	7.1	7.8	16.4	26.8	33.4	12.2
Zr	108	253	115	126	113	166	200	237	122
Nb	2.78	3.06	4.09	3.94	3.38	6.24	10.89	10.89	3.58
Cs	13.01	2.12	0.87	2.82	3.25	2.00	5.07	6.25	4.10
Ba	272	156	654	886	786	168	346	295	922
Ta	0.19	0.17	0.25	0.27	0.21	0.42	0.71	0.72	0.23
Pb	19.37	32.71	31.62	37.66	56.11	12.00	12.67	10.15	46.06
Th	3.24	26.88	9.63	13.51	9.83	2.52	4.32	3.80	7.03
U	1.07	1.92	2.23	2.62	2.09	0.59	14.63	0.95	0.96
La	12.53	100.07	43.87	40.53	31.36	14.85	17.38	21.31	38.37
Ce	20.91	155.26	71.33	73.91	57.21	34.45	40.61	48.66	76.47
Pr	2.33	17.00	7.85	7.28	5.92	4.58	5.04	6.26	8.43
Nd	8.86	53.40	26.82	23.70	19.57	19.43	21.57	26.96	31.40
Sm	1.97	6.24	4.03	3.23	2.95	4.80	4.87	6.64	4.82
Eu	0.58	1.29	0.90	0.75	0.69	1.46	0.97	1.26	1.14
Gd	2.15	4.40	3.24	2.35	2.24	4.59	4.77	6.69	3.93
Tb	0.32	0.45	0.40	0.27	0.31	0.63	0.73	0.96	0.46
Dy	1.90	2.02	2.12	1.33	1.55	3.51	4.80	6.23	2.50
Ho	0.39	0.34	0.38	0.24	0.30	0.69	1.15	1.36	0.47
Er	1.14	0.92	1.08	0.71	0.80	1.99	3.80	4.54	1.32
Tm	0.16	0.13	0.15	0.11	0.10	0.32	0.62	0.72	0.17
Yb	1.02	0.77	0.91	0.59	0.69	2.57	4.89	5.29	1.09
Lu	0.16	0.15	0.15	0.09	0.10	0.40	0.77	0.86	0.16
La/Yb_{cn}	8.31	87.95	32.61	46.04	30.52	3.89	2.39	2.71	23.69
La/Sm_{cn}	3.99	10.08	6.83	7.89	6.68	1.94	2.24	2.02	5.01
Gd/Yb_{cn}	1.71	4.64	2.89	3.21	2.62	1.44	0.79	1.02	2.91
(Eu/Eu*)cn	0.86	0.75	0.76	0.84	0.82	0.95	0.62	0.58	0.80
(Ce/Ce*)cn	0.93	0.91	0.93	1.04	1.01	1.01	1.05	1.02	1.02
Al_2O_3/TiO_2	32.04	48.13	42.92	45.54	41.86	16.60	15.69	15.84	26.10
Nb/Ta	14.46	17.97	16.05	14.39	16.11	14.92	15.39	15.03	15.81
Zr/Y	8.99	27.23	10.49	17.79	14.60	10.10	7.44	7.11	10.03
Ti/Zr	28.00	11.82	18.73	15.18	18.73	33.25	24.57	20.10	30.77
(Nb/Nb*)pm	0.18	0.02	0.08	0.07	0.08	0.41	0.51	0.49	0.09
(Zr/Zr*)pm	1.81	0.97	0.77	1.01	1.04	1.20	1.36	1.24	0.70
(Ti/Ti*)pm	0.82	0.67	0.50	0.68	0.65	0.79	0.56	0.42	0.75
ΣREE	54.43	342.43	163.23	155.10	123.80	94.27	111.98	137.73	170.72
North	64°51.359'	64°51.446'	64°51.446'	64°52.912'	64°52.912'	64°43.597'	64°43.597'	64°43.394'	64°43.527'
West	50°11.553'	50°11.409'	50°11.409'	50°13.083'	50°13.083'	49°58.033'	49°58.033'	50°00.442'	49°59.737'

LDL = lower than detection limit.

The chemical index of alteration CIA = $100(Al_2O_3/[Al_2O_3+Na_2O+K_2O+CaO^*])$ is calculated in molar proportions where CaO* represents CaO only in silicates (see Nesbitt and Young, 1984; Fedo et al., 1995).

Table 3.4. (*Continued*)

	Ivisaartoq belt, lower metasedimentary unit			
	Quartzitic gneisses			
	496101	498294	498296	498299
SiO_2 (wt.%)	77.7	76.3	72.0	81.6
TiO_2	0.28	0.32	0.61	0.16
Al_2O_3	11.73	11.42	10.89	11.09
Fe_2O_3	2.83	5.12	8.02	1.41
MnO	0.05	0.05	0.10	0.02
MgO	0.62	0.75	1.58	0.46
CaO	1.92	0.90	3.13	0.69
Na_2O	2.57	3.29	2.50	1.63
K_2O	2.22	1.79	0.97	2.88
P_2O_5	0.04	0.04	0.15	0.02
LOI (%)	0.98	0.85	0.46	1.17
Mg-number (%)	30	22	28	39
CIA (%)	54	56	51	61
Sc (ppm)	4	7	12	2
V	LDL	LDL	LDL	LDL
Cr	LDL	LDL	LDL	LDL
Co	1	1	5	1
Ni	7	5	9	4
Ga	88	93	76	74
Rb	57	48	20	77
Sr	37	40	50	25
Y	140.4	103.9	143.6	102.3
Zr	618	702	438	237
Nb	12.22	19.89	13.08	15.25
Cs	2.95	5.65	2.07	4.68
Ba	278	303	230	266
Ta	0.87	0.70	0.90	1.04
Pb	7.60	14.58	4.95	11.77
Th	4.51	7.86	4.99	7.84
U	1.00	1.50	0.96	1.44
La	29.93	56.96	39.08	21.02
Ce	78.51	130.78	88.34	137.97
Pr	11.13	19.03	12.95	9.04
Nd	54.02	86.48	60.36	39.15
Sm	17.00	24.30	17.81	11.46
Eu	3.13	3.33	3.60	1.79
Gd	22.52	27.38	23.94	12.43
Tb	4.10	4.13	4.10	2.51
Dy	27.18	23.35	26.90	18.37
Ho	5.85	4.37	5.65	4.20
Er	17.89	12.37	16.40	13.36
Tm	2.67	1.83	2.52	1.93
Yb	17.90	12.64	16.70	12.60
Lu	2.61	1.98	2.45	1.83
La/Yb_{cn}	1.13	3.03	1.58	1.12
La/Sm_{cn}	1.11	1.47	1.38	1.15
Gd/Yb_{cn}	1.02	1.75	1.16	0.80
(Eu/Eu*)cn	0.49	0.40	0.53	0.46
(Ce/Ce*)cn	1.04	0.96	0.95	2.41
Al_2O_3/TiO_2	42.01	36.18	17.92	70.58
Nb/Ta	14.06	28.50	14.58	14.70
Zr/Y	4.40	6.76	3.05	2.31
Ti/Zr	2.71	2.70	8.32	3.98
(Nb/Nb*)pm	0.43	0.38	0.38	0.48
(Zr/Zr*)pm	1.43	1.07	0.93	0.78
(Ti/Ti*)pm	0.03	0.04	0.07	0.03
ΣREE	294.43	408.95	320.82	287.67
North	64°43.420'	64°43.597'	64°43.568'	64°43.391'
West	50°00.013'	49°59.045'	49°59.516'	50°00.856'

Table 3.5. Summary of significant geochemical characteristics and trace element ratios for metavolcanic and metasedimentary rocks

	Group 1 amphibolites	Group 2 amphibolites	Group 3 amphibolites	Group 4 amphibolites
SiO_2 (wt%)	48-53	47-55	48-51	51-54
TiO_2	0.6-1.0	0.4-1.0	0.8-1.2	0.26-0.33
Al_2O_3	13.6-15.6	13.1-16.3	14.6-16.2	14.6-18.6
Fe_2O_3	10.1-13.2	9.9-15.7	11.3-13.4	6.9-10.8
MgO	6.8-11.2	5.6-11.3	6.3-9.3	10.8-13.1
CaO	10.2-14.3	7.7-14.1	9.1-10.8	7.2-9.5
Zr (ppm)	35-58	18-60	43-67	20-29
Ni	79-433	59-171	100-190	124-178
Cr	187-603	37-618	219-319	99-765
ΣREE	23-38	13-37	25-41	16-20
Al_2O_3/TiO_2	14-22	16-36	13-20	44-71
Ti/Zr	93-105	90-137	105-111	55-97
Nb/Ta	14-19	12-20	14-21	16-20
Zr/Y	2.6-3.1	1.3-2.4	2.3-2.9	1.7-3.9
La/Yb_{cn}	0.84-1.24	0.32-0.61	0.55-0.91	0.81-2.58
La/Sm_{cn}	0.77-1.14	0.53-1.02	0.69-0.84	1.64-2.42
Gd/Yb_{cn}	1.10-1.21	0.68-0.95	0.96-1.22	0.57-1.01
(Eu/Eu*)cn	0.88-1.02	0.63-1.06	0.84-1.01	1.01-1.24
(Nb/Nb*)pm	0.60-0.79	0.32-0.67	0.92-1.15	0.28-0.42
(Ti/Ti*)pm	0.86-0.92	0.59-0.82	0.84-0.94	0.59-0.74
(Zr/Zr*)pm	0.97-1.07	0.94-1.63	1.06-1.19	1.13-1.47

Table 3.5. (*Continued*)

	Plagioclase-rich amphibolites	Ultramafic rocks (picritic cumulus)	Biotite schists	Quartzitic gneisses
SiO_2 (wt%)	55-67	42-49	53-72	72-82
TiO_2	0.6-1.0	0.1-0.4	0.3-0.9	0.2-0.6
Al_2O_3	10.6-14.8	3.8-9.4	12.6-24.0	10.9-11.7
Fe_2O_3	3.5-13.4	8.3-15.5	2.5-10.2	1.4-8.0
MgO	2.8-6.3	19.7-39.1	1.3-8.4	0.5-1.6
CaO	6.7-11.3	0.5-9.5	1.3-7.7	0.7-3.1
Zr (ppm)	87-146	4-21	108-253	237-702
Ni	63-130	658-2212	53-328	4.1-8.7
Cr	132-229	2377-6312	51-753	< 30
ΣREE	86-102	2.4-17.2	54-342	288-409
Al_2O_3/TiO_2	10-26	11-45	17-48	18-71
Ti/Zr	24-70	102-151	12-30	2.7-8.3
Nb/Ta	14-16	8-18	14-18	14-29
Zr/Y	5.9-15.9	1.3-3.6	7.1-27.2	2.3-6.8
La/Yb_{cn}	6.29-15.64	0.31-2.48	2.39-87.95	1.12-3.03
La/Sm_{cn}	1.78-3.21	0.65-1.83	1.94-10.08	1.11-1.47
Gd/Yb_{cn}	2.61-3.12	0.47-1.32	0.79-4.64	0.80-1.75
(Eu/Eu*)cn	0.87-0.93	0.34-1.03	0.58-0.95	0.40-0.53
(Nb/Nb*)pm	0.21-0.55	0.31-0.94	0.02-0.51	0.38-0.48
(Ti/Ti*)pm	0.89-0.98	0.80-1.59	0.42-0.82	0.03-0.07
(Zr/Zr*)pm	0.66-1.23	0.84-3.29	0.70-1.81	0.78-1.43

CHAPTER 4

The Neoarchean 2800-2840 Ma Storø greenstone belt, SW Greenland: Field and geochemical evidence for an intra-oceanic supra-subduction zone geodynamic setting

4.1. Introduction

The Nuuk region in southern West Greenland comprises several Eo- to Neoarchean (3850-2800 Ma) tectono-stratigraphic terranes assembled into a single super-terrane during prolonged continent-continent collisional events taking place between 2960 and 2650 Ma (Friend et al., 1988; 1996; Nutman et al., 1989; McGregor et al., 1991; Friend and Nutman, 2005; Nutman and Friend, 2007). Terrane amalgamation resulted in polyphase regional amphibolite-granulite facies metamorphism and multi-stage ductile deformation (Nutman and Friend, 2007). The allochtonous terranes are dominated by Archean tonalite-trondhjemite-granodiorite (TTG) associations and include small fragments of greenstone belts < 5 km in width. The accretion of allochtonous terranes in the Nuuk region is one of the best documented examples of an Archean collisional orogeny (Nutman and Friend, 2007). The collisional orogenic model proposed for the Nuuk region has important implications for the geodynamic origin of Archean greenstone belts (cf. Nutman and Friend, 2007). In Phanerozoic collisional orogens, supra-subduction zone ophiolites have been obducted into continents during the progressive closure of ocean basins (Dilek and Flower, 2003; Flower and Dilek, 2003; Pearce, 2003; Şengör and Natal'in, 2004). Therefore, the tectonic terrane model suggests that some greenstone belts from the Nuuk region may represent the Archean analogues of Phanerozoic ophiolites (cf., De Wit, 2004). Or alternatively, they may also represent remnants of continental flood

and rift volcanic sequences deformed during collisional tectonics (cf. Bickle et al., 1994; Hunter et al., 1998; Bleeker, 2002; Thurston, 2002; Hartlaub, et al., 2004; Shimizu et al., 2005).

Recent field and geochemical investigations in the region have shown that the Mesoarchean (3070-3075 Ma) Ivisaartoq, Ujarassuit, and Qussuk greenstone belts display lithological and geochemical characteristics that are characteristic of Phanerozoic intra-oceanic subduction zone geodynamic settings (Garde, 2007; Polat et al., 2007, 2008; Ordóñez-Calderón et al., 2008a,b). These characteristics include: 1) pyroclastic andesites in the Qussuk belt (Garde, 2007); 2) epidosites in pillow basalts in the Ivisaartoq belt (Polat et al., 2007) resembling those recovered from modern sea-floor hydrothermal systems in the Tonga-Kermadec forearc (cf. Banerjee et al., 2000); 3) amphibolites with basaltic composition and pronounced negative Nb-Ta anomalies in primitive mantle-normalized diagrams (Polat et al., 2007; 2008; Ordóñez-Calderón et al., 2008a,b); 4) ultramafic rocks with geochemical composition similar to those of island arc picrites; and 5) boninite-like rocks in the Ujarassuit greenstone belt (Polat et al., 2007; 2008; Ordóñez-Calderón et al., 2008a,b). The above lithological-geochemical associations suggest that the central Nuuk region comprises dismembered fragments of Mesoarchean supra-subduction zone oceanic crust (Garde, 2007; Polat et al., 2007, 2008; Ordóñez-Calderón et al., 2008a,b).

The Neoarchean (2800-2840 Ma) Storø greenstone belt consists of metamorphosed basalts, ultramafic rocks, anorthosites, and siliciclastic sedimentary rocks. These lithological characteristics are broadly similar to those of the Mesoarchean Ivisaartoq and Ujarassuit greenstone belts. The geochemical characteristics and geodynamic setting of the Storø volcanic and sedimentary rocks are not well understood. Accordingly, we report

new high precision major and trace element data for 17 samples of metavolcanic rocks and 12 samples of metasedimentary rocks from the Storø belt to investigate its petrogenesis, geodynamic setting of origin, and sedimentary provenance. The new field and geochemical data are compared with those reported for the Mesoarchean greenstone belts in the Nuuk region to understand Meso- to Neoarchean magmatic and sedimentological processes.

4.2. Regional geology and field characteristics

The Nuuk region consists of several Eo- to Neoarchean (3850-2800 Ma) tectono-stratigraphic terranes bounded by folded amphibolite facies mylonites (Friend et al., 1987, 1988, 1996; Nutman et al., 1989; McGregor et al., 1991; Crowley, 2002; Friend and Nutman, 2005). These allochtonous terranes comprise TTG-gneisses, gabbro-anorthosite complexes, and fragments of greenstone belts (Black et al., 1971; Moorbath et al., 1973; McGregor, 1973; Bridgwater et al., 1974; McGregor and Mason, 1977; Chadwick, 1990; Nutman et al., 1996; Garde, 2007; Polat et al., 2007). Terrane accretion was diachronous and appears to have taken place between ca. 2960 and 2600 Ma resulting in polyphase of deformation and metamorphism (Friend and Nutman, 1991; Friend et al., 1996; Friend and Nutman, 2005; Nutman and Friend, 2007).

The Storø greenstone belt is the oldest component of the ca. 2825-2780 Ma Tre Brødre terrane (Fig. 4.1). The precise age of the belt is not well constrained. However, zircons in volcaniclastic-sedimentary rocks indicate maximum depositional ages between 2800 and 2840 Ma (Hollis, 2005; Knudsen et al., 2007; Nutman et al., 2007). The belt was metamorphosed at upper amphibolite facies conditions between 2650 and 2600 Ma (Hollis, 2005; Nutman et al., 2007). The thickest section of the belt is exposed in central

Storø Island where the belt is folded into synformal and antiformal structures that are overturned to the west towards the terrane boundary (Fig. 4.1). The Storø greenstone belt comprises a sequence of amphibolites (metabasalts) interleaved with a ca. 100 to 200 m thick unit composed of garnet-biotite schists and quartzitic gneisses (metavolcaniclastic-sedimentary rocks) (Fig. 4.1). The amphibolites are finely layered and isoclinally folded (Fig. 4.2a). They are commonly intercalated with garnet-biotite schists at outcrop scale (Fig. 4.2b). The amphibolites in the uppermost part of the belt contain relict pillow structures (Hollis et al., 2004). The Storø greenstone belt shows evidence for superposed folding (Fig. 4.2b-d). Lenses of serpentinized ultramafic rocks are abundant at the top of the sequence. The base of the tectono-stratigraphic sequence of the belt is intruded by a metagabbro-meta-anorthosite complex (Figs. 4.1 and 4.2e). Tectonic transposition and multi-stage folding (Fig. 4.2c) have obliterated the primary characteristics of the contact between the Storø greenstone belt and the surrounding TTG-gneisses. However, in the northern part of the belt, it is intruded by the ca. 2825 Ma Ikkatoq gneisses of the Tre Brødre terrane (Hollis et al., 2004). In contrast, at some localities thrust sheets of the Eoarchean Færingehavn terrane truncate the stratigraphic sequence of the belt. In addition, the Storø greenstone belt has undergone several stages of postmagmatic alteration resulting in calc-silicate metasomatism, silicification, quartz veining (Fig. 4.2f), and gold mineralization (see Juul-Pedersen et al., 2007). The hydrothermal event associated with gold mineralization appears to have taken place at ca. 2635 Ma at upper amphibolite facies metamorphic conditions (see Knudsen et al., 2007; Nutman et al., 2007).

4.3. Petrography

The studied rock types rarely preserve primary igneous mineralogy or sedimentary textures. They consist mostly of amphibolite facies metamorphic assemblages with well developed tectonic foliation.

Amphibolites are composed mainly of hornblende (60-70 %), plagioclase (20-35 %), and quartz (5-10 %) (Fig. 4.3a-b). They also include accessory (< 2%) minerals such as zircon, apatite, magnetite, and titanite. Garnet, biotite, and actinolite are locally present. Biotite is a retrograde metamorphic mineral and generally replaces hornblende and garnet.

Ultramafic rocks are strongly altered to serpentine (> 90%) (Fig. 4.3c). These rocks occasionally preserve relict igneous cumulus texture consisting of serpentinized coarse-grained olivine, orthopyroxene, and clinopyroxene. Talc, actinolite, tremolite, and magnetite are also common alteration minerals. Ultramafic rocks do not exhibit evidence for spinifex texture.

Garnet-biotite schists (Fig. 4.3d-e) are composed mainly of quartz (20-30%), plagioclase (40-50%), garnet (5-20%), biotite (10-20%), sillimanite (0-10%), and hornblende (0-10%). Accessory minerals may include epidote, kyanite, magnetite, titanite, and zircon.

Quartzitic gneisses (Fig. 4.3f) consist of quartz (50-70%), plagioclase (10-20%), biotite (5-15%), muscovite (0-10%), and K-feldspar (0-5%). They sometimes contain garnet (2%). Accessory minerals include magnetite, zircon, and epidote.

4.4. Analytical methods

Samples were pulverized using an agate mill in the Department of Earth and Environmental Sciences of the University of Windsor, Canada. Major elements and some

trace elements (Sc and Zr) were analyzed on a Thermo Jarrel-Ash ENVIRO II ICP-OES in Activation laboratories Ltd. (ATCLABS) in Ancaster, Canada. The samples were mixed with a flux of lithium metaborate and lithium tetraborate, and fused at 1000 °C in an induction furnace. The molten beads were rapidly digested in a solution of 5% HNO_3 containing an internal standard, and mixed continuously until complete dissolution. Loss on ignition (LOI) was determined by measuring weight loss upon heating to 1100 °C over a three hour period. Totals of major elements are 100 ± 1 wt.% and their analytical precisions are of 1-2% for most major elements. The analytical precisions for Sc and Zr are better than 10%.

Transition metals (Ni, Co, Cr, and V), REE, HFSE, and LILE were analyzed on a high-sensitivity Thermo Elemental X7 ICP-MS in the Great Lakes Institute for Environmental Research (GLIER), University of Windsor, Canada, following the protocols of Jenner et al. (1990). Sample dissolution was conducted under clean lab conditions with double distilled acids. Approximately 100-130 mg of sample powder was used for acid digestion. Samples were dissolved in Teflon bombs in a concentrated mixture of HF-HNO_3 at a temperature of 120 °C for 3 days and then further attacked with 50% HNO_3 until no solid residue was left. Hawaiian basalt standards BHVO-1 and BHVO-2 were used as reference materials to estimate precision and accuracy. Analytical precisions are estimated as follows: 3-10% for REE, Y, Nb, Ta, Rb, Sr, Cs, Ba, and Co; 10-20% for Ni, and Th; and 20-30% for U, Pb, V, and Cr.

Major element analyses were recalculated to 100 wt.% anhydrous basis for inter-comparisons. Chondrite and primitive mantle reservoir compositions are those of Sun and McDonough (1989) and Hofmann (1988), respectively. The Eu (Eu/Eu*), Ce (Ce/Ce*),

Nb (Nb/Nb*), Ti (Ti/Ti*), and Zr (Zr/Zr*) anomalies were calculated with the following equation after Taylor and McLennan (1985):

$$A/A^* = A_N/([(B_N)(C_N)]^{1/2}$$

Where

A/A^* = Element anomaly

A_N = Chondrite normalization for Eu and Ce anomalies, and primitive mantle normalization for Nb, Ti, and Zr anomalies.

B_N and C_N = Neighboring immobile elements as follow: Sm and Gd for Eu/Eu*; La and Pr for Ce/Ce*, Th and La for Nb/Nb*, Nd and Sm for Zr/Zr*, and Tb and Dy for Ti/Ti*.

Mg-numbers (%) were calculated as the molecular ratio of $Mg^{2+}/(Mg^{2+} + Fe^{2+})$ where Fe^{2+} is assumed to be 90% of the total Fe.

4.5. Geochemistry

4.5.1. Amphibolites

Amphibolites consistently plot in the field of basaltic rocks on Zr/Ti versus Nb/Y diagram (Fig. 4.4). They possess Zr/Y ratios (Zr/Y = 1.7-3.9) within the range of those of modern tholeiitic basalts (Zr/Y = 2.0-4.5) (see Barrett and MacLean, 1994) (Table 4.1). Amphibolites of the Storø and the Ivisaartoq-Ujarassuit greenstone belts display near-collinear trends of major elements, HFSE, and REE on variation diagrams of Zr indicating comparable compositions (Table 4.1; Fig. 4.5). They have Mg-numbers ranging from 41 to 61 and variable concentrations of SiO_2 (43.1-55.3 wt%), TiO_2 (0.6-2.5 wt%), Fe_2O_3 (9.5-19.7 wt%), Al_2O_3 (9.9-15.6 wt%), MgO (4.7-14.1 wt%), Zr (30-150 ppm), ΣREE (20-101 ppm), and Ni (59-262 ppm). Amphibolites in the Storø belt possess

lower concentrations of Cr (45-211 ppm) than those of the Ivisaartoq-Ujarassuit counterparts (Cr = 104-2030 ppm).

On chondrite- and primitive mantle-normalized diagrams, most amphibolites in the Storø belt exhibit coherent near-flat to slightly enriched LREE (La/Sm_{cn} = 0.91-1.48) and relatively flat HREE patterns (Gd/Yb_{cn} = 1.0-1.28) (Fig. 4.6a-b). They display consistent negative Nb anomalies (Nb/Nb* = 0.34-0.73), and negative to positive anomalies of Eu (Eu/Eu* = 0.67-1.18), Zr (Zr/Zr* = 0.74-1.19), and Ti (Ti/Ti* = 0.75-1.14) (Fig. 4.6a-b). In addition, they possess sub-chondritic Al_2O_3/TiO_2 (6.1-19.9) and Nb/Ta (13.7-16.2) ratios, and sub- to super-chondritic Ti/Zr (67-136) (Table 4.1). The above geochemical characteristics and trace element patterns are similar to those displayed by well preserved pillow basalts and least altered Group 1 amphibolites of the Ivisaartoq and Ujarassuit greenstone belts (see Polat et al., 2007; Ordóñez-Calderón et al., 2008a,b).

A few amphibolites display different and more variable trace element patterns than those described above (Fig. 4.6c-d). These include strongly depleted to strongly enriched LREE patterns (La/Sm_{cn} = 0.47-4.81), slightly fractionated HREE (Gd/Yb_{cn} = 0.77-1.26), pronounced-negative to near-absence anomalies of Nb (Nb/Nb* = 0.41-0.95), and strong negative to positive Eu anomalies (Eu/Eu* = 0.55-3.25). Amphibolites with strong LREE depletion (sample 493126; Fig. 4.6c-d) display similar trace element patterns to those of altered Group 3 and Group 2 amphibolites in the Ivisaartoq and Ujarassuit greenstone belts, respectively, and amphibolites in the Qussuk greenstone belt, northwest of Storø (Garde, 2007; Ordóñez-Calderón et al., 2008a).

4.5.2. Ultramafic rocks

Sample 493124 (Fig. 4.3c) was collected from a serpentinized ultramafic body that extends for approximately 2 km along the belt. This rock possesses low CaO (5.1 wt%), Al_2O_3, (7.14 wt%), TiO_2 (0.40 wt%), Zr (35.5 ppm), and ΣREE (11.3 ppm), and high contents of MgO (31.9 wt%), Ni (1173 ppm), and Cr (1575 ppm) (Table 4.1). On chondrite- and primitive mantle-normalized diagrams (Fig. 4.6c-d) this sample displays a flat REE pattern (La/Sm_{cn} =1.08; Gd/Yb_{cn} = 0.98), lack of Nb (Nb/Nb* = 1.09) and Eu (Eu/Eu* = 0.99) anomalies, and exhibits pronounced positive Zr (Zr/Zr* = 2.11) and Ti (Ti/Ti* = 1.32) anomalies.

4.5.3. Garnet-biotite schists and quartzitic gneisses

Garnet-biotite schists straddle the compositional fields of basalts and andesites on the Zr/Ti versus Nb/Y diagram (Fig. 4.4). They possess variable concentrations of SiO_2 (48.8-66.9 wt%), MgO (1.96-4.68 wt%), Fe_2O_3 (5.7-16.8 wt%), TiO_2 (0.82-2.64 wt%), Al_2O_3 (14.9-23.2 wt%), Zr (102-250 ppm), and high concentrations of Ni (26-154 ppm), Sc (13-58 ppm), Cr (7-166 ppm), and V (62-452 ppm) (Table 4.2; Fig. 4.5). On chondrite- and primitive mantle-normalized diagrams, the garnet-biotite schists display LREE enriched patterns (La/Sm_{cn} = 1.38-3.23) and near-flat to fractionated HREE patterns (Gd/Yb_{cn} =1.05-2.24) (Fig. 4.7a-b). In addition, they exhibit pronounced negative anomalies of Nb (Nb/Nb* = 0.25-0.61), and negative to positive Eu (Eu/Eu* = 0.56-1.22), Zr (Zr/Zr* = 0.79-1.56), and Ti (Ti/Ti* = 0.52-1.87) anomalies.

Quartzitic gneisses in the Storø greenstone belt have high concentrations of SiO_2 (82.5-87.4 wt%). Relative to the garnet-biotite schists, they are depleted in Al_2O_3 (6.3-8.6 wt%), MgO (0.68-1.19 wt%), TiO_2 (0.22-0.45 wt%), Zr (60.7-74.2 ppm), ΣREE (60.1-

45.9 ppm), and transition metals (Ni < 50 ppm) (Table 4.2). They have Zr/Ti and Nb/Y ratios similar to those of andesites and basaltic andesites (Fig. 4.4). On chondrite and primitive mantle normalized diagrams, they display enriched LREE and fractionated HREE patterns (La/Sm_{cn} = 3.17-3.79; Gd/Yb_{cn} = 1.45-5.06) (Fig. 4.7c-d). In addition, they possess pronounced negative Nb (Nb/Nb* = 0.15-0.17) and Ti (Ti/Ti* =0.68-0.79) anomalies, shallow-negative Eu anomalies (Eu/Eu* = 0.77-1.02), and positive anomalies of Zr (Zr/Zr* = 1.01-1.30) (Fig. 4.7c-d).

4.6. Discussion

4.6.1. Element mobility in metavolcanic rocks

The Storø greenstone belt has undergone high-grade metamorphism, and a complex history of hydrothermal alteration indicated by calc-silicate metasomatism, silicification, shear-zone hosted quartz veins (Fig. 4.2f), and high-temperature (> 300 °C) amphibolite-facies gold mineralization (see Juul-Pedersen et al., 2007; Knudsen et al., 2007; Nutman et al., 2007). This processes appear to have resulted in significant major and trace element mobility. To circumvent the geochemical effects of metamorphism and hydrothermal alteration, most geochemical studies of Archean greenstone belts rely on the systematics of HFSE (Th, Nb, Ta, Zr, and Ti), REE (La-Lu), and transition metals (Ni, Sc, V, Cr, and Co), given that these group of elements are relatively immobile under various geological conditions (Hart et al., 1974; Condie et al., 1977; Ludden and Thompson, 1979; Gélinas et al., 1982; Ludden et al., 1982; Middelburg et al., 1988; Ague, 1994; Arndt, 1994; Staudigel et al., 1996; Alt, 1999; Polat and Hofmann, 2003; Polat et al., 2003; Masters and Ague, 2005). However, numerous studies have also indicated that HFSE and REE may be mobile under high-temperature magmatic, metamorphic, and hydrothermal

alteration conditions (Gieré, 1990; Rubin et al., 1993; Van Baalen, 1993; Valsami-Jones, 1997; Tilley and Eggleton, 2005; Galley et al., 2000; Jiang et al., 2005; Ordóñez-Calderón et al., 2008a).

In the Storø belt, most amphibolites display coherent and near-parallel trace element patterns on chondrite- and primitive mantle-normalized diagrams (Fig. 4.6a-b). Samples with the lowest concentrations of trace elements (ΣREE < 13 x chondrite) possess higher Mg-numbers (55-61) than those with larger contents of trace elements (ΣREE > 19 x chondrite, Mg-numbers = 41-53). These geochemical variations are commonly exhibited by unaltered Phanerozoic volcanic rocks and reflect various degrees of fractional crystallization (e.g., Green et al. 2006). In addition, HFSE (e.g., Ti and Nb), transition metals (e.g., Sc), and REE exhibit excellent correlation with Zr on variation diagrams (Fig. 4.5). Therefore, amphibolites with flat to slightly enriched LREE patterns (Fig. 4.6a-b) are interpreted to preserve their near-primary magmatic geochemical signatures.

In contrast, altered amphibolites display trace element patterns that are not parallel to those of the least altered counterparts (Fig. 4.6c-d; Table 4.1). For instance, strong silicification of sample 485492 (SiO_2 = 82.9 wt%) resulted in significant dilution of major and trace element contents (e.g., TiO_2 = 0.12 wt%; Ni = 9.3 ppm) and a U-shape REE pattern. In the Ivisaartoq greenstone belt, the U-shape REE patterns of Group 2 amphibolites appear to have resulted from strong HFSE and REE mobility during regional prograde metamorphism (see Ordóñez-Calderón et al., 2008a).

Amphibolites with depleted LREE patterns (Fig. 4.6c-d; samples 493109, 493114, and 493126) are compositionally similar to Group 2 and Group 3 amphibolites in the Ujarassuit and Ivisaartoq belts, respectively, and amphibolites in the Qussuk belt in the Akia Terrane (see Garde, 2007; Ordóñez-Calderón et al., 2008a,b). Given that these

amphibolites do not exhibit evidence for significant major element metasomatism (e.g., silicification or calc-silicate alteration) their origin is controversial. In Qussuk peninsula they have been interpreted to retain their near primary magmatic geochemical signatures (Garde, 2007). In contrast, in the Ivisaartoq and Ujarassuit greenstone belts the depleted LREE patterns have been ascribed to trace element mobility during regional amphibolite facies metamorphism (Ordóñez-Calderón et al., 2008a,b). Geochronological evidence renders unlikely a cogenetic link among metavolcanic rocks in those greenstone belts. Nonetheless, the compositional resemblance may reflect a similar origin. For example, in those belts, amphibolites with larger depletion of LREE ($La/Yb_{cn} < 0.70$) display the most pronounced negative Ti anomalies ($Ti/Ti^* = < 0.70$) (cf. Ordóñez-Calderón et al., 2008b). These geochemical characteristics may reflect either breakdown of Ti- and LREE-bearing minerals (e.g., hornblende and titanite) during high-grade metamorphism, or alternatively, a primary magmatic signature derived from a depleted mantle source with residual amphibole after partial melting. In the Storø belt, amphibolites with depleted LREE patterns occur randomly within the same outcrops of amphibolites with near-flat LREE patterns (e.g., samples 493108 and 493109). This suggests that LREE may have been remobilized and therefore amphibolites with depleted LREE patterns (Fig. 4.6c-d) are not taken into account for petrological and geodynamic interpretations.

4.6.2. Provenance for metasedimentary rocks

Relative to the amphibolites, garnet-biotite schists and quartzitic gneisses display independent covariation trends of TiO_2 and HREE on variation diagrams of Zr (Fig. 4.5), and different inter-element ratios of HFSE, REE, and transition metals (Fig. 4.8). Therefore, it is unlikely that garnet-biotite schists and quartzitic gneisses represent the

metamorphosed products of hydrothermally altered (e.g., intense silicification or sericitisation) basaltic rocks (cf. Knudsen et al., 2007).

Strong deformation (Fig. 4.2b-d) and high-grade metamorphism have obliterated primary sedimentary structures. Nevertheless, a volcaniclastic-sedimentary protolith is suggested by the presence of detrital zircons ranging in age from 3180 to 2830 Ma (Hollis, 2005; Knudsen et al., 2007; Nutman et al., 2007). This indicates a wide range of felsic source rocks and recycling of older continental crust.

The contribution of felsic source regions to the protolith of garnet-biotite schists and quartzitic gneisses is also evident in normalized trace element patterns with strongly enriched incompatible elements (mainly Th, LREE, and Zr), relative to HREE and Y (Fig. 4.7). In addition, moderate to high concentrations of transition metals (Ni up to 153 ppm) also suggest that mafic igneous rocks were significant source rocks. Inter-element ratios of transition metals against HFSE and LREE clearly display geochemical trends that are consistent with mixing of detritus derived from felsic and mafic end members (Fig. 4.8) (cf. Condie and Wronkiewicz, 1990; Hofmann, 2005).

During weathering of source rocks, CaO, Na_2O, and K_2O are progressively removed into solution whereas Al_2O_3 remains immobile (Nesbitt and Young, 1984). Accordingly, the chemical index of alteration ($CIA = 100[Al_2O_3/ (Al_2O_3 + CaO^* + Na_2O + K_2O)]$), where CaO* is CaO in the silicate fraction, measures the residual enrichment of Al_2O_3 in the detrital component. Therefore the CIA is widely used as a parameter that quantifies the degree of weathering of the source rocks (Nesbitt and Young, 1984; Fedo et al., 1995; Nesbitt et al., 1996). Experimental and empirical studies have shown that chemical weathering normally result in geochemical trends that parallel the A-CN side of the A-CN-K diagram (Fig. 4.9) (Nesbitt and Young, 1984; Nesbitt and Markovics, 1997;

Nesbitt, 2003; McLennan et al., 2003). Garnet-biotite schists and quartzitic gneisses do not follow the predicted weathering trends but rather straddle the trends for mafic to felsic source rocks (Fig. 4.9). The scattering on the A-CN-K diagram may be the result of several processes including post-depositional mobility of Ca, Na, and K, geochemical fractionation owing to sedimentary sorting of the clay and sand fraction, and mixing of detritus derived from mafic to felsic source rocks (see McLennan et al., 1993; Nesbitt et al., 1996, 1997; McLennan et al., 2003). Although mobility of Ca, Na, and K, likely occurred during metamorphism, the scattered pattern in the A-CN-K diagram is consistent with mixing of mafic to felsic detritus (Figs. 4.8 and 4.9), and different clay/sand ratios in the sedimentary protoliths as is indicated by large variations in the Al_2O_3 contents (Table 4.2).

Garnet-biotite schists and quartzitic gneisses possess CIA values (50 to 71; one sample with 81) moderately higher than those of unweathered igneous rocks (38 to 51), but lower than average Archean shales (ca. 76) (Condie, 1993) (Fig. 4.9; Table 4.2). The low CIA values, moderate Al_2O_3 contents (14.9 to 23.2 wt%), and inter-element ratios (Figs. 4.8 and 4.9) strongly suggest those rocks were derived from mafic to felsic source rocks that experienced low rates of chemical weathering. Garnet-biotite schists are interpreted to represent compositionally immature graywackes whereas the quartzitic gneisses likely represent more mature quartz-rich arkoses.

Detrital zircons of 3180 Ma, in quartzitic gneisses and garnet-biotite schists, suggest erosion of old continental rocks (Knudsen et al., 2007). However, zircons with ages between 2880 and 2830 Ma, close to the age of the belt, appear to be the dominant population (Knudsen et al., 2007). Therefore, zircon geochronology and the geochemical evidence presented in this study indicate that the protolith of quartzitic gneisses and

garnet-biotite schists in the Storø greenstone belt contain detritus derived from Mesoarchean continental rocks, and reworked felsic to mafic Neoarchean volcaniclastic detritus. Given the dominant basaltic composition of the Storø belt, the felsic source rocks were likely distal relative to the belt.

4.6.3. Petrogenesis and geodynamic origin of metavolcanic rocks

In amphibolites, positive correlation of REE, Nb, and Th, and negative correlation of Al_2O_3, MgO, and transition metals (Sc, V, Ni, Co, Cr) with increasing Zr contents are consistent with fractionation of olivine, pyroxene, and plagioclase (Fig. 4.5). In addition, TiO_2 increases with Zr contents suggesting that Fe-Ti oxides (ilmenite and titanomagnetite) were not significant mineral phases during fractionation. The sub-parallel near-flat enrichment of trace element patterns (La/Yb_{cn} = 0.91-1.48) on chondrite- and primitive mantle-normalized diagrams (Fig. 4.6) indicate that fractionation took place without significant contamination with upper continental crust rocks. This is also consistent with field evidence indicating fault bounded contacts between amphibolites and TTG-gneisses (Fig. 4.1). Therefore, the basaltic protoliths of the amphibolites in the Storø greenstone belt were likely erupted in an intra-oceanic tectonic setting.

Amphibolites display pronounced negative Nb-Ta anomalies on primitive-mantle normalized diagrams (Fig. 4.6) which is consistent with a subduction zone geochemical signature (Saunders et al., 1991; Hawkesworth et al., 1993; Kelemen et al., 2003). They consistently plot within the field of Phanerozoic subduction-related volcanic rocks on the Th/Yb versus Nb/Yb diagram (Fig. 4.10). These characteristics indicate that the Storø greenstone belt formed in a supra-subduction zone geodynamic setting.

Ultramafic rock 493124 possesses high MgO (31.9 wt.%), Ni (1173 ppm) and Cr (1575 ppm) concentrations, and Mg-number (86) indicating a cumulate picritic composition (cf. Le Bas, 2000). These geochemical characteristics are similar to ultramafic rocks in the Ivisaartoq and Ujarassuit greenstone belts which have been interpreted as island arc picrites (Polat et al., 2007, 2008; Ordóñez-Calderón et al., 2008a,b). The ultramafic rock in this study, however, lacks the distinctive negative Nb-Ta anomaly of island arc picrites (cf. Eggins, 1993; Kamenetsky et al., 1995; Schuth et al., 2004; Rohrback et al., 2005). In the Ivisaartoq and Ujarassuit belts, only the least altered ultramafic rocks with relict igneous mineralogy preserve the negative Nb-Ta anomalies (Polat et al., 2007, 2008; Ordóñez-Calderón et al., 2008a,b). Postmagmatic element mobility of LREE and Th, relative to Nb and Ta, resulted in variable negative to positive Nb-Ta anomalies (Polat et al., 2007, 2008; Ordóñez-Calderón et al., 2008a,b). Given the strong serpentinization of sample 493124 (Fig. 4.3c), it is likely that the original magmatic trace element signature has been obliterated. In the Storø belt, the spatial association of the ultramafic rocks (Fig. 4.1) and amphibolites with subduction zone geochemical signatures suggests that the ultramafic rocks represent Archean island arc picrites.

Less fractionated amphibolites (MgO > 8 wt%) exhibit lower concentrations of HREE and HFSE (mainly Nb, Ta, Zr, and Ti), relative to average modern N-MORB (Hofmann, 1988) (Fig. 4.6a-b). These trace element characteristics are also exhibited by primitive Phanerozoic island arc tholeiites (IAT) (e.g., Maury et al., 1992; Kelemen et al., 2003). Fluid fluxing from the downgoing slab lowers the solidus temperature of the mantle wedge and induces high melt production rates (e.g., Maury et al., 1992; Hawkesworth et al., 1993; Pearce and Peate, 1995). Accordingly, the lower

concentrations of HFSE and HREE in arc magmas, relative to N-MORB, result from larger degrees of partial melting in subduction zones than in mid-ocean ridge settings. However, studies of mantle xenoliths in arc magmas from the western Pacific island arcs have shown that the sub-arc mantle may be more depleted in trace elements (HFSE and HREE) than depleted upper mantle at mid-ocean ridges (e.g., Dick and Bullen, 1984; Maury et al., 1992; Arai et al., 2007; Ishimaru et al., 2007; Arai and Ishimaru, 2008). The degree of depletion of the sub-arc mantle depends on the partial melting history before arc inception and during arc development. Therefore, the low concentrations of HFSE and HREE in modern IAT result from a combination of processes including large degrees of flux melting in a depleted sub-arc mantle.

Amphibolites of the Storø belt are enriched in Fe_2O_3 (Fe_2O_3 = 12.0-17.8 wt% at MgO > 8 wt%) relative to modern N-MORB (9.8 to 11.6 wt%) and primitive IAT (8.9-10.6 wt%) at similar MgO contents (Hofmann, 1988; Kelemen et al., 2003). These compositional differences between Archean and Phanerozoic tholeiitic basalts have been previously documented and have been attributed to larger degrees of partial melting in an Archean mantle that was at least 120 °C hotter than the modern upper mantle (e.g., Glikson, 1971; Nisbet and Fowler, 1983; Ohta et al., 1996; Pollack, 1997). Given the immobile behavior of Nb and Yb in slab-derived fluids, the Nb/Yb ratios of tholeiitic basalts reflect the degree of depletion of incompatible elements in the mantle source (cf. Hawkesworth et al., 1993; Pearce and Peate, 1995; Becker et al., 2000; Schmidt and Poli, 2003; Pearce, 2008). Less fractionated amphibolites in the Storø greenstone belt possess slightly lower Nb/Yb ratios (0.55-0.76 versus 0.90 in N-MORB) than average N-MORB (see Hofmann, 1988). Accordingly, the major and trace element characteristics of these rocks suggest large degrees of partial melting of a depleted sub-arc mantle. In addition,

the flat HREE patterns indicate shallow melting (< 80 km) and absence of residual garnet in the mantle source (cf. Johnson, 1994; Hirschmann and Stolper, 1996; van Westrenen et al., 2001).

4.7. Implications and conclusions

The Neoarchean (2800-2840 Ma) Storø greenstone belt possesses comparable lithological and geochemical characteristics to those of the Mesoarchean (3075 Ma) Ivisaartoq and (3070 Ma) Ujarassuit greenstone belts (Polat et al., 2007; 2008; Ordóñez-Calderón et al., 2008a,b). These include: 1) amphibolites with an island arc tholeiitic (IAT) geochemical composition, 2) intercalations of ultramafic cumulates (metapicrites), 3) metamorphosed gabbro-anorthosite complexes at the base of the tectono-stratigraphic sequence, and 4) reworked metavolcaniclastic-sedimentary rocks with mixed felsic to mafic provenance. The Storø greenstone belt, however, does not include boninite-like rocks.

In southern West Greenland, the spatial and temporal association of amphibolites (IAT), metapicrites, and metagabbro-meta-anorthosite complexes has been interpreted as fragments of Archean oceanic crust (Windley et al., 1981; Weaver et al., 1982; Ashwal and Myers, 1994; Polat et al., 2008; Windley and Garde, 2008). On the basis of field, geochronological, and geochemical evidence from the Ivisaartoq belt, Polat et al. (2008) proposed that the Archean oceanic crust may have consisted of a lower layer of cumulate gabbro and anorthosites, and an upper layer of basaltic to ultramafic flows. The intra-oceanic origin of the Ivisaartoq and Ujarassuit greenstone belts has also been substantiated by the recognition of boninites (Ordóñez-Calderón et al., 2008b). In the Storø greenstone belt, the geochemical characteristics of metavolcanic rocks and

structural contacts between orthogneisses and supracrustal rocks are consistent with an intra-oceanic subduction zone oceanic crust. Therefore, lithological and geochemical similarities between the Storø and the Ivisaartoq-Ujarassuit greenstone belts suggest broadly similar petrologic processes in the generation of Meso- to Neoarchean supra-subduction zone oceanic crust. These processes include: 1) hot subduction zones, likely owing to subduction of young and hot oceanic lithosphere or spreading-ridge subduction; 2) large degrees of partial melting; 3) heterogeneous depleted- to strongly refractory-mantle; 4) metasomatism of the sub-arc mantle with slab-derived fluids and melts prior to or during partial melting; and 5) supra-subduction zone extension.

Despite the dominant mafic-ultramafic composition of the Storø greenstone belt, metavolcaniclastic-sedimentary rocks display geochemical evidence for mixing of mafic and felsic detritus (Fig. 4.8). Low CIA values (Fig. 4.9) and the presence of a significant population of ca. 2830 to 2880 Ma detrital zircons (see Hollis, 2005; Nutman et al., 2007) suggest that the more differentiated siliciclastic components represent reworked mildly-weathered felsic to intermediate volcanic-plutonic detritus. These source rocks may have been part of more mature Neoarchean island arc complexes which are not represented in the geologic record. In the Ivisaartoq and Ujarassuit greenstone belts, the source rocks for felsic to intermediate detritus also appear to have been eroded away (Ordóñez-Calderón et al., 2008b). Nonetheless, the occurrence of a rare mature ca. 3071 Ma island arc complex in the Qussuk greenstone belt, Akia Terrane, supports the coexistence of subduction zone basalts and felsic to intermediate volcanic arc complexes (Garde, 2007).

Given that mature island arcs have thicker and less dense crust than juvenile arcs, more evolved arc complexes may have been thrust into the uppermost crustal levels during the prolonged collisional tectonics of the Nuuk region (Bridgwater et al., 1974;

Friend et al., 1988; Nutman et al., 1989; Friend and Nutman, 2005; Nutman and Friend, 2007). The Nuuk region exposes high-grade amphibolite-granulite facies metamorphic rocks which clearly suggest that at least 15 km of the uppermost crust have been eroded away. Therefore, the absence of mature volcanic arc sequences in the region may be explained by the present level of erosion (see Garde, 2007; Ordóñez-Calderón et al., 2008b). In contrast, other Archean granite-greenstone terranes in the Superior Province, eastern Yilgarn Craton, and the Baltic shield, consist of low-grade greenschist facies metavolcanic rocks, clearly indicating that the uppermost crustal levels have not been deeply eroded (cf. Ludden and Hubert, 1986; Ludden et al., 1986; Laflèche et al., 1992a,b; Kimura et al., 1993; Polat et al., 1998; Puchtel et al., 1998, 1999; Smithies et al., 2007; Barley et al., 2008). In the Nuuk region, high-grade greenstone belts are less than 5 km in width. In contrast, low-grade greenstone belts may be more than 20 km wide (op. cit.). Accordingly, the high-grade metamorphic rocks of the Nuuk region represent the roots of an Archean collisional orogen and therefore a significant portion of the supracrustal stratigraphy has been removed by erosion.

The presence of quartz-rich metasedimentary rocks and old detrital zircons (> 3000 Ma) sourced from Mesoarchean continental rocks (see Hollis, 2005; Knudsen et al., 2007) do not invalidate the oceanic origin of the belt, but rather provide additional constraints for its geodynamic origin. For instance, Knudsen et al. (2007) suggested that the Storø belt formed in a back-arc setting close to old continental crust. However, in the SW Pacific Ocean island arcs, turbidity currents have transported continental sediments, derived from New Zealand, into the Tonga-Kermadec arc (Graham et al., 1997). Therefore, a juvenile arc or forearc geodynamic origin cannot be rule out for the Storø greenstone belt.

4.8. Acknowledgements

We thank Z. Yang, and J.C. Barrette for their help during the ICP-MS analyses. This is a contribution of PREA and NSERC grant 250926 to A. Polat, and NSERC grant 83117 to B. Fryer. Field worked was funded by the Bureau of Minerals and Petroleum in Nuuk and the Geological Survey of Denmark and Greenland (GEUS).

4.9. References

Ague, J.J., 1994. Mass transfer during Barrovian metamorphism of pelites, south-central Connecticut. I: Evidence for changes in composition and volume. American Journal of Science 294, 989-1057.

Alt J. C., 1999. Hydrothermal alteration and mineralization of oceanic crust: Mineralogy, geochemistry, and processes. In: Barrie, C.T., Hannington, M.D., (Eds.). Volcanic-Associated Massive Sulphide Deposits: Processes and Examples in Modern and Ancient Settings. Reviews in Economic Geology 8, 133-155.

Appel, P.W.U., Bliss, I.C., Coller, D.W., Grahl-Madsen, L., Petersen, J.S., 2000. Recent gold discoveries in Archaean rocks of central West Greenland. Transactions-Institution of Mining and Metallurgy. Section B. Applied Earth Science 109, 34-41.

Arai, S., Abe, N., Ishimaru, S., 2007. Mantle peridotites from the Western Pacific. Gondwana Research 11, 180-199.

Arai, S., Ishimaru, S., 2008. Insights into petrological characteristics of the lithosphere of mantle wedge beneath arcs through peridotites xenoliths: a review. Journal of Petrology 49, 665-698.

Arndt, N.T., 1994. Archean komatiites. In: Condie, K.C. (Ed.). Archean Crustal Evolution. Developments in Precambrian Geology 11, 11-44.

Ashwal, L.D., Myers, J., 1994. Archean anorthosites. In: Condie, K.C., (Ed.). Archean Crustal Evolution. Elsevier, Amsterdam, 315-355.

Banerjee, N.R., Gillis, K.M., Muehlenbachs, K., 2000. Discovery of epidosites in a modern oceanic setting, the Tonga forearc. Geology 28, 151-154.

Barley, M.E., Brown, S.J.A., Krapež, B., Kositcin, N., 2008. Physical volcanology and geochemistry of a Late Archaean volcanic arc: Kurnalpi and Gindalbie Terranes, Eastern Goldfields Superterrane, Western Australia. Precambrian Research 161, 53-76.

Barrett, T.J., MacLean, W.H., 1994. Chemostratigraphy and hydrothermal alteration in exploration for VHMS deposits in greenstones and younger volcanic rocks. In: Lentz, D.R., (Ed.). Alteration and alteration processes associated with ore-forming systems. Geological Association of Canada, Short course notes 11, 433-467.

Becker, H., Jochum, K.P., Carlson, R.W., 2000. Trace element fractionation during dehydration of eclogites from high-pressure terranes and the implications for element fluxes in subduction zones. Chemical Geology, 163, 65-99.

Bickle, M.J., Nisbet, E.G., Martin, A., 1994. Archean greenstone belts are not oceanic crust. Journal of Geology 102, 121-138.

Black, L.P., Gale, N.H., Moorbath, S., Pankhurst, R.J., McGregor, V.R., 1971. Isotopic dating of very early Precambrian amphibolite facies gneisses from the Godthaab district, West Greenland. Earth and Planetary Science Letters 12 (3), 245-259.

Bleeker, W., 2002. Archean tectonics, a review, with illustrations from the Slave craton. In: Fowler, C.M.R., Ebinger, C.J., Hawkesworth, C.J. (Eds.). The Early Earth: Physical,

Chemical and Biological Development. Geological Society of London, Special Publications 199, 151-181.

Bridgwater, D., McGregor, V.R.,. Myers, J.S., 1974. A horizontal tectonic regime in the Archean of Greenland and its implications for early crustal thickening. Precambrian Research 1, 179-197.

Chadwick, B., 1990. The stratigraphy of supracrustal rocks within high-grade orthogneisses and its bearing on Late Archean structure in southern West Greenland. Journal of the Geological Society of London 147, 639-652.

Condie, K.C., 1993. Chemical composition and evolution of the upper continental crust: Contrasting results from surface samples and shales. Chemical Geology 104, 1-37.

Condie, K.C., Viljoen, M.J., Kable, E.J.D., 1977. Effects of alteration on element distributions in Archean tholeiites from the Barberton greenstone belt, South Africa. Contributions to Mineralogy and Petrology 64, 75-89.

Condie, K.C., Wronkiewicz, D.J., 1990. The Cr/Th ratio in Precambrian pelites from the Kaapvaal Craton as an index of craton evolution. Earth and Planetary Science Letters 97 (3-4), 256-267.

Crowley, J.L., 2002. Testing the model of late Archean terrane accretion in southern West Greenland: a comparison of the timing of geological events across the Qarliit Nunaat Fault, Buksefjorden region. Precambrian Research 116 (1-2), 57-79.

De Wit, M.J., 2004. Archean greenstone belts do contain fragments of ophiolites. In: Kusky, T.M., (Ed.). Precambrian ophiolites and related rocks. Developments in Precambrian Geology, Elsevier vol. 13, 599-614.

Dick, H.J.B., Bullen, T., 1984. Chromian spinel as a petrogenetic indicator in abyssal and alpine-type peridotites and spatially associated lavas. Contributions to Mineralogy and Petrology 86, 54-76.

Dilek, Y., Flower, M.F.J., 2003. Arc-trench rollback and forearc accretion: 2. A model template for ophiolites in Albania, Cyprus, and Oman. In: Dilek, Y., Robinson, P.T. (Eds.). Ophiolites in earth history. Geological Society of London, Special Publications 218, 43-68.

Eggins SM, 1993. Origin and differentiation of picritic arc magmas, Ambae (Aoba), Vanuatu. Contributions to Mineralogy and Petrology 114, 79-100.

Fedo, C.M., Nesbitt, H.W., Young, G.M., 1995. Unraveling the effects of potassium metasomatism in sedimentary rocks and paleosols, with implications for paleoweathering conditions and provenance. Geology 23, 921-924.

Fedo, C.M., Whitehouse, M.J., 2002. Metasomatic origin of quartz-pyroxene rock, Akilia, Greenland, and implications for earth's earliest life. Science 296, 1448-1452.

Flower, M.F.J., Dilek, Y., 2003. Arc-trench rollback and forearc accretion: 1. A collision induced mantle flow model for Tethyan ophiolites. In: Dilek, Y., Robinson, P.T. (Eds.). Ophiolites in earth history. Geological Society of London, Special Publications 218, 21-41.

Friend, C.R.L., Nutman, A.P., 2005. New pieces of the Archaean terrane jigsaw puzzle in the Nuuk Region, southern West Greenland: steps in transforming a simple insight into a complex regional tectonothermal model. Journal of the Geological Society of London 162, 147-162.

Friend, C.R.L., Nutman, A.P., 1991. Refolded nappes formed during late Archaean terrane assembly, Godthåbsfjord, southern West Greenland. Journal of the Geological Society of London 148, 507-519.

Friend, C.R.L., Nutman, A.P., Baadsgaard, H., Kinny, P.D., McGregor, V.R., 1996. Timing of late Archean terrane assembly, crustal thickening and granite emplacement in the Nuuk region, southern West Greenland. Earth and Planetary Science Letters 142, 353-365.

Friend, C.R.L., Nutman, A.P. & McGregor, V.R., 1987. Late-Archaean tectonics in the Færingehavn-Tre Brødre area, south of Buksefjorden, southern West Greenland. Journal of the Geological Society of London 144, 369-376.

Friend, C.R.L., Nutman, A.P., McGregor, V.R., 1988. Late Archean terrane accretion in the Godthåb region, southern West Greenland. Nature 335, 535-538.

Galley, A.G., Jonasson, I.R., Watkinson, D.H., 2000. Magnetite-rich calc-silicate alteration in relation to synvolcanic intrusions at the Ansil volcanogenic massive sulfide deposit, Rouyn-Noranda, Quebec, Canada. Mineralium Deposita 35, 619-637.

Garde, A.A., 2007. A mid-Archean island arc complex in the eastern Akia terrane, Godthåbsfjord, southern West Greenland. Journal of the Geological Society of London 164, 565-579.

Gélinas, L., Mellinger, M., Trudel, P., 1982. Archean mafic metavolcanics from the Rouyn-Noranda district, Abitibi Greenstone Belt, Quebec. 1. Mobility of the major elements. Canadian Journal of Earth Sciences 19, 2258-2275.

Gieré, R., 1990. Hydrothermal mobility of Ti, Zr and REE: examples from the Bergell and Adamello contact aureoles (Italy). Terra Nova 2, 60-67.

Glikson, A.Y., 1971. Primitive Archaean element distribution patterns: Chemical evidence and geotectonic significance. Earth and Planetary Science Letters 12, 309-320.

Graham, I.J., Glasby, G.P., Churchman, G.J., 1997. Provenance of the detrital component of deep-sea sediments from the SW Pacific Ocean based on mineralogy, geochemistry and Sr isotopic composition. Marine Geology 140, 75-96.

Greene, A.R., Debari, S.M., Kelemen, P.B., Blusztajn, J., Clift, P.D., 2006. A detailed geochemical study of island arc crust: the Talkeetna arc section, south-central Alaska. Journal of Petrology, 1051-1093.

Hart S. R., Erlank A. J., Kable E. J. D., 1974. Sea-floor basalt alteration: Some chemical and isotopic effects. Contributions to Mineralogy and Petrology 44, 219–230.

Hartlaub, R.P., Heaman, L.M., Ashton, K.E., Chacko, T., 2004. The Archean Murmac Bay Group: evidence for a giant Archean rift in the Rae Province, Canada. Precambrian Research 131, 345-372.

Hawkesworth, C.J., Gallagher, K., Hergt, J.M., McDetmott, F., 1993. Mantle and slab contributions in arc magmas. Annual Review of Earth and Planetary Sciences 21, 175-204.

Hirschmann, M.M., Stolper, E.M., 1996. A possible role for garnet pyroxenite in the origin of "garnet signature" in MORB. Contribution to Mineralogy and Petrology 124, 185-208.

Hofmann, A., 2005. The geochemistry of sedimentary rocks from the Fig Tree Group, Barberton greenstone belt: Implications for tectonic, hydrothermal and surface processes during mid-Archaean times. Precambrian Research 143, 23-49.

Hofmann, A.W., 1988. Chemical differentiation of the Earth: the relationship between mantle, continental crust, and oceanic crust. Earth and Planetary Science Letters 90, 297-314.

Hollis, J.A., (Ed.) 2005. Greenstone belts in central Godthåbsfjord region, southern West Greenland: Geochemistry, geochronology and petrology arising from 2004 field work, and digital map data. Danmarks Og Grønlands Geologiske Undersøgelse Rapport 42, 214 pp.

Hollis, J.A., van Gool, J.A.M., Steenfelt, A., Garde, A.A., 2004. Greenstone belts in the central Godthåbsfjord region, southern West Greenland: Preliminary results from field work in 2004. Danmarks Og Grønlands Geologiske Undersøgelse Rapport 110, 110 pp.

Hunter, M.A., Bickle, M.J., Nisbet, E.G., Martin, A., Chapman, H.J., 1998. Continental extensional setting for the Archean Belingwe greenstone belt, Zimbabwe. Geology 26, 883-886.

Ishimaru, S., Arai, S., Ishida,Y., Shirasaka, M., Okrugin, V.M., 2007. Melting and multi-stage metasomatism in the mantle wedge beneath a frontal arc inferred from highly depleted peridotite xenoliths from the Avacha volcano, southern Kamchatka. Journal of Petrology 48, 395-433.

Jenner, G. A., Longerich, H. P., Jackson, S. E., Fryer, B. J., 1990. ICP-MS; a powerful tool for high-precision trace-element analysis in earth sciences; evidence from analysis of selected U.S.G.S. Reference samples. Chemical Geology 83, 133-148.

Jiang, S.Y., Wang, R.C., Xu, X.S., Zhao, K.D., 2005. Mobility of high field strength elements (HFSE) in magmatic-, metamorphic-, and submarine-hydrothermal systems. Physics and Chemistry of the Earth 30, 1020-1029.

Johnson, K., 1994. Experimental cpx/and garnet/melt partitioning of REE and other trace elements at high pressures: petrogenetic implications. Mineralogical Magazine 58A, 454-455.

Juul-Pedersen, A., Frei, R., Appel, P.W.U., Persson, M.F., Konnerup-Madsen, J., 2007. A shear zone related greenstone belt hosted gold mineralization in the Archean of West Greenland. A petrographic and combined Pb-Pb and Rb–Sr geochronological study. Ore Geology Reviews 32, 20-36.

Kamenetsky, V.S., Sobolev, A.V., Joron J.L., Semet, M.P., 1995. Petrology and geochemistry of Cretaceous ultramafic volcanics from eastern Kamchatka. Journal of Petrology 36 (3), 637-662.

Kelemen, P.B., Hanghøj, K., Greene, A.R., 2003. One view of the geochemistry of subduction-related magmatic arcs, with emphasis on primitive andesite and lower crust. Treatise on Geochemistry, Elsevier, vol. 3, 593-659.

Kemp, A.I.S., Hawkesworth, C.J., 2003. Granitic perspectives on the generation and secular evolution of the continental crust. Treatise on Geochemistry vol. 3, 349-410.

Kimura, G., Ludden, J.N., Desrochers, J.P., Hori, R., 1993. A model of ocean-crust accretion for the Superior Province, Canada. Lithos 30, 337-355.

Knudsen, C., van Gool, J.A.M., Østergaard, C., Hollis, J.A., Rink-Jørgensen, M., Persson, M., Szilas, K., 2007. Gold-hosting supracrustal rocks on Storø, southern West Greenland: lithologies and geological environment. Geological Survey of Denmark and Greenland Bulletin 13, 41-44.

Laflèche, M.R., Dupuy, C., Bougault, H., 1992a. Geochemistry and petrogenesis of Archean mafic volcanic rocks of the southern Abitibi Belt, Québec. Precambrian Research 57, 207-241.

Laflèche, M.R., Dupuy, C., Dostal, J., 1992b. Tholeiitic volcanic rocks of the late Archean Blake River Group, southern Abitibi greenstone belt: Origin and geodynamic implications. Canadian Journal of Earth Sciences 29, 1448-1458

Le Bas, M.J., 2000. IUGS Reclassification of the high-Mg and picritic volcanic rocks. Journal of Petrology 41, 1467-1470.

Ludden, J.N., Gélinas, L., Trudel, P., 1982. Archean metavolcanics from the Rouyn-Noranda district, Abitibi greenstone belt, Québec. 2. Mobility of trace elements and petrogenetic constraints. Canadian Journal of Earth Sciences 19, 2276-2287.

Ludden, J., Hubert, C., 1986. Geologic evolution of the late Archean Abitibi greenstone belt of Canada. Geology 14, 707-711.

Ludden, J., Hubert, C., Gariepy, C., 1986. The tectonic evolution of the Abitibi greenstone belt of Canada. Geological Magazine 123, 153-166.

Ludden, J.N., Thompson, G., 1979. An evaluation of the behavior of the rare earth elements during the weathering of sea-floor basalts. Earth and Planetary Science Letters 43, 85-92.

Manning, C.E., Mojzsis, S.J., Harrison, T.M., 2006. Geology, age and origin of supracrustal rocks at Akilia, West Greenland. American Journal of Science 306 (5), 303-366.

Masters, R.L., Ague, J.J., 2005. Regional-scale fluid flow and element mobility in Barrow's metamorphic zones, Stonehaven, Scotland. Contributions to Mineralogy and Petrology 150, 1-18.

Maury, R.C., Defant, M.J., Joron, J.L., 1992. Metasomatism of the sub-arc mantle inferred from trace elements in Philippine xenoliths. Nature 360, 661-663.

Middelburg, J.J., van der Weijden, C.H., Woittiez, J.R.W., 1988. Chemical processes affecting the mobility of major, minor and trace elements during weathering of granitic rocks. Chemical Geology 68, 253-273.

McGregor, V.R., Friend, C.R.L., Nutman, A.P., 1991. The late Archaean mobile belt through Godthabsfjord, southern West Greenland; a continent-continent collision zone? Bulletin of the Geological Society of Denmark 39 (3-4), 179-197.

McGregor, V.R., 1973. The early Precambrian gneisses of the Godthaab District, West Greenland. Philosophical Transactions of the Royal Society of London, Series A 273, 343-358.

McGregor, V.R., Friend, C.R.L., Nutman, A.P., 1991. The late Archean mobile belt through the Godthåbsfjord, southern West Greenland; a continent-continent collision zone? Bull. Geol. Soc. Denmark 39, 179-197.

McGregor, V.R., Mason, B., 1977. Petrogenesis and geochemistry of metabasaltic and metasedimentary enclaves in the Amîtsoq gneisses, West Greenland. American Mineralogist 62, 887- 904.

McLennan, S.M., Bock, B., Hemming, S.R., Hurowitz, J.A., Lev, S.M., McDaniel, DK., 2003. The role of provenance and sedimentary processes in the geochemistry of sedimentary rocks. In: Lentz, D.R. (Ed.). Geochemistry of sediments and sedimentary rocks: Evolutionary considerations to mineral-deposit forming environments. GeoText 4, Geological Association of Canada, 7-38.

McLennan, S.M., Hemming, S., McDaniel, DK., Hanson, G.N., 1993. Geochemical approaches to sedimentation, provenance, and tectonics. In: Johnsson, M.J., Basu, A., (Eds.). Processes controlling the composition of clastic sediments. Geological Society of America, Special Paper 284, 21-40.

McLennan, S.M., Murray, R.W., 1999. Geochemistry of sediments. In: Marshall, C.P., Fairbridge, R.W. (Eds.). Encyclopedia of Geochemistry. Kluwer Academic Publishers, 282-292.

Moorbath, S., O'Nions, R.K., Pankhurst, R.J., 1973. Early Archaean age for the Isua Iron Formation, West Greenland. Nature 245, 138-139.

Nesbitt, H.W., 2003. Petrogenesis of siliciclastic sediments and sedimentary rocks. In: Lentz, D.R. (Ed.). Geochemistry of sediments and sedimentary rocks: Evolutionary considerations to mineral-deposit forming environments. GeoText 4, Geological Association of Canada, 39-51.

Nesbitt, H.W., Fedo, C.M., Young, G.M., 1997. Quartz and feldspar stability, steady and non-steady-state weathering, and petrogenesis of siliciclastic sands and muds. The Journal of Geology 105, 173-191.

Nesbitt, H.W., Markovics, G., 1997. Weathering of granodioritic crust, long-term storage of elements in weathering profiles, and petrogenesis of siliciclastic sediments. Geochimica et Cosmochimica Acta 61, 1653-1670.

Nesbitt, H.W., Young, G.M., 1982. Early Proterozoic climates and plate motions inferred from major element chemistry of lutites. Nature 299, 715-717.

Nesbitt, H.W., Young, G.M., 1984. Prediction of some weathering trends of plutonic and volcanic rocks based on thermodynamic and kinetic considerations. Geochimica et Cosmochimica Acta 48, 1523-1534.

Nesbitt, H.W., Young, G.M., McLennan, S.M., Keays, R.R., 1996. Effects of chemical weathering and sorting on the petrogenesis of siliciclastic sediments, with implications for provenance studies. Journal of Geology 104, 525-542.

Nisbet, E.G., Fowler, C.M.R., 1983. Model for Archean plate tectonics. Geology 11, 376-379.

Nutman, A.P., Christiansen, O., Friend, C.R.L., 2007. 2635 Ma amphibolite facies gold mineralisation near a terrane boundary (suture?) on Storø, Nuuk region, southern West Greenland. Precambrian Research 159, 19-32.

Nutman, A.P., Friend, C.R.L., 2007. Adjacent terranes with ca. 2715 and 2650 Ma high-pressure metamorphic assemblages in the Nuuk region of the North Atlantic Craton, southern West Greenland: Complexities of Neoarchaean collisional orogeny. Precambrian Research 155, 159-203.

Nutman, A.P., Friend, C.R.L., Baadsgaard, H., McGregor, V.R., 1989. Evolution and assembly of Archean Gneiss Terranes in the Godthåbsfjord Region, Southern West Greenland: structural, metamorphic, and isotopic evidence. Tectonics 8 (3), 573-589.

Nutman, A.P., McGregor, V.R., Friend, C.R.L., Bennett, V.C., Kinny, P.D., 1996. The Itsaq gneiss complex of southern West Greenland; the world's most extensive record of early crustal evolution (3900-3600 Ma). Precambrian Research 78 (1-3), 1-39.

Ohta, H., Maruyama, S., Takahashi, E., Watanabe, Y., Kato, Y., 1996. Field occurrence, geochemistry and petrogenesis of the Archean Mid-Ocean Ridge Basalts (AMORBs) of the Cleaverville area, Pilbara Craton, Western Australia. Lithos 37, 199-221.

Ordóñez-Calderón, J.C., Polat, A., Fryer, B.J., Gagnon, J.E., Raith, J.G., Appel, P.W.U., 2008a. Evidence for HFSE and REE mobility during calc-silicate metasomatism, Mesoarchean (~3075 Ma) Ivisaartoq greenstone belt, southern West Greenland. Precambrian Research 161, 317-340.

Ordóñez-Calderón, J.C., Polat, A., Fryer, B.J., Appel, P.W.U., van Gool, J.A.M., Dilek, Y., Gagnon, J.E., 2008b. Geodynamic origin of dismembered fragments of

Mesoarchean oceanic crust in the Ujarassuit and Ivisaartoq greenstone belts, SW Greenland. (Submitted to Lithos)

Pearce, J.A., 1996. A user's guide to basalt discrimination diagrams. In: Wyman, D.A. (Ed.). Trace element geochemistry of volcanic rocks: applications for massive sulphide exploration. Geological Association of Canada, Short Course Notes 12, 79-113.

Pearce, J.A., 2003. Supra-subduction zone ophiolites: The search for modern analogues. In: Dilek, Y., Newcomb, S., (Eds.). Ophiolite concept and the evolution of the geological thought. Geological Society of America Special Paper 373, 269-293.

Pearce, J.A., 2008. Geochemical fingerprinting of oceanic basalts with applications to ophiolite classification and the search for Archean oceanic crust. Lithos 100, 14-48.

Pearce, J.A., Peate, D.W., 1995. Tectonic implications of the composition of volcanic arc magmas. Annual Reviews of Earth and Planetary Sciences 23, 251-285.

Polat, A., Appel, P.W.U., Frei, R., Pan, Y., Dilek, Y., Ordóñez-Calderón, J.C., Fryer, B., Raith, J.G., 2007. Field and geochemical characteristics of the Mesoarchean (~3075 Ma) Ivisaartoq greenstone belt, southern West Greenland: Evidence for seafloor hydrothermal alteration in a supra-subduction oceanic crust. Gondwana Research 11, 69-91.

Polat, A., Frei, R., Appel, P.W.U., Dilek, Y., Fryer, B., Ordóñez-Calderón, J.C., Yang, Z., 2008. The origin and compositions of Mesoarchean oceanic crust: evidence from the 3075 Ma Ivisaartoq greenstone belt, SW Greenland. Lithos 100, 293-321.

Polat, A., Hofmann, A.W., 2003. Alteration and geochemical patterns in the 3.7-3.8 Ga Isua greenstone belt, West Greenland. Precambrian Research 126, 197-218.

Polat, A., Hofmann, A.W., Münker, C., Regelous, M., Appel, PW.U., 2003. Contrasting geochemical patterns in the 3.7-3.8 Ga pillow basalt cores and rims, Isua greenstone belt, Southwest Greenland: implications for postmagmatic alteration processes. Geochimica et Cosmochimica Acta 67 (3), 441-457.

Polat, A., Kerrich, R., Wyman, D.A., 1998. The late Archean Schreiber-Hemlo and White River-Dayohessarah greenstone belts, Superior Province: collages of oceanic plateaus, oceanic arcs, and subduction-accretion complexes. Tectonophysics 289, 295-326.

Pollack, H.N., 1997. Thermal characteristics of the Archean mantle. In: de Wit, M., Ashwal, L.D., (Eds.). Greenstone belts. Oxford Monographs on Geology and Geophysics 35, 223-232.

Puchtel, I.S., Hofmann, A.W., Amelin, Y.V., Garbe-Schönberg, C.-D., Samsonov, A.V., Shchipansky, A.A., 1999. Combined mantle plume-island arc model for the formation of the 2.9 Ga Sumozero-Kenozero greenstone belt, SE Baltic Shield: Isotope and trace element constraints. Geochimica et Cosmochimica Acta 63, 3579-3595.

Puchtel, I.S., Hofmann, A.W., Mezger, K., Jochum, K.P., Shchipansky, A.A., Samsonov, A.V., 1998. Oceanic plateau model for continental crustal growth in the Archaean: A case study from the Kostomuksha greenstone belt, NW Baltic Shield. Earth and Planetary Science Letters 155, 57-74.

Rohrbach, A., Schuth, S., Ballhaus, C., Münker, C., Matveev, S., Qopoto, C., 2005. Petrological constraints on the origin of arc picrites, New Georgia Group, Solomon Islands. Contributions to Mineralogy and Petrology 149, 685-698.

Rubin, J.N., Henry, C.D., Price, J.G., 1993. The mobility of zirconium and other "immobile" elements during hydrothermal alteration. Chemical Geology 110, 29-47.

Saunders, A.D., Norry, M.J., Tarney, J., 1991. Fluid influence on the trace element compositions of subduction zone magmas. Philosophical Transactions: Physical Sciences and Engineering, Royal Society of London 335, 377-392.

Schmidt, M.W., Poli, S., 2003. Generation of mobile components during subduction of the oceanic crust. Treatise on Geochemistry, Elsevier, vol. 3, 567-591.

Schuth, S., Rohrbach, A., Münker, C., Ballhaus, C., Garbe-Schönberg, D., Qopoto, C., 2004. Geochemical constraints on the petrogenesis of arc picrites and basalts, New Georgia Group, Solomon Islands. Contribution to Mineralogy and Petrology 148, 288-304.

Şengör, A.M.C., Natal'in, B.A., 2004. Phanerozoic analogues of Archean oceanic basement fragments: Altaid ophiolites and ophirags. In: Kusky, T.M., (Ed.). Precambrian ophiolites and related rocks. Developments in Precambrian Geology, Elsevier vol. 13, 675-726.

Shimizu, K., Nakamura, E., Maruyama, S., 2005. The geochemistry of ultramafic to mafic volcanics from the Belingwe greenstone belt, Zimbabwe: magmatism in an Archean continental large igneous province. Journal of Petrology 46, 2367-2394.

Smithies, R.H., Van Kranendonk, M.J., Champion, D.C., 2007. The Mesoarchean emergence of modern-style subduction. Gondwana Research 11, 50-68.

Staudigel, H., Plank, T., White, B., Schmincke, H-U., 1996. Geochemical fluxes during sea floor alteration of the basaltic upper oceanic crust: DSDP sites 417 and 418. In: Bebout, G.E., Scholl, S.W., Kirby, S.H., Platt, J.P. (Ed.). Subduction: Top to bottom. American Geophysical Union, Washington, 19-38.

Sun, S.S., McDonough, W.F., 1989. Chemical and isotopic systematics of oceanic basalts: implications for mantle composition and processes. Geological Society of London, Special Publications 42, 313-345.

Taylor, S.R., McLennan, S. M., 1985. The continental crust: Its composition and evolution. Blackwell, Oxford, 312 pp.

Thurston, P.C., 2002. Autochthonous development of Superior Province greenstone belts? Precambrian Research 115, 11-36.

Tilley, D.B., Eggleton, R.A., 2005. Titanite low-temperature alteration and Ti mobility. Clays and Clay Minerals 53 (1), 100-107.

Valsami-Jones, E., Ragnarsdóttir, K.V., 1997. Controls on uranium and thorium behaviour in ocean-floor hydrothermal systems: examples from the Pindos ophiolite, Greece. Chemical Geology 135, 263-274.

Van Baalen, M.R., 1993. Titanium mobility in metamorphic systems: a review. Chemical Geology 110, 233-249.

Van Westrenen, W., Blundy, J., Wood, B., 2001. High field strength element/rare earth fractionation during partial melting in the presence of garnet: implications for identifications of mantle heterogeneities. Geochemistry, Geophysics, Geosystems 2, Paper number 2000GC000133.

Weaver, B.L., Tarney, J., Windley, B., Leake, B.E., 1982. Geochemistry and petrogenesis of Archean metavolcanic amphibolites from Fiskenaesset, S.W. Greenland. Geochimica et Cosmochimica Acta 46, 2203-2215.

Winchester, J.A., Floyd, P.A., 1977. Geochemical discrimination of different magma series and their differentiation products using immobile elements. Chemical Geology 20, 325-343.

Windley, B.F., Bishop, F.C., Smith, J.V., 1981. Metamorphosed layered igneous complexes in Archean granulite-gneiss belts. Annual Review of Earth and Planetary Sciences 9, 175-196.

Windley, B.F., Garde, A.A., 2008. Arc-generated blocks with crustal sections in the North Atlantic Craton of west Greenland: New implications for mechanisms of crustal growth in the Archean with modern analogue. Journal of the Geological Society of London (Manuscript in revision).

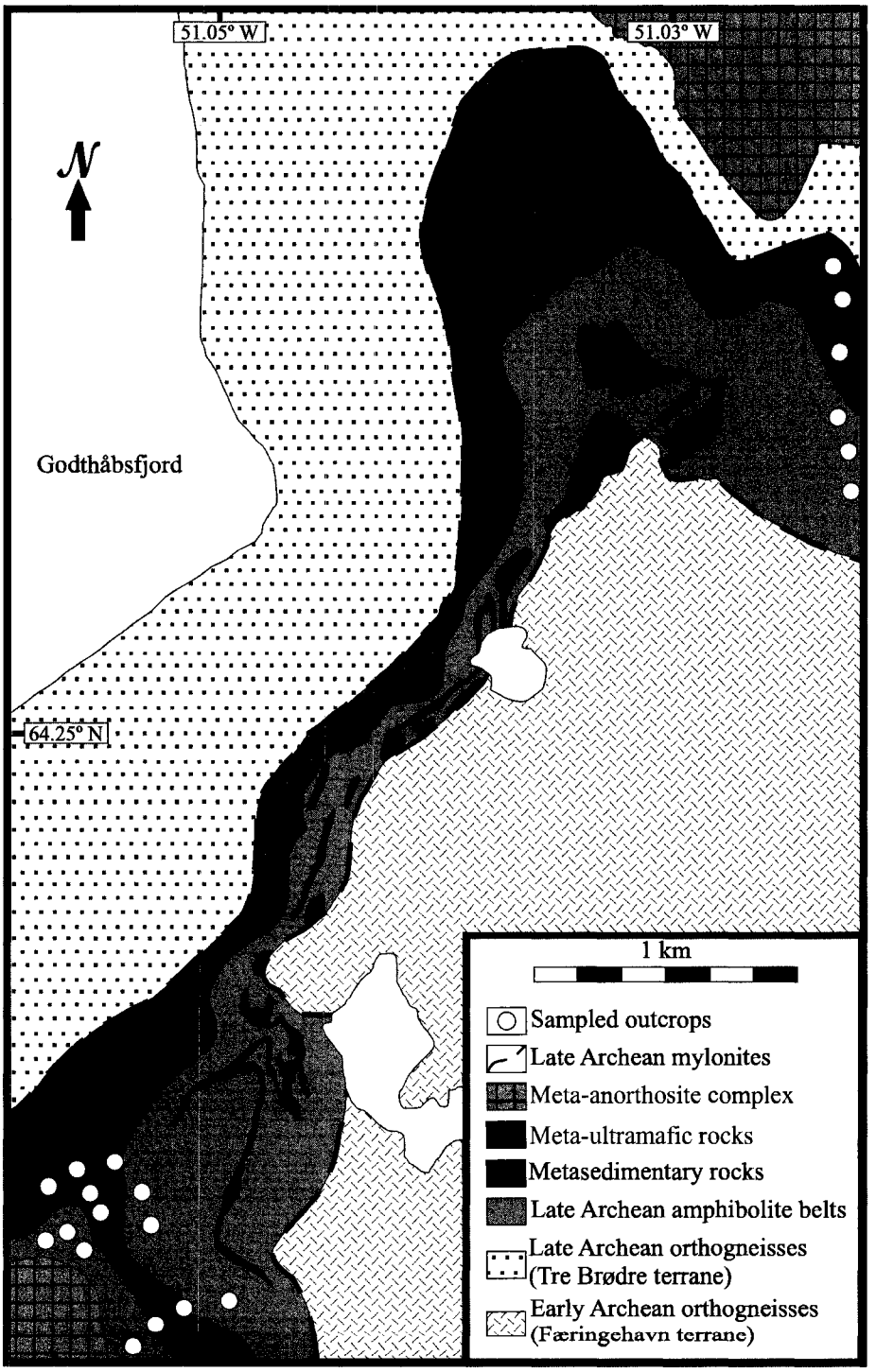

Figure 4.1. Geological map of central Storø greenstone belt with approximate sample locations. Modified from Juul-Pedersen et al. (2007).

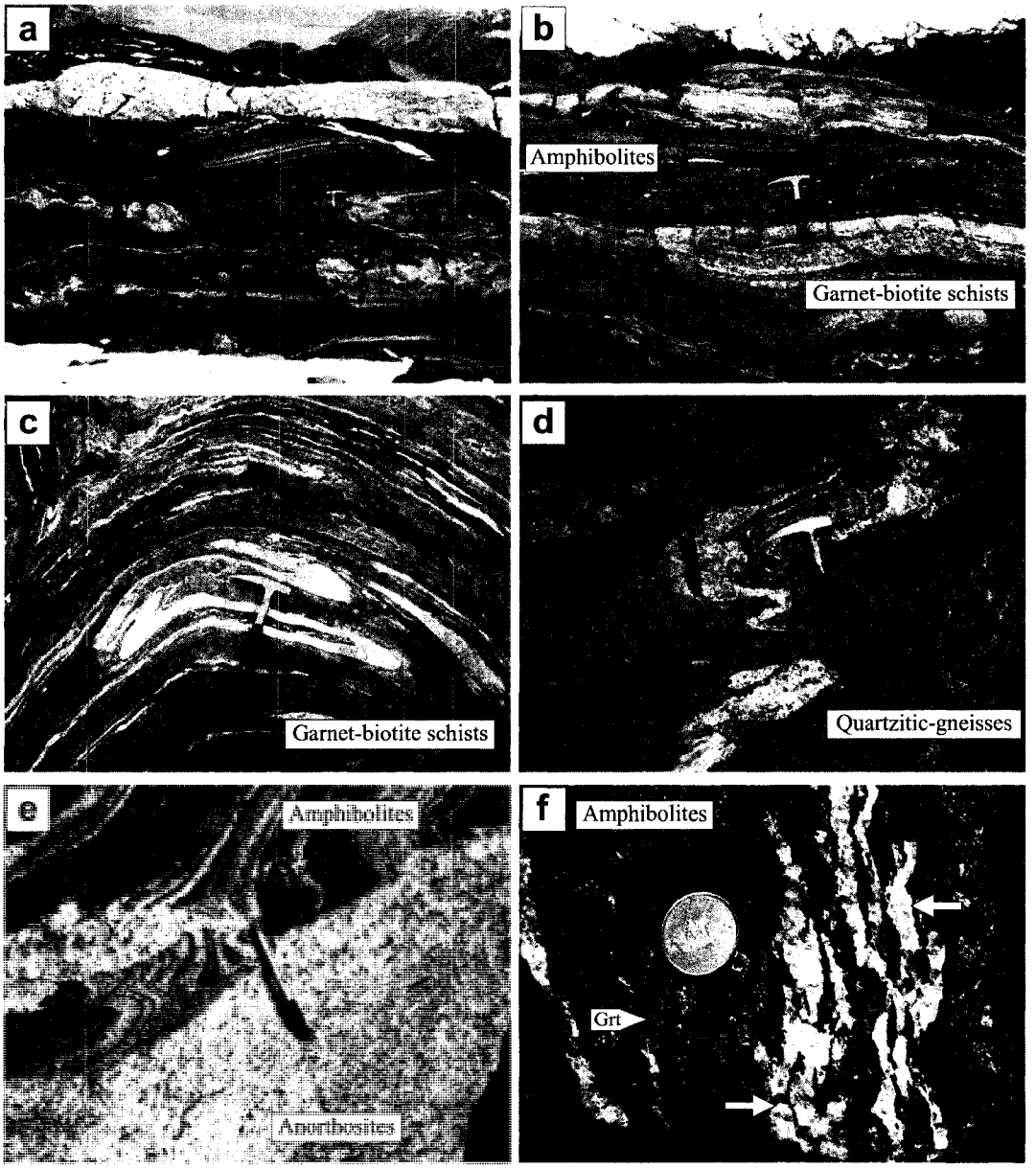

Figure 4.2. Field photographs of rock types in the Storø greenstone belt. (a) Tight isoclinal folds in amphibolites. (b) Intercalation of amphibolites and garnet-biotite schists. (c) Superposed folds on garnet-biotite schists. (d) Tightly folded quartzitic gneisses. (e) Amphibolites intruded by anorthosites. (f) Garnet-bearing altered amphibolites with abundant quartz-veins.

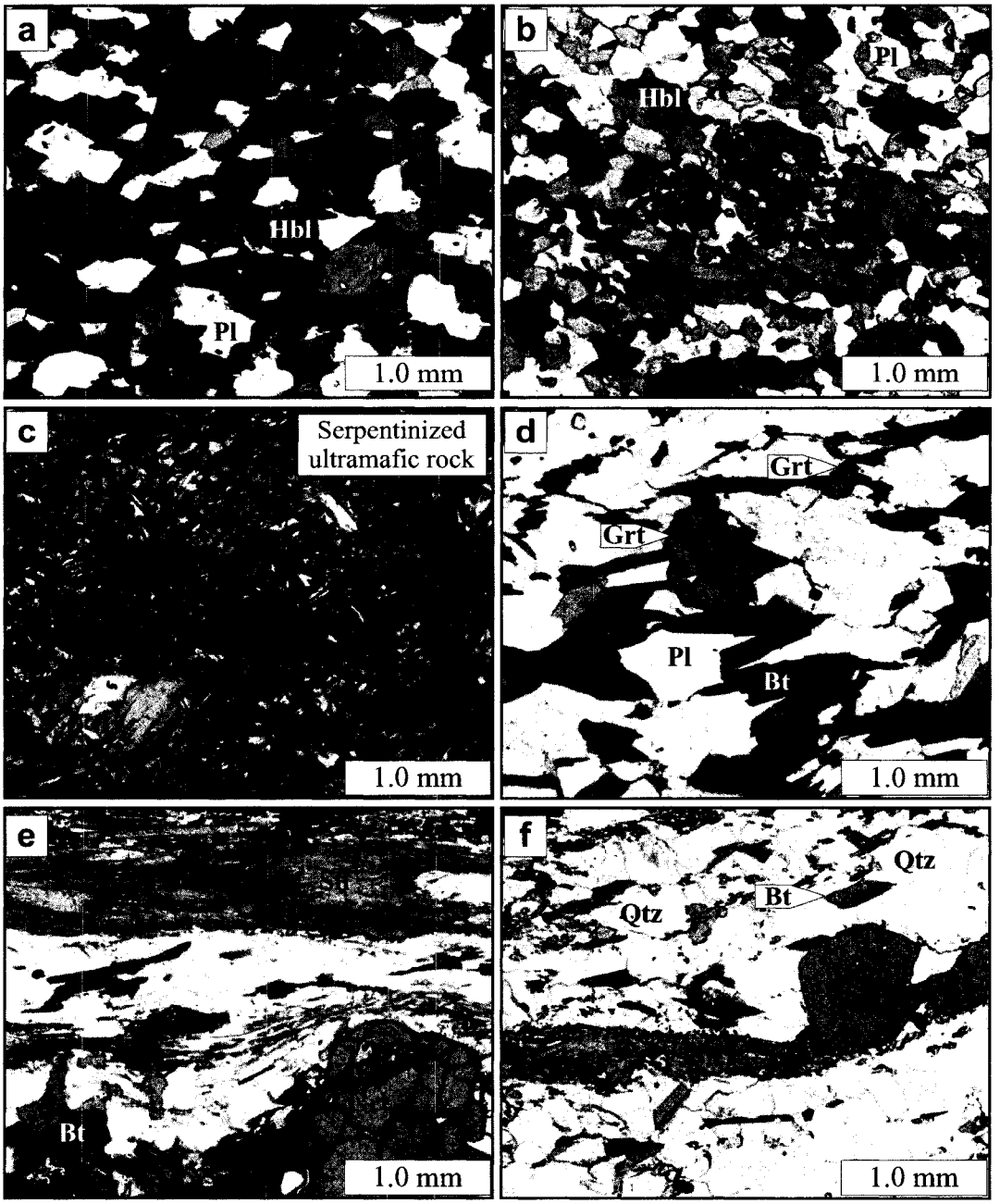

Figure 4.3. Photomicrographs of various rock types in the Storø greenstone belt. (a-b) Amphibolites. (c) Serpentinized ultramafic rock. (d) Garnet-biotite schists. (e) Garnet-biotite schists with fibrous sillimanite. (f) Quartzitic gneisses with accessory garnet and sillimanite. Abbreviations: Bt, biotite; Grt, garnet; Hbl, hornblende; Sil, sillimanite; Pl, plagioclase; Qtz, quartz. Plane polarized light for (a-b) and (d-f), and crossed polarized light for (e).

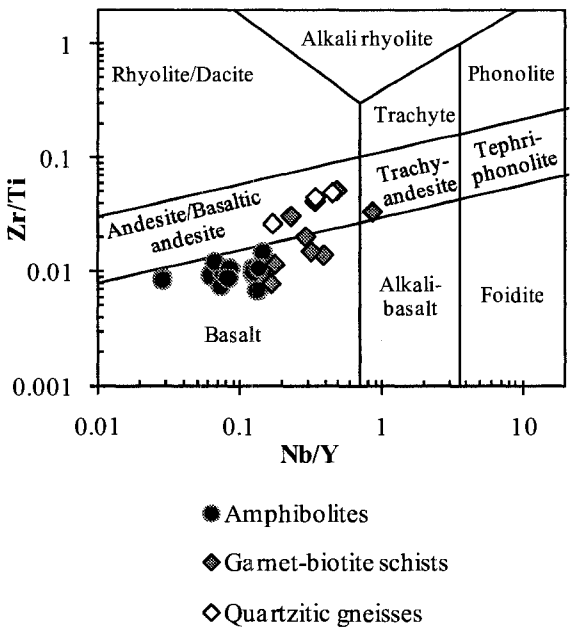

Figure 4.4. Zr/Ti versus Nb/Y classification diagram for metavolcanic (amphibolites) and metavolcaniclastic-sedimentary (garnet-biotite schists and quartzitic gneisses) rocks in the Storø greenstone belt. Compositional fields revised by Pearce (1996) after Winchester and Floyd (1977).

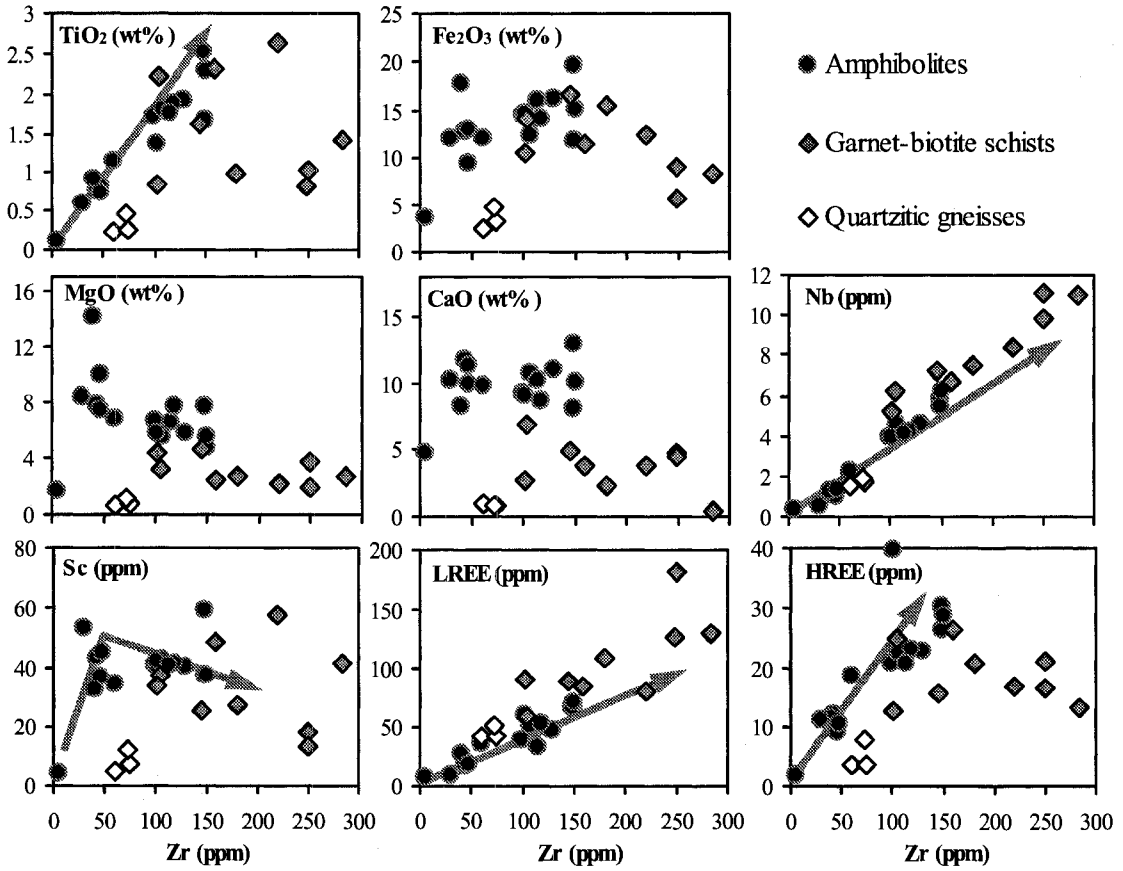

Figure 4.5. Variation diagrams of Zr versus selected major and trace elements for metavolcanic (amphibolites) and metavolcaniclastic-sedimentary (garnet-biotite schists and quartzitic gneisses) rocks. Arrows represent the deduced magmatic trends for metavolcanic rocks in the Ivisaartoq greenstone belt (see Ordóñez-Calderón et al., 2008a).

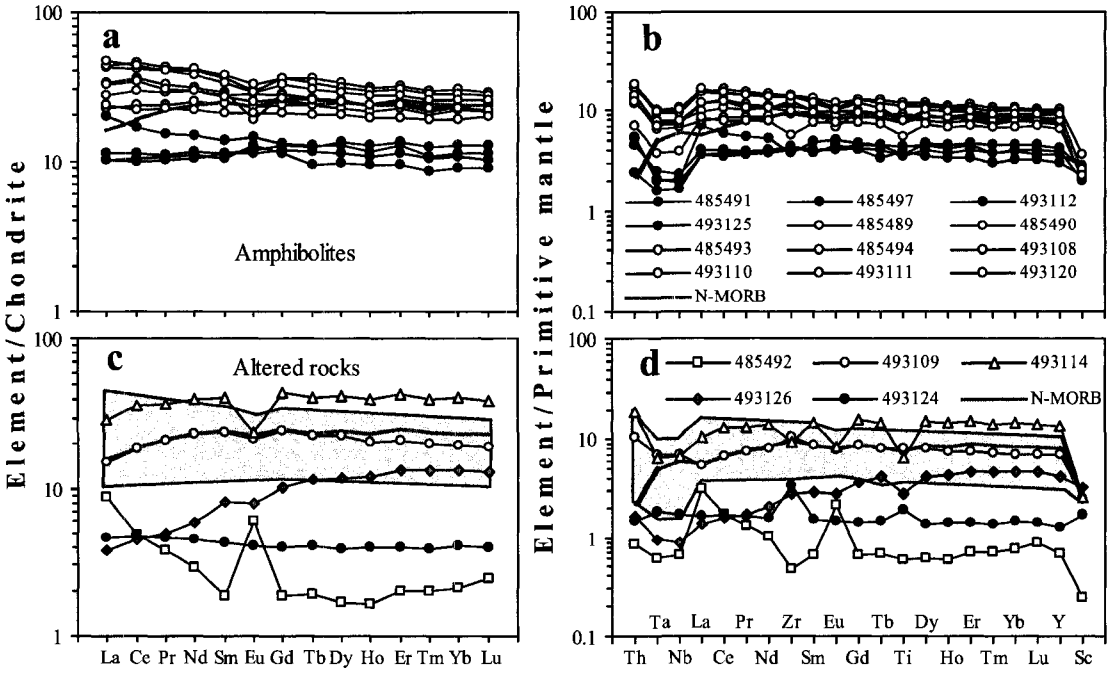

Figure 4.6. Chondrite- and primitive-mantle normalized diagrams for metavolcanic rocks in the Storø greenstone belt. (a-b) Least altered amphibolites. (c-d) Altered amphibolites and serpentinized ultramafic rock (493124). Chondrite normalization values from Sun and McDonough (1989). Primitive mantle normalization values and average geochemical composition of modern N-MORB from Hofmann (1988).

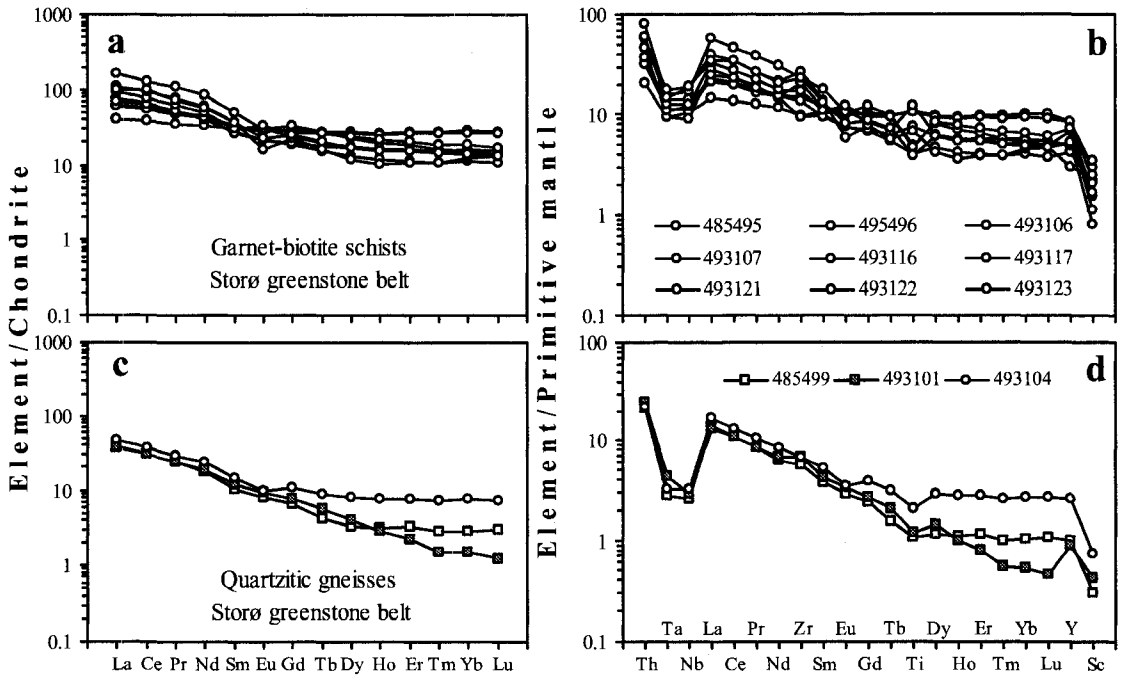

Figure 4.7. Chondrite- and primitive-mantle normalized diagrams for metavolcaniclastic-sedimentary rocks in the Storø greenstone belt. (a-b) Garnet-biotite schists. (c-d) Quartzitic gneisses. Normalization values as in Figure 4.6.

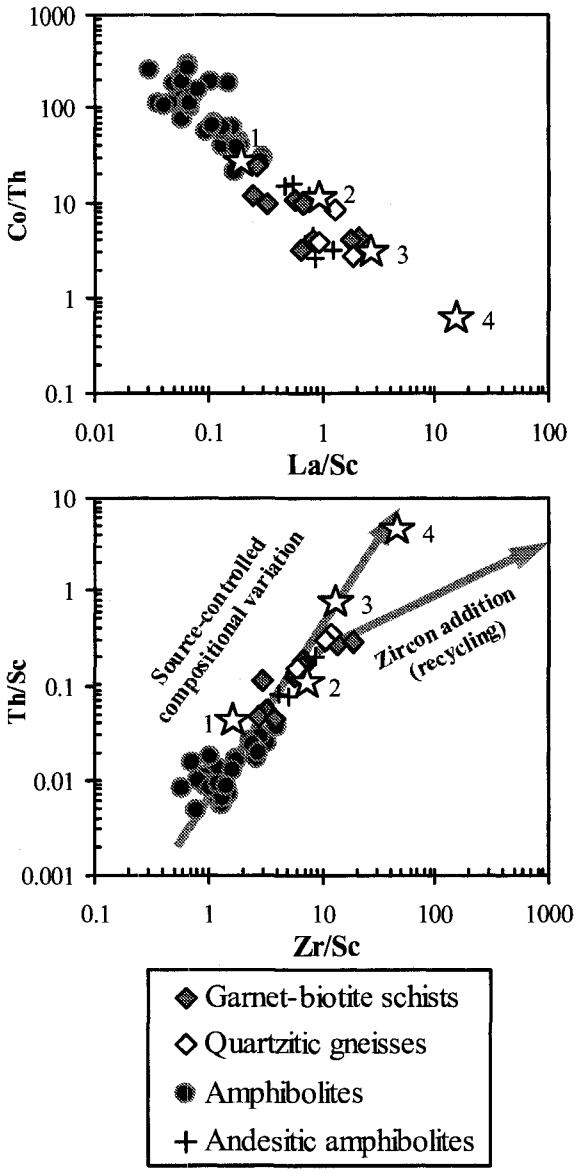

Figure 4.8. Selected trace element ratios for metavolcaniclastic-sedimentary rocks (garnet-biotite schists and quartzitic gneisses) in the Storø greenstone belt. Amphibolites (metabasalts) are those from Storø, Ivisaartoq, and Ujarassuit greenstone belts (see Ordóñez-Calderón et al., 2008a,b). Amphibolites with an andesitic geochemical composition are those from Qussuk and Ujarassuit greenstone belts (Garde, 2007; Ordóñez-Calderón et al., 2008b). Numbered stars represent the following reservoir compositions: 1 = average oceanic island arc tholeiitic basalt (Kelemen et al., 2003); 2 = average andesite (Kelemen et al., 2003); 3 = average > 3.5 Ga upper continental crust (Condie, 1993); 4 = average Archean calc-alkaline granite (Kemp and Hawkesworth, 2003).

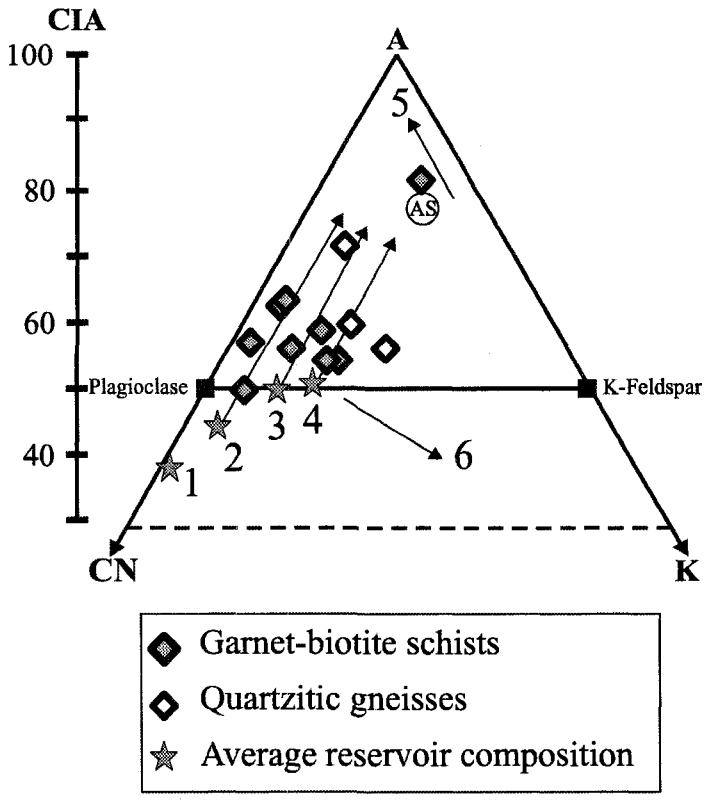

Figure 4.9. Ternary A-CN-K diagram for metavolcaniclastic-sedimentary rocks (garnet-bioite schists and quartzitic gneisses) from the Storø greenstone belt. The ternary diagram is plotted in molecular proportions of Al_2O_3 (A)-CaO*+Na_2O (CN)-K_2O (K) where CaO* represents the amount of CaO in the silicate fraction (Nesbitt and Young, 1982, 1984; Fedo et al., 1995). The scale for the chemical index of alteration (CIA) is illustrated to the left (McLennan and Murray, 1999). Numbered stars as in Figure 4.8. AS = Archean shale; arrows parallel to the A-CN side represent the predicted weathering trend for intermediate to felsic protoliths (stars 2-4); arrow 5 represent the trend of extremely weathered rocks, and arrow 6 the trend of sediments affected by potassium metasomatism.

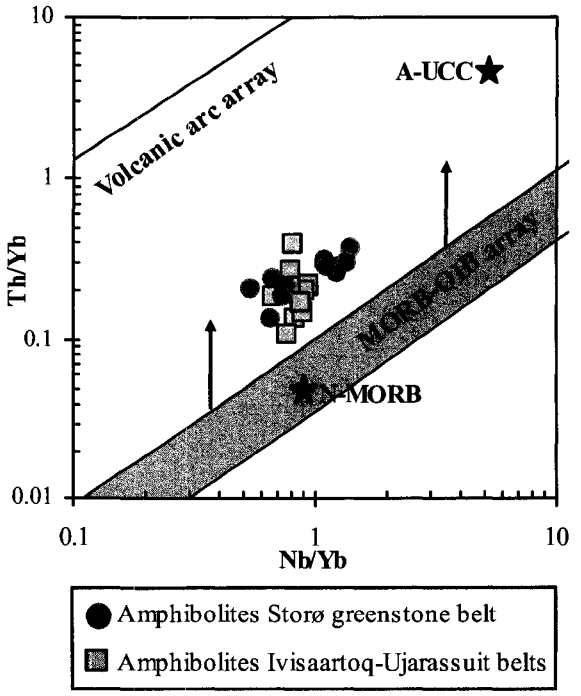

Figure 4.10. Th/Yb versus Nb/Yb diagram showing the fields of modern MORB-OIB and volcanic arc arrays (see Pearce and Peate, 1995 and Pearce, 2008). Less altered amphibolites from the Storø, Ivisaartoq, and Ujarassuit greenstone belts plot in the field of modern subduction-related volcanic rocks. Amphibolites from the Ivisaartoq and Ujarassuit greenstone belt after Ordóñez-Calderón et al. (2008a,b). Average composition of modern N-MORB and Archean (> 3.5 Ga) upper continental crust (A-UCC) after Hofmann (1988) and Condie (1993), respectively.

Table 4.1. Major (wt.%) and trace element (ppm) concentrations and significant element ratios for metavolcanic rocks in the Storø greenstone belt.

	Least altered amphibolites								
	485491	485497	493112	493125	485489	485490	485493	485494	493108
SiO_2 (wt.%)	49.1	46.6	47.2	55.3	50.9	49.8	43.1	49.1	47.6
TiO_2	0.78	0.83	0.92	0.73	1.71	1.87	2.52	2.30	1.92
Al_2O_3	15.55	15.39	9.85	13.93	13.18	14.28	15.35	14.22	14.12
Fe_2O_3	12.89	13.04	17.79	9.51	14.68	14.23	19.73	15.10	16.36
MnO	0.20	0.26	0.25	0.18	0.18	0.19	0.29	0.21	0.23
MgO	7.93	9.94	14.14	7.53	6.77	7.74	7.75	5.58	5.85
CaO	11.76	11.34	8.30	10.00	9.29	8.68	8.15	10.11	11.09
Na_2O	1.55	2.14	1.09	2.65	2.97	2.66	2.31	2.58	2.33
K_2O	0.12	0.34	0.26	0.09	0.14	0.29	0.46	0.51	0.20
P_2O_5	0.07	0.13	0.18	0.06	0.22	0.22	0.31	0.32	0.28
LOI (%)	0.62	0.98	1.05	0.26	0.19	0.45	0.28	0.18	0.18
Mg-number (%)	55	60	61	61	48	52	44	42	41
Sc (ppm)	43	37	33	45	41	41	59	37	40
V	184	123	128	290	236	224	291	223	207
Cr	73	139	84	211	51	50	54	16	46
Co	54	58	80	44	43	47	53	38	51
Ni	158	189	262	99	73	91	92	59	111
Ga	35	51	30	32	44	58	57	76	46
Rb	1.3	14.2	14.8	0.7	1.2	9.4	17.3	4.5	2.6
Sr	113	60	17	80	57	102	69	121	117
Y	18.3	13.0	16.6	15.9	31.3	34.0	44.1	41.8	33.0
Zr	43.3	47.0	40.6	47.1	99.4	118.4	149.0	150.1	129.3
Nb	1.15	0.98	1.23	1.35	3.94	4.21	5.52	6.22	4.59
Cs	0.21	0.64	1.76	LDL	0.07	1.48	2.70	0.39	LDL
Ba	3.87	124.39	19.31	6.92	17.42	98.47	49.29	174.49	21.12
Ta	0.08	0.06	0.08	0.10	0.26	0.29	0.37	0.41	0.31
Pb	2.11	3.62	2.04	3.92	2.70	4.96	3.75	3.65	23.38
Th	0.44	0.20	0.44	0.38	1.06	1.19	1.42	1.39	0.99
U	0.09	0.30	0.30	0.21	0.22	0.54	0.94	1.80	1.48
La	2.49	2.47	4.87	2.73	5.44	8.14	10.41	10.61	6.65
Ce	6.29	6.69	10.55	7.21	14.76	22.44	26.38	28.88	18.65
Pr	0.97	1.02	1.45	1.05	2.26	3.10	3.83	4.09	2.78
Nd	4.97	5.23	6.89	5.41	11.66	14.51	19.02	19.44	13.72
Sm	1.73	1.59	2.07	1.72	3.66	4.36	5.49	5.71	4.21
Eu	0.67	0.74	0.82	0.65	1.32	1.09	1.68	1.87	1.59
Gd	2.59	2.29	2.66	2.42	4.79	5.62	7.19	7.24	5.52
Tb	0.47	0.35	0.48	0.43	0.88	0.97	1.32	1.23	0.96
Dy	3.36	2.43	3.22	2.87	5.64	6.41	8.38	7.87	6.25
Ho	0.72	0.53	0.66	0.60	1.21	1.33	1.74	1.67	1.31
Er	2.18	1.55	2.10	1.87	3.69	3.94	5.23	4.96	3.91
Tm	0.32	0.22	0.27	0.26	0.52	0.59	0.75	0.71	0.55
Yb	2.10	1.47	1.84	1.76	3.60	3.80	4.94	4.63	3.74
Lu	0.32	0.23	0.28	0.26	0.54	0.59	0.72	0.69	0.54
La/Yb_{cn}	0.80	1.13	1.79	1.05	1.02	1.44	1.42	1.54	1.20
La/Sm_{cn}	0.91	0.97	1.48	1.00	0.93	1.17	1.19	1.17	0.99
Gd/Yb_{cn}	1.00	1.25	1.17	1.11	1.08	1.20	1.18	1.26	1.20
(Eu/Eu*)cn	0.97	1.18	1.07	0.98	0.96	0.67	0.82	0.89	1.01
(Ce/Ce*)cn	0.98	1.02	0.96	1.03	1.01	1.08	1.01	1.06	1.05
Al_2O_3/TiO_2	19.94	18.60	10.70	19.13	7.69	7.64	6.10	6.20	7.36
Nb/Ta	14.04	15.38	15.26	13.76	14.91	14.61	14.79	15.34	14.71
Zr/Y	2.37	3.62	2.44	2.97	3.18	3.48	3.38	3.60	3.92
Ti/Zr	107.91	105.56	135.79	92.60	103.37	94.69	101.27	91.70	89.00
(Nb/Nb*)pm	0.45	0.57	0.34	0.54	0.67	0.55	0.58	0.66	0.73
(Zr/Zr*)pm	1.03	1.14	0.75	1.08	1.06	1.04	1.02	1.00	1.19
(Ti/Ti*)pm	0.80	1.14	0.95	0.84	0.98	0.96	0.97	0.94	1.00
ΣREE	29.18	26.80	38.15	29.23	59.97	76.90	97.09	99.60	70.38
North	64°24.530'	64°24.280'	64°24.227'	64°25.654'	64°24.494'	64°24.517'	64°24.524'	64°24.533'	64°24.487'
West	51°05.621'	51°05.510'	51°05.625'	51°01.709'	51°05.637'	51°05.614'	51°05.624'	51°05.658'	51°05.642'

LDL = Lower than detection limit

*Serpentinized ultramafic rocks. Other samples are least altered and altered mafic amphibolites

Table 4.1. (*Continued*)

	Least altered amphibolites			Altered amphibolites and ultramafic rocks				
	493110	493111	493120	485492	493109	493114	493126	493124*
SiO_2 (wt.%)	52.5	51.5	53.8	82.9	48.7	53.0	52.2	44.3
TiO_2	1.80	1.15	1.67	0.12	1.76	1.37	0.59	0.40
Al_2O_3	13.61	15.46	13.66	5.80	13.65	13.31	13.66	7.14
Fe_2O_3	12.54	12.17	11.96	3.60	16.13	14.76	12.03	10.68
MnO	0.22	0.19	0.34	0.06	0.23	0.21	0.19	0.15
MgO	5.61	6.84	4.74	1.67	6.67	5.81	8.45	31.87
CaO	10.71	9.84	12.95	4.80	10.16	9.09	10.26	5.05
Na_2O	2.69	2.47	0.62	0.99	2.24	1.97	2.37	0.42
K_2O	0.18	0.21	0.07	LDL	0.14	0.27	0.19	LDL
P_2O_5	0.16	0.19	0.23	0.04	0.26	0.24	0.05	0.02
LOI (%)	0.22	0.65	0.27	0.37	0.12	0.34	0.53	6.88
Mg-number (%)	47	53	44	48	45	44	58	86
Sc (ppm)	42	34	37	4	41	42	54	28
V	223	121	347	48	203	148	351	149
Cr	54	96	84	LDL	52	25	80	1576
Co	46	36	46	10	48	34	50	97
Ni	81	94	72	9	98	59	82	1173
Ga	44	45	40	16	44	47	34	15
Rb	2.1	2.7	1.2	1.8	2.2	4.5	2.6	2.4
Sr	91	109	100	64	187	71	78	24
Y	33.8	27.9	40.1	2.9	30.5	59.6	18.0	5.6
Zr	107.1	60.6	149.7	5.0	114.4	101.9	30.3	35.5
Nb	4.58	2.30	5.87	0.39	4.18	3.99	0.52	1.00
Cs	LDL	0.07	0.06	0.52	LDL	LDL	0.05	0.26
Ba	25.02	39.42	16.86	13.25	31.75	20.25	20.04	0.88
Ta	0.28	0.15	0.39	0.02	0.27	0.26	0.04	0.08
Pb	4.57	5.44	4.07	14.35	6.75	4.32	1.51	2.33
Th	1.03	0.57	1.54	0.07	0.87	1.57	0.14	0.12
U	0.40	0.48	0.39	2.27	0.37	0.47	0.12	0.03
La	7.91	5.70	11.38	2.16	3.67	7.18	0.93	1.13
Ce	21.58	13.93	27.33	3.10	11.88	23.43	2.84	3.03
Pr	2.87	2.13	3.87	0.36	2.05	3.60	0.47	0.44
Nd	13.85	10.40	17.80	1.35	10.96	18.97	2.79	2.12
Sm	4.11	3.20	5.06	0.28	3.73	6.42	1.24	0.66
Eu	1.43	1.20	1.65	0.35	1.26	1.38	0.46	0.24
Gd	5.29	4.27	6.63	0.38	5.04	8.95	2.07	0.82
Tb	0.93	0.75	1.12	0.07	0.86	1.55	0.43	0.15
Dy	6.28	5.12	7.23	0.43	5.75	10.78	2.99	0.99
Ho	1.31	1.09	1.54	0.09	1.18	2.30	0.69	0.22
Er	3.92	3.21	4.53	0.33	3.54	7.16	2.20	0.66
Tm	0.56	0.48	0.64	0.05	0.51	1.02	0.34	0.10
Yb	3.64	3.12	4.18	0.35	3.23	6.87	2.18	0.68
Lu	0.55	0.50	0.64	0.06	0.49	0.99	0.33	0.10
La/Yb_{cn}	1.46	1.23	1.83	4.18	0.76	0.70	0.29	1.12
La/Sm_{cn}	1.21	1.12	1.41	4.81	0.62	0.70	0.47	1.08
Gd/Yb_{cn}	1.18	1.11	1.28	0.89	1.26	1.05	0.77	0.98
(Eu/Eu*)cn	0.94	0.99	0.87	3.25	0.89	0.55	0.87	0.99
(Ce/Ce*)cn	1.09	0.96	0.99	0.84	1.04	1.11	1.03	1.04
Al_2O_3/TiO_2	7.56	13.49	8.20	46.75	7.76	9.69	23.00	17.68
Nb/Ta	16.17	15.38	15.04	16.32	15.19	15.61	13.52	13.32
Zr/Y	3.17	2.17	3.73	1.72	3.75	1.71	1.69	6.35
Ti/Zr	100.78	113.41	66.75	147.48	92.24	80.78	117.30	68.12
(Nb/Nb*)pm	0.65	0.52	0.57	0.41	0.95	0.48	0.59	1.09
(Zr/Zr*)pm	0.99	0.74	1.10	0.57	1.25	0.65	1.14	2.11
(Ti/Ti*)pm	0.95	0.75	0.75	0.91	1.01	0.43	0.67	1.32
ΣREE	74.24	55.09	93.58	9.37	54.16	100.60	19.95	11.34
North	64°24.496'	64°24.220'	64°25.475'	64°24.530'	64°24.486'	64°24.245'	64°25.851'	64°25.604'
West	51°05.636'	51°05.628'	51°00.900'	51°05.621'	51°05.656'	51°05.597'	51°01.340'	51°01.661'

Table 4.2. Major (wt.%) and trace element (ppm) concentrations and significant element ratios for metavolcaniclastic-sedimentary rocks in the Storø greenstone belt.

	Garnet-biotite schists								
	485495	485496	493106	493107	493116	493117	493121	493122	493123
SiO_2 (wt.%)	55.3	52.8	52.2	48.8	50.3	60.5	55.3	59.6	67.0
TiO_2	2.32	2.23	0.85	2.64	1.62	1.02	0.99	1.43	0.82
Al_2O_3	20.46	18.78	21.77	21.98	16.49	15.92	18.52	23.24	14.89
Fe_2O_3	11.49	14.19	10.53	12.53	16.75	9.16	15.50	8.30	5.67
MnO	0.18	0.24	0.10	0.18	0.24	0.16	0.16	0.13	0.11
MgO	2.42	3.27	4.41	2.23	4.68	3.77	2.70	2.70	1.96
CaO	3.80	6.89	2.71	3.88	4.90	4.71	2.33	0.40	4.49
Na_2O	2.83	0.77	3.98	4.76	0.67	0.95	3.48	0.85	3.55
K_2O	1.04	0.62	3.43	2.75	4.08	3.53	0.94	3.22	1.31
P_2O_5	0.15	0.20	0.06	0.22	0.24	0.23	0.06	0.09	0.19
LOI (%)	0.13	0.10	0.79	0.55	0.80	0.86	LDL	1.30	0.27
CIA (%)	62	57	59	56	54	54	63	81	50
Mg-number (%)	29	31	45	26	36	45	26	39	41
Sc (ppm)	49	37	34	58	25	18	27	42	13
V	404	452	257	275	153	63	177	224	84
Cr	93	105	166	50	13	7	64	65	LDL
Co	26	41	42	31	31	21	20	21	15
Ni	61	87	154	73	50	41	49	60	26
Ga	80.5	88.3	117.2	113.5	135.5	189.0	62.4	138.7	83.5
Rb	37.2	20.1	300	196	162	140	37.1	101	61.8
Sr	93.9	89.5	282.7	115.4	67.6	77.4	161.0	41.5	205.0
Y	37.4	36.9	18.1	21.5	22.7	28.9	32.2	13.0	22.9
Zr	159	104	102	220	145	250	180	284	249
Nb	6.66	6.20	5.27	8.36	7.22	9.81	7.45	11.05	11.06
Cs	4.07	2.65	30.94	23.18	7.21	4.68	1.98	4.74	4.34
Ba	220.91	212.64	422.90	320.32	529.98	823.57	196.97	568.21	291.73
Ta	0.45	0.38	0.38	0.56	0.44	0.62	0.50	0.59	0.71
Pb	14.01	8.59	20.61	23.74	9.83	9.03	23.22	8.84	7.14
Th	2.65	1.72	3.85	2.64	3.12	4.83	4.91	6.59	3.81
U	0.74	0.45	1.71	4.48	0.56	0.85	0.98	1.58	1.69
La	15.89	10.02	19.25	14.47	16.97	39.19	22.76	27.18	23.87
Ce	36.71	24.39	41.50	35.24	41.37	82.56	49.66	60.58	62.31
Pr	4.80	3.39	5.07	4.49	5.02	10.30	5.97	7.27	7.04
Nd	20.79	15.59	19.72	19.91	20.07	41.13	23.48	28.39	27.41
Sm	5.22	4.57	4.16	4.91	4.05	7.62	4.70	5.82	5.75
Eu	1.60	1.64	1.24	1.76	1.23	1.72	1.98	0.94	1.29
Gd	6.11	5.78	3.83	4.88	4.05	6.89	5.27	4.50	5.02
Tb	1.02	1.02	0.56	0.74	0.67	1.03	0.98	0.60	0.75
Dy	6.98	6.69	3.30	4.39	4.24	5.77	6.04	3.01	4.36
Ho	1.50	1.43	0.66	0.89	0.88	1.10	1.23	0.57	0.86
Er	4.61	4.43	1.90	2.63	2.57	3.07	3.38	1.82	2.50
Tm	0.70	0.65	0.28	0.39	0.36	0.40	0.48	0.28	0.36
Yb	4.72	4.32	1.84	2.61	2.42	2.49	3.05	2.06	2.26
Lu	0.71	0.65	0.27	0.39	0.35	0.35	0.43	0.33	0.33
La/Yb_{cn}	2.27	1.56	7.04	3.74	4.72	10.59	5.03	8.88	7.12
La/Sm_{cn}	1.91	1.38	2.91	1.85	2.63	3.23	3.05	2.93	2.61
Gd/Yb_{cn}	1.05	1.08	1.68	1.51	1.35	2.24	1.40	1.76	1.80
(Eu/Eu*)cn	0.87	0.97	0.95	1.10	0.93	0.73	1.22	0.56	0.74
(Ce/Ce*)cn	1.01	1.01	1.01	1.05	1.08	0.99	1.03	1.04	1.16
Al_2O_3/TiO_2	8.83	8.42	25.65	8.33	10.17	15.62	18.77	16.24	18.17
Nb/Ta	14.87	16.34	13.92	14.97	16.39	15.82	14.98	18.78	15.56
Zr/Y	4.26	2.82	5.63	10.22	6.41	8.63	5.60	21.77	10.88
Ti/Zr	87.14	128.26	49.94	71.91	66.78	24.47	32.81	30.23	19.71
(Nb/Nb*)pm	0.42	0.61	0.25	0.55	0.40	0.29	0.29	0.34	0.47
(Zr/Zr*)pm	1.07	0.86	0.79	1.56	1.13	0.99	1.20	1.54	1.39
(Ti/Ti*)pm	1.11	1.09	0.80	1.87	1.24	0.53	0.52	1.37	0.58
ΣREE	111.35	84.57	103.58	97.71	104.26	203.63	129.40	143.34	144.11
North	64°24.538'	64°24.494'	64°24.455'	64°24.470'	64°25.305'	64°25.305'	64°25.525'	64°25.541'	64°25.539'
West	51°05.671'	51°05.695'	51°05.641'	51°05.609'	51°00.249'	51°00.277'	51°01.033'	51°01.020'	51°00.698'

LDL = lower than detection limit.

The chemical index of alteration CIA = $100(Al_2O_3/[Al_2O_3+Na_2O+K_2O+CaO^*])$ is calculated in molar proportions where CaO* represents CaO only in silicates (see Nesbitt and Young, 1984; Fedo et al., 1995).

Table 4.2. (*Continued*)

	Quartzitic gneisses		
	485499	493101	493104
SiO_2 (wt.%)	87.4	85.6	82.5
TiO_2	0.22	0.25	0.45
Al_2O_3	6.27	6.34	8.60
Fe_2O_3	2.45	3.27	4.74
MnO	0.03	0.02	0.07
MgO	0.68	0.79	1.19
CaO	1.01	0.86	0.85
Na_2O	0.62	0.77	0.69
K_2O	1.27	2.07	0.84
P_2O_5	0.04	0.05	0.04
LOI (%)	0.46	0.75	0.61
CIA (%)	60	56	71
Mg-number (%)	35	32	33
Sc (ppm)	5	7	12
V	23	22	50
Cr	16	21	31
Co	5	17	7
Ni	10	50	14
Ga	61.0	89.7	54.2
Rb	36.0	51.9	29.4
Sr	40.6	90.5	85.8
Y	4.3	3.8	11.2
Zr	60.7	74.2	71.9
Nb	1.49	1.73	1.93
Cs	2.22	2.74	2.39
Ba	275.02	443.20	206.64
Ta	0.11	0.17	0.13
Pb	5.59	16.10	8.63
Th	1.77	2.08	1.83
U	0.76	4.36	0.56
La	9.62	9.03	11.55
Ce	19.47	19.67	23.82
Pr	2.25	2.30	2.84
Nd	8.36	8.89	11.27
Sm	1.60	1.79	2.20
Eu	0.47	0.55	0.56
Gd	1.35	1.52	2.21
Tb	0.16	0.21	0.32
Dy	0.83	1.03	2.03
Ho	0.17	0.16	0.44
Er	0.54	0.37	1.27
Tm	0.07	0.04	0.18
Yb	0.47	0.24	1.23
Lu	0.08	0.03	0.19
La/Yb_{cn}	13.72	24.97	6.32
La/Sm_{cn}	3.79	3.17	3.29
Gd/Yb_{cn}	2.31	5.06	1.45
(Eu/Eu*)cn	0.98	1.02	0.77
(Ce/Ce*)cn	1.01	1.04	1.00
Al_2O_3/TiO_2	27.88	25.42	19.16
Nb/Ta	13.55	10.02	15.06
Zr/Y	14.02	19.50	6.43
Ti/Zr	22.18	20.17	37.41
(Nb/Nb*)pm	0.15	0.16	0.17
(Zr/Zr*)pm	1.16	1.30	1.01
(Ti/Ti*)pm	0.79	0.68	0.71
ΣREE	45.44	45.86	60.12
North	64°24.472'	64°24.472'	64°24.455'
West	51°05.760'	51°05.760'	51°05.687'

CHAPTER 5

Conclusions and Implications

5.1. Effects of multistage alteration on the original magmatic geochemical fingerprints

Most Archean greenstone belts have undergone a prolonged and complex history of postdepositional hydrothermal alteration. Alteration may occur in a wide variety of geological conditions including sea-floor hydrothermal alteration, regional metamorphism, and late stage felsic plutonism (Gruau et al., 1992; 1996; Lahaye et al., 1995; Polat et al., 2003; Terabayashi et al., 2003; Weiershäuser and Spooner, 2005). These geological processes cause variable changes in the original geochemical characteristics of volcanic rocks in greenstone belts. Precise determination of the original magmatic geochemical signatures can only be done through a detailed investigation of the postmagmatic geochemical changes. Therefore, understanding of how and to what extent the original geochemical fingerprints of igneous rocks in greenstone belts were modified by hydrothermal alteration, metamorphism, and deformation is fundamental in Archean geology. In high-grade granite-greenstone terranes, like the Nuuk region in SW Greenland, evaluating alteration is crucial in understanding the magmatic and tectonic evolution of greenstone belts, given that the original stratigraphic and structural relationships have been obscured during polyphase metamorphism and deformation. I have addressed the alteration issue by taken a holistic approach, integrating knowledge of the regional geology, field observations, detailed petrographic analysis, and high precision whole-rock major and trace element geochemical data. This thesis has made a significant contribution by providing evidence that alteration processes may form trace

element patterns that resemble those of unaltered Phanerozoic volcanic rocks formed in various geodynamic environments (Chapter 2) (Ordóñez-Calderón et al., 2008). Therefore, investigation of the alteration history is the first important step in understanding the geochemical and tectonic evolution of high-grade Archean greenstone belts. The most important results concerning the metasomatic history of the Meso- to Neoarchean Ivisaartoq, Ujarassuit, and Storø greenstone belts are:

- In the Ivisaartoq belt (see Chapter 2), well preserved pillowed lavas show field evidence for seafloor hydrothermal alteration (see also Polat et al., 2007; Ordóñez-Calderón et al., 2008). This alteration resulted in the formation of epidosites (stage-I calc-silicate alteration) in pillow cores and inter-pillow breccia (Fig. 2.3a-b). Major elements (MgO, CaO, Fe_2O_3, Na_2O, and K_2O), LILE (e.g., Rb, Sr, Ba, and Pb), and LREE (mainly La, Ce, and Eu) were significantly remobilized during this alteration event. In contrast, the concentrations of HREE and HFSE (Th, Nb, Ta, Zr, and Ti) were not changed (Fig. 2.11a-b).
- In the Ivisaartoq belt (see Chapter 2), metavolcanic rocks were also affected by a second stage of calc-silicate alteration. This metasomatic alteration occurred along shear zones developed during the regional amphibolite facies metamorphism. Calc-silicate rocks are of strata-bound appearance and consists of diopside + garnet + epidote + plagioclase + quartz + titanite ± vesuvianite ± calcite ± actinolite ± scheelite. In addition to strong mobility of major elements and LILE, the stage-II calc-silicate alteration also modified the original magmatic geochemical composition of LREE, MREE, and HFSE (mainly Th, Nb, and Ta) (Figs. 2.10 and 2.12). In contrast, transition metals remained relatively immobile during this metasomatic event.

- An interesting finding was the recognition of a cryptic alteration in mafic and ultramafic amphibolites (metabasalts and metapicrites) from the Ivisaartoq belt (Chapter 2). This alteration did not cause major element metasomatism, and therefore altered and less altered samples are not easily identified using mineralogical criteria (e.g., calc-silicates, silicification, chloritization, etc). Altered amphibolites occur along high strain zones and are spatially associated with stage-II calc-silicate rocks, suggesting that they formed during regional amphibolite facies metamorphism. Most trace elements were remobilized, including the LREE, MREE, and HFSE (Th, Nb, Ta, and Ti). The cryptic alteration produced trace element patterns that resemble those of Phanerozoic boninites, mid-ocean-ridge basalts (N-MORB), and LREE-depleted island-arc tholeiites (Fig. 2.8c-h) (see also Ordóñez-Calderón et al., 2008).
- In the Ujarassuit, Storø, and Qussuk greenstone belts (Fig. 1.1), amphibolites with depleted LREE patterns and negative Nb-Ta anomalies are geochemically similar to Group 3 amphibolites (with cryptic alteration) in the Ivisaartoq belt (Fig. 2.8e-f; 3.8c-d; and 4.6c-d) (cf. Garde, 2007; Ordóñez-Calderón et al., 2008). Like the Ivisaartoq counterpart, those belts exhibit evidence for significant metasomatic alteration, high-grade metamorphism, and strong ductile deformation. Therefore, it is likely that the LREE were depleted during high-grade metamorphism, as has been well documented in the Ivisaartoq belt (Ordóñez-Calderón et al., 2008).

5.2. Evidence for relict Meso- to Neoarchean suprasubduction zone oceanic crust

The intra-oceanic or intra-continental origin of Archean greenstone belts is one of the most debated issues and fundamental problems to be resolved in Archean geology (Bickle

et al., 1994; Ridley et al., 1997; Hamilton, 1998, 2003; Bleeker, 2002; De Wit, 2004; Eriksson et al., 2004; Eriksson and Catuneanu, 2004; Thurston and Ayres, 2004; Polat and Kerrich, 2006). This is because interpretations regarding the magmatic evolution of greenstone belts, geochemical characteristics of their mantle source, recognition of Archean oceanic crust, and geodynamic models for the origin of Archean granite-greenstone terranes, ultimately rely on precise understanding of the depositional environment in which Archean volcanic rocks were erupted. Resolving that essential problem is complicated, given that the original stratigraphic relationships and volcanic facies are normally obliterated during high-grade metamorphism and ductile deformation. I investigated the issues mentioned above by carefully integrating, outcrop- to belt-scale field and structural observations, petrographic analysis, and whole rock major and trace element geochemistry of a wide variety of metamorphosed volcanic rocks from the Ivisaartoq, Ujarassuit, and Storø greenstone belts (Fig. 1.1). The most important results are:

- The following field and geochemical characteristics indicate an intra-oceanic origin for the Ivisaartoq, Ujarassuit, and Storø greenstone belts: (1) epidosites in pillow basalts from the Ivisaartoq belt are reminiscent of those recovered from modern sea-floor hydrothermal systems in the Tonga-Kermadec forearc (cf. Polat et al., 2007; Ordóñez-Calderón et al., 2008; Banerjee et al., 2000) (Fig. 2.3a-b); (2) the contact between greenstone belts and older orthogneisses is bounded by high-grade mylonites (Fig. 3.2d-e); (3) in a given tectono-stratigraphic terrane, the TTG-gneisses intrude into the supracrustal rocks and contain amphibolite xenoliths with an earlier tectonic foliation (Fig. 3.2g); (4) amphibolites do not

display geochemical trends indicating that their volcanic protoliths were contaminated with felsic crustal rocks (Figs. 3.13 and 4.10).

- Field and geochemical characteristics of amphibolite rocks in the Ujarassuit and Ivisaartoq greenstone belts indicate different volcanic protoliths including pillow basalts, picrites, boninites, and andesites (Chapters 3 and 4). These rocks display near-flat to enriched LREE patterns and pronounced negative Nb-Ta anomalies in primitive mantle-normalized diagrams, which is consistent with a subduction zone geochemical signature (Figs. 3.8 and 3.9). Amphibolites with a basaltic composition consistently plot in the field of volcanic arc rocks on the Th/Yb versus Nb/Yb diagram (3.13a). Therefore, the Ujarassuit and Ivisaartoq greenstone belt were formed in an intra-oceanic suprasubduction zone setting. In addition, the occurrence of boninites, picrites, and epidosites suggests that the Ivisaartoq and Ujarassuit greenstone belts represent a fragment of Archean forearc or back-arc oceanic crust. Similar geochemical signatures in mafic and ultramafic rocks from the Storø greenstone belt also suggest a suprasubduction zone origin.
- The geochemical characteristics of ultramafic to mafic rocks in this study indicate that the Meso- and Neoarchean mantle was geochemically heterogeneous, more depleted in trace elements than modern depleted upper mantle, and experienced significant metasomatism owing to slab derived components. The above characteristics are also common in the sub-arc mantle from the western Pacific island arcs (e.g. Maury et al., 1992; Arai et al., 2007; Ishimaru et al., 2007; Arai and Ishimaru, 2008).

5.3. Missing felsic to intermediate volcanic arc rocks: Evidence from metasedimentary rocks

The primary geochemical characteristics of siliciclastic sedimentary rocks are controlled by a number of factors including source rock composition, intensity of chemical weathering, mixing of multi-source detritus, hydrodynamic sorting, sediment recycling, and diagenesis (Argast and Donnelly, 1987; Nesbitt and Young, 1989; Johnsson, 1993; Korsch et al., 1993; McLennan et al., 1993, 2003; Fedo et al., 1995; Nesbitt et al., 1996; Fralick and Kronberg, 1997; Nesbitt, 2003; Kiminami and Fujii, 2007). Those factors are ultimately controlled by the tectonic setting of deposition (Dickinson and Suczek, 1979; Bhatia, 1983; Bhatia and Crook, 1986). Siliciclastic rocks normally include detritus derived from large geographic areas, providing important information about the paleogeography and the geochemical characteristics of upper crustal rocks being eroded during the time of sedimentation (e.g. Haughton et al., 1991). In complexly metamorphosed and deeply eroded terranes, metasedimentary rocks may contain the only source of information about sediment source rocks, which are no longer preserved in the geological record. In this study, I have assessed the geochemical characteristics of metasedimentary rocks in the Ujarassuit, Ivisaartoq, and Storø greenstone belts (Chapters 3 and 4), to investigate their provenance and to constraint the tectonic setting of origin of these belts. The most significant results are:

- In the Ujarassuit, Ivisaartoq, and Storø greenstone belts, biotite schists and quartzitic gneisses represent metamorphosed volcaniclastic-sedimentary rocks (Figs. 3.2; 3.3; 3.5; 4.2; and 4.3). These rocks display low chemical indexes of alteration (CIA = 46-71) indicating poorly weathered source rocks (Figs. 3.12a

and 4.9). Trace element ratios of Co/Th, La/Sc, Th/Sc, and Zr/Sc show covariations suggesting a mixed-provenance of detritus derived from felsic, intermediate, and mafic source rocks (Figs. 3.12 and 4.8). The majority of detrital zircons in metasedimentary rocks have yielded U-Pb ages that are similar to the age of volcanic rocks within the same greenstone belt (Nutman et al., 2004; Hollis et al., 2006; Knudsen et al., 2007). Therefore, the protoliths of metasedimentary rocks are interpreted to represent first-cycle sediments derived from mafic to felsic volcanic rocks, or their intrusive equivalents. However, a minor population of detrital zircons (< 5%) is older than the associated greenstone volcanism (op. cit.). This suggests that those belts were deposited relatively close to older continental rocks.

- The intermediate and felsic source rocks are not represented in the geological record. Meso- to Neoarchean greenstone belts in the area are dominated by metabasaltic rocks. The Qussuk belt, however, comprises a significant proportion of amphibolites with andesitic composition which have been interpreted as remnant of a volcanic arc complex (Garde, 2007). Those magmatically more evolved complexes are not common in the region. Therefore, with the exception of the Qussuk belt, their existence appears to be recorded only in the metasedimentary rocks.

5.4. Implications for Meso- to Neoarchean crustal evolution in the Nuuk region

The processes by which the early continental crust was formed are still contentious. There are two complementary models: the island arc and the oceanic plateau models (e.g., Taylor, 1967; Moorbath, 1977; Schubert and Sandwell, 1989; Abbott, 1996; Albarède,

1998; Condie, 1999; Kelemen et al., 2003; Mueller and Nelson, 2004; Pirajno, 2007). The island arc model suggests that most of the continental crust was formed at subduction zones. This model is supported by geochemical estimates, which show that the bulk continental crust has a high-Mg andesitic composition, and exhibits enrichment of incompatible elements (e.g., Th, Rb, Ba, Cs, and LREE), pronounced negative Nb-Ta anomalies, and relatively flat HREE patterns in primitive mantle-normalized diagrams (cf. Kelemen et al., 2003; Kemp and Hawkesworth, 2003; Rudnick and Gao, 2003). These trace element characteristics are remarkably similar to those of subduction-related igneous rocks. However, given that island arcs are dominated by basaltic rocks (e.g., Kelemen et al., 2003), a bulk crust with andesitic composition can only be produced by significant intracrustal differentiation processes. These include: remelting of basaltic crust; fractional crystallization of mafic melts; mixing of mafic to felsic magmas; and delamination of mafic to ultramafic lower crustal rocks (Taylor and McLennan, 1995; Rudnick and Fountain, 1995; Rudnick and Gao, 2003). In contrast, the oceanic plateau model suggests that the buoyant thick-crust of oceanic plateaus is the major precursor of the continental crust. In this model, the basaltic crust of oceanic plateaus is transformed into bulk andesitic continental crust through intracrustal melting and subduction inception along their margins (Abbott, 1996, Condie, 1997, 1999, 2001; Albarède, 1998). Such processes are currently seen in the Solomon and Antilles island arcs, which are developed along the southern margin the Ontong-Java Plateau, and the eastern edge of the Caribbean Plateau, respectively (Condie, 2001). However, intra-crustal melting of oceanic plateaus can also take place in environments not related to subduction. For instance, in Iceland, partial melting of amphibolite facies basaltic crust has produced calc-alkaline rhyolites and dacites with negative Nb-Ta anomalies (see Jónasson et al., 1992).

An Archean example of plume-related crustal growth includes the 3.53-3.17 Ga east Pilbara terrane in Western Australia. In this greenstone belt, plume-related komatiites and basalts were erupted in three major episodes at 3.53-3.43, 3.35-3.29, and 3.27-3.24 Ga (Van Kranendonk et al., 2007a,b; Smithies et al., 2007a). Intracrustal melting of basaltic rocks and fractionation of basaltic melts gave rise to significant TTG and granite magmatism (Hickman, 2004; Champion and Smithies, 2007; Van Kranendonk et al., 2004, 2007a,b; Smithies et al., 2007a,b). Accordingly, crustal growth in the east Pilbara craton does not appear to involve Phanerozoic-like subduction processes. In contrast, the 2.9 Ga Sumozero-Kenozero greenstone belt in the Baltic shield, comprises a lower stratigraphic unit of mafic to ultramafic oceanic-plateau volcanic rocks, which are intruded and overlaid by an upper unit of mafic to felsic subduction-related volcanic rocks (Puchtel et al., 1999). In the 2.7 Ga Wawa-Abitibi greenstone belts in the southern Superior province of Canada, oceanic plateau- and subduction-related volcanic rocks were tectonically imbricated owing to subduction-accretion processes (see Mueller et al., 1996; Polat et al., 1998; Polat and Kerrich, 2001). Therefore, plume and arc magmatism in the Archean contributed significantly to the generation and differentiation of the continental crust.

In contrast to the above Archean greenstone belts, the results presented in this thesis indicate that plume-related magmatism was not significant in the Meso- to Neoarchean evolution of the Nuuk region. Instead, rock associations such as boninites, picrites, island arc tholeiites, and andesites are consistent with crustal growth by accretionary processes at subduction zone settings. The Meso- to Neoarchean accretionary history of the Nuuk region covers a time span of approximately 400 Ma (Nutman and Friend, 2007). In a comparable period of time (630 to 245 Ma), subduction-accretion processes formed a

collage of unrelated crustal blocks and suprasubduction zone ophiolites, giving rise to the Altaid orogenic system in central Asia (Şengör, 1990; Şengör and Natal'in, 2004). Therefore, this study leads to the conclusion that Phanerozoic-like subduction processes may well explain the collisional history and crustal evolution of the Nuuk region. This resulted in the formation, accretion, and fragmentation of Meso- to Neoarchean ophiolites.

5.5. References

Albarède, F., 1998. The growth of the continental crust. Tectonophysics 296, 1-14.

Abbott, D.H., 1996. Plumes and hotspots as sources of greenstone belts. Lithos 37, 113-127.

Arai, S., Abe, N., Ishimaru, S., 2007. Mantle peridotites from the Western Pacific. Gondwana Research 11, 180-199.

Arai, S., Ishimaru, S., 2008. Insights into petrological characteristics of the lithosphere of mantle wedge beneath arcs through peridotites xenoliths: a review. Journal of Petrology 49, 665-698.

Argast, S.T., Donnelly, W., 1987. The chemical discrimination of clastic sedimentary components. Journal of Sedimentary Research 57, 813-823.

Banerjee, N.R., Gillis, K.M., Muehlenbachs, K., 2000. Discovery of epidosites in a modern oceanic setting, the Tonga forearc. Geology 28, 151-154.

Bhatia, M.R., 1983. Plate tectonics and geochemical composition of sandstones. Journal of Geology 91, 611-627.

Bhatia, M.R., Crook, K.A.W., 1986. Trace element characteristics of greywackes and tectonic setting discrimination of sedimentary basins. Contributions to Mineralogy and Petrology 92, 181-193.

Bickle, M.J., Nisbet, E.G., Martin, A., 1994. Archean greenstone belts are not oceanic crust. Journal of Geology 102, 121-138.

Bleeker, W., 2002. Archean tectonics, a review, with illustrations from the Slave craton. In: Fowler, C.M.R., Ebinger, C.J., Hawkesworth, C.J. (Eds.). The early earth: physical, chemical and biological development. Geological Society of London Special Publications 199, 151-181.

Champion, D.C., Smithies, R.H., 2007. Geochemistry of Paleoarchean granites of the east Pilbara terrane, Pilbara craton, Western Australia: Implications for early Archean crustal growth. In: Van Kranendonk, M.J., Smithies, R.H., Bennett, V.C., (Eds.). Earth's oldest rocks. Developments in Precambrian Geology 15, 369-409.

Condie, K.C., 1997. Contrasting sources for upper and lower crust: The greenstone connection. Journal of Geology 105, 729-736.

Condie, K.C., 1999. Mafic crustal xenoliths and the origin of the lower continental crust. Lithos 46, 95-101.

Condie, K.C., 2001. Mantle plumes and their record in the earth history. Cambridge University, 306 pp.

De Wit, M.J., 2004. Archean greenstone belts do contain fragments of ophiolites. In: Kusky, T.M., (Ed.). Precambrian ophiolites and related rocks. Developments in Precambrian Geology 13, 599-614.

Dickinson, W.R., Suczek, C.A., 1979. Plate tectonics and sandstone compositions. AAPG Bulletin 63, 2164-2182.

Eriksson, P.G., Catuneanu, O., 2004. A commentary on Precambrian plate tectonics. In: Eriksson, P.G., Altermann, W., Nelson, D.R., Müeller, W.U., Catuneanu, O., (Eds.).

The Precambrian earth: Tempos and events. Developments in Precambrian Geology 12, 201-213.

Eriksson, P.G., Catuneanu, O., Nelson, D.R., Mueller, W.U., Alterman, W., 2004. Towards a synthesis. In: Eriksson, P.G., Altermann, W., Nelson, D.R., Müeller, W.U., Catuneanu, O., (Eds.). The Precambrian earth: Tempos and events. Developments in Precambrian Geology 12, 739-769.

Fedo, C.M., Nesbitt, H.W., Young, G.M., 1995. Unraveling the effects of potassium metasomatism in sedimentary rocks and paleosols, with implications for paleoweathering conditions and provenance. Geology 23, 921-924.

Fralick, P.W., Kronberg, B.I., 1997. Geochemical discrimination of clastic sedimentary rock sources. Sedimentary Geology 113, 111-124.

Garde, A.A., 2007. A mid-Archean island arc complex in the eastern Akia terrane, Godthåbsfjord, southern West Greenland. Journal of the Geological Society of London 164, 565-579.

Gruau, G., Rosing, M., Bridgwater, D., Gill, R.C.O., 1996. Resetting of Sm-Nd systematics during metamorphism of >3.7-Ga rocks: implications for isotopic models of early Earth differentiation. Chemical Geology 133, 225-240.

Gruau, G., Tourpin, S., Fourcade, S., Blais S., 1992. Loss of isotopic (Nd, O) and chemical (REE) memory during metamorphism of komatiites: New evidence from eastern Finland. Contributions to Mineralogy and Petrology 112, 66-82.

Hamilton, W.B., 1998. Archean magmatism and deformation were not products of plate tectonics. Precambrian Research 91, 143-179.

Hamilton, W.B., 2003. An alternative earth. GSA Today 13 (11), 4-12.

Haughton, P.D.W., Todd, S.P., Morton, A.C., 1991. Sedimentary provenance studies. In: Morton, A.C., Todd, S.P., Haughton, P.D.W., (Eds.). Developments in sedimentary provenance studies. Geological Society of London Special Publication 57, 1-11.

Hickman, A.H., 2004. Two contrasting granite-greenstone terranes in the Pilbara Craton, Australia: Evidence for vertical and horizontal tectonic regimes prior to 2900 Ma. Precambrian Research 131, 153-172.

Hollis, J.A., Frei, D., van Gool, J.A.M., Garde, A.A., Persson, M., 2006. Using zircon geochronology to resolve the Archaean geology of southern West Greenland. Geological Survey of Denmark and Greenland Bulletin 10, 49-52.

Ishimaru, S., Arai, S., Ishida,Y., Shirasaka, M., Okrugin, V.M., 2007. Melting and multi-stage metasomatism in the mantle wedge beneath a frontal arc inferred from highly depleted peridotite xenoliths from the Avacha volcano, southern Kamchatka. Journal of Petrology 48, 395-433.

Jónasson, K., Holm, P.M., Pedersen, A.K., 1992. Petrogenesis of silicic rocks from the Króksfjördur central volcano, NW Iceland. Journal of Petrology 33, 1345-1369.

Johnsson, M.J., 1993. The system controlling the composition of clastic sediments. In: Johnsson, M.J., Basu, A., (Eds.). Processes controlling the composition of clastic sediments. Geological Society of America Special Paper 284, 1-19.

Kelemen, P.B., Hanghøj, K., Greene, A.R., 2003. One view of the geochemistry of subduction-related magmatic arcs, with emphasis on primitive andesite and lower crust. Treatise on Geochemistry 3, 593-659.

Kemp, A.I.S., Hawkesworth, C.J., 2003. Granitic perspectives on the generation and secular evolution of the continental crust. Treatise on Geochemistry 3, 350-410.

Kiminami, K., Fujii, K., 2007. The relationship between major element concentration and grain size with sandstones from four turbidite sequences in Japan. Sedimentary Geology 195, 203-215.

Korsch, R.J., Roser, B.P., Kamprad, J.L., 1993. Geochemical, petrographic and grain-size variations within single turbidite beds. Sedimentary Geology 83, 15-35.

Knudsen, C., van Gool, J.A.M., Østergaard, C., Hollis, J.A., Rink-Jørgensen, M., Persson, M., Szilas, K., 2007. Gold-hosting supracrustal rocks on Storø, southern West Greenland: lithologies and geological environment. Geological Survey of Denmark and Greenland Bulletin 13, 41-44.

Lahaye, Y., Arndt, N.T., Byerly, G., Chauvel, C., Fourcade, S., Gruau, G., 1995. The influence of alteration on the trace-element and Nd isotopic compositions of komatiites. Chemical Geology 126, 43-64.

Maury, R.C., Defant, M.J., Joron, J.L., 1992. Metasomatism of the sub-arc mantle inferred from trace elements in Philippine xenoliths. Nature 360, 661-663.

McLennan, S.M., Bock, B., Hemming, S.R., Hurowitz, J.A., Lev, S.M., McDaniel, DK., 2003. The role of provenance and sedimentary processes in the geochemistry of sedimentary rocks. In: Lentz, D.R. (Ed.). Geochemistry of sediments and sedimentary rocks: Evolutionary considerations to mineral-deposit forming environments. GeoText 4, Geological Association of Canada, 7-38.

McLennan, S.M., Hemming, S., McDaniel, D.K., Hanson, G.N., 1993. Geochemical approaches to sedimentation, provenance, and tectonics, 1993. In: Johnsson, M.J., Basu, A., (Eds.). Processes controlling the composition of clastic sediments. Geological Society of America Special Paper 284, 21-40.

Moorbath, S., 1977. Ages, isotopes and evolution of Precambrian continental crust. Chemical Geology 20, 151-187.

Moorbath, S., O'Nions, R.K., Pankhurst, R.J., 1973. Early Archaean age for the Isua iron formation, West Greenland. Nature 245, 138-139.

Mueller, W.U., Daigneault, R., Mortensen, J.K., Chown, E.H., 1996. Archean terrane docking: upper crust collision tectonics, Abitibi greenstone belt, Quebec, Canada. Tectonophysics 265, 127-150.

Mueller, W.U., Nelson, D.R., 2004. Generation of continental crust. In: Eriksson, P.G., Altermann, W., Nelson, D.R., Müeller, W.U., Catuneanu, O., (Eds.). The Precambrian Earth: Tempos and Events. Developments in Precambrian Geology 12, 65-66.

Nesbitt, H.W., 2003. Petrogenesis of siliciclastic sediments and sedimentary rocks. In: Lentz, D.R. (Ed.). Geochemistry of sediments and sedimentary rocks: Evolutionary considerations to mineral-deposit forming environments. GeoText 4, Geological Association of Canada, 39-51.

Nesbitt, H.W., Young, G.M., 1989. Formation and diagenesis of weathering profiles. Journal of Geology 97, 129-147.

Nesbitt, H.W., Young, G.M., McLennan, S.M., Keays, R.R., 1996. Effects of chemical weathering and sorting on the petrogenesis of siliciclastic sediments, with implications for provenance studies. Journal of Geology 104, 525-542.

Nutman, A.P., Friend, C.R.L., Barker, S.L.L., McGregor, V.R., 2004. Inventory and assessment of Palaeoarchaean gneiss terrains and detrital zircons in southern West Greenland. Precambrian Research 135, 281-314.

Ordóñez-Calderón, J.C., Polat, A., Fryer, B.J., Gagnon, J.E., Raith, J.G., Appel, P.W.U., 2008. Evidence for HFSE and REE mobility during calc-silicate metasomatism, Mesoarchean (~3075 Ma) Ivisaartoq greenstone belt, southern West Greenland. Precambrian Research 161 (3-4), 317-340.

Pirajno, F., 2007. Ancient to modern earth: The role of mantle plumes in the making of continental crust. In: Van Kranendonk, M.J., Smithies, R.H., Bennett, V.C., (Eds.). Earth's oldest rocks. Developments in Precambrian Geology 15, 1037-1064.

Polat, A., Appel, P.W.U., Frei, R., Pan, Y., Dilek, Y., Ordóñez-Calderón, J.C., Fryer, B., Raith, J.G., 2007. Field and geochemical characteristics of the Mesoarchean (~3075 Ma) Ivisaartoq greenstone belt, southern West Greenland: Evidence for seafloor hydrothermal alteration in a supra-subduction oceanic crust. Gondwana Research 11, 69-91.

Polat, A., Frei, R., Appel, P.W.U., Dilek, Y., Fryer, B., Ordóñez-Calderón, J.C., Yang, Z., 2008. The origin and compositions of Mesoarchean oceanic crust: Evidence from the 3075 Ma Ivisaartoq greenstone belt, SW Greenland. Lithos 100, 293-321.

Polat, A., Hofmann, A.W., Münker, C., Regelous, M., Appel, PW.U., 2003. Contrasting geochemical patterns in the 3.7-3.8 Ga pillow basalt cores and rims, Isua greenstone belt, Southwest Greenland: implications for post-magmatic alteration processes. Geochimica et Cosmochimica Acta 67 (3), 441-457.

Polat, A., Kerrich, R., 2001. Geodynamic processes, continental growth, and mantle evolution recorded in late Archean greenstone belts of the southern Superior Province, Canada. Precambrian Research 112, 5-25.

Polat, A., Kerrich, R., 2006. Reading the geochemical fingerprints of Archean hot subduction volcanic rocks: Evidence for accretion and crustal recycling in a mobile

tectonic regime. In: Benn, K., Mareschal, J-C., Condie, K.C., (Eds.). Archean geodynamics and environments. American Geophysical Union Geophysical Monograph 164, 189-213.

Polat, A., Kerrich, R., Wyman, D.A., 1998. The late Archean Schreiber-Hemlo and White River-Dayohessarah greenstone belts, Superior Province: collages of oceanic plateaus, oceanic arcs, and subduction-accretion complexes. Tectonophysics 289, 295-326.

Ridley, J.R., Vearncombe, J.R., Jelsma, H.A., 1997. Relations between Greenstone Belts and Associated Granitoids. *In*: de Wit, M., Ashwal, L.D., (Eds.). Greenstone Belts. Oxford Monographs on Geology and Geophysics 35, 376-397.

Rudnick, R.L., Fountain, D.M., 1995. Nature and composition of the continental crust: A lower crustal perspective. Reviews of Geophysics 33, 267-309.

Rudnick, R.L., Gao, S., 2003. Composition of the continental crust. Treatise on Geochemistry 3, 1-64.

Schubert, G., Sandwell, D., 1989. Crustal volumes of the continents and of oceanic and continental submarine plateaus. Earth and Planetary Science Letters 92, 234-246.

Şengör, A.M.C., 1990. Plate tectonics and orogenic research after 25 years: A Tethyan perspective. Earth Science Reviews 27, 1-201.

Şengör, A.M.C., Natal'in, B.A., 2004. Phanerozoic analogues of Archean oceanic basement fragments: Altaid ophiolites and ophirags. In: Kusky, T.M., (Ed.). Precambrian ophiolites and related rocks. Developments in Precambrian Geology, Elsevier 13, 675-726.

Smithies, R.H., Champion, D.C., Van Kranendonk, M.J., 2007b. The oldest well-preserved felsic volcanic rocks on earth: Geochemical clues to the early evolution of the Pilbara supergroup and implications for the growth of a Paleoarchean

protocontinent. In: Van Kranendonk, M.J., Smithies, R.H., Bennett, V.C., (Eds.). Earth's oldest rocks. Developments in Precambrian Geology 15, 339-367.

Smithies, R.H., Van Kranendonk, M.J., Champion, D.C., 2007a. The Mesoarchean emergence of modern-style subduction. Gondwana Research 11, 50-68.

Taylor, S.R., 1967. The origin and growth of continents. Tectonophysics 4, 17-34.

Taylor, S.R., McLennan, S.M., 1995. The geochemical evolution of the continental crust. Reviews of Geophysics 33, 241-265.

Terabayashi, M., Masada, Y., Ozawa, H., 2003. Archean ocean-floor metamorphism in the North Pole area, Pilbara Craton, Western Australia. Precambrian Research 127, 167-180.

Thurston, Ayres, L.D., 2004. Archean and Proterozoic Greenstone belts: Setting and evolution. In: Eriksson, P.G., Altermann, W., Nelson, D.R., Müeller, W.U., Catuneanu, O., (Eds.). The Precambrian earth: Tempos and events. Developments in Precambrian Geology 12, 311-333.

Van Kranendonk, M.J., Collins, W.J., Hickman, A., Pawley, M.J., 2004. Critical tests of vertical vs. horizontal tectonic models for the Archean East Pilbara Granite-Greenstone Terrane, Pilbara Craton, Western Australia. Precambrian Research 131, 173-211.

Van Kranendonk, M.J., Smithies, R.H., Hickman, A.H., Champion, D.C., 2007a. Paleoarchean development of a continental nucleus: The east Pilbara terrane of the Pilbara craton, Western Australia. In: Van Kranendonk, M.J., Smithies, R.H., Bennett, V.C., (Eds.). Earth's oldest rocks. Developments in Precambrian Geology 15, 307-337.

Van Kranendonk, M.J., Smithies, R.H., Hickman, A.H., Champion, D.C., 2007b. Review: Secular tectonic evolution of Archean continental crust: Interplay between horizontal and vertical processes in the formation of the Pilbara Craton, Australia. Terra Nova 19, 1-38.

Weiershäuser, L., Spooner, E.T.C., 2005. Seafloor hydrothermal fluids, Ben Nevis area, Abitibi greenstone belt; implications for Archean (approximately 2.7 Ga) seawater properties. Precambrian Research 138, 89-123.

Appendix A: copyright release from Elsevier

Attached in the next page is the permission and copyright release from Elsevier to include in Chapter 2 of this Ph.D. dissertation the following manuscript published in Precambrian Research:

Ordóñez-Calderón, J.C., Polat, A., Fryer, B.J., Gagnon, J.E., Raith, J.G., Appel, P.W.U., 2008. Evidence for HFSE and REE mobility during calc-silicate metasomatism, Mesoarchean (~3075 Ma) Ivisaartoq greenstone belt, southern West Greenland. Precambrian Research 161 (3-4), 317-340. doi:10.1016/j.precamres.2007.09.004.

ELSEVIER LICENSE
TERMS AND CONDITIONS

Sep 08, 2008

This is a License Agreement between Juan Carlos Ordóñez-Calderón ("You") and Elsevier ("Elsevier"). The license consists of your order details, the terms and conditions provided by Elsevier, and the payment terms and conditions.

Supplier	Elsevier Limited The Boulevard,Langford Lane Kidlington,Oxford,OX5 1GB,UK
Registered Company Number	1982084
Customer name	Juan Carlos Ordóñez-Calderón
Customer address	401 Sunset Avenue, University of Windsor, Earth Sciences windsor, ON N9B 3P4
License Number	2013720001745
License date	Aug 21, 2008
Licensed content publisher	Elsevier
Licensed content publication	Precambrian Research
Licensed content title	Evidence for HFSE and REE mobility during calc-silicate metasomatism, Mesoarchean (~3075 Ma) Ivisaartoq greenstone belt, southern West Greenland
Licensed content author	J.C. Ordóñez-Calderón, A. Polat, B.J. Fryer, J.E. Gagnon, J.G. Raith and P.W.U. Appel
Licensed content date	10 March 2008
Volume number	
Issue number	
Pages	0
Type of Use	Thesis / Dissertation
Portion	Full article
Format	Print
You are an author of the Elsevier article	Yes
Are you translating?	No
Purchase order number	
Expected publication date	Sep 2008
Elsevier VAT number	GB 494 6272 12

Appendix B: Table B1 with structural data

Attached in the next page is Table B1 with the structural data for foliations, lineations, and isoclinal fold axis in the western and eastern flanks of the Ujarassuit greenstone belt.

Table B.1. Structural data for foliations, lineations, and isoclinal fold axis in the Western and Eastern flanks of the Ujarassuit greenstone belt. All structural data follow the right hand rule.

Lithology	North	West	Strike	Dip angle
Foliations, Western flank				
Amphibolite	64°51.196'	50°12.660'	6	51
Amphibolite	64°51.194'	50°12.658'	186	61
Amphibolite	64°51.164'	50°12.661'	158	61
Amphibolite	64°51.126'	50°12.685'	176	61
Amphibolite	64°51.008'	50°12.631'	150	80
Amphibolite	64°50.965'	50°12.642'	186	86
Amphibolite	64°50.932'	50°12.728'	198	72
Amphibolite	64°50.854'	50°12.627'	20	82
Amphibolite	64°50.827'	50°12.510'	176	80
Amphibolite	64°50.713'	50°12.490'	21	73
Amphibolite	64°51.228'	50°12.191'	165	56
Amphibolite	64°50.206'	50°12.872'	30	61
Amphibolite	64°51.109'	50°11.921'	18	82
Amphibolite	64°51.194'	50°11.994'	166	64
Amphibolite	64°50.161'	50°13.010'	0	64
Amphibolite	64°50.098'	50°13.052'	22	52
Amphibolite	64°49.747'	50°13.462'	32	33
Amphibolite	64°49.726'	50°12.973'	26	65
Amphibolite	64°48.973'	50°14.124'	28	82
Amphibolite	64°51.437'	50°11.845'	10	40
Biotite schist	64°51.445'	50°11.406'	210	83
Biotite schist	64°51.852'	50°11.959'	150	61
Amphibolite	64°53.576'	50°12.875'	350	86
Amphibolite	64°53.452'	50°12.965'	0	83
Amphibolite	64°52.700'	50°13.186'	0	90
Amphibolite	64°53.956'	50°12.896'	12	85
Amphibolite	64°54.085'	50°13.010'	186	88
Amphibolite	64°54.101'	50°13.010'	4	85
Amphibolite	64°54.289'	50°13.111'	0	68
Amphibolite	64°54.266'	50°13.166'	6	85
Amphibolite	64°54.170'	50°13.374'	352	72
Metagabbro	64°54.119'	50°13.634'	0	68
Amphibolite	64°54.042'	50°13.590'	14	58
Amphibolite	64°51.132'	50°12.662'	198	60
Amphibolite	64°51.136'	50°12.649'	184	66
Amphibolite	64°51.001'	50°12.634'	190	68
Amphibolite	64°50.962'	50°12.649'	180	86
Amphibolite	64°50.869'	50°12.606'	28	63
Amphibolite	64°50.903'	50°12.618'	180	88
Amphibolite	64°50.856'	50°12.627'	8	82
Amphibolite	64°50.885'	50°12.389'	184	84
Amphibolite	64°51.203'	50°12.205'	188	62
Amphibolite	64°51.218'	50°12.164'	180	70
Amphibolite	64°51.184'	50°12.174'	8	69
Amphibolite	64°50.202'	50°12.837'	22	60
Amphibolite	64°50.162'	50°12.995'	28	64
Amphibolite	64°49.667'	50°13.494'	14	60
Amphibolite	64°49.455'	50°13.696'	20	58
Amphibolite	64°51.170'	50°12.260'	190	68
Biotite schist	64°51.483'	50°11.421'	172	60
Amphibolite	64°51.806'	50°12.636'	174	50
Amphibolite	64°53.566'	50°12.867'	350	72
Amphibolite	64°53.312'	50°12.971'	344	80
Amphibolite	64°52.959'	50°13.087'	146	80
Amphibolite	64°52.912'	50°13.083'	150	60

Table B.1 *(Continued)*

Lithology	North	West	Strike	Dip angle
Foliations, Western flank				
Amphibolite	64°52.717'	50°13.201'	150	80
Amphibolite	64°52.693'	50°13.178'	350	80
Amphibolite	64°52.668'	50°12.784'	174	70
Amphibolite	64°53.974'	50°12.924'	147	60
Amphibolite	64°54.043'	50°13.027'	6	80
Amphibolite	64°54.103'	50°13.116'	2	80
Amphibolite	64°54.132'	50°13.146'	16	54
Metagabbro	64°54.118'	50°13.627'	0	60
Amphibolite	64°54.133'	50°13.327'	5	68
Amphibolite	64°54.159'	50°13.879'	5	66
Amphibolite	64°54.142'	50°13.996'	10	70
Foliations, Eastern flank				
Amphibolite	64°52.063'	50°02.060'	9	61
Orthogneiss	64°52.001'	50°02.310'	0	58
Amphibolite	64°52.001'	50°02.310'	6	68
Amphibolite	64°51.854'	50°01.520'	23	66
Amphibolite	64°51.514'	50°02.840'	29	68
Amphibolite	64°51.424'	50°03.570'	329	63
Amphibolite	64°51.314'	50°01.400'	355	38
Amphibolite	64°51.017'	50°03.670'	357	37
Orthogneiss	64°52.329'	50°00.990'	339	73
Amphibolite	64°52.313'	50°03.320'	0	50
Amphibolite	64°52.390'	50°03.410'	340	51
Amphibolite	64°52.032'	50°00.100'	349	63
Amphibolite	64°50.919'	50°00.030'	18	68
Amphibolite	64°50.929'	50°00.680'	17	65
Amphibolite	64°50.909'	50°01.820'	8	63
Amphibolite	64°50.997'	50°04.060'	7	59
Amphibolite	64°51.047'	50°04.420'	342	45
Amphibolite	64°51.092'	50°04.790'	18	53
Amphibolite	64°51.212'	50°09.800'	333	57
Amphibolite	64°50.834'	50°05.210'	13	63
Metagabbro	64°52.022'	50°00.236'	12	50
Orthogneiss	64°51.958'	50°00.216'	12	48
Orthogneiss	64°51.735'	50°00.139'	348	52
Metagabbro	64°51.511'	50°00.309'	334	44
Amphibolite	64°51.425'	50°00.355'	320	62
Amphibolite	64°51.316'	50°00.142'	348	62
Amphibolite	64°51.302'	50°00.103'	30	52
Mylonite	64°52.323'	50°00.100'	340	60
Mylonite	64°52.955'	50°00.658'	338	62
Amphibolite	64°50.971'	50°00.202'	44	50
Orthogneiss	64°52.415'	50°00.137'	350	52
Mylonite	64°52.350'	50°00.201'	20	70
Mylonite	64°52.432'	50°00.236'	350	32
Metagabbro	64°52.580'	50°00.222'	318	56
Orthogneiss	64°52.620'	50°00.097'	344	62
Lineations, Western flank				
Amphibolite	64°50.190'	50°12.150'	162	40
Amphibolite	64°53.312'	50°12.971'	180	50
Amphibolite	64°52.717'	50°13.201'	158	40
Amphibolite	64°53.974'	50°12.924'	160	42
Amphibolite	64°54.043'	50°13.027'	180	40

Table B.1 *(Continued)*

Lithology	North	West	Strike	Dip angle
Lineations, Western flank				
Orthogneiss	64°53.523'	50°14.389'	140	42
Orthogneiss	64°53.593'	50°14.282'	148	40
Orthogneiss	64°53.634'	50°14.298'	150	42
Orthogneiss	64°53.433'	50°14.522'	154	40
Orthogneiss	64°53.424'	50°14.585'	144	40
Orthogneiss	64°53.061'	50°15.166'	144	38
Orthogneiss	64°52.992'	50°15.171'	136	48
Orthogneiss	64°52.768'	50°14.819'	150	52
Orthogneiss	64°53.170'	50°14.231'	160	50
Amphibolite	64°54.142'	50°13.996'	102	60
Amphibolite	64°53.956'	50°14.912'	150	46
Amphibolite	64°53.816'	50°15.657'	132	38
Amphibolite	64°53.799'	50°15.778'	134	42
Amphibolite	64°53.785'	50°15.157'	132	44
Orthogneiss	64°53.633'	50°16.067'	144	30
Orthogneiss	64°53.587'	50°16.173'	146	32
Orthogneiss	64°53.608'	50°16.374'	156	32
Amphibolite	64°50.827'	50°12.510'	182	36
Amphibolite	64°50.772'	50°12.629'	180	36
Amphibolite	64°50.713'	50°12.490'	190	52
Amphibolite	64°50.587'	50°12.569'	172	46
Amphibolite	64°50.161'	50°13.010'	188	32
Amphibolite	64°48.973'	50°14.124'	182	32
Amphibolite	64°53.576'	50°12.875'	148	68
Amphibolite	64°53.452'	50°12.965'	160	42
Amphibolite	64°53.291'	50°12.961'	133	70
Amphibolite	64°53.956'	50°12.896'	152	63
Amphibolite	64°54.949'	50°12.514'	182	62
Orthogneiss	64°54.983'	50°12.425'	120	52
Amphibolite	64°55.006'	50°11.584'	142	63
Orthogneiss	64°54.948'	50°10.337'	162	21
Amphibolite	64°54.954'	50°09.947'	167	18
Amphibolite	64°54.942'	50°09.082'	152	40
Amphibolite	64°53.465'	50°15.698'	151	38
Amphibolite	64°53.536'	50°15.769'	142	35
Amphibolite	64°53.762'	50°15.745'	141	37
Lineations, Eastern flank				
Amphibolite	64°51.364'	49°59.898'	100	50
Amphibolite	64°51.480'	49°59.689'	40	40
Metagabbro	64°51.802'	49°59.603'	16	52
Orthogneiss	64°53.111'	49°56.566'	20	60
Amphibolite	64°52.998'	49°56.497'	288	76
Amphibolite	64°53.002'	49°56.826'	40	60
Amphibolite	64°52.879'	49°57.143'	320	66
Amphibolite	64°52.855'	49°57.233'	310	70
Orthogneiss	64°53.297'	49°57.515'	50	58
Orthogneiss	64°53.390'	49°57.856'	52	52
Orthogneiss	64°53.421'	49°58.250'	50	74
Orthogneiss	64°52.942'	49°59.761'	20	52
Mylonite	64°52.955'	50°00.658'	30	40
Amphibolite	64°50.941'	49°59.203'	40	74
Orthogneiss	64°51.458'	49°59.485'	24	60
Orthogneiss	64°52.215'	49°59.885'	42	44
Orthogneiss	64°52.310'	49°59.789'	42	50

Table B.1 *(Continued)*

Lithology	North	West	Strike	Dip angle
Lineations, Eastern flank				
Amphibolite	64°51.355'	50°01.319'	150	28
Orthogneiss	64°51.335'	50°01.440'	240	30
Orthogneiss	64°52.640'	49°59.516'	50	50
Orthogneiss	64°52.631'	49°59.596'	32	44
Orthogneiss	64°52.415'	50°00.137'	48	52
Mylonite	64°52.350'	50°00.201'	30	54
Mylonite	64°52.580'	50°00.222'	24	50
Orthogneiss	64°52.620'	50°00.097'	24	52
Orthogneiss	64°52.961'	49°59.915'	22	60
Orthogneiss	64°53.090'	49°59.049'	50	60
Isoclinal fold axis, Western flank				
Amphibolite	64°51.203'	50°12.205'	180	28
Amphibolite	64°51.063'	50°12.192'	188	28
Amphibolite	64°51.264'	50°12.200'	160	22
Amphibolite	64°49.820'	50°12.840'	208	38
Amphibolite	64°51.170'	50°12.260'	188	20
Biotite schist	64°51.359'	50°11.553'	190	50
Orthogneiss	64°51.882'	50°12.557'	174	30
Amphibolite	64°52.959'	50°13.087'	150	32
Amphibolite	64°52.693'	50°13.178'	174	40
Amphibolite	64°53.974'	50°12.924'	151	50
Orthogneiss	64°53.501'	50°14.442'	140	38
Orthogneiss	64°53.634'	50°14.298'	144	42
Orthogneiss	64°53.643'	50°14.263'	162	40
Orthogneiss	64°53.515'	50°14.359'	162	44
Orthogneiss	64°53.170'	50°14.231'	156	50
Amphibolite	64°53.799'	50°15.778'	152	50
Orthogneiss	64°53.606'	50°16.074'	154	24
Orthogneiss	64°53.696'	50°16.398'	150	32
Amphibolite	64°51.200'	50°12.203'	190	30
Amphibolite	64°51.228'	50°12.191'	150	38
Amphibolite	64°51.185'	50°12.182'	183	29
Amphibolite	64°51.065'	50°12.195'	182	29
Amphibolite	64°50.206'	50°12.872'	174	52
Amphibolite	64°50.967'	50°11.783'	220	72
Orthogneiss	64°49.823'	50°12.836'	196	38
Amphibolite	64°48.973'	50°14.124'	199	32
Amphibolite	64°51.362'	50°11.554'	188	78
Amphibolite	64°51.807'	50°12.630'	206	68
Amphibolite	64°53.291'	50°12.961'	133	70
Amphibolite	64°53.009'	50°13.076'	174	53
Amphibolite	64°53.956'	50°12.896'	196	42
Orthogneiss	64°53.993'	50°12.946'	150	50
Orthogneiss	64°54.983'	50°12.425'	178	64
Orthogneiss	64°54.878'	50°10.657'	168	52
Isoclinal fold axis, Eastern flank				
Orthogneiss	64°51.735'	50°00.139'	148	30
Orthogneiss	64°51.425'	50°00.355'	140	20
Amphibolite	64°51.316'	50°00.142'	110	38
Amphibolite	64°51.302'	50°00.103'	186	28
Orthogneiss	64°51.382'	50°00.383'	160	30
Amphibolite	64°51.355'	50°01.319'	138	42
Orthogneiss	64°51.308'	50°01.515'	136	44
Amphibolite	64°51.029'	50°00.904'	194	40

Vita Auctoris

Juan Carlos Ordóñez was born in 1974 in Girón, Colombia. He studied Geology at the Universidad Industrial de Santander, in Colombia, where he obtained his B.Sc. in geology in 2001, and graduated with the Summa Cum Laude distinction. The same year he earned a scholarship from the Inter-American Development Bank and went on to Shimane University, in Japan, where he obtained his M.Sc. degree in 2003. After successfully completing his M.Sc., he returned back to Colombia and worked as a lecturer in the Department of Geology of the Universidad Industrial de Santander, where he taught Physical Geology and Mineralogy. In June 2004, he moved on to the University of Windsor in Canada, where he started his Ph.D. and is currently a doctoral candidate. He hopes to graduate in September.